Design of a multi-analysis and real time multi-organ-on-chip in the context of blood sugar regulation and type 2 diabetes

Marie Monchablon

THÈSE PRÉSENTÉE
POUR OBTENIR LE GRADE DE

DOCTEURE DE L'UNIVERSITÉ DE BORDEAUX

ECOLE DOCTORALE DES SCIENCES PHYSIQUES ET DE L'INGENIEUR

SPECIALITE ELECTRONIQUE

Par Marie MONCHABLON

Développement d'un multi-organe-sur-puce multi-analyse et temps réel dans le contexte de la régulation glycémique et du diabète de type 2.

Design of a multi-analysis and real time multi-organ-on-a-chip in the context of bloodsugar regulation and type 2 diabetes.

Sous la direction de **Sylvie RENAUD** et de **Matthieu RAOUX**

Soutenue le 19 décembre 2023

Membres du jury :

Mme Thérèse Leblois	Professeure des Universités - Université de Franche-Comté, Femto-st	Rapporteur
Mme Christel Vanbesien	Maîtresse de Conférence - Université de Lille, IEMN	Rapporteur
M. Guillaume Wantz	Professeur des Universités - Bordeaux INP, IMS	Président
M. Karim Bouzakri	Docteur - Centre européen d'étude du Diabète	Examinateur
Mme Sylvie Renaud	Professeure des Universités - Bordeaux INP, IMS	Directrice de thèse
M. Matthieu Raoux	Maître de Conférence - Université de Bordeaux, CBMN	Co-directeur de thèse
M. Antoine Pirog	Maître de conférence - Junia, IMS	Invité
M. Brice Sorli	Maître de conférence - Université de Montpellier, IES	Invité

Résumé

Depuis 4 décennies, un modèle intermédiaire entre les traditionnelles approches *in vivo* et *in vitro* émerge : les Systèmes MicroPhysiologiques (SMP). Ils sont construits pour recréer différents niveaux de la physiologie humaine, du simple organe à leurs interactions. Ils améliorent l'environnement de culture grâce à des microstructures accueillant des modèles d'architecture 3D et multicellulaire, et intègrent des microcapteurs monitorant l'activité cellulaire et leur environnement.

Ce nouvel outil d'investigation intéresse la recherche fondamentale sur les maladies comme le diabète. Dans le cas de cette maladie incurable, la régulation du glucose sanguin, résultant d'interactions complexes entre les îlots pancréatiques, le foie, les adipocytes et les muscles, est altérée. Un Multi-Organe-sur-Puce (MOsP) est un SMP pouvant reproduire ces interactions, et représente donc un modèle pertinent pour la recherche sur le diabète. En effet, la régulation inter-organe n'est pas entièrement reproduite par les modèles *in vitro* usuels, et requiert de multiples capteurs, ce qui est éthiquement et techniquement impossible *in vivo*. Dans le contexte du diabète, il n'existe aucun MOsP reproduisant l'action des îlots sur les muscles, malgré l'importance des muscles squelettiques dans la régulation glycémique.

Cette thèse propose une méthodologie pour construire un MOsP étudiant les interactions d'îlot à muscle dans la régulation glycémique. Les 3 objectifs du MOsP étaient : atteindre des concentrations physiologiques d'insuline grâce à des îlots sécrétant en réponse à une élévation physiologique de glucose, induisant une prise de glucose mesurable par les muscles, et monitorer l'expérience en direct. Pour cela, les recherches ont été menées avec une approche interdisciplinaire, utilisant et confrontant des résultats venant d'expériences biologiques *in vitro* et de simulations modélisant la biologie et la physique.

Ce manuscrit détaille les étapes de la méthodologie, et délivre différents designs pour progressivement construire un MOsP comprenant une puce microfluidique contenant les cellules et un capteur de glucose connecté directement au flux. Les principaux résultats sont :

- Un milieu et une procédure de co-culture entre îlots primaires et lignée de myotubes ont été démontrés.
- Un substrat de culture commun de type Matrice de MicroElectrodes a été trouvé.
- Des îlots ont été cultivés en puce microfluidique, et ont présenté une sécrétion d'insuline en réponse au glucose durant des expériences en fluidique. Des myotubes ont pu se différentier dans une puce, et ont présenté une prise de glucose basale (insuline indépendant).
- Une stratégie *in vitro-in silico* pour dimensionner le MOsP a été développée et implémentée. Un modèle *in silico* simplifié d'îlot a été développé pour rapidement explorer 2 designs de puce. Des expériences *in vitro* de sécrétion d'insuline, ont été menées et confrontées aux expériences *in silico*. Les résultats ont soulevé l'hypothèse que les îlots n'avaient pas une fonctionnalité optimale dans nos petits volumes de culture. La

même constatation a été faite concernant les myotubes, où la prise de glucose insuline dépendante a été démontrée en macro volumes, mais en micro volumes, la réponse observée (uniquement à concentration physiologique d'insuline) doit être reproduite avec des expériences plus robustes pour démontrer leur présence.

- Un capteur de glucose compatible avec le système microfluidique a été caractérisé lors d'expériences *in vitro* et *in silico*.
- Un multi-potentiostat a été développé dans la perspective de futures mesures électrochimiques multiples et intégrées.

Les bases et perspectives présentées ici permettront d'achever le MOsP îlot-muscle par de futurs travaux. La méthodologie peut aussi être réutilisée et étendue pour l'ajout de nouveaux organes (foie, adipocytes) complétant le MOsP, qui permettra de mieux comprendre les dérégulations intervenant dans le diabète de type 2.

Keywords : Multi-organe-sur-puce, Diabète, Ilots de Langerhans, Muscles squelettiques, Capteur enzymatique, Matrice de MicroElectrodes

Abstract

Over the past 4 decades, an intermediate model between the traditional *in vivo* and *in vitro* approaches has emerged: the MicroPhysiological Systems (MPS). MPS are designed to recapitulate different levels of human physiology, from the single organ to organs crosstalk. They upgrade the culture environment by patterning microstructures hosting 3D and multicellular architecture models and integrate microsensors monitoring cell activity and environment.

This new investigation tool is of interest in fundamental research on diseases such as diabetes. In this incurable disease, blood glucose regulation, resulting from a complex organs interplay between the pancreatic islets, the liver, the adipocytes and the muscles, is impaired. A Multi-Organ-on-a-Chip (MOoC) is a MPS that can recapitulate these organs crosstalk and represents a relevant model for diabetes research. Indeed, inter-organ regulations are not recapitulated by usual *in vitro* models, and deciphering these interactions requires multiple sensors, which is not ethically and technically possible *in vivo*. In the context of diabetes, MOoCs reproducing the islets to skeletal muscles communication do not exist so far, despite the importance of the skeletal muscles impact on blood glucose, under islets action.

In this thesis, we propose a methodology to design a MOoC deciphering islets to muscles interactions in blood glucose regulation. The MOoC objectives were to: (i) attain physiological insulin concentration secreted by islets in response to physiological glucose elevation, (ii) that induces a measurable glucose uptake by the muscle cells, (iii) monitor online relevant parameters. To that end, the investigations were conducted with an interdisciplinary approach, using and confronting results from both *in vitro* biological experiments and *in silico* modelling of biology and physics.

This manuscript details the methodology steps, delivering different designs for progressive validation toward a complete MOoC that comprises a microfluidic chip with cells and an online glucose sensor. During the MOoC construction, our main findings were the following:

- A co-culture medium and procedure for primary islets and LHCN-M2 myotubes were demonstrated.
- A common MicroElectrodes Array-based substrate was found suited for co-culture in a single microfluidic chip.
- Islets were cultured in microfluidic chips, and presented an insulin secretory response to glucose during fluidic experiments. Myotubes were successfully differentiated in microfluidic chips, and presented a measurable basal (insulin-independent) glucose uptake.
- An *in silico* and *in vitro* informed MOoC scaling strategy was developed and implemented. A simplified *in silico* islet model was developed to rapidly explore chip designs. Corresponding *in vitro* insulin secretion experiments were conducted and confronted to the *in silico* experiments. Results raised the hypothesis that islets function

was sub optimal when cultured in our low volume. Similar observation was made concerning myotubes scaling, where insulin-dependent glucose uptake was demonstrated in macro volumes experiments, but in micro volumes, the observed insulin response (only at physiological insulin concentration), has to be further repeated with improved experiments to explicitly demonstrate its presence.

- A glucose biosensor compatible with microfluidic was characterized under different injection protocols, using *in vitro* and *in silico* experiments.
- A multi-potentiostat was developed in the perspective of multiple and integrated electrochemical sensing in the MOoC.

From the grounds and perspectives presented in this thesis, future work can be conducted to further complete this islet-muscle MOoC. The methodology can be re-used and extended in the perspective of adding new organs (liver, adipocytes) in this MOoC in order to better address the interorgan crosstalk deregulations in type 2 diabetes pathophysiology.

Keywords: Multi-organ-on-chip, Diabetes, Islets of Langerhans, Skeletal muscles, Enzymatic sensor, MicroElectrodes Array

Thèse réalisée dans les laboratoires :

IMS
au sein du groupe
Technologies Innovantes Pour la Santé
Université de Bordeaux
CNRS UMR-5218 - Bordeaux INP
351 cours de la libération
33405 TALENCE Cedex
France

CBMN
au sein du groupe
Cell biology and Biosensors
Université de Bordeaux
CNRS UMR-5248
1 All. Geoffroy Saint-Hilaire
33600 PESSAC
France

Remerciements

Le travail présenté dans ce manuscrit est le fruit d'une compilation de méthodes, réflexions, stratégies, approches, expériences et interprétations provenant de différents domaines scientifiques. Ceci a été permis par de (très) nombreuses interactions, collaborations, échanges, parfois animés, avec des scientifiques de différents domaines et laboratoires.

Je remercie donc en premier lieu le laboratoire de l'Intégration du Matériau au Système (IMS) et l'institut de Chimie et Biologie des Membranes et Nanoobjets (CBMN), dirigés respectivement par Yann Deval puis Cristell Maneux, et Sophie Lecomte, qui m'ont accueillie.

Pour évaluer un tel travail, la constitution du jury ne fut pas simple, et je remercie naturellement les membres ayant accepté la lourde tâche de lire mon manuscrit pour l'évaluer. Je remercie tout particulièrement Christel Vanbesien et Thérèse Leblois pour la qualité de leur lecture, reflétée par la profondeur de leur analyse et la pertinence de leurs questions, donnant naissance à des rapports extrêmement détaillés. Je les remercie chaleureusement pour leurs retours extrêmement positifs, qui valorisent ce travail dont l'aspect tentaculaire donne un sentiment d'inachevé malgré de nombreuses avancées. Je remercie ensuite Karim Bouzakri, qui aura accepté le rôle d'examinateur, et qui l'aura endossé malgré la maladie le jour J. Je remercie ensuite Guillaume Wantz, le second examinateur, également président du jury, pour la fraîcheur apportée à cette soutenance. Je remercie enfin Brice Sorli et Antoine Pirog pour avoir accepté d'être membres invités, un grand merci pour leurs questions qui ont ouvert la discussion à des problématiques et perspectives qui n'ont pu être abordées pendant la soutenance.

Merci Antoine pour cette transition, car plus qu'un membre invité, tu accompagnais Sylvie et Matthieu dans la lourde tâche d'encadrer ce travail. Je vous remercie tous 3 pour les nombreux *points thèse* et donc pour le temps que vous m'avez accordé dans vos agendas si chargés. Vous m'avez donné bien sûr plus que du temps, me transmettant la philosophie de la recherche. Elle est nécessaire à la survie de tout chercheur face à l'inconnu, surtout quand il y a des cellules dans les environs de l'inconnu. Même s'il y eu de nombreux désaccords, nous avons toujours et jusqu'au bout réussi à converger pour arriver sans encombre au terme de mon voyage, plus que jamais enrichi de différents modes de pensées. J'espère que le voyage de DIAMOCHIP se poursuivra avec la même dynamique. Mais je n'en doute pas avec ta capacité, Matthieu, à remuer ciel et terre pour ton projet (comme l'ont démontré les derniers déboires administratifs). Le projet est entre de bonnes mains. Ce fut un réel plaisir de travailler avec vous, vous m'avez laissé m'épanouir dans mon projet, cherché à adoucir mon regard trop exigent sur mon travail. Merci Antoine pour ta bienveillance, cherchant toujours à aider autrui, même du travail jusqu'au cou. Enfin merci Sylvie, dont j'ai beaucoup appris sur la manière de faire sa place dans un univers très masculin et d'obtenir le respect sans jamais élever la voix. Merci pour les petites astuces transmises explicitement ou implicitement. Je m'appliquerai dans la suite de ma carrière à faire vivre ces principes, et j'espère bénéficier d'une carrière aussi remplie et épanouissante que la tienne, qui aura

toujours laissé de la place pour la vie de maman.

Je souhaite ensuite remercier les partenaires de l'Institut d'Electronique et des Systèmes de Montpellier, Benoît Charlot et Audrey Sebban-Pellicer, pour votre bonne humeur dans nos quelques réunions DIAMOCHIP, ainsi que votre imagination débordante concernant la microfabrication! Je remercie également Gilles Carnac de PhyMedExp pour ses conseils au tout début de l'aventure concernant les myotubes.

Côté laboratoires d'accueil, je remercie en premier lieu, au sein du CBMN, Flora Bouvet et Anthony Bouter pour leur initiation à la biologie cellulaire des myotubes, et leur précieuse aide dans mes expériences. Je remercie à nouveau Stéphane Arbault pour avoir accompagné mes premiers pas dans l'électrochimie, alors que la chimie aura toujours été pour moi une science obscure. Concernant l'équipe Lang, devenue Raoux en cours de route, je remercie bien sûr Julien et Alexandra qui ont eux aussi accompagné mes premiers pas en culture cellulaire. Certains moments resteront mémorables, provenant du léger choc culturel, induisant des comportements et questions qui étaient souvent loufoques pour vous. J'espère que vous aurez trouvé ça tout aussi enrichissant (et amusant) que moi. Je n'aurai déclenché l'alarme à CO2 du labo qu'une fois, *a priori* aucun incendie ou décès à déplorer, ça ne me paraît pas trop mal. Un grand merci à Pier qui m'aura aussi à l'occasion aidée avec Dorian. Enfin un merci à vous Jochen, j'ai pu constater l'apport immense des années sur un regard scientifique. J'espère atteindre un jour votre esprit critique 360°. Un grand merci également pour votre retour après ma soutenance, ces petites phrases qui marquent et qui permettent de sauter hors du nid avec confiance. De manière moins scientifique, merci d'avoir apporté un peu d'Est dans cet Ouest (vous étiez aussi content, je pense, quand au moins une personne avait compris « il faudrait putzer la microfluidique »).

Viennent ensuite mes fellows de l'open space, si nombreux sur ces 3 années. D'abord merci à Manon, Myriam, et Emilie de l'équipe Lang à l'époque, qui m'ont accompagnée dans mes premiers pas de la thèse. Mais celles de cette époque lointaine qui m'auront accompagnée jusqu'au bout de l'aventure sont Critsina, et Lua. Que de souvenirs sur ces 3 années, dans ou en dehors de l'open space. Vous aurez été là jusqu'au bout du bout, avec le chargement de ma camionnette mon dernier soir : le trio de début et de fin. Un merci particulier pour toi Lua qui a permis à l'open space d'être un endroit si convivial où il faisait bon venir le matin. Merci ensuite à toi Karen, la nouvelle ancienne, pour les moments chaleureux au labo et en dehors, cette gentillesse inouïe, ton exemplarité dans la qualité de tes expériences. Merci à toi Dorian le stagiaire, qui a toujours été bien plus, un vrai partenaire de ma thèse (GLUT 4ever), et un ami. Tu es un grand maintenant, avec ton propre projet de thèse, auquel je souhaite tout le succès possible. In the same register a giant thank you to you Eleftheria as intern (my favorite one, of course), but also as friend. Your good vibes during a hard season with unsatisfying experiments helped me a lot, and I was even happier when you came for my defense. I hope to remain your favourite supervisor ever, and prepare yourself to welcome me in Athens soon! Je remercie ensuite Alice et Léonie, mes successives voisines d'en face. Merci Alice pour tes conseils et ton écoute bienveillante de post-doc déjà passée par là. Ton regard aiguisé aura été d'un grand soutien. Merci à toi Léonie pour les papotes autour de tes « p'tits chats trop mignons », de la cuisine, et des loisirs créatifs. Toujours dans l'équipe Arbault, merci Samuel pour ta bonne humeur, les mots croisés du midi, et les magnifiques conseils d'escalade sur les appuis! Même si nous nous sommes vues en pointillées, merci Mélanie, notamment pour m'avoir fait découvrir ton second pays ! Merci enfin à Anouk et Romane, les dernières arrivantes de mon aventure à qui je souhaite tout le meilleur pour la suite. N'oublions pas les personnes que j'ai pu croiser dans l'open space : Yujie, Emilie, Pauline, Léna, Iyette, Noémie, Léa.

Pour la fin de l'open space, je garde Marie et Michel. Ton lunatisme Michele est inimitable, tout comme ta cuisine digne d'une Mama (un peu psychorigide, oui, ok, pas de saucisses dans la tarte ricotta épinards...) qui m'aura régalée. J'espère que je vous aurais régalés aussi avec mes recettes de fromages « pou-ants », et que ton nouveau tablier deviendra ton meilleur allié dans tes futures aventures culinaires. Et enfin merci est un euphémisme Marie, ta rare gentillesse, ton ouverture d'esprit et ta sincérité manqueront à mon quotidien. Je te remercie aussi professionnellement pour les petits tips qu'on ne pensait pas toujours à me dire mais qui étaient cruciaux, et aussi pour nos longues catharsis quand ça n'allait pas. J'espère avoir pu être là autant que tu l'as été pour moi. On n'en restera pas là !

Passons maintenant à l'IMS ! Je remercie mes voisins de bureau pendant l'écriture qui auront été un soutien quotidien dans cette période que vous connaissez si bien. Merci donc à Jean, Adrien, Noëlle, et plus récemment Florian qui a rejoint l'équipe de permanents. Je remercie également Romain et Jérémy, voisins de mon 3ème bureau) vos discussions techniques de hardware auront bercé ma rédaction. Merci ensuite à Gilles, le Père Castor du midi, qui racontait parfois des histoires et blagues pas pour les enfants. L'électrochimie fut bien plus sympathique à tes côtés. Merci ensuite à toi Jean-Luc, que j'associe à Gilles pour votre bonhomie, votre et sourire inébranlable qui m'ont réchauffé le cœur dans des moments de doute. Que d'énergie Jean-Luc, et longue vie aux apéros au port sur le rafio-bar de Lulu. Enfin merci à toi Yannick, je regrette déjà tes délicieuses gaufres et ton humour !

Je remercie ensuite « les biologistes » de l'étage, une espèce rare dans un laboratoire d'électronique. Vous êtes des oiseaux rares à plusieurs titres, et vous apportez un air exotique propice à arrondir les pensées anguleuses d'ingénieurs. Merci Yann d'animer ce petit monde, et certains midis, avec tes problèmes de riche comme tu dis ou tes super voyages qui hérissent le poil de Loïc. Merci également pour tes encouragements sur mon avenir, j'espère qu'ils s'avèreront exacts. Merci ensuite à toi Florence, tu es épatante, pouvant passer d'un restaurant chic du cap Ferret au labo à vider un rat de son sang, le tout toujours élégamment habillée. Ton sens pratique des manips de bio allant à l'efficacité et la rapidité aura été très enrichissant pour mon initiation à la biologie.

Je remercie enfin notre petit groupe de thésards. D'abord Anne et Lorenza, mes cothésardes de toujours. L'été de rédaction aura été bien plus sympa à stresser avec vous. Merci Anne pour les soirées jeux de société, switch, carressage de Biscuit, ou juste apéro, dans ton appartement du fin fond de la métropole bordelaise. Merci aussi pour les sorties Bistro Régent-cinéma, toujours avec Roland et Camille à l'avant-garde! Merci Roland, ou Biscotte, ou le Marseillais, pour toutes les petites discussions tissées de fous rires à ton bureau. Ton mot résume à merveille les 2 ans partagés, nos petites blagues, mais aussi ta personnalité blagueuse et sympathique derrière ce Bulgare baraqué, et enfin une maîtrise incontestable des jeux de mots (incroyable la façon dont tu as réussi à caser de façon diplomatiquement correcte le titre de mon morceau de piano préféré...). Je ne rigolerai plus jamais autant que tu as pu me faire rire, un grand merci. Je te souhaite de profiter du restant de ta thèse, et n'oublie pas d'être fier de ton travail. Je remercie ensuite Alexia et Loïc, qui auront muté de thésards à post-docs pendant ces 3 années, mais qui seront toujours restés les mêmes bons vivants à proposer des soirées au bar. Merci aussi Alexia pour avoir partagé cette expérience rare qui est la culture cellulaire quand on est ingénieur, ça rend perplexe parfois... et de partager les petits trucs qui marchent, trucs que tu as toujours su admirablement trouver. Merci Loïc pour ton sponsoring de Janco et EDF tempo le midi, j'ai peur de ne pas retrouver de « bobologue » aussi averti que toi. Les midis auront aussi été bien animés avec vous Rosa, Jana, Anabelle, Patricia, et plus récemment Mélissa Amélie et Emilie. Je vous souhaite à toutes de profiter de l'IMS et de la super équipe, car à peu près toutes vous avez vocation à rester. Un petit *ping* pour Emilie, déjà citée précédemment, qui m'aura

fait découvrir Bordeaux et son vignoble, et un fort bon caviste qui aura régalé les papilles de la famille. Tu as maintenant tout pour t'épanouir avec plus récemment un petit bout, plus qu'à entretenir le cocon et en profiter à fond. Je remercie ensuite Amandine, qui composa ma super team de stagiaires. Ce picomètre nous en aura fait voir de toutes les couleurs, et je suis ravie de t'avoir accompagnée dans tes premiers pas de l'électronique pour la biologie (même si tu es partie sur la RF ensuite...). Je remercie enfin Killian, ou Kiki, pour la visio de la défense, mais surtout de reprendre mon bébé. Il ne peut pas être entre de meilleures mains, et tu ne peux être entre de meilleures mains ou mieux entouré. Pas besoin de te dire bonne chance, plutôt profite bien. Je remercie enfin ceux qui auront croisé mon chemin pendant une courte durée, ou de manière plus occasionnelle : merci Charlie, Adrien, Mélodie, Clémence, et Pierre-Marie.

Pour la partie sciences, j'aimerais enfin remercier Nicolas Andreff. Un an avant de postuler pour la thèse, je ne savais ni ce que c'était réellement, ni pensais en être capable. Si ce travail existe, une des raisons premières est votre soutien et vos encouragements dans cette direction. Je vous remercie donc chaleureusement car l'expérience vaut d'être vécue, et elle oriente mon parcours professionnel dans une direction qui me plaît.

Je veux ensuite remercier ceux qui auront occupé mes soirées et weekends en dehors de mes super équipes. Merci d'abord aux latinos, Olivia, Andres, Stefi, Ilse, et les pas latinos Adrian Nico et Sébastien. Merci ensuite à Jérémy, Lamia, et Sophie, les « Z'izis » de Bordeaux. On n'était pas nombreux à représenter l'élite du dispositif médical made in Franche-Comté côté Ouest, je suis navrée de vous abandonner. En tout cas merci pour les soirées, à se rappeler le bon vieux temps, Besançon, les collègues partis en Suisse pour le plus grand bonheur du porte-monnaie, sans oublier la Qualité et le Réglementaire. Merci Lamia pour les petites virées ensemble, et mon baptême de bateau. Merci ensuite aux amis du lycée Justine, Nico, Alice et Eléanor, pour leur soutient notamment à nos retrouvailles de Noël. Merci Alice et Eléanor d'avoir assisté à ma soutenance (surtout toi Eléanor car tu as fait l'aller-retour entre 2 consultations !!). Enfin un immense merci à toi Denis, pour avoir pris soin de moi tout ce temps, même à distance. Ta capacité de travail tout comme ta capacité à te préserver psychologiquement sont admirables, et tu auras tout fait pour m'en transmettre les principes afin que la thèse se passe comme sur des roulettes. Je garde des kilos de photos et bons souvenirs, et j'espère prochainement planifier mon voyage en Equateur pour voir ton pays qui promet beaucoup.

Enfin je remercie ma famille, que j'ai eu peu l'occasion de voir ces 3 dernières années, mais qui aura toujours été une bulle d'évasion en dehors de la science et des technologies. Un remerciement tout particulier à ceux qui ont assisté à ma soutenance de bout en bout : Mamie et Dominique, Martine et Daniel, et enfin Isa. Merci Mamie aussi car c'est bien toi qui m'auras appris l'exigence du travail parfaitement réalisé ou rien du tout, à travers le tricot et broderie notamment. Et planter un tubing dans une entrée de puce microfluidique n'est pas si différent que de rentrer un fil dans un chas d'aiguille. Merci ensuite à toi Lia, ma première maîtresse devenue vraiment maîtresse, j'espère que tu es fière de ta première élève et piti sœur. En tout cas je suis fière de te voir t'épanouir dans l'éducation, et j'espère te voir un jour te confronter à l'exercice de la thèse dans ce domaine, car tu relèveras l'exercice avec brio. Merci Raphaël pour les délicieuses gougères, qui ne se seront pas vues mourir le jour du pot! Et enfin grand merci Mamounette, pour l'adulte que je suis devenue avec ton éducation, qui a pu réaliser tout ça. Merci de mettre du doux dans ma vie.

Ces quelques pages ne sont pas suffisantes pour exprimer à toutes le personnes mentionnées ma gratitude pour ces 3 années, années qui m'auront marquée avec tant de positif. Un dernier merci à tous avec toute la sincérité du monde pour ce que vous m'avez apporté, et apporté à ce travail.

Contents

List of Abbreviations

ADP	Adenosin Diphosphate
Ag/AgCl	Silver/Silver Chloride
Akt	Protein Kinase B
pAkt	Phosphorylated form of Akt
ATP	Adenosin Triphosphate
BSA	Bovine Serum Albumin
BST	Bio Sensor Technology
CAD	Computer-Assisted Design
CE	Counter Electrode
CK-MB	Creatin Kinase MB
CMRL	Connaught Medical Research Laboratories
DAPI	4,6-diamidino-2-phenylindole
DMEM	Dulbecco's Modified Eagle Medium
ECM	Extra Cellular Matrix
ELISA	Enzyme-Linked Immunosorbent Assay
EUROoCS	European Organ on Chip Society
FAD	Flavin Adenine Dinucleotide
FDA	Food and Drug Administration
GAPDH	Glyceraldehyde 3-phosphate dehydrogenase
GLP-1	Glucagon-like Peptide 1
GLUT	Glucose Transporter
GST-α	Glutathione Transferase
GSV	GLUT4 storage vesicle
GUA	Glucose Uptake Assay
H_2O_2	Hydrogen Peroxide
HAM's F10	Hamster F10
ID	Internal Diameter
IEQ	Islet Equivalency
IL-1β	Interleukin 1 β
IL-6	Interleukin 6
IMPSS	International MicroPhysiological Systems Society
IP-10	IFN-gamma-inducible protein 10
iPSC	Induced Pluripotent Stem Cell
IR	Insulin Receptor
KCL	Potassium Chloride
KMEM	Standard proliferation medium of LHCN-M2
KMEMdiff	Standard differentiation medium of LHCN-M2
LHCN-M2	Immortalized Human Skeletal Myoblasts Myogenic clone n°2
MCS	MultiChannel Systems
MEA	MicroElectrode Array
MED	Micro Electrode Devices

MEM-Eagle	Minimum Essential Media from Harry Eagle
MIN6	Mouse Insulinoma 6
MPS	Micro-Physiological Systems
MOoC	Multi-Organs on a Chip
2-NBDG	2-(N-(7-nitrobenz-2-oxa-1,3-diazol-4-yl)amino)-2-desoxyglucose
NIH	National Institute of Health
OD	Outer Diameter
OoC	Organ On a Chip
Op Amp	Operational Amplifier
ORCHID	Organ on Chip In Development
PBS	Phosphate Buffered Saline
PDMS	PolyDiMethylSiloxane
PEEK	Polyether Ether Ketone
PET	Polyethylene Terephthalate
PLA	Polylactic Acid
PMMA	Polymethyl methacrylate)
PP	Pancreatic Polypeptide
RE	Reference Electrode
RPMI	Roswell Park Memorial Institute Medium
RT-qPCR	Quantitative reverse transcription polymerase chain reaction
SiN	Silicon Nitrade
TNF-α	Tumor Necrosis Factor α
WE	Working Electrode

"Si l'on ne se préoccupait trop de l'achèvement des choses, on n'entreprendrait jamais rien"
"If we worried about the completion of things, we would never carry out anything"

François 1er, roi de France du XVI^{me} siècle,
à propos du château de Chambord

Introduction

Over the past 4 decades, the concept of bringing forward classic cell culture by combining microtechnics and bioengineering has emerged. The aim is to provide fundamental research and pharmaceutical industry intermediate models between the traditional *in vivo* and *in vitro* approaches, preserving the interest of each model while overcoming their respective drawbacks. This new generation of models emerging is called MicroPhysiological Systems (MPS). They are not relying on living organisms, thus they prevent ethical issues, and also try to limit costs that are associated to *in vivo* models. The cellular model and/or culture process in MPS is not as basic as in classical *in vitro* models. Indeed, the culture environment is upgraded using: microtechnics to pattern microstructures hosting the cellular/micro-organ models, as well as microsensors monitoring cell activity and/or their environment. The cellular model is also improved by recapitulating a 3D and multi-cellular architecture using bioengineering techniques such as scaffolds and bioprinting. The MPS are designed to recapitulate different levels of human physiology, from the single organ to physiological processes involving organs crosstalks. When the MPS focuses on the organ level it is called an Organ-on-a-chip (OoC), and from 2 organs it is called a Multi-Organ-on-a-Chip (MOoC).

The pharmaceutical industrialists find in MPS the perspective to limit the drug discovery failure rate, where a suboptimal translation of *in vitro* and animal *in vivo* results to human is incriminated. These systems are also particularly of interest fundamental research on diseases like diabetes where complex organs interplay is involved: inter-organ regulations cannot be accurately recapitulated by *in vitro* model, and deciphering these interactions requires multiple sensors monitoring cellular activity, which is not possible with *in vivo* model for ethical and technical reasons.

Diabetes is an incurable disease linked to an impaired blood glucose regulation (also called glucose homeostasis) and leading to various complications such as cardiovascular diseases or blindness. The prevalence of diabetes has dramatically increased according to reports, and projections foresee a persistent dynamic in the next decades. This disease is the focus of numerous clinical and fundamental investigations, to understand the underlying processes and/or to develop innovative therapies. The current MPS systems in the context of diabetes are generally focusing on the 4 main organs interacting to regulate the blood glucose concentration: the pancreas (through the action of embedded micro-organs, named the islets of Langerhans), the liver, the adipocytes and the muscles. The diabetes-related literature is composed of OoCs but few MOoCs were proposed up to now to emulate organs interactions between 2 or 3 organs. Interestingly, despite the fact that skeletal muscles constitute the main organ reducing blood glucose concentration under the islets action, MOoCs reproducing islets to skeletal muscles communications has no precedent in scientific literature.

In this context, this thesis proposes a methodology to design a MOoC targeting to decipher islets to skeletal muscles interactions in glucose homeostasis. More precisely, the objectives were to:

- attain a physiological insulin concentration secreted by islets in response to physiological glucose elevation,
- induce a measurable glucose uptake by the muscles model,
- and monitor online relevant physiological parameters.

The investigations were conducted with a interdisciplinary approach, using and confronting results from both *in vitro* biological experiments and *in silico* modeling with multiphysics simulation.

This interdisciplinary work and investigation method were allowed by facilities coming from the 2 host laboratories: the IMS and CBMN, in 2 teams respectively involved in microelectronics for biology (from stimulation to signal acquisition and processing), and islets biology and diabetes research. The two involved teams, *Technologie pour la santé* and *Cell biology and Biosensors*, collaborate since 2008. The development of such new biotehnological tool to investigate diabetes is the beginning of a new collaborating project. This PhD thesis had been funded by a grant awarded by the University of Bordeaux for this interdisciplinary collaboration.

This PhD thesis is the first step to the development of a future 4-organ MOoC, which would represent a new powerful investigation tool to decipher blood glucose deregulation leading to diabetes and to screen pharmacological compounds for future therapies.

The work reported in this PhD thesis is organized as follows. In the first chapter, the scientific context and the elementary notions necessary to understand the interdisciplinary work will be presented. The second chapter presents how the cell culture requirements of the different cell types constrained the design (i.e the cells adhesion and the co-culture). The third chapter establishes and implements a scaling methodology for the MOoC. Finally, the fourth chapter reports the integration of a glucose sensor for real-time monitoring.

Chapter 1

Scientific context and preliminary notions

1.1 Glucose homeostasis: physiology and pathophysiology

1.1.1 Glucose homeostasis

In human metabolism, several physical constants (e.g. temperature, pH, osmolarity) and concentration of chemicals must be kept in a precise and narrow range of values for survival, and to permit an optimal metabolism and cells/organs function. The molecule of interest in this thesis work is the glucose, whose concentration in blood must remain for human in the narrow range of 3.9-7.8 mM[1][Leal et al., 2021]. In order to achieve this regulation of blood glucose, human physiology possesses a complex and multi-organ process, called the ***glucose homeostasis***.

The main organs involved in glucose homeostasis are [Röder et al., 2016][Gerich, 2010]: the pancreas, the liver, the adipose tissue (fat), the skeletal muscles, the nervous system, the gut and the kidney. The *pancreas*[2] acts at the center of this complex system by detecting the blood glucose level, and secreting *insulin* and *glucagon*, the 2 main hormones of glucose homeostasis. In case of hyperglycaemia (*i.e.* a blood glucose higher than the normal range), insulin is secreted by the pancreas. Upon the insulin action, the *liver*, *adipose tissue*, and *muscles* uptake glucose from the blood and/or stop to produce and release glucose in order to rapidly decrease the circulating concentration. On the contrary, upon glucagon action, the *liver* produces glucose to increase the circulating concentration. The liver is the first organ in contact with these hormones, which act more distally on muscles and adipocytes. These relationships are illustrated in Fig. 1.1.

Glucose is not the only molecule modulating insulin and glucagon secretion. Other nutrients, namely amino-acids and lipids, also influence their secretion. In addition, many other hormones and neuromediators secreted by the above mentioned organs and by the *pancreas* itself regulate finely the glycaemia. For example, somatostatin is a well-known inhibitor of insulin and glucagon secretion. Inspired from [Röder et al., 2016], a non exhaustive map of hormonal/neurohormonal interactions is presented in Fig. 1.2. Indeed, the map from [Röder et al., 2016] is not exhaustive as muscles secrete other myokines than IL-6, such as TNF-α, IL-1β, IP-10 for example [Langlois et al., 2022]. The complexity of the map comes also from many not elucidated actions: some pancreatic hormones listed on the figure, such as the pancreatic polypeptide, have a not fully defined action on glucose homeostasis; or

[1] mM stands for mmol/l, a common concentration unit in biology
[2] More precisely the endocrine pancreas, notion introduced later

IL-6 exact role and action on pancreas is not yet clarified [Ellingsgaard et al., 2008][Suzuki et al., 2011].

Therefore, glucose homeostasis is a very complex process controlled by a system of organs interacting through multiple hormones [Chandra and Liddle, 2009].

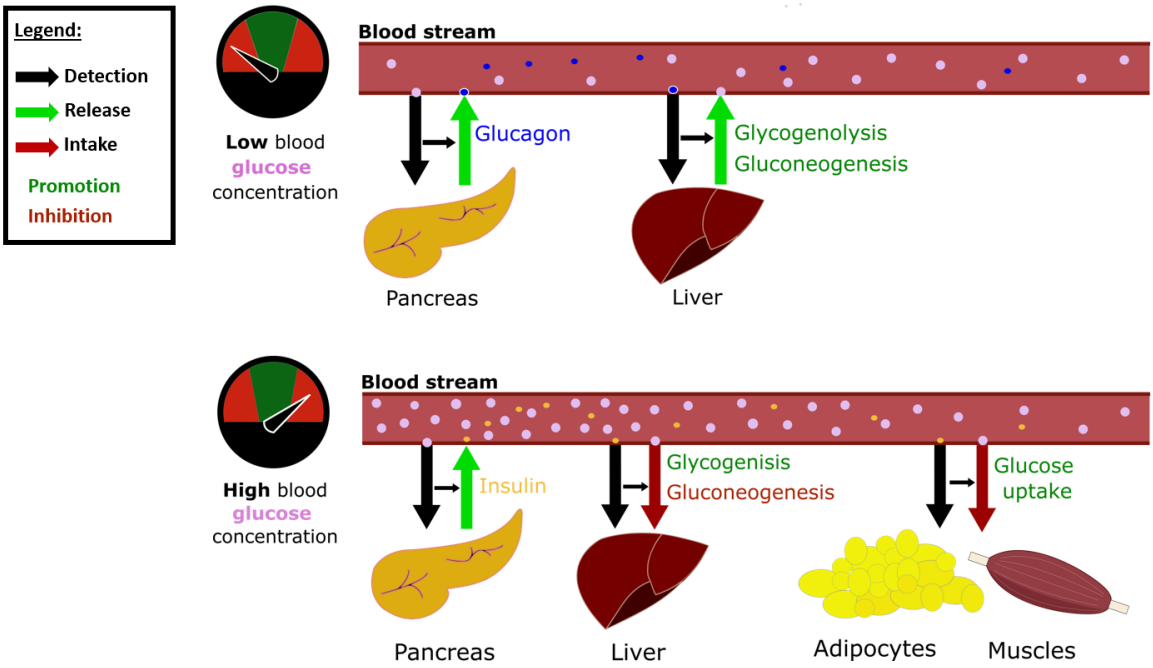

FIGURE 1.1: Glycaemia regulation, involving interactions between the pancreas, the liver, the muscles and the adipose tissue.

1.1.2 Pancreas-muscles axis in glucose homeostasis

1.1.2.1 Pancreas and pancreatic islets

Pancreas The pancreas plays a key role in the regulation of nutrients digestion and energy homeostasis through the release of *digestive enzymes* and *hormones* as previously mentionned (insulin and glucagon notably) [Röder et al., 2016]. The pancreas is composed of an exocrine part, secreting the digestive enzymes into the bile duct to reach the gut, and the endocrine pancreas, secreting the pancreatic hormones like insulin and glucagon, directly into the blood stream. In this work we focus on the endocrine pancreas, as we previously saw the major role of pancreatic hormones in glucose homeostasis.

Islets: the pancreatic micro-organs involved in glucose homeostasis The endocrine pancreas is composed of micro-organs, the islets, that are surrounded by the exocrine pancreas. They represent only 1-2% of the total pancreatic mass. They were discovered in 1869 by Paul Langerhans [Hoffmann and Langerhans, 1869], and therefore were named the *islets of Langerhans*. Mice have about 1,100 pancreatic islets, while human have >1 million of islets [Rorsman and Ashcroft, 2018]. Their role is to secrete the main hormones regulating the

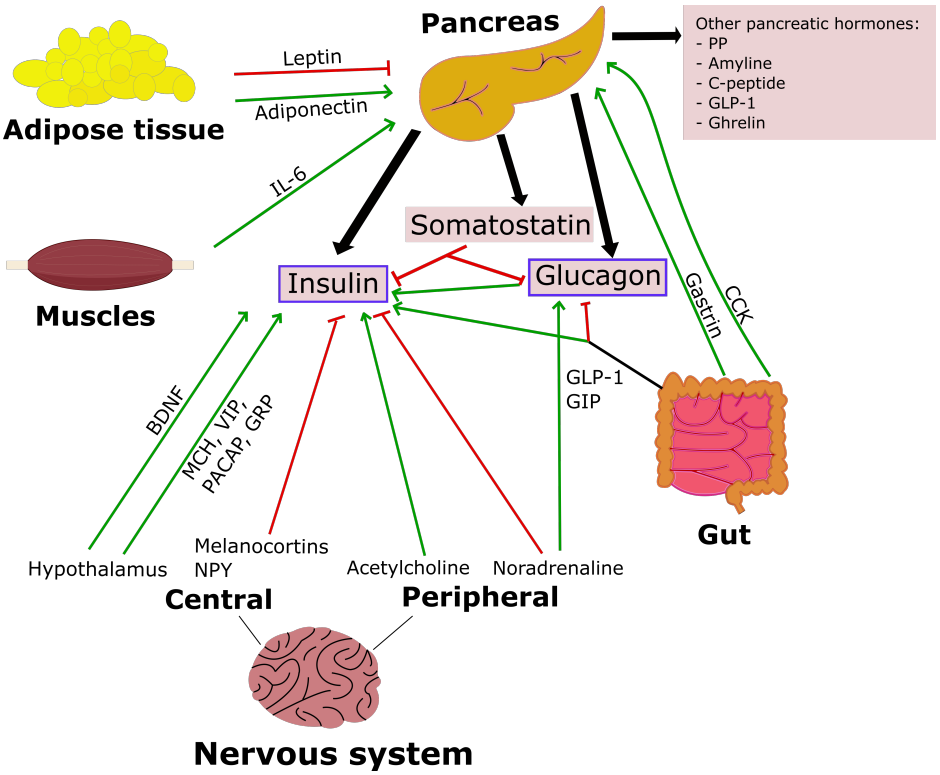

FIGURE 1.2: Some hormonal and neurohormonal interactions between the main organs involved in glucose homeostasis, inspired from [Röder et al., 2016]. The pancreatic hormones have a pink background (non-exhaustive list), and the 2 main hormones for glucose homeostasis have a purple frame. The hormones regulating directly the secretion have arrows and straights toward the pancreatic hormones concerned; and hormones regulating indirectly, or in a not elucidated way, have arrows toward the pancreas. BNDF, Brain-Derived Neurotrophic Factor; CCK, CholeCystokinin; GIP, Glucose-dependent Insulinotropic Peptide; GLP-1, Glucagon-Like Peptide 1; GRP, Gastrin-Releasing Peptide; IL-6, Interleukin 6; MCH, Melanin Concentrating Hormone; NPY, Neuropeptide Y; PACAP, Pituitary Adenylate Cyclase-Activating Polypeptide; POMC, Pro-opiomelanocortin; PP, Pancreatic Polypeptide; VIP, Vasoactive Intestinal Peptide.

glycaemia, (Fig. 1.2), but also regulating nutrient homeostasis since islets are also involved in amino-acids and lipids metabolisms.

The diversity of hormones secreted comes from the diversity of cells composing an islet: this micro-organ is an aggregate of different cell types. The proportion of each cell type in an islet differs depending on the species and localisation within the pancreas. Still, the predominant islet cell type are amylin-, C-peptide- and insulin-secreting β-cells (50% in humans, 75% in mice), glucagon- and GLP1-releasing α-cells (35-40% in humans, 15-20% in mice) and somatostatin-secreting δ-cells (10% in humans, 5% in mice). There are also minor cell types: the pancreatic polypeptide (PP)-producing γ-cells, and the ghrelin-producing ϵ-cells, which represent less than 1% of the total [Röder et al., 2016][Aamodt and Powers, 2017]. The islets include of other cell types such as macrophages, and are connected to nervous system and blood stream by numerous capillaries passing through islets. A schematic composition of an islet and its micro-environment is represented in Fig. 1.3.

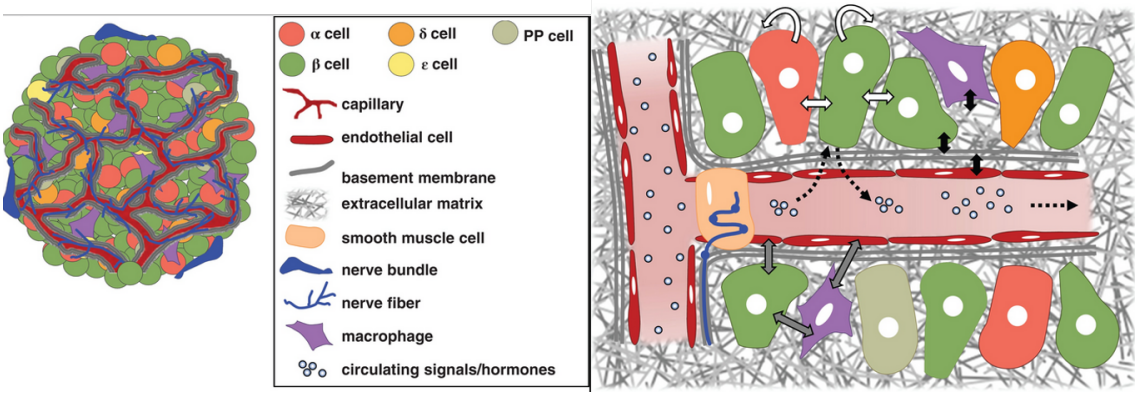

FIGURE 1.3: Islets composition, micro-environment, and different kind of interactions: endocrine cell response to circulating signals (dashed arrows); intra-endocrine signaling (white arrows); multi-cellular interactions, with all cell types (gray arrows); cell to extracellular matrix interaction (black arrows). From [Aamodt and Powers, 2017].

Islets and Micro-Electrode Arrays Cells within a tissue interact together and with their environment by receptors at cell's surface, or via molecules circulating in the extracellular and the intracellular media, as represented by the different arrows in Fig. 1.3.

In the case of glucose, the cells express at their membrane GLUcose Transporters (GLUTs) for a facilitated transport of glucose in the intracellular compartment [Navale and Paranjape, 2016]. Some GLUTs are ubiquitous isoforms, that are present in all tissues, to provide energy needed by the cells. Other isoforms such as GLUT 2 and 4, are more specifically involved in glycaemia regulation. GLUT 4 is expressed by skeletal muscle cells and will be detailed in section 1.1.2.2. Concerning **mouse** islets, GLUT 2 is responsible, in the insulin-secreting β cells, of quick equilibrium between the extracellular and intracellular concentrations of glucose [Thorens, 2015]. This permits β cells to quickly start insulin secretion in response to hyperglycaemia. In brief, *glucose is metabolised by β cells*, which *generate energy molecules*, namely Adenosine TriPhosphate (ATP). The increase of ATP in the intracellular medium increases the ATP/ADP ratio [3], *that then triggers ionic fluxes across the membrane* through specific ion channels opening or closing, thus producing *variations of the membrane potential*. The final result is the *exocytosis* which is the fusion of insulin-containing vesicles with the plasma membrane, so that *insulin is released by the β cell* [Lang, 1999].

Thus a pivotal part of the islets metabolism relies on ionic currents, which generate detectable electrical signals. The recording and analysis of such signals is called *Electrophysiology*. To measure these signals over time, different technologies have been developed [Spanu, Martines, and Bonfiglio, 2021]: *intracellular sharp microelectrodes* (Patch Clamp), *MicroElectrodes Array* (MEA) and *Transistors* (like *Organic ElectroChemical Transistors*, *Ion Sensitive Field-Effect Transistor*). These signals can be studied to better understand the endogenous "algorithms" governing islets function. Recently, the biologists and electronic engineering teams at CBMN and IMS have jointly demonstrated that insulin secretion by C57Bl6J mouse islets is strongly correlated with their electrical activity measured by MEA [Jaffredo et al., 2021]. As we intended to exploit electrical signals to monitor the islets activity in our project, we included the MEA technology in our specifications.

MEAs are fabricated using clean room microtechnologies to deposit patterns of electrodes, tracks and pads on a glass substrate. The material for the electrodes is selected

[3] ADP are the molecules of ATP that provided their phosphate group to supply energy

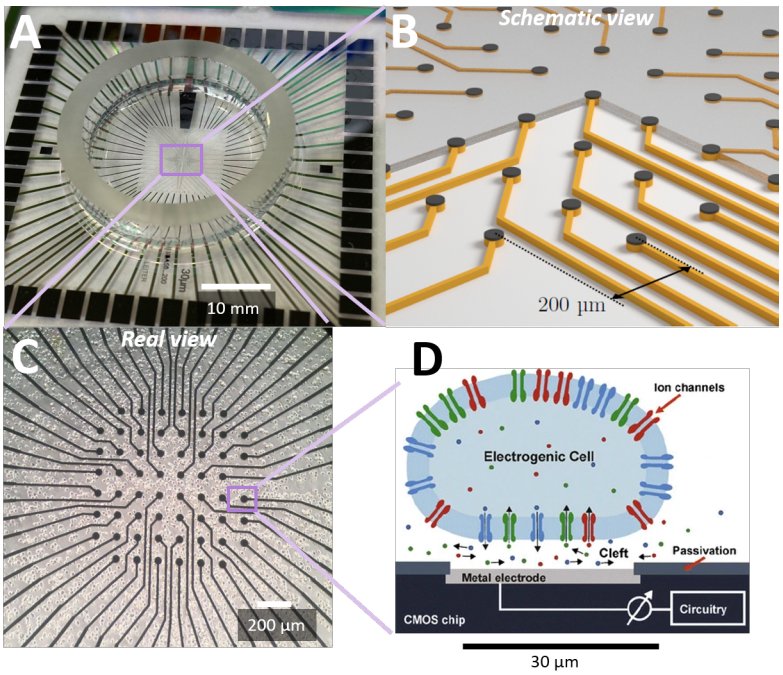

FIGURE 1.4: Presentation of the MicroElectrodes Array. (A) Macro-view of a MEA, with the bonded ring to hold the cell culture medium. (B) Schematic representation of the layers constitutive of a MEA, from [Chen et al., 2007]. (C) Zoom on the electrode area with cells. (D) Zoom at the cell and electrode level: schematic representation of a cell with ionic exchanges between intra- and extra- cellular media through ion channels. The electrode below the cell detects field potentials related to the electrical activity of the cell. From [Jones et al., 2011].

to provide the best signal-to-noise ratio, or possibly for its physical properties like transparency (like Indium Tin Oxide). A passivation layer is deposited to isolate the tracks and let free only the electrodes (in contact with the cells) and the pads (in contact with the pins of the signal acquisition system). Fig. 1.4 shows different views of a MEA. An acquisition setup is necessary to process (amplify, filter) and record the signals. In our framework we use the preamplifyier MEA1060-BC-PA from Multi Channel Systems (MCS) (illustrated in Fig. 1.5) and a computer with the MC_card to digitize and acquire the signal.

β cells and insulin secretion kinetics When β cells detect hyperglycaemia, the metabolism described above increases, leading in 1 to 2 min to insulin secretion. The secretion profile has a particular shape with two phases: the first phase (5-15 min) with a peak of secretion followed by a decrease called the *Nadir*, and a second phase which is an "oscillating plateau" [Nunemaker et al., 2006], until normoglycaemia.

Each phase of this biphasic secretion targets different organs [Nunemaker et al., 2006]. The higher secretion during the first phase saturates the liver (2/3 of the insulin released by the pancreas is kept by the liver). The production of glucose by the liver is then rapidly stopped, in parallel to glucose uptake starts. The second phase acts mainly on distal organs such as muscles and adipocytes. The oscillations of the second phase limits the β cells exhaustion and the insulin resistance of the targeted organs. In [Alcazar and Buchwald, 2019], insulin secretion by C57Bl6J islets was measured upon different glucose concentrations. The insulin kinetics contain the first phase, the Nadir, and the second phase (Fig. 1.6).

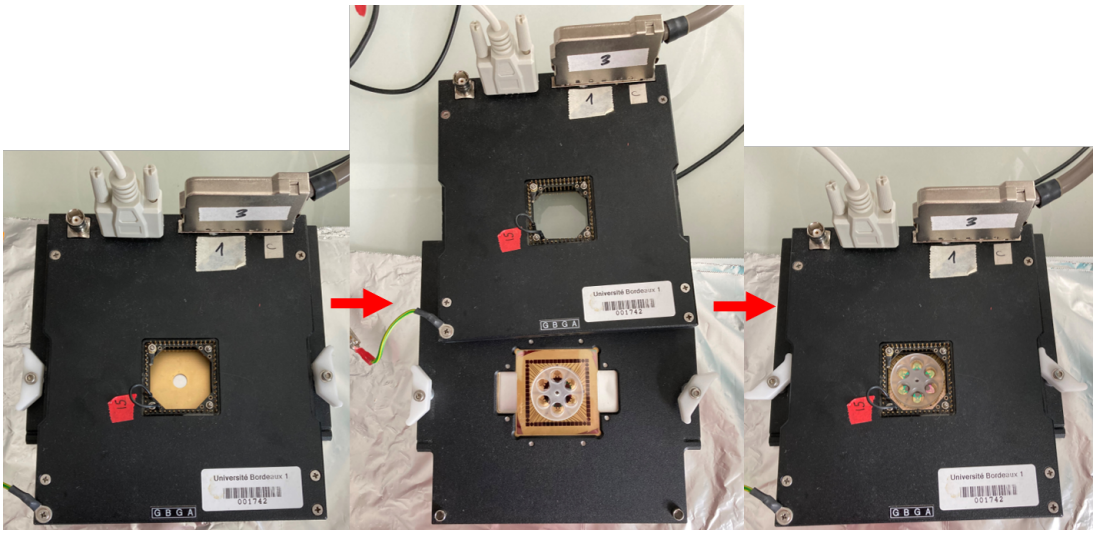

FIGURE 1.5: The preamplification system from MCS: stand-alone, opened to place a MEA, closed with the MEA.

1.1.2.2 Skeletal muscles

Anatomical introduction According to [Noto, Leavitt, and Edens, 2023], human muscles are categorized in three families: **skeletal** and **cardiac** (both included in a larger category named striated muscles), and **smooth** muscles. The function and physiology of each category is different. While skeletal muscles are involved in voluntary movements, smooth muscles are present throughout the gastrointestinal, reproductive, urinary, vascular, and respiratory systems, for involuntary movement. Finally cardiac muscles encompass the heart.

The skeletal muscles are the most important in terms of mass, representing 40% of total body weight [Frontera and Ochala, 2015]. This thesis work focuses on skeletal muscles as it is the main contributor to glucose uptake [Sylow et al., 2021].

Skeletal muscles are composed of fibers called *fascicles*, which themselves are composed of smaller fibers, the *myofibers* (also referred as *muscles fibers*, *muscle cells* or *myocytes*), as illustrated in Fig 1.7 (A.a). The myofibers are cells of usually of 100 µm width and 1 cm length [Frontera and Ochala, 2015].

The Fig. 1.8 shows a detailed composition of a fascicle, constituted of myofibers, surrounded by capillaries bringing nutrients, and nerve endings. In addition, immune cells, fibroblasts and satellite cells are found in a fascicle. Satellite cells are the adult stem cells of skeletal muscles. When activated by myogenic factors, they proliferate and differentiate into new muscle fibers. Thus they contribute to muscle growth, repair, and regeneration [Frontera and Ochala, 2015].

Myofiber/muscle fibers composition Myofibers are particular ***cells*** with a well structured organisation [Sylow et al., 2021]. Myofibers are composed of multitude of contractile units, the myofibrils (see Fig. 1.7 (A.b)). It is estimated that each muscle fiber is made of thousands of myofibrils [Frontera and Ochala, 2015].

These myofibrils are repetitions of a small protein network called the *sarcomere*. Two categories of protein assemblies compose the sarcomere: the thin and thick filaments (see Fig. 1.7 (A.c)). The relative movement of these 2 types of filaments generate the contraction and the movement. The proteins constituting the filaments include the *myosin*, *actin*,

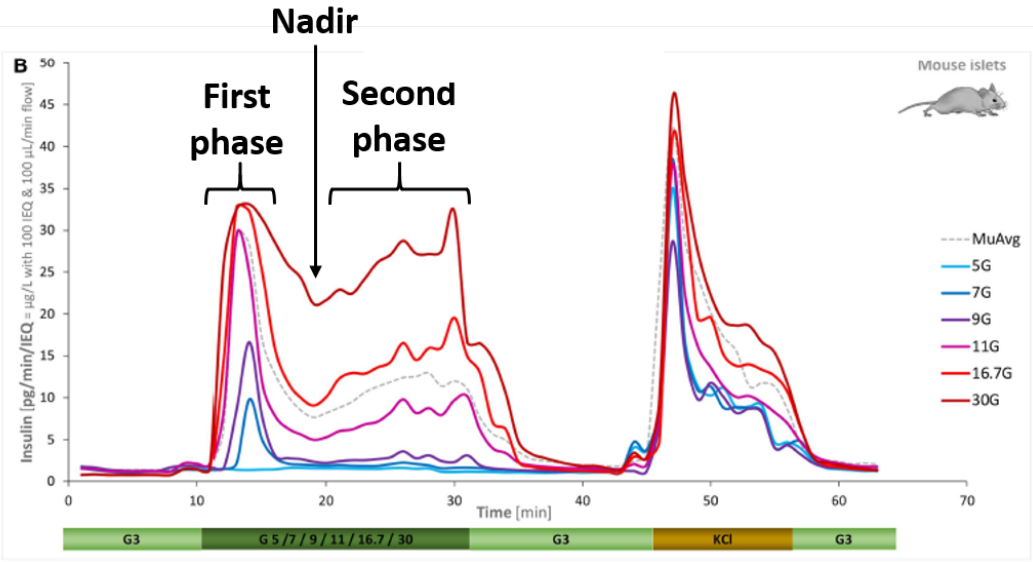

FIGURE 1.6: Insulin secretion kinetics measured in islets from C57Bl6J mice upon different glucose stimulations, adapted from [Alcazar and Buchwald, 2019]. Original caption: "Concentration dependence of insulin secretion in murine islets. Summary of experimental data for murine islets perifused using standard equipment and parallel stepwise incoming glucose stimulations (3 mM → 5/7/9/11/16.7/30 mM → 3 mM as indicated; plus 10 min KCl and 10 min low; corrected to ~100 IEQ per chamber; n = 3–12 per group). Averages of all data obtained in our labs for the G3 → G11 protocol are included as dashed gray lines for reference."

troponins, *tropomyosin*. The proteins binding the filaments, and appearing as a *Z lines* on electron microscope images, are made of *α-actinin*.

Myogenesis In adult muscles, myoblasts are produced from satellite cells. They then fuse and differentiate into myotubes (see Fig. 1.7 (B)). Myotubes keep on growing by fusion and the sarcomeric organization gets structured, until forming large well striated myofibers in which nuclei are at the periphery [Lauritzen and Schertzer, 2010][Toral-Ojeda et al., 2018][Fernández-Costa et al., 2021]. The myofibers are thus ***polynucleated cells***, comprising up to several thousand of nuclei [Sylow et al., 2021]. The differentiation steps are illustrated in Fig. 1.7 (B), with the transcription factors driving each step. The transcription factors are proteins regulating the production of specific proteins, by turning-on/off, increasing/decreasing their production from DNA. In a more general point of view, this orchestration of protein production by transcription factors regulates the cell metabolism, proliferation, differentiation and death [Lambert et al., 2018].

In vitro, skeletal muscle cell differentiation is a complex and not fully understood process. The current 2D and 3D cultures do not succeed yet to fully mature into myofibers but rather the intermediate myotubes state, as *in vitro* culture does not recapitulate the complex *in vivo* environment including neural innervation, presence of endogenous hormonal factors and mechanical stimulations [Lauritzen and Schertzer, 2010][Sylow et al., 2021][Rogal et al., 2019].

Therefore in *in vitro* culture it is important to assess the level of maturity of myotubes.

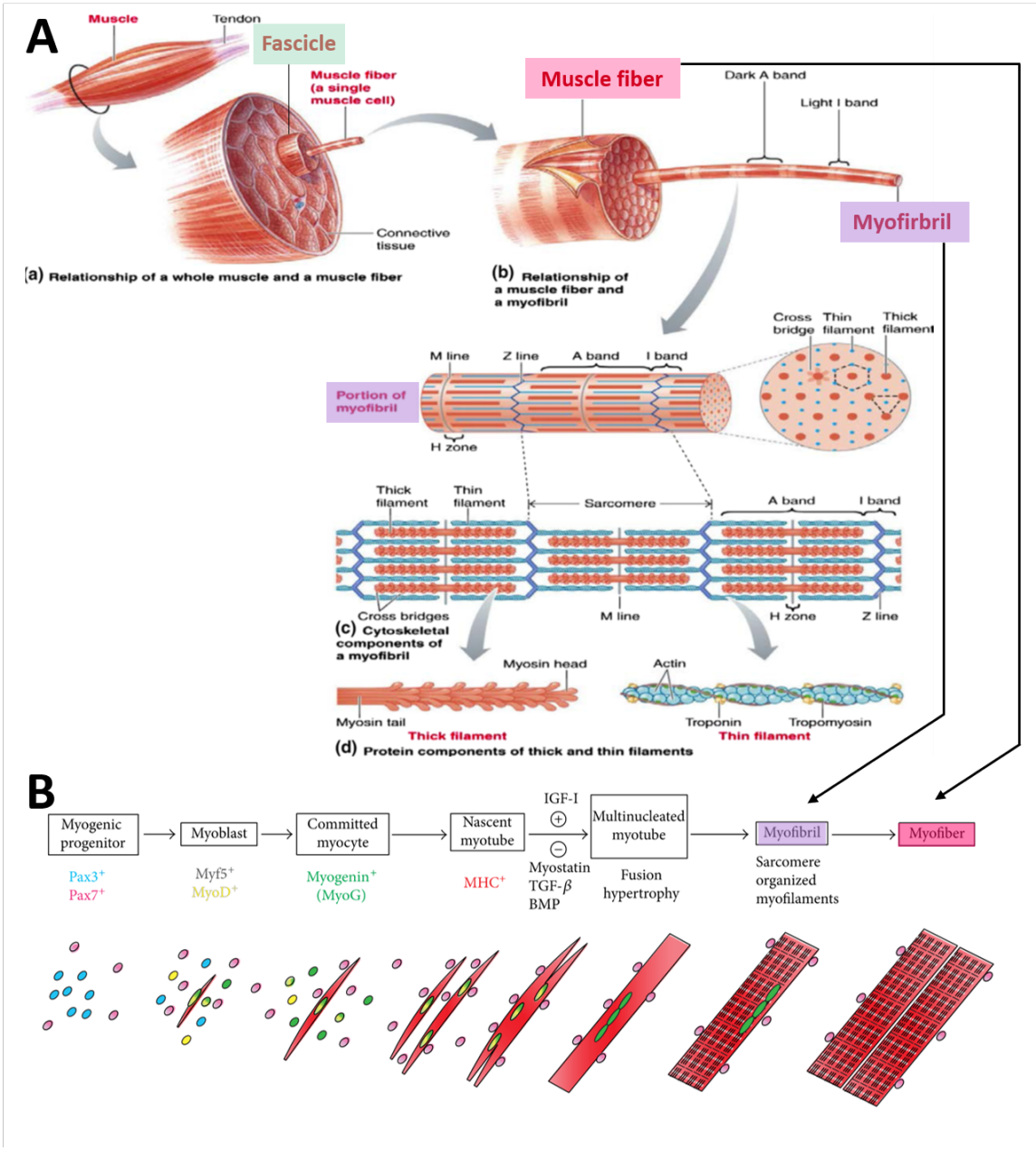

FIGURE 1.7: (A) Anatomical structure of a muscle, from [Frontera and Ochala, 2015]. (B) The differentiation of myoblasts into myofibers, with the transcription factors involved in each step, from [Jiwlawat et al., 2018]. BMP, Bone Morphogenetic Protein; IGF-I, Insulin-like Growth Factor-I; MHC+, Myosin Heavy Chain; Myf, Myogenic factor; MyoD, Myoblast determination protein; MyoG, Myogenin; Pax, Paired box transcription factor; TGF-β, Transforming Growth Factor-β

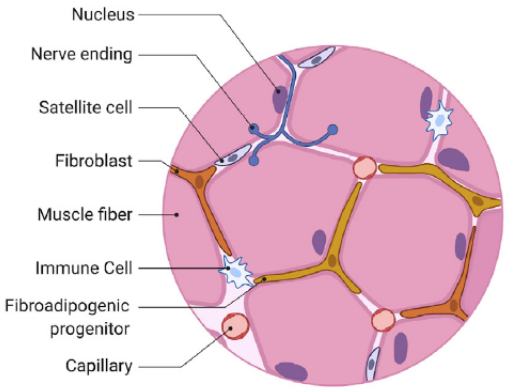

FIGURE 1.8: Diversity of the cellular composition and its distribution in a fascicle, from [Sylow et al., 2021].

To do so, the expression of specific proteins and their organisation can be observed by immunostaining: Troponin-T and α-actinin reveal the presence of sarcomeres, and the striated organisation reveals the level of maturity toward myofibrils (see Fig. 1.7 (A.c)).

Myofibers and glucose homeostasis Myofibers, or muscle cells, detect insulin when this hormone binds specific receptors at the plasma membrane, which triggers a signalling pathway leading to the translocation of vesicles containing GLUT 4 toward the plasma membrane. These vesicles fuse with the membrane, thus integrating the glucose transporter in it. This process increases the glucose uptake by muscle cells, as illustrated in the overview of the metabolic pathways presented in Fig. 1.9a.

Fig. 1.9b shows the complexity of the mechanisms in more details. The translocation of GLUT4 is actually a permanent process but with a short lifetime; at steady state (without insulin), GLUT4 are located mainly on vesicles inside the cell rather than at the plasma membrane. When insulin binds to its receptor, cascades of phosphorylation occur on different molecules to *increase* the translocation of GLUT4 to the membrane [Sylow et al., 2021]. One pivotal step in this cascade is the phosphorylation of *Akt*, also known as Protein kinase B. The ratio of phosphorylated Akt (pAkt) on unphosphorylated Akt increases in myotubes/myofibers upon insulin. The quantification of the increase of this ratio represents a classical method of validation of myotube functional maturity. We focus on this part of the metabolic pathway, as this characterization method was used in section 2.1.3.5.

1.1.3 Diabetes, the main disorder related to glucose homeostasis deregulation

The complex organs interactions ensuring glucose homeostasis can be disturbed at different levels and for different reasons related to genetic and environmental factors. This group of pathologies is named *diabetes*, which is a "group of metabolic diseases characterised by hyperglycaemia resulting from defects in the secretion or action of insulin, or both combined" (according to the American Diabetes Association [American Diabetes Association, 2013]).

The 2 main types (amongst 4 [Artasensi et al., 2020]) of diabetes [American Diabetes Association, 2013] are:

- Type I diabetes (T1D) results from the auto-immune destruction of β cells, and induces a defect in insulin. T1D represents 10% of the diabetes cases.

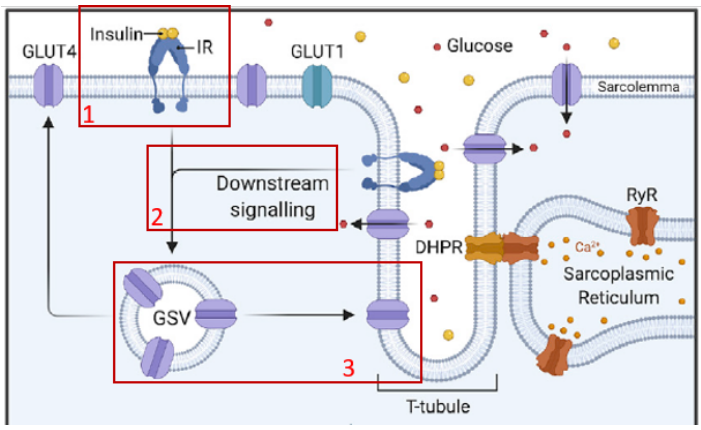

(A) Overview of GLUT 4 translocation in response to insulin. 1) Insulin binds to its receptor (IR), 2) metabolic cascade, 3) GLUT 4, expressed on vesicles (GSV), translocates at the membrane. This increases the glucose uptake capabilities of the myofiber. From [Sylow et al., 2021].

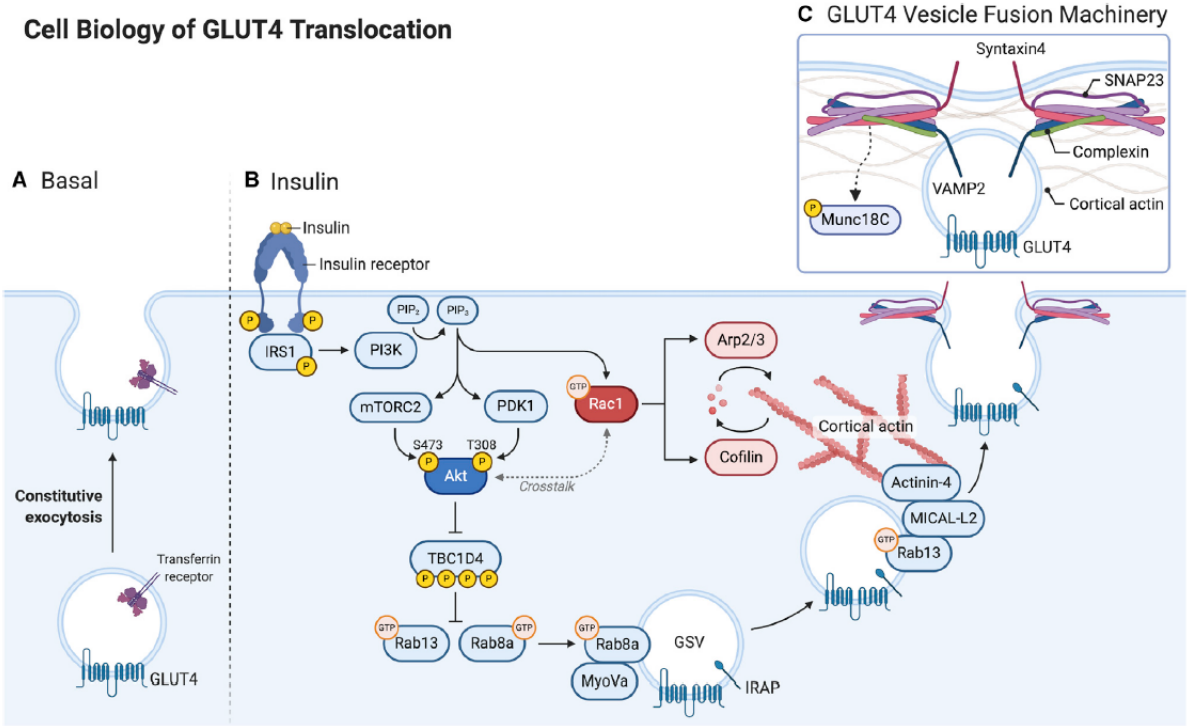

(B) Detailed signalling pathway involved in GLUT 4 translocation in response to insulin. Note the presence in this cascade of the pivotal step of Akt phosphorylation. Adapted from [Sylow et al., 2021].

FIGURE 1.9: Quick and detailed overviews of metabolic cascade leading to GLUT4 translocation.

- Type II diabetes (T2D) is the most widespread type, characterized by a defect in insulin secretion from β cells and an insulin resistance of the targeted tissues: insulin is no longer able to decrease glucose production by the liver and to increase glucose uptake by muscles and adipose tissue. T2D involves complex interplay between genetic and environmental factors. [Barroso and McCarthy, 2019]

The boundary between these 2 types of diabetes becomes more and more blurred with underlying processes appearing more and more complex [Balasubramanyam, 2021].

1.1.4 Diabetes, a worldwide public health issue

Hyperglycemia phases are characteristic in diabetes and lead to dramatic complications at macrovascular and microvascular level, resulting in cardiovascular diseases, or kidney, retina and nervous affections. The complications of T2D are very common and can lead to the full failure of these organs: for instance, the main origin of blindness is actually diabetes [American Diabetes Association, 2013].

The main risk factors and origins of T2D are the lack of physical exercise and unhealthy diet, and the related obesity. In developed or developing countries, the increasing incidence of obesity and the population ageing (but also better survival of people and better diagnosis) lead to a worrying increase of diabetes incidence [Zheng, Ley, and Hu, 2018]. Over the world, diabetes incidence has been estimated to 285 million people in 2009, 382 million in 2013, 425 million in 2017, and recently 529 million in 2021 [Ong et al., 2023]. T1D is also rising for unknown reasons [Ong et al., 2023], which leads to consider diabetes as an epidemic [Zheng, Ley, and Hu, 2018]. By 2050, it is expected that more than 1.31 billion (1.22–1.39 with 95% uncertainty interval) will suffer from diabetes [Ong et al., 2023].

Although China and India are the 2 main epidemic centers so far [Zheng, Ley, and Hu, 2018], the recent projections of 2023 show the emergence of new countries with a quickly increasing prevalence of diabetes in 2 super regions: *north Africa and Middle East* and *Latin America and Caribbean* [Ong et al., 2023].

Unfortunately no cure exists so far to counteract this epidemic. The treatment of T1D involves rigorous life management, the administration of insulin and self-monitoring of patients blood glucose levels. For T2D, the first medication is the lifestyle improvement, including weight loss, increase of physical activity and respect of a healthy diet [Zheng, Ley, and Hu, 2018]. In addition, pharmacological medications can be prescribed [Artasensi et al., 2020]: drugs either stimulating insulin secretion (secretagogues) or glucose disposal (non secretagogues). The latters mainly rely on decreasing liver gluconeogenesis (metabolic pathway producing glucose), improving insulin sensitivity and increasing GLP-1 secretion from the gut. Interestingly, the exact operating mode of this type of drug is not yet fully clarified.

Diabetes is therefore a complex pathology becoming a worldwide health issue and requiring new tools to investigate its underlying processes.

(A) Main culture substrates used for cell culture, from Corning supplier website.

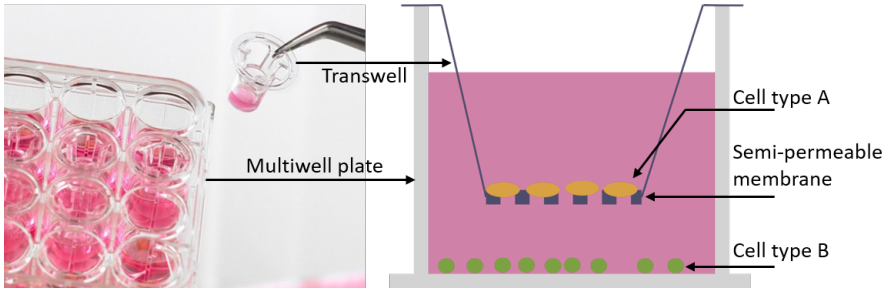

(B) The transwell system to study cell crosstalk in traditional cell culture. Left: real view (from Corning website), right: schematic representation with cells.

FIGURE 1.10: Presentation of the main culture supports in the traditional static and 2D cell culture.

1.2 Microphysiological systems

1.2.1 An emerging need

The traditional 2D *in vitro* culture, or more commonly called *cell culture*, appeared one century ago, causing some scepticism at the time [K. Young and J. Beebe, 2010][Segeritz and Vallier, 2017]. Indeed, 2D *in vitro* culture consists in maintaining cells or biological tissues outside a living organism. Biological materials are usually placed in transparent plastic recipient (the usual culture supports are illustrated in Fig. 1.10a), filled with a "complex nutritive medium" according to the Good Cell Culture Practice [Bal-Price and Coecke, 2011]. This medium is frequently renewed to replace nutrients and remove the metabolic wastes. The culture is maintained in a strictly controlled environment in terms of temperature, pH, oxygen and sterility [Bal-Price and Coecke, 2011]. To study crosstalk between cells, biologists often use transwells. As illustrated in Fig. 1.10b; transwells are smaller wells that can be inserted to split a traditional culture well in 2 compartments. A semi-permeable membrane physically separate the cells, but allows nutrients and mediators secreted by cells to pass from one side to the other.

A cell culture is ***a model*** of the *in vivo* reality, not representing the full complexity of the cell environment. Its simplicity of use, as well as the favorable ethical and cost aspects, explain why cell culture became the main approach in cellular biology at the end of 20^{th} century for both academia and industry [K. Young and J. Beebe, 2010]. The scientists can indeed isolate a part of the full system they want to study and test specific parameters, protocols and drug effects on the cells.

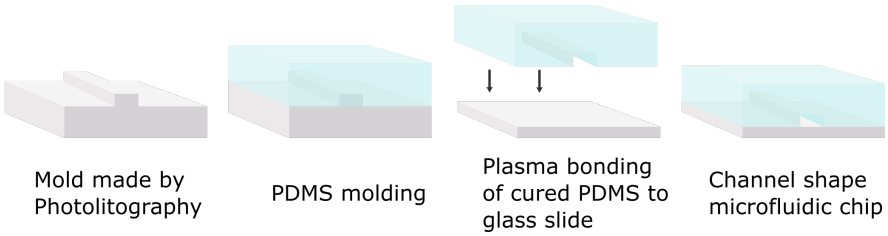

FIGURE 1.11: Soft lithography and bonding steps to produce a microfluidic chip.

However the simplicity may limit the relevance of certain studies as evidenced by [Shroff et al., 2022][Ingber, 2022][Zhang et al., 2023][Li and Tian, 2018]: (i) a cell culture often minimizes the interaction of the cells with their extracellular matrix, and the interaction between cells in a given organ and also between organs; (ii) the cell model is generally reduced to one cell type cultured in 2D, while tissues are 3D and multi-cellular. Their 3D architectures is important, as it influences cells' gene expression, metabolism, maturity and function [Jensen and Teng, 2020][Shroff et al., 2022][Zhang et al., 2023]. Furthermore, the fact that the culture is essentially static (without circulation of medium) cannot recapitulate the dynamic environment of cells and prevent automatized and continuous monitoring during the experiments.

This simplicity is considered by a certain community as the main reason of the high failure rate in drug discovery [Esch, Bahinski, and Huh, 2015][Shroff et al., 2022][Ingber, 2022][Zhang et al., 2023]. This new scientific community suggests a new *in vitro* model to provide an intermediate tool between *in vitro* and *in vivo*, to accelerate fundamental research in biology, as well as drug development by pharmaceutical industry. It is interesting to note that in 2000 a study evaluating accuracy of *in vitro* models to identify human toxicity of drugs concluded of relevance of these tools [Olson et al., 2000], with the non rodents models predictive for 63% of human toxicities and rodents ones for 43%. However nowadays the figures provided in this study are considered as not sufficient by this community [Zhang et al., 2023], as they induce an unsustainable cost for healthcare and industrialists.

1.2.2 ... and an emerging technology...

MicroPhysiological Systems (MPS) technology may represent this more sophisticated tool between classical 2D *in vitro* cell culture and *in vivo*. This large family of system that will be detailed later in this section first started with Organ-on-a-Chips (OoC).

This technology appeared thanks to the development of soft lithography, and the conceptualization of its use in Biology and Biochemistry in the 90's [K. Young and J. Beebe, 2010][Whitesides et al., 2001][Leung et al., 2022]. Soft lithography consists in molding elastomeric material using a mold micropatterned by photolithography. The most common elastomeric material is the Polydimethylsiloxane (PDMS), a low cost oxygen permeable and biocompatible material [Radisic and Loskill, 2021]. By bonding the molded piece to a rigid substrate (glass or else), a microchannel can be created, as illustrated in Fig. 1.11.

An OoC is created when cells are loaded inside the microchannel. The microfluidic chip can be designed with sophisticated patterns and shapes, to create physiologically relevant microstructures (e.g. pillars for cell attachment [Fernández-Costa et al., 2022], or grooves to orientate the cells [Duc et al., 2021]). A continuous flow can circulate within the channel to mimic the biological fluxes such as blood stream, but some systems are based on static culture like in [Duc et al., 2021]. The channel volumes can be adjusted to better recapitulate the metabolites concentrations and dynamics [Picollet-D'hahan et al., 2021], but some technical

constraints, like in [Skardal et al., 2017] where a recirculating loop was implemented , lead to use millilitres contrary to the usual microliters in microfluidics. The low volume of medium surrounding the cells is preferred (characterized by the medium to cell ratio) as it prevents dilution of secreted molecules [Leung et al., 2022], and allow amplification of concentration variations [Modena et al., 2018].

From this initial concept, many subtypes of systems have been derived [Picollet-D'hahan et al., 2021]. The biological material inside the microfluidic chip are from a variety of origin and size. They can be cell lines (immortalized cells), primary cells (taken from human donors or animals) or differentiated from stem cells. They can be organized in 3D spheroids or organoids (bioprinted or aggregated in molds), or be *ex vivo* tissues (biopsies). The environment of the cells can be closer to *in vivo* reality, using scaffolds, hydrogels, microstructure, membranes, in order to recapitulate the micro-environment. To reproduce some molecular, mechanical (muscles) and electrical (nerves) stimuli on the organ of interest, electrodes or microstructures acting as actuators can be integrated on-chip. Furthermore, it is also possible to couple several OoC together to study inter-organ regulation, thus creating a Multi-OoC or **MOoC**. As an example, in [Bailleul et al., 2022], the authors stimulated the muscular contraction of C2C12 myotubes with electromagnetic field to characterize muscular fatigue, which models the action of nerves on the muscle cells; while in [Duc et al., 2021], a coculture of neurons and muscle cells emulated neuro-muscular junctions to study their disruption in neurodegenerative diseases. Note that a MOoC can be in a single chip as in [Duc et al., 2021], or in several interconnected chips as in [Skardal et al., 2017] with a liver-on-chip, connected to a heart-on-chip and a lung-on-chip.

The different systems described above (classical 2D *in vitro* and MPS) correspond to different model levels, deciphering from single cell activity to overall cell population when 3D and multi-cellular are investigated in MOoCs.

All the above mentioned systems were qualified in the literature with different names, often related to their mainstream feature: body-on-chip, organoid-on-chip, multi-organ-on-chip or micro-physiological system (MPS). Except rare articles ([Mandenius, 2018]), MPS usually refers to the whole family of systems aiming at improving the classical 2D *in vitro* culture using better biological models and a better cell culture environment.

In the rest of this work, we will refer to MPS when it concerns this general family, and we will use OoC and MOoC when the system will be mono- or multi-organ.

1.2.3 ... with an exponentially growing interest

Despite the fact that cells have already been cultured in PDMS during the early 2000s [Leclerc, Sakai, and Fujii, 2003][Shoji et al., 2023], usually it is considered that the first OoC is the lung-on-chip of Donald Ingber in 2010 [Huh et al., 2010]. This pioneer publication is different compared to the previous cultures by its study of the physiological relevance of the system . It tooks 10 years to Donald Ingber to obtain the published results, after presenting his device concept in 2001 in [Whitesides et al., 2001].

Then during the next decade, OoC-related publications have been exponentially growing, with an average annual increase of 50% between 2011 and 2022. As a comparison, in parallel publications on tumor research were "only" increasing by 5.3% annually [Shoji et al., 2023]. Accordingly, the OoC technology was selected in 2016 by The World Economic Forum, as one of the top ten emerging technologies [Leung et al., 2022].

1.2.4 Key players and environment in MPS

1.2.4.1 Stakeholders

The MPS environment is rich of contributors, and understanding their roles and their relationships allows to better understand the technology roadmap.

The MPS technology would not bring as much enthusiasm (and fundings) without the ***pharmaceutical industry***. It strongly pushes the development of this new tool to improve and reduce costs of drug discovery, and adapt to the more stringent animal use regulations. Indeed, the European Parliament adopted a text in 2021 "Plans and actions to accelerate a transition to innovation without the use of animals in research". In Europe, the Swiss company Roche is a key actor in MPS, sponsoring conferences and actively pushing MPS development in their products [Reardon, 2015].

This stakeholder does not develop MPS, it is the role of ***biotechnology or MPS industrialists*** that develop MPS closely with ***academia***. These are indeed frequently spin-offs of academic research, and keep on participating to research grants to demonstrate the interest of their system through publications. The most famous is Emulate: this spin-off appeared after Donald Ingber's article [Huh et al., 2010], from Harvard Wyss Institute (USA). Emulate supplies industrialists, including Roche and Johnson & Johnson, using them in their investigations [Reardon, 2015]. In Europe, collaborations exist too, such as between Astrazeneca (Sweden) and TissUse GmbH, a German biotechnology company [Bauer et al., 2017][Rigal, 2023].

In academic laboratories, the MPS community is split in two: an engineering community and a biologist/bioengineer community, with a different approach of MPS. On the first hand the engineering community develops system integration, miniaturization, sensing, and more recently standardization; on the other hand, the biology/bioengineering community focuses on organoids/iPSC development (see brief definition section 1.5.1 p. 28), vascularization and micro-environment emulation through hydrogel/membranes. Companies like TissUse and Emulate are mostly oriented towards the biology community, that generally seeks plug-and-play systems to focus on the fundamental biology part. The members of engineering community often produce their own systems with specific architectures and custom integration of sensors/actuators, and thus is a minor market for MPS industrialists.

Last but not least, MPS valuing is also driven by the reactivity of the ***regulatory instances***, specific to each country. For example, the pharmacological industry can only exploit MPS in a preclinical validation process if the local regulatory instances authorizes it. Considering the potential of MPS, the FDA (the American Food and Drug Administration) has decided to get involved in the MPS technology development. This institution also created a working group on alternative methods to limit animal use [FDA, 2022]. In that frame, FDA actively collaborates with MPS industrialists, (eg. CN bio and Emulate) [Shoji et al., 2023]. The FDA issued in 2022 the "*FDA Modernization Act 2.0.*", which has updated its previous 1938 act [*The FDA Modernization Act 2.0 - What does it mean?* 2023][Akash, Arnob, and Uddin, 2023]. In this amendment, the FDA opened the possibility to use non-animal testing for pre-clinical tests such as *in silico* simulations, artificial intelligence, and finally MPS.

1.2.4.2 Countries and regions

It is also interesting to see the hotpots of the MPS research. The greatest contributors to academic publications are the USA (35% of total articles studied in the meta analysis in [Shoji et al., 2023]) followed by Europe (32%) and China (9%). In general, inside the leading

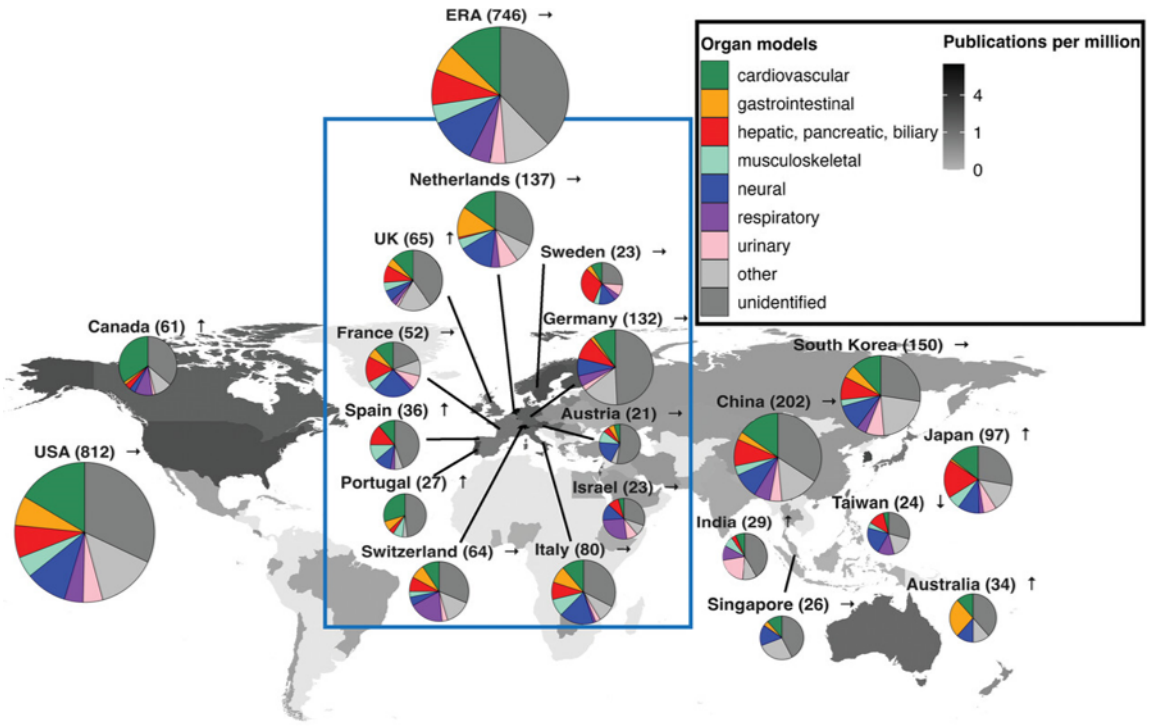

FIGURE 1.12: Original caption from [Shoji et al., 2023]: "Global trends in organoid and OoC research. World map of A) organoid and B) OoC research and trends of countries/regions. Pie charts of selected countries/regions are shown along with number of research articles. Arrows indicate recent trends of publication counts. For better visibility of smaller pies, diameters of the pie charts are in a cube root scale such that the area nonlinearly correlates with the number of research articles. The grayscale gradient on the map shows the sum of fractional counts of contributions of each country, adjusted for the population size. "Unidentified" as an organ model category consists of research articles in which the algorithm did not detect an organ model type"

countries/regions, OoC research predominantly focuses on "cardiovascular" and "hepatic pancreatic biliary" models (see Fig. 1.12)[Shoji et al., 2023].

In Europe, as illustrated in Fig. 1.12, Netherlands is the greatest contributor followed by Germany; France being the 6^{th} country. However in the category "hepatic pancreatic biliary", France is the second country in Europe with the largest proportion of articles. An important contributor is the CEA Leti and BIOMICS in Grenoble, involved in endocrine and exocrine pancreas MPS projects [Quintard et al., 2022][Navarro et al., 2021][Papoz et al., 2022]. Note also in France the great proportion of "neuronal" organ models, possibly related to the presence of a french company supplying *neuro-organs-on-chip platforms* [*NETRI - Digitizing human biology* 2023].

The number of publications per country shows the political interest of Europe to gather their efforts, as 11 countries of the European area are required to get closer of the massive number of publications of USA alone (746 publications for Europe, and 812 for USA).

1.2.4.3 Organizations/societies

Two main societies represent the MPS community: the European Organ on Chip Society (EUROoCS) and the International MicroPhysiological Systems Society (IMPSS).

EUROoCS was created after the Horizon 2020 FET-Open project Organ-on-Chip In Development (ORCHID), in which the group of experts, after analyzing the technological landscape and stakeholders, rose the need of a society gathering the communities to enhance European research [Mastrangeli, 2019]. The first conference took place in Graz (Austria) in 2019. The community gathers every year in Europe since then.

The more recent society is the IMPSS. Despite the claimed "International" label, this society sounds more USA driven. The society has been incorporated under the Law of Washington DC [*IMPSS BY-LAWS* n.d.], and 7 over the 19 board members are from USA, with 3 out of 4 in the bureau. So far the locations of the conferences, named the "Microphysiological World Summit", were New Orleans in 2022, Berlin in 2023 (hosted by Uwe Marx, Chief Scientific Officer of TissUse company), and Seattle in 2024.

Covering the great diversity of objectives stirring the MPS community, both conferences gather a large panel of stakeholders. EUROoCS conferences are more technology and engineering oriented than IMPSS conferences. So far, the regulatory and clinical applications has in turn been more predominant in the IMPSS conferences.

1.2.4.4 Diabetes and MOoCs

The meta analysis explores also the multi-organ systems, the MOoCs. The most important trend goes towards the investigation of the liver-intestine interaction, followed by the heart-kidney-lung [Shoji et al., 2023]. This is illustrated in Fig. 1.13, showing the distribution of OoCs and MOoCs publications.

Regarding diabetes-related MOoCs, islet-liver and muscle-liver are present in a significant amount of publications (see Fig. 1.13). More specifically, islet-liver MOoCs are presented in [Bauer et al., 2017][Tao et al., 2022][Essaouiba et al., 2020]. Concerning the adipocyte-islet axis, [Lu, Dugan, and Kennedy, 2018] studied the action of adipocytes on islets' insulin secretion. Coming to the islet-muscle axis, a recent study investigated the impact of IL-6 secreted by muscle cells on the islets [Fernández-Costa et al., 2022].

Very few studies have so far presented experimental results from MOoC with more than 2 organs: [Lee et al., 2019] proposed a methodology to develop an in-silico muscle-liver-islet interactions, and [Kim et al., 2023] studied liver-islet-adipocyte.

Surprisingly, there is currently in the MOoC literature no publication demonstrating the increased glucose uptake of skeletal muscle cells under the action of insulin, which is one of the most important interaction in glucose homeostasis (see section 1.1.2.2). [Rogal et al., 2019] also emphasizes in the lack of studies using skeletal muscle cells in type 2 diabetes research.

1.2.5 Technological challenges of MOoCs

As previously mentioned, MPS is a new technology, involving recent domains of sciences that are evolving alongside with MPS:

- complex multi- and 3D cellular models,
- barriers, gradients recapitulation,
- recapitulation of the full environment in terms of chemical composition and concentrations, mechanical properties, or scaling,
- microfluidic equipment integration (pump, valves),
- online sensing development, integration,

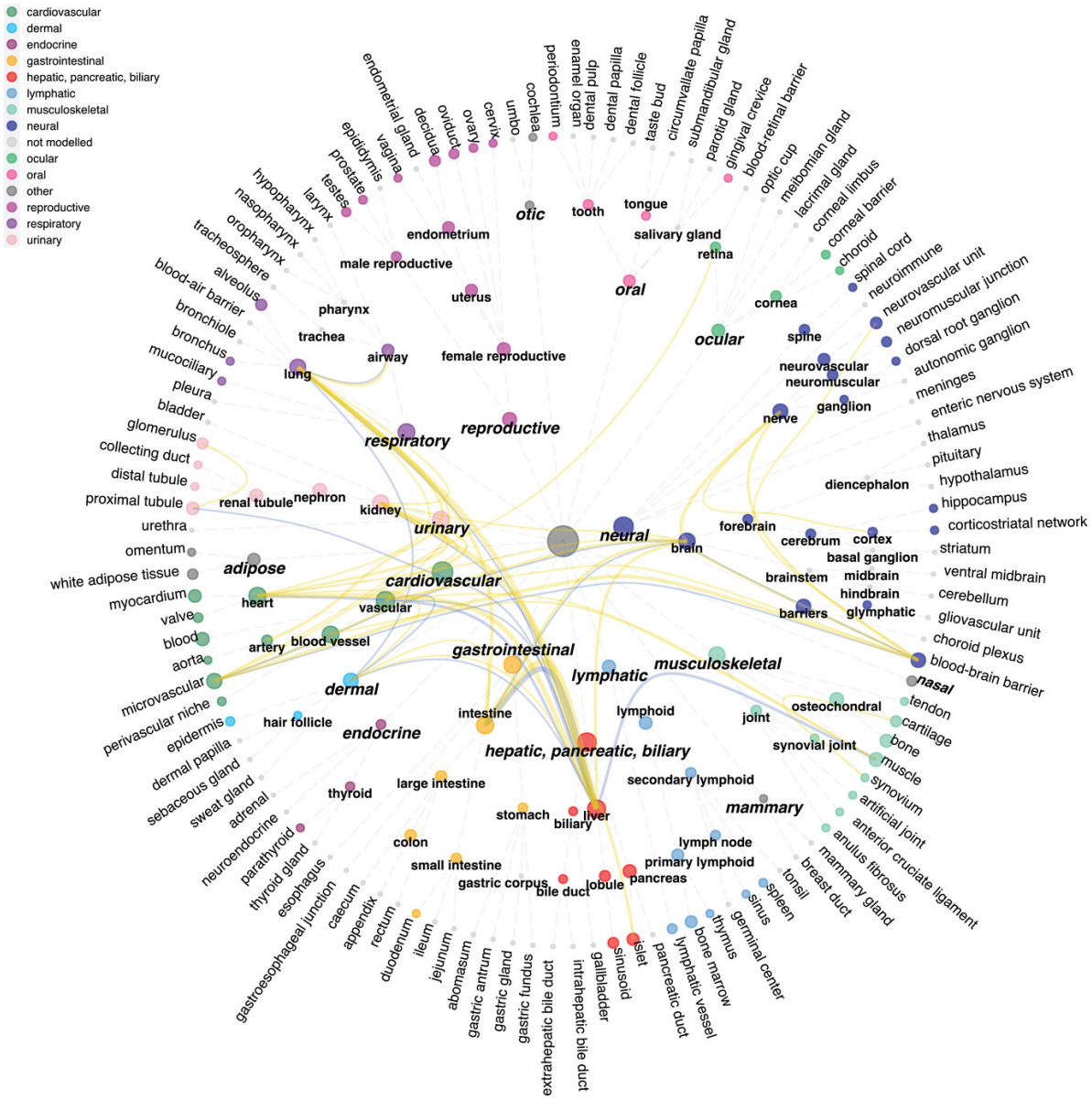

FIGURE 1.13: Original caption from [Shoji et al., 2023]: "Organs and substructures collectively researched by OoC. The dendrogram shows hierarchically categorized organs and substructures that are modeled by OoC, with edge bundling to show collectively researched organs/substructures. Spheres representing organs/substructures are sized according to publication counts and color-coded according to level 1 organ categories. Spheres corresponding to substructures that are only modeled by organoids but not by OoC are colored in light grey. Curved lines connect organs/substructures that are mentioned in combination in OoC in research articles, and are only drawn for organ/substructure combinations that appear in 2 or more articles. The colors of the curved lines indicate publication year (blue: 2010–2019; orange: 2020 onwards), with their width reflecting publication counts. The widest line (intestine–liver in orange) corresponds to 13 research articles."

- automation and standardization.

MPS projects are usually focusing on 1 or 2 of these main technological challenges above listed. Considering the scientific background of the laboratories involved in this PhD work, the 2 challenges tackled here are the *online sensing* and the *scaling*. Thus we will focus more particularly on the technological context related to these domains.

1.2.5.1 Online sensors

Many physical measures are of interest in the MPS: myriads of molecules secreted by cells, nutrients and oxygen concentrations, pH or temperature. These measurements are useful to validate the cells health and micro-environment, to respect the Good Cell Culture Practice [Bal-Price and Coecke, 2011], and can also help decipher the temporal interactions of cells.

Traditional *in vitro* cell culture frequently uses offline sensing, which requires the experimenter to collect samples (cells or medium) and conduct assays. These assays are well established techniques, with a huge scientific historic (Western Blots, Immunochemistry, ELISA, RT-qPCR for the most usual). However these techniques are generally destructive and/or endpoint (one measure made at the end of the experiment) thus preventing dynamic monitoring. Moreover, they are not optimised for very low volume samples (in the order of the microliter). In the perspective of MPS accomplishment, online sensors are required. Online measurement in a MPS corresponds to an analysis occurring during the experiment without requiring a specific action from the experimenter, using sensors directly integrated in the chip or at the extremity of tubing connected to the MPS [Leung et al., 2022].

Despite a large set of very optimistic reviews listing the diversity of sensors and successful stories of sensor integration in MPS [Leung et al., 2022][Modena et al., 2018] [Ino and Shiku, 2019] [Soucy et al., 2019], online sensing remains a great technological challenge in the MPS. The main challenges identified in the literature are:

- **Integration** of the sensor, which itself includes:
  - The miniaturization of the sensing part and the electronic acquisition system.
  - The compatibility of the sensor microfabrication with the microfluidic chip fabrication. Indeed as illustrated in [Dornhof et al., 2022], sensor components can be chemically or heat sensitive, thus the fabrication protocol of the system (sensor and chip) requires that each step respects the already deposited elements.
  - The working conditions of the sensor have to fit with the culture conditions (37°C, pH and oxygen levels) [Fuchs et al., 2023]
- **Regeneration** of sensors, notably the *biosensors* that have a short life time (less than a week so far) [Kilic et al., 2018] [Zhang et al., 2017]
- **Interference** of the sensor with the experiment, by modifying the physical or chemical cells' environment. For instance, H_2O_2 can be generated by some electrochemical sensors and can interfere with cells [Fuchs et al., 2023][Dornhof et al., 2022] and is more precisely known to produce exercise-like effects on myotubes [Carter and Solomon, 2019]. The enzyme-based sensors are also known to consume oxygen [Weltin et al., 2014]
- **Automation** of the sensing for long term and high-throughput experiments [Kilic et al., 2018]

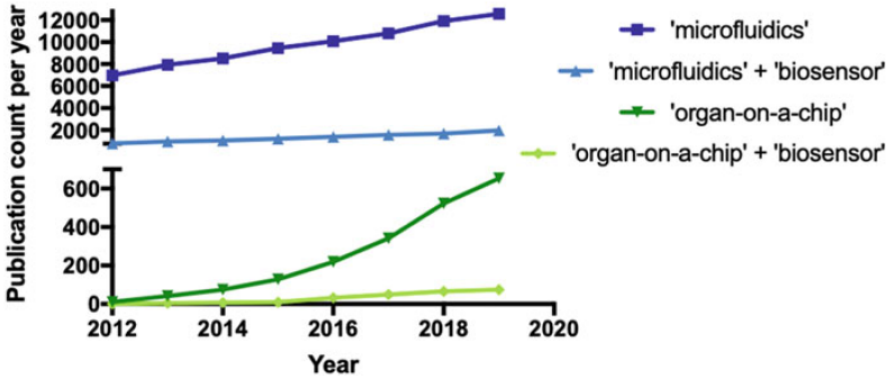

FIGURE 1.14: Scopus search results with the 3 keywords: organ-on-a-chip, microfluidics and biosensor, and their combinations. From [Rothbauer and Ertl, 2021].

To overcome these challenges and achieve sensor integration, a great diversity of technical skills are required as well as equipment such as costly clean room facilities [Rothbauer and Ertl, 2021]. This may explain that many MPS use so far the classical offline sample analysis, like immunostaining, western blots, ELISA or RT-qPCR [Bauer et al., 2017][Kim et al., 2023][Essaouiba et al., 2020][Tao et al., 2022][Pediaditakis et al., 2022].

[Rothbauer and Ertl, 2021] plotted the Scopus search results related to the keywords "microfluidics" and "organ-on-a-chip", and then with the addition of the keyword "biosensor" (see Fig. 1.14). Results including the organ-on-a-chip + biosensor keywords only appeared in 2015, and their increase is much lower than the one of publications dealing with organ-on-a-chip. Thus, progressively, the MPS engineering community develops online sensing and go beyond the limits of these techniques.

Insulin sensing In the context of diabetes, in the most recent publications found, [Lu, Dugan, and Kennedy, 2018] developed an online insulin sensing system using immunolabelling (a fluorescent probe binds to insulin thanks to an antibody targeting insulin). This system was integrated on chip, to monitor insulin secretion after the action of adipocytes on islets. Similarly, [L. Glieberman et al., 2019] designed an online immunolabelling system for automated sensing of insulin release by islets. In [Fernández-Costa et al., 2022], the authors developed a sensing platform using plasmon resonance to detect the insulin secreted by β cells stimulated by "trained" myotubes (electrically stimulated) secreting interleukin-6.

Insulin sensing is definitely crucial for the community of diabetes MPS, as well as in clinical context. The rarity of such crucial sensors may be related to the size of insulin, the low physiological insulin concentration, and the difficulty to achieve sufficient selectivity against other interfering molecules [Soffe, Nock, and Chase, 2019].

Glucose sensing Among the multitude of glucose sensors, two technologies mainly emerge [*Organ on Chip in Development, ORCHID Project,* 2019] [Leung et al., 2022]:

- **Electrochemical** sensors rely on a chemical reaction between the analyte and a biological "receptor" (in the case of glucose it is an enzyme), generating a measurable current. This category of sensor, used in our work, will be further detailed in Chapter 4, section 4.1.2.

- **Optical** sensors rely on fluorescent dyes, quantum dots, or plasmonic nanoantennas. The interaction of these substrates with glucose generates a measurable electromagnetic field.

As reported by [*Organ on Chip in Development, ORCHID Project,* 2019], optical glucose sensors are less common than the electrochemical ones as they require specific and expensive equipment, and require optical accessibility in the MPS. On the contrary, electrochemical biosensing is considered an easy and low cost technique [Shanbhag et al., 2023][Grieshaber et al., 2008].

Electrochemical glucose sensing is an old technique dating from the 60s, with the invention of the Clark electrode using a Glucose oxidase [Sabu et al., 2019]. Since this invention, glucose sensing is still relying on enzymes. In the MPS publications, we can find offline assays (glucose dosage using reagents) and test stripes from clinical devices [Bauer et al., 2017][Zambon et al., 2014][Lee et al., 2019] related to enzyme detection. As an alternative, some enzymatic sensor suppliers developed a PMMA case called *flow cell* that can host test stripes. The flow cell creates microfluidic and electronic contact with the sensor strip, forming an online glucose sensor. This type of system has been used by [Bavli et al., 2016] and [Matthiesen et al., 2022]. Custom made glucose sensors are also common in the literature, based on a direct deposition of Glucose oxidase on a chip electrode: [Misun et al., 2016][Dornhof et al., 2022].

A recent publication of [Fuchs et al., 2023] shows an interesting and unusual use of the enzymatic sensor: instead of measuring the electrical current generated by the enzyme reaction with glucose, they measured the oxygen depletion induced by the enzyme reaction, using oxygen sensitive phosphorescent particles. This sensing is enzyme-based but the final readout is optical.

Cells' electrical activity sensing As introduced in section 1.1.2.1, the MicroElectrodes Arrays are used to detect electrical activity of electrogenic cells, like islets in the research spectrum of the CBMN, or neurons and muscles. In the context of MPS, this sensor is commonly used for electrical detection in neurons [Duc et al., 2021][Oleaga et al., 2018], and muscles (almost only cardiomyocytes) [Oleaga et al., 2018][M. Maoz et al., 2017][Duc et al., 2021]. Note that the MEA can also be used to measure tissues bioimpedance as in [Bailleul et al., 2022].

Lactate sensing Lactate is another metabolite of interest, as in [Dornhof et al., 2022] [Bavli et al., 2016][Matthiesen et al., 2022]: lack of oxygen in the MPS will induce lactate production by the cells, therefore monitoring lactate levels indirectly assesses the oxygen availability in the culture.

Multi-sensing platform At this moment, the most advanced system, regarding online sensing, might be the platforms realized in [Zhang et al., 2017]. They developed 2 sensing platforms, one for the metabolites of interest in their liver and heart MOoC (Albumin, GST-*alpha*, CK-MB) and one for temperature, pH and oxygen. The first sensing platform uses electrochemical sensors, and the second platform optical ones: the medium absorbance was related to pH with the presence of phenol red, a pH-sensitive dye; the fluorescence was also related to oxygen thanks to a sensitive dye, the ruthenium; and the temperature was measured with a probe (no more information about it).

As already mentioned, the electrochemical sensors suffer from a short life time notably when antibodies are used for the detection, like in [Zhang et al., 2017]. In this work, they developed a very complete microfluidic sensing platform which is capable to renew the

antibodies automatically to maintain sensing in the long term. Considering no publications has been found so far reproducing or reusing this work (including by the authors), and the number of authors (31) and laboratories (18) involved, this great work does not appear to be yet scalable to the MOoCs projects, probably in terms of funding and competences required.

From this rapid bibliographic study, we conclude that online sensing in MPS is already present in the literature, but remains marginal due to its implementation and usage complexity.

1.2.5.2 Scaling

The definition of "scaling", as we understand it in this work, is as follows: how to dimension the organ volume/size, number of cells, flow rate, concentrations, shear stress [Picollet-D'hahan et al., 2021] to recapitulate the physiology at a smaller scale (see Fig. 1.15).

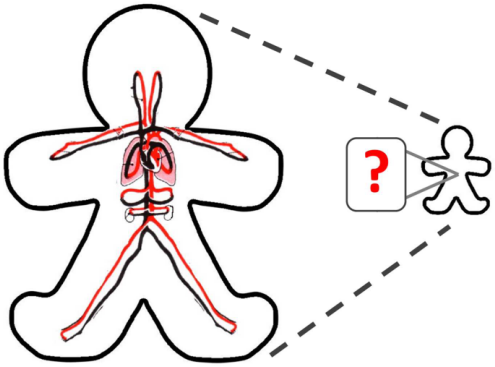

FIGURE 1.15: Illustration of the scaling question, from [Moraes et al., 2013].

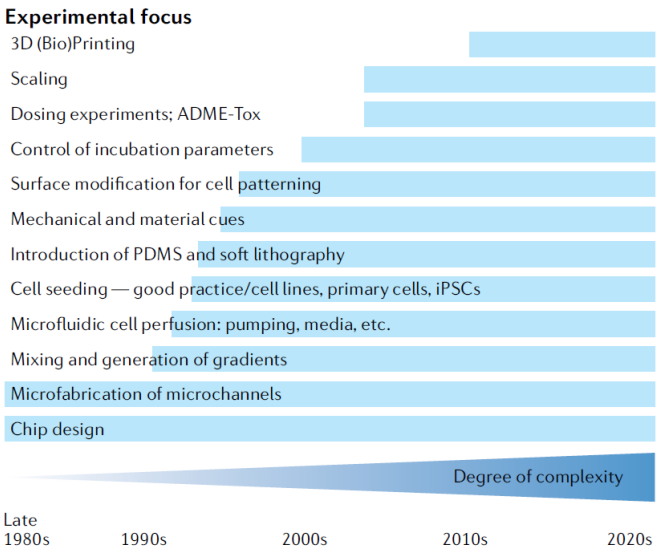

FIGURE 1.16: The research topics emerging through time with the MPS technology, from [Leung et al., 2022].

The scaling question is among the most recent in the MPS field as illustrated in Fig. 1.16. In that exploratory part of MPS research, categories of scaling are not yet fully defined [Park

et al., 2020]. Still, the most common scaling categories are the following: proportional, allometric and functional [Picollet-D'hahan et al., 2021]. Otherwise we can find: direct scaling, residence time-based scaling, allometric scaling and multifunctional scaling [Leung et al., 2022]. A brief description of each methodology is given below:

- The **proportional scaling**, or also called **direct scaling**, consists in estimating the number of cells for each organ by dividing the *in vivo* number of cells by an arbitrary scaling factor. This technique has been used for example by [Bauer et al., 2017].
- The **allometric scaling** relies on the hypothesis that there is a law relating the mass of the organs (M_{organ}) to the mass of the body (M_{body}):

$$M_{organ} = A \times {M_{body}}^{B} \tag{1.1}$$

  A and B are empirically determined coefficients [Moraes et al., 2013] that depend on the species and the organ. However, it has been demonstrated that this scaling can be irrelevant [P. Wikswo et al., 2013]: the mass of an organ may be larger than the mass of the body. This type of scaling is also considering that the cells metabolism *in vivo* is maintained in the chip, which is not the reality [Moraes et al., 2013] (as for proportional scaling). However, allometric scaling is an easy to apply technique thanks to coefficients already provided in the literature [P. Wikswo et al., 2013]. This technique has been used in [Lee et al., 2019].
- The **residence time** based scaling [Sung, Wang, and Shuler, 2019], consists in setting the cells' chamber volume so that the *in vivo* residence time of blood in an organ is respected, preserving the reaction kinetics (consumption and production of molecules by cells). The residence time is deduced from the ratio between the flow and the volume. The size of the organ is considered in this scaling mode as linearly related to the organism mass, contrary to allometric scaling. This methodology has been set up by the Shuler's group, a pioneer in MOoCs scaling research [Moraes et al., 2013][Sung, Wang, and Shuler, 2019][Leung et al., 2022]. Besides, Michael L. Shuler co-founded in 2015 Hesperos (USA), a spin off of a NIH project, an important MOoCs provider [Sung, Wang, and Shuler, 2019][*About - Hesperos Inc. - Leader in Organ-on-a-Chip Technology* 2018].
- The **functional** scaling consists in defining the main function the organ that is desired to recapitulate, and then to scale the device accordingly, depending on the physical constrains and cells availability [P. Wikswo et al., 2013][Moraes et al., 2013].
- Functional scaling may be limited by the fact that the organs play different roles (for example the islets secrete insulin and glucagon in glucose homeostasis). The scaling targeting one function can lead to scale improperly another function of the organ [Moraes et al., 2013]. The **multifunctional** scaling has been introduced to prevent this issue: it is based on mechanistic models, where multiple parameters are specified to describe a multifunctional target. An algorithm optimizes the parameters to find the best combination resulting in an optimal outcome for the experiments, and the MPS is scaled to fit theses parameters.

[Sung, Wang, and Shuler, 2019] summarizes and compares the pros and cons of the different scaling strategies (see Table in Fig. 1.17).

However, although no consensus has been found so far, scaling remains an under-considered topic in the MPS community while it's crucial to emulate as best as possible the actual human physiology [Picollet-D'hahan et al., 2021][Moraes et al., 2013].

Methods	Direct scaling	Residence time-based scaling	Allometric scaling	Functional scaling	Multifunctional scaling
Main principles	Multiplication of organ sizes by a scaling factor	Match the fluid (blood) residence time for each organ	Physiological parameters should follow allometric power laws at microscale	Define major functional parameter for each organ	Specify multiple objective parameters and numerically derive design parameters
Pros	• Very simple	• Ensures physiologically realistic dynamics between organs	• Plenty of literature sources for allometric relationship for various parameters	• Mathematically robust and easy to apply once data is provided	• Works well for a specific purpose (for example, PK study)
Cons	• Likely to cause imbalance between organ functions at microscale • Ignores flow rates or circulation time	• Each organ module should have physiological level of intrinsic activity • Mass transfer within the tissue needs to be considered	• Allometric scaling law may not hold at microscale • Often requires further refinement by considering cell number, flow rates, etc.	• Issues with organs with multiple functions • Difficult to define quantitative parameters for some organ functions	• Can be mathematically complex when the system becomes larger

FIGURE 1.17: Table summarizing the different scaling methodologies and their pros and cons. From [Sung, Wang, and Shuler, 2019].

For example, [Fernández-Costa et al., 2022] measured the insulin secreted by islets under the action of interleukin-6 (IL-6), itself secreted by stimulated skeletal muscle cells. However there is no mention of the scaling strategy demonstrating the relevance of the IL-6 levels, which questions the relevance of the measured inter-organ crosstalk. This issue emerges in other large scale projects of MPS, where open-top chips are designed to culture organoids [Ronaldson-Bouchard et al., 2022][Bauer et al., 2017]. This is convenient as the cells can be extracted after experiments for off line analysis, but requires large volumes inducing dilutions of biological factors [Leung et al., 2022].

1.3 Scientific historic of teams: toward MPS

This thesis work is the result of a collaboration between two research teams: *Technologie pour la santé* (IMS UMR 5218) and *Cell biology and Biosensors* (CBMN UMR 5248), experts in microelectronics and islets electrophysiology, respectively. These teams have a collaboration history that started in 2008. Through experiments, hardware and software tools and *in silico* models, they have since that date tried to decipher the islets electrical activity used as a proxy for insulin secretion.

The team *Technologie pour la santé* of the IMS UMR 5218 is part of the *Bioelectronics* group gathering researchers in electronics but also biology. The two other teams in the group are working either on neuromorphic computing, or on bioelectromagnetism. *Technologie pour la santé* addresses circuits and systems at the interface with biology. Such interfaces can either be unidirectional in the case of biological tissue stimulation or signal acquisition, or bidirectional, potentially forming a bio-electronics closed-loop including real-time signal processing. Before this thesis work, a system for real-time acquisition and analysis of islets electrical activity detected by MEA was developed and exploited [Pirog et al., 2017], in collaboration with the biologists at CBMN. Together, IMS and CBMN demonstrated a correlation between the insulin secretion by islets and their electrical activity. More recently in IMS, a PhD project developed a platform to electromagnetically stimulate myotubes cultured on MEA and measure their bioimpedance as a marker of fatigue [Bailleul et al., 2022].

The *Biomedical Research: Fundamental and Translational* pole of the CBMN UMR 5248 laboratory works on a broad range of topics: biofilms, antibiotics resistance, muscular dystrophies, and diabetes. The *Cell biology and Biosensors* team studies islets with an unusual approach: they analyze the islet electrical activity and relate it to islets secretion activity, using MEA and more recently OECT [Abarkan et al., 2022]. They developed a microfluidic chip with a barrier system allowing to trap islets on a MEA electrodes integrated in the chip [Perrier et al., 2018]. Capitalizing on the demonstrated monitoring of insulin secretion via electrical recordings (see above paragraph), the group developed in a recent thesis a microfluidic channel including a MEA [Jaffredo et al., 2021]: the islets, placed on electrodes, can be infused with solutions and the secreted insulin is analyzed in the flowing out medium, while the electrical activity is recorded in parallel.

An other team of this pole provided an important support to our work: the team *Réparation membranaire et vésicules extracellulaire*, which investigates membrane repair defects involved in myopathies like the Duschene disease. They are familiar with the LHCN-M2 human cell line, which they use in their experiments. They kindly provided the cells and the support to perform LHCN-M2 cultures, and helped us setting up co-culture medium experiments and conducting some of them.

The long and tight collaboration between CBMN and IMS and their experience in their respective research fields led them to consider to integrate MPS technology in their mutual research roadmap. This PhD thesis was the opportunity for both teams to enter the MPS community (stakeholders, conferences, GDR) but also new or relatively new technologies and methods implied by design of MPS (microfluidics, biological cell co-culture, scaling, electrochemical sensors, multiphysics simulation, muscle cells culture).

As this PhD thesis was the first one on the topic of MOoC for both groups, it represented a huge challenge, in addition to the absence of specific ANR funding (an ANR grant was obtained at the end the last year of my PhD). The thesis was supported by and Interdisciplinary PhD Grant from University of Bordeaux.

It was co-supervised by Pr S. Renaud (IMS) and Dr M. Raoux (CBMN). PhD research was conducted in both laboratories (approximately 50% in each): biology experiments, microfluidics tests, and sensor characterization were performed at CBMN, that possesses the cell culture equipment and the cell lines and primary islets, as well as the microfluidic equipment; multiphysics simulations and electronics tests on custom potentiostat happened in IMS, that owns the ad hoc software and computers, and proper electronic equipment.

1.4 Thesis research objectives

We presented the diabetes disease and showed that MPS are a new tool able to go beyond 2D *in vitro* cell culture and help investigate the complex interactions involved in this multi-organ pathology: it allows multi-organ interactions study, with relevant scaling for relevant concentrations and kinetics, and in parallel, integrated online sensors give access to real time analysis.

In that context, and in line with the research roadmap of CBMN and IMS, we define the main objective of this PhD as **the design of a MOoC suitable for the analysis of glucose homeostasis**.

A bibliographic study on MPS and diabetes revealed that no system exists to study the insulin mediated glucose uptake from skeletal muscles, even though this is the main organ reducing glycaemia under insulin action. We decided to target our research on the interactions between these two organ, also considering that dealing directly with the 4 main

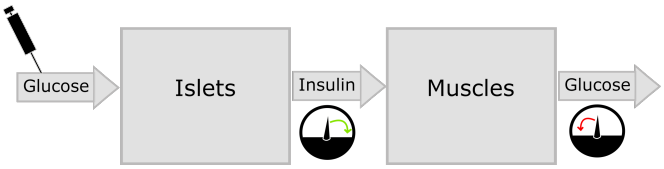

FIGURE 1.18: Block chain representing the targeted interactions to observe with the MOoC.

organs involved in glucose homeostasis without preliminary foundations was unrealistic. This work focuses therefore on the **endocrine pancreas or islets to skeletal muscles axis of the glucose homeostasis**, for its great interest in understanding glucose homeostasis, type 2 diabetes pathophysiology, and finding new treatments [Langlois et al., 2022].

We propose a methodology to design and scale a MOoC recreating the pancreas to skeletal muscle action, respecting **verifiable physiological conditions**. More precisely, we intend to:

- **attain a physiological insulin concentration generated by islets in response to physiological glucose elevation**
- **that induces a measurable glucose uptake by the muscles model**
- **monitor online relevant physiological parameters**.

The above mentioned objectives are illustrated in Fig. 1.18. They also include intermediate objectives, like managing to: co-culture the 2 cell types, culture them in microfluidic chip, define a scaling strategy exploiting *in silico* modelling, and select a sensor and characterize it.

Fulfilling these objectives requires an interdisciplinary approach, that involves engineering and biology in a continuously joint effort.

1.5 Preliminary specifications of the MOoC

Capitalizing on the scientific history and the equipment of IMS and CBMN, we agreed on preliminary specifications for the MOoC-to-be that are related to the cell models, the chip material, and the sensors, as explained below.

1.5.1 Cells models

The pancreas in our system is considered as an insulin source, thus we reduced it to the hormone secreting part of pancreas, namely **islets**. The biological model we selected is the **C57Bl6J mouse islets**. This choice is based on our preliminary work in CBMN and IMS, where we demonstrated on that biological model the correlation between insulin secretion and islets electrical activity measured by MEA [Jaffredo et al., 2021]. By selecting this cell model, we can monitor insulin release activity through a MEA acting as proxy sensor. In addition, an *in silico* model of C57Bl6J islets has been previously developed by [Alcazar and Buchwald, 2019], which represents a key point for our hybrid *in silico-in vitro* design methodology developed further in Chapter 3.

Primary mouse islets from C57Bl6J mice are more relevant in MOoCs than:

- **human islets**, which are are not optimal during the first development steps of a MOoC, due to the variability between donors and the difficult access to primary human islets [Hart and Powers, 2019].

- **cell lines**. For example in [Fernández-Costa et al., 2022] in which a myotubes-islets MOoC was developed, the authors used the mouse MIN6 cell model which is poorly responsive to physiological glucose concentrations. Like any cell lines (endoC, INS-1, RIN, HIT) they do not contain all islet cell types (while for example alpha cells represent about 40% of islet cells in human). Moreover, the response to other nutrients than glucose is not known, which could be critical in the context of MPS.

- **human iPSC** [4] are not optimal neither. Indeed, the protocols are costly, long, providing cell with a high inter-batch variability, and often poorly responsive to glucose. Very few groups in the world are able to generate glucose-responsive iPSC-derived *beta*-cells, and even in the last published protocols, the cells show differences with native *beta*-cells regarding their metabolism [Balboa et al., 2022].

In addition, mouse islets are highly accessible with few variability between animals in terms of age, genetic background, pathology, diet and environment.

Regarding the skeletal muscle model, the LHCN-M2 human cell line was selected as it is a human model, well established in the field of muscle biology [Toral-Ojeda et al., 2018]. After maturation, the length and shape of the plurinucleated myotubes obtained resemble those of primary myotubes, in a better way than the C2C12 mouse cell line largely used as skeletal muscle model [Zhu et al., 2007]. The *Réparation membranaire* team at CBMN is experienced in using this cell model, which was a precious advantage in the development of the MOoC.

1.5.2 MEA-based microfluidic chip

The interaction of the 2 micro-organ/cell types integrated in the MOoC (islets and myotubes) will be analysed by monitoring two essential markers: insulin secretion (islets) and glucose consumption (muscle cells).

Insulin secretion will be measured, as previously mentioned, through its electrical image obtained on a MEA. This MEA will be the substrate of the MOoC microfluidic chip. Note that a MEA also permit to record the electrical activity of LHCN-M2 cells as they are electrogenic cells. The CBMN is experienced in integrating MEA in PDMS microfluidic chips [Jaffredo et al., 2021], which is similar to PDMS-glass bonding: the Silicon atom involved in the bonding of PDMS to glass is also present in the Silicon Nitride top layer of MEAs [Ren et al., 2015].

Therefore the material selected for the microfluidic chip is the PDMS, not only for its easy bonding on MEA, but also for its convenient patterning, biocompatibility and oxygen permeability.

Regarding glucose monitoring, we opted for the integration of an enzymatic glucose sensor compatible with microfluidics (Bio Sensor Technology (BST), Berlin, Germany). This sensor was previously used in a liver-on-chip [Prill, Jaeger, and Duschl, 2014][Ezra et al., 2015][Bavli et al., 2016]. An other interest of this sensor is the possibility to co-detect lactate, which represents an interesting perspective. The choice of this glucose sensor and its use are further detailed in the section 4.2, dedicated to the online glucose sensing.

These pre-specified design elements of the expected islets-skeletal muscles MOoC are summarized in Fig. 1.19.

[4] Induced Pluripotent Stem Cell, which are bioengineered cells able to proliferate as cell lines and differentiate in the desired cell type using appropriate growth factors

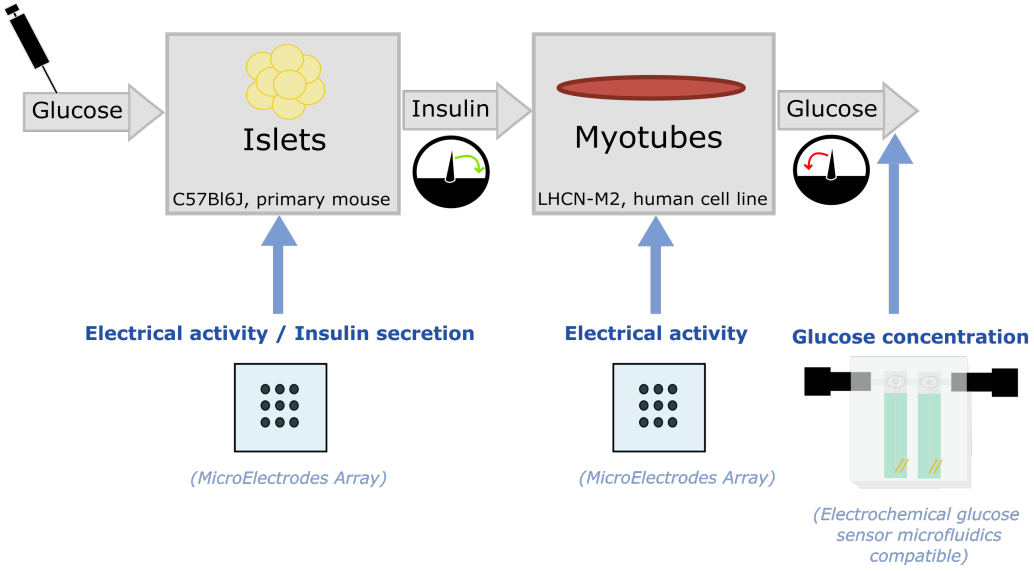

FIGURE 1.19: Details of the block chain in 1.18 with specified cellular models and sensors to monitor culture conditions and cellular metabolism.

Chapter 2

System design : meeting cell culture requirements

In this chapter, we will discuss how the requirements of pancreatic islets and LHCN-M2 myotubes culture have driven the general design of the microfluidic chip. Indeed their culture particularities drove the choice of a culture substrate on which both cell types adhere, as well as determined the possibility of co-culturing them in the same medium. The results of these investigations impacted the design of the microfluidic chip, as it defined the chip substrates and the overall geometry as explained in the following sections.

2.1 Co-culture and microfluidic chip design

2.1.1 Introduction

The design of the microfluidic chip highly depends on the possibility to co-culture primary islets from C57Bl6J mice and LHCN-M2 skeletal muscle cell line. By co-culture it is intended 2 notions: finding a *co-culture medium* where the different cell types survive, normally proliferate and differentiate (for muscle cells), ensure their function, while the molecular messengers such as insulin from one organ can reach the other organ; as well as finding a common culture protocol. Indeed the LHCN-M2 are classically cultured with 2 steps and 2 media, while islets require a single step and a single medium. The first step for LHCN-M2 cells (myoblasts) is a proliferation phase in a first medium, named *KMEM*. Then, when myoblasts reach 80% of confluence on the surface, the medium is changed for the KMEMdiff medium to induce myoblasts fusion into LHCN-M2 myotubes. The islets are primary cells thus not requiring this maturation protocol in 2 steps.

It was very uncertain to be able to co-culture islets and LHCN-M2 myotubes. No previous example of such co-culture was present in the literature before the 2-OoC of [Fernández-Costa et al., 2022], which was released at the end of the PhD. They co-cultivated a beta cell line (MIN6) and skeletal muscle cell line (C2C12), using a medium very close to the medium of the MIN6, and also of the medium of this PhD. Even though, they did not precisely validate the functionality of the myotubes in this unusual culture medium, and did not evaluate their response to insulin as it was out of the scope of their study. The other challenge we faced was this 2-step protocol for LHCN-M2 cells that we had to reduce to one medium and one step.

This justified the parallel work between: the design of a microfluidic chip versatile enough to allow *separate culture*, and then communication *experiments reuniting* cells (that we will see in section 2.1.2); the development and validation of a co-culture medium and protocol (that we will see in section 2.1.3).

2.1.2 Chip design in case co-culture is not possible

2.1.2.1 Introduction

In the case no co-culture is possible between the 2 cell types, the design has to work in 2 different modes:

- **static mode** for the long term culture, where the cells are in their dedicated medium with their dedicated culture procedure
- **microfluidic mode** for the interactions experiments where a flow is applied to induce communication. The infused medium in this microfluidic mode will be a minimal solution for cell survival used in biology for short term experiments (< 1 day), described in [Lebreton et al., 2015]: 24m M KCl, 6 mM $MgCl_2$, 6 mM $CaCl_2$, 50 mM $HEPES$, 661.25 mM $NaCl$.

The challenge posed in designing a device compatible with both models is finding a balance between having enough volume for the static mode and as few as possible for the microfluidic mode. Indeed, static mode calls for a volume that is sufficiently large for a low frequency of medium renewals by the experimenters (typically each 2-3 days), to remove accumulated metabolic waste and supply new nutrients. The lower the volume is, the higher the frequency of renewal is. Conversely, microfluidic mode requires a sufficiently small volume to prevent over-dilution of secreted metabolites, as this may prevent the device from reaching physiological concentrations of metabolites and generate concentrations below the detection threshold of the measurement equipment.

Criteria Considering the objectives of the MOoC, and the general observation above, this dual mode microfluidic chip needs to satisfy the following requirements:

(1) The chip must use a MicroElectrodes Array (MEA) substrate compatible with the Multi Channel Systems (MCS, Reutlingen, Germany) acquisition systems as presented in Fig. 1.5.

(2) There must be no floating metallic pieces that may cause electrical noise during electrophysiology recordings.

(3) The volume of culture medium must be maximized for the static mode (minimum 250 µl, the smallest volume of culture observed in the experiments of the CBMN biologists team).

(4) The shear stress in microfluidic mode should be limited to 6 mPa for the islets and to tens of mPa for the myotubes according to the limitations introduced in 2.1.2.1. A system where molecules are brought to the cells by diffusion would be ideal and physiologically relevant.

(5) The response time of the system (*ie* the time taken by the system to reach steady-state) should be limited. We defined arbitrarily that a switch in glucose concentration should take less than 10 min, and the insulin concentration should be attained under 30 min.

(6) The number of islets cultured in the device must be sufficient to generate physiological insulin concentrations (300 pM to 1 nM). There should ideally be between 10 (minimum number of islets to minimize biological variability) and 150 islets (number of islets typically obtained after dissection of a C57Bl6J mouse).

(7) The well must have homogeneous shear stress and concentration gradient.

(8) The time lag between the 2 wells must be reduced as much as possible in order to avoid nonsynchronous metabolism in both cells types.

Brief introduction to shear stress The constraint (4) requires the introduction of the *shear stress*. A cell within a microfluidic channel where a flow is applied to the circulating medium is exposed to a stress named the shear stress [M. Walker, C. Zeringue, and J. Beebe, 2004]. This phenomenon is illustrated on the Fig 2.1, where the cell is deformed by the action of the flowing fluid.

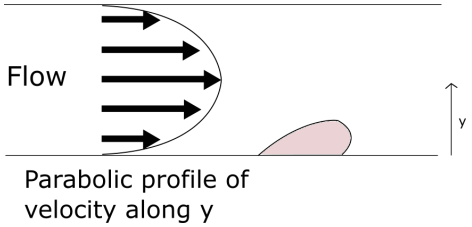

FIGURE 2.1: Schematic of a cell exposed to shear stress inside a microfluidic channel. The parabolic profile of the velocity is represented, showing the gradient of speed toward y axis, responsible for shear stress.

This intuitive phenomenon can be formalized, in the 2D case of Fig 2.1, by the following equation:

$$\tau = \mu \times \frac{du}{dy} \tag{2.1}$$

With τ the shear stress, μ the dynamic viscosity of water, u the velocity and y the axis gowing toward the channel top. This relation expresses the fact that the shear stress at a point depends on the velocity variation along an axis (here y). In the case of a microfluidic channel, the velocity is not homogeneous along the y axis: the speed is null at the borders and increases with the distance to the borders.

When generalized to 3D, the equation becomes [L. Glieberman et al., 2019]:

$$\tau = \mu \times \nabla \vec{u} \tag{2.2}$$

Regarding our islet-muscle MOoC, shear stress limits have to be implemented to ensure the cells safety, and will impact the microfluidic geometry. We identified from the literature the limit shear stress for islets at 6 mPa [L. Glieberman et al., 2019]. For myotubes, maximal shear stress value is not clearly set, probably as shear stress is inherently present *in situ* in the environment of muscle cells as contractile organ. However, based on the muscles-on-chip literature, we were able to define a relevant range for shear stress. [Anene-Nzelu et al., 2013] observed the synergy between a micropatterned substrate and an alignment of C2C12 cells, at a shear stress level between 30 mPa to 1.5 Pa. In [Naskar, Kumaran, and Basu, 2017], the effect of shear stress on C2C12 cells differentiation was evaluated from 3 to 42 mPa, and was optimal at 16 mPa. Therefore, we considered 1 Pa as the maximum limit, and worked preferentially in the range of tens of mPa for muscle cells.

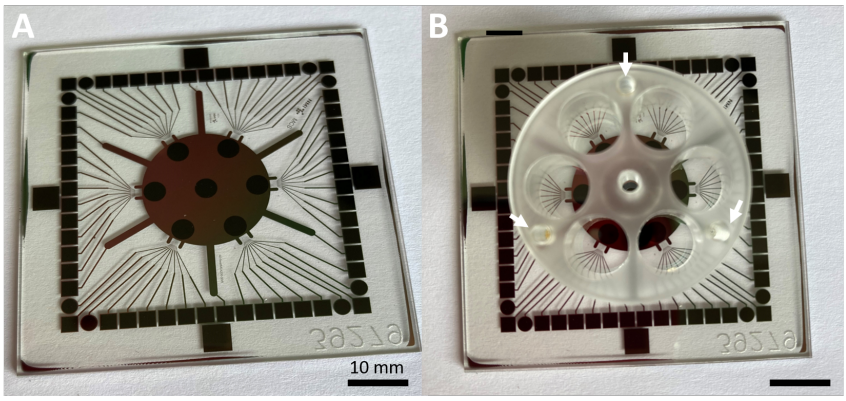

FIGURE 2.2: (A) 60-6wellMEA200/30iR-Ti MEA from MCS with 6 areas of 9 electrodes. (B) This MEA with the dedicated ring creating 6 wells. The arrows show where holes were drilled to screw the cover.

2.1.2.2 Description of the chip

Considering the designs constraints above listed, a system has been designed as described in the following paragraphs. The general design selected is briefly 2 culture wells, that can be reunited in the microfluidic mode using a channel inside the cover sealing the wells. The precise description of the system is provided hereafter.

The system takes advantage of the geometry of MCS's 60-6wellMEA200/30iR-Ti MEAs, which features 6 active areas with sufficient spacing to position distinct culture wells. Each well contains 9 recording electrodes and a common reference electrode. This MEA works in combination with a ring that creates 6 separated wells. This MEA and the dedicated ring are the base of the dual mode chip (see Fig. 2.2). Thanks to the 6 wells, a single MEA can host up to 3 MOoCs of 2 organs.

For sealing and medium injection, a cover is screwed on top of the ring thanks to drilled holes as shown in Fig. 2.2 panel (B). Each cover is constituted of a removable PDMS disk and a PMMA disk. We designed two different types of covers, one for each mode of the chip (it is then easy to switch from a mode to an other thanks to the screwing system). The 2 covers are illustrated with CAD representations in the Fig. 2.3 for the microfluidic mode and the Fig. 2.4 for the static mode.

In static mode (see Fig. 2.4), a thick disk of PDMS is used to extend the walls of the resin ring, thus increasing the culture volumes if required. The PDMS disk is indeed punched to create 6 wells aligned to the ring wells. A corresponding PMMA cover is also designed with holes aligned with the wells of the PDMS and ring layers. Nylon screws (chosen to satisfy constraint (2)) are used to seal the PDMS disk to the ring by pressing them together.

For the microfluidic mode (see Fig. 2.3), the PDMS disk is changed to a thinner variant, which hosts a channel linking the 2 wells of the chip. The channel dimensions are shown in the Fig. 2.5 panel (C). It also helps sealing the PMMA cover to the ring and the inlet and outlet tubes to the cover. Fig. 2.5 panel (A) shows a cover from the top with the tubes attached. Panel (B) reveals the inside of the wells when the cover is screwed on a ring.

A first version of this chip used an external tubing linking the 2 wells by the top. The flow was not stable, neither repeatable, and sometimes interrupted. We suspected the hydraulic resistance of the tubing was too high. Therefore we designed a channel inside the PDMS disk with a larger section and a shorter length than the previous tubing, to lower the hydraulic resistance. The height of the ring had also been reduced from 10 mm height to 5.3 mm,

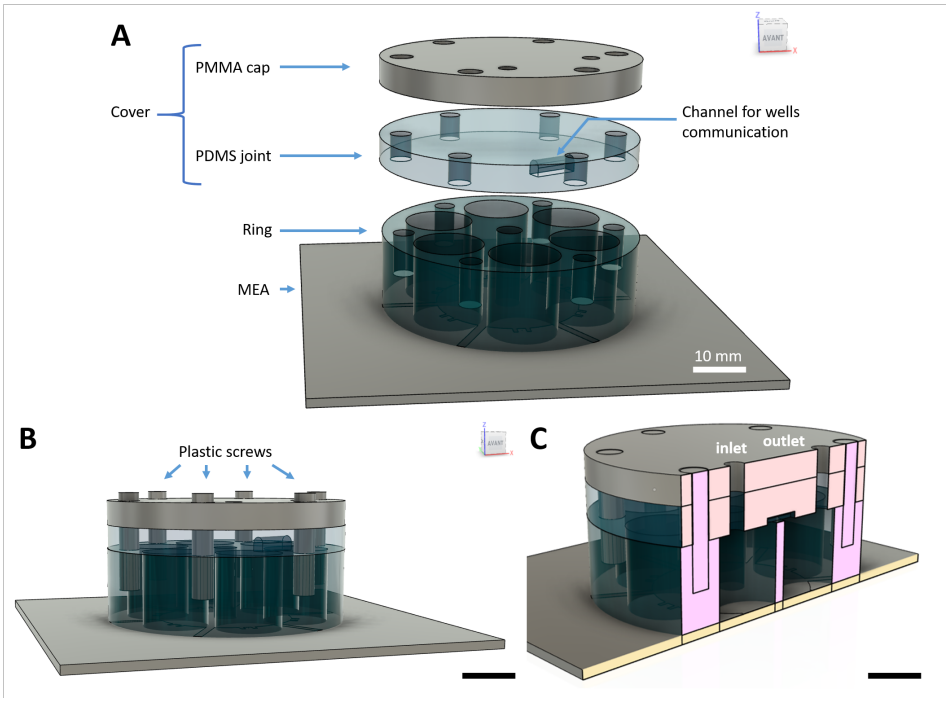

FIGURE 2.3: CAD views of the chip design 1 in microfluidic mode. (A) Exploded view and description of the system components. (B) Chip view when the cover is screwed. (C) Cut view of the CAD model showing the inner part of the chip when the cover is screwed.

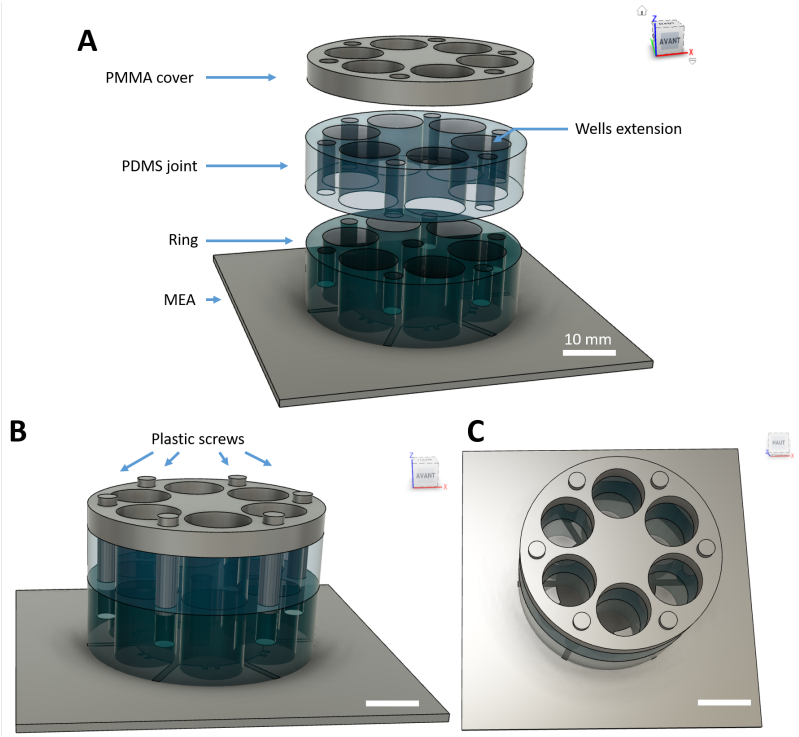

FIGURE 2.4: CAD views of the chip design 1 in static mode. (A) Exploded view and description of the system components. (B) Chip view when the cover is screwed. (C) Top view of the CAD model showing the deep wells created by the PDMS disk.

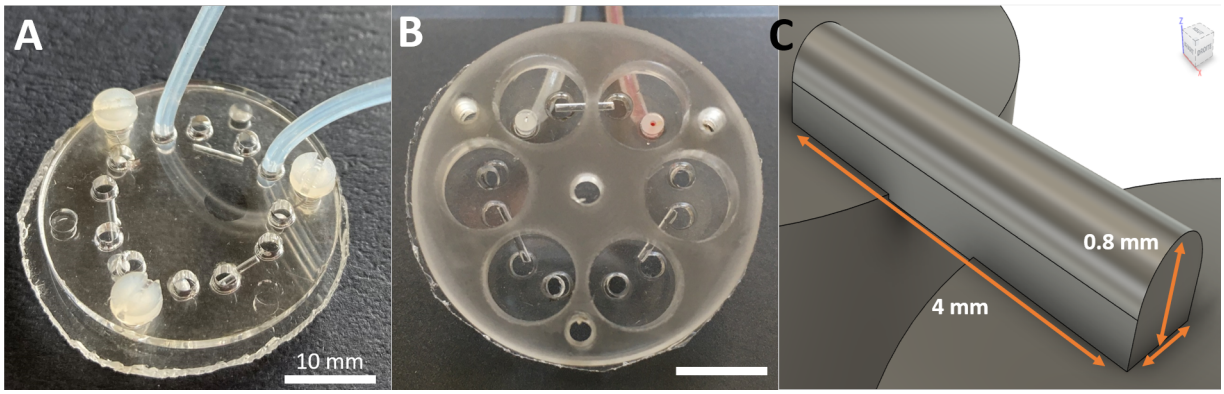

FIGURE 2.5: Cover for the microfluidic mode. (A) Top view. (B) View from the bottom when the cover is screwed on the ring. (C) Schematic view of the channel that bridges 2 wells.

to lower the chamber volumes. The final volumes of the system in the 2 modes are the following:

- For the static mode, each well volume is at minimum 250 µl; the volume can be increased if necessary by playing on the PDMS disk thickness.
- For the microfluidic mode, the volume is determined by the height of the ring. After the height reduction (from 10 to 5 mm), the volume is 250 µl. This is the minimal height and volume possible due to 2 reasons: a minimal height of about 3 mm is required to allow the screwing, and the reduction is limited by the technique, which consists in eroding the ring with a rotating tool getting closer of the piece. This is called a lathe, and the technique requires to hold sufficiently the piece for safety, which corresponded here on holding on 5 mm over the 10 mm height.

This system allows to validate the requirements (1) (2) (3) as listed in section 2.1.2.1. The final prototype chip is showed in the Fig. 2.6 in panels (A) and (B). The panels (C) and (D) show this same chip when placed inside the MCS pre-amplifier.

2.1.2.3 Chip fabrication

The MEA we used as microfluidic substrate is the 60-6wellMEA200/30iR-Ti-rcr from MCS. Usually the macrolon resin ring creating the wells is also provided with the chip at this reference, glued on the MEA substrate thanks to a silicone glue. But for this work, the rings were ordered separately to customize them prior to gluing them using PDMS:

- The ring height was reduced using a lathe from initial 10 mm to 5.3 mm. The surface smoothness obtained with this technique is sufficient to ensure no leakage when assembling the chip
- 3 holes were drilled and tapped to screw the cover. The drilling was made using a 2 mm diameter drill bit, and the tapping with a manual tap.

The cover is a 2 mm-thick PMMA piece, whose holes for the screws, wells (static mode chip), and tubings (microfluidic mode) were laser cut.

The PDMS joint of the microfluidic mode was made in 1:10 w/w (curing agent : silicon) PDMS (Ref SYLGARD™ 184 Silicone Elastomer Kit ; Dow corning), poured in a petri dish.

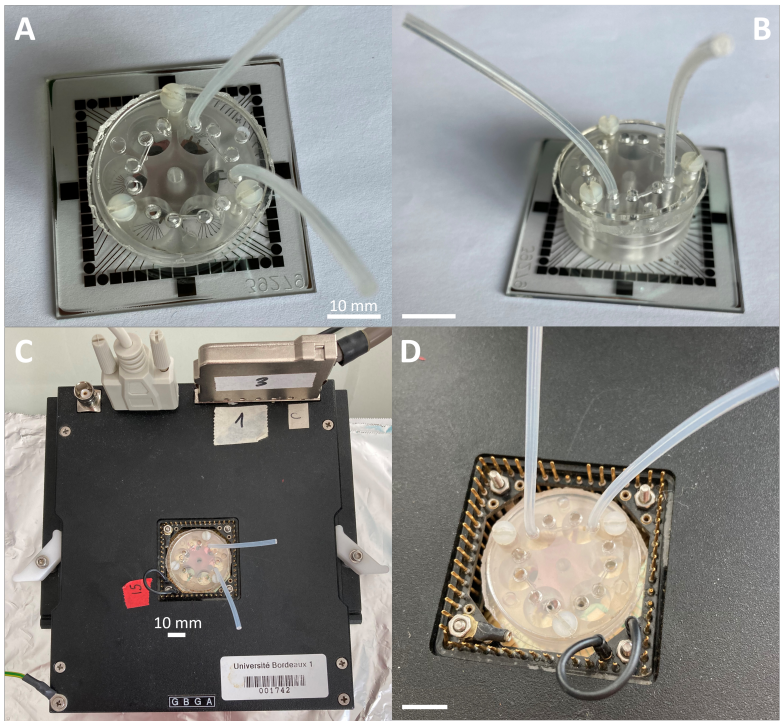

FIGURE 2.6: chip n°1 in the microfluidic mode. (A) and (B) top and profile views. (C) and (D) the chip n°1 in the MCS amplifier.

We used a petri dish to exploit its transparency: a draw of the future wells was printed and placed at its back to correctly place pieces of PEEK tubings (Ref PEEK Yel 1/32 x 0.007 inch 1577, IDEX) of 2 mm length, which will further be the channels between wells. The PDMS was cured 6 hours at 60°C, corresponding to the highest temperature recommended for the plastic dish's manufacturer. Once the PDMS was reticulated, the PEEK tubings were removed from the PDMS with a scalpel, creating the channels. The holes for the screws and the tubing were drilled using 2 mm diameter puncher. Finally the PDMS disk was cut using a scalpel. The screws were Nylon (Ref RS PRO Nylon Hexagon Head Machine Screws, RS Components), cut to fit the height of the ring.

Prior to using this technique, we tried 3D printed molds that were intended to directly shape the disk of PDMS and the holes for tubings. We tested different 3D printing techniques like PLA (PolyLactic Acid) filament (MakerBot replicator 2 printer), that did not show satisfying surface finishing ; and resin (Mars Pro Elegoo 3D printer) showing a better surface finish and Z axis resolution (see Fig. 2.7, panels (A) and (B), respectively left and right). We also tested 2 generations of designs, a first more elaborated (see Fig. 2.7, panels (A) and (B)) that was intended to be placed in a petri dish as shown in the panel (A) of Fig. 2.7, and have PDMS poured inside the ring. However the PDMS was hard to turn out, therefore a second generation was designed, intended to simply create marks to guide the puncher and the cut (Fig. 2.7, panel (E)). Once more the removal from the tin was not perfect due to bad PDMS curing. This issue is mentioned in the literature [Venzac et al., 2021], and can be solved by precisely setting the values of temperature/duration of heating and UV exposition for a perfect reticulation of a given resin. Due to the complexity of this procedure, we selected the final solution previously explained for the prototyping of the chip n°1, that provided satisfying results despite its simplicity.

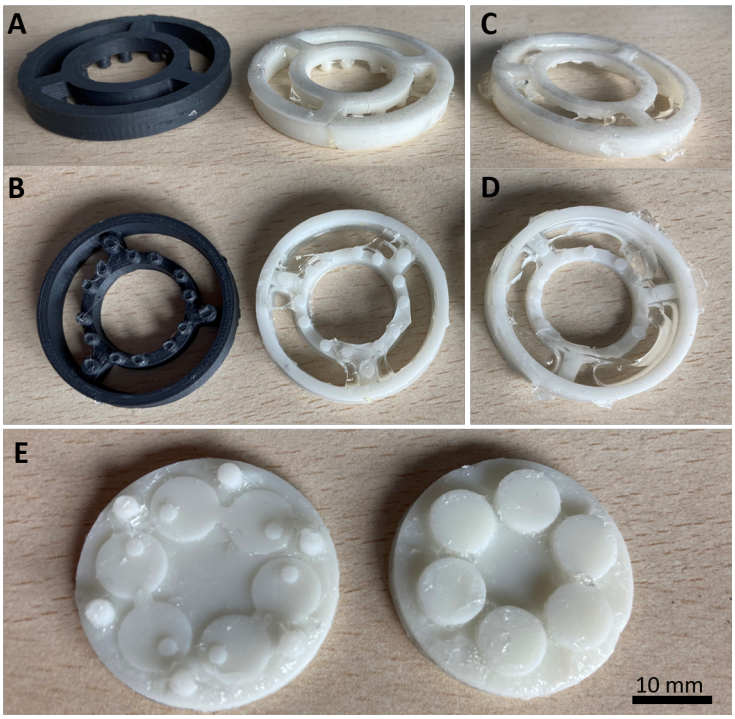

FIGURE 2.7: 3D printed molds tested prior to the final molding technique using a petri dish and PEEK tubings. (A) first generation, filament on the left, resin on the right, top view. (B) First generation, filament on the left, resin on the right, bottom view showing the pillars. (C) Second generation, top view. (D) Second generation, bottom view showing the pillars. (E) Third generation, for the microfluidic mode (left) and the static mode (right).

2.1.2.4 Chip validation

Watertightness and usability assessement The aim of the test was to check the sealing of the chip :

- Are 3 screws sufficient to completely seal the cover ?
- Does the surface finish of the ring top cause any leaks ?
- Are tubing connections watertight ?
- Usability of the chip i.e. ability to screw and unscrew easily the covers

The test was realised by injecting distilled water colored with Phenol red, a colored pH indicator frequently used in cell culture. The flow was pressure-driven thanks to a pump and pressure controller (MFCS-EZ series, Fluigent). Different pressures were tested over the possible range of the pressure controller (0-1 bar). To check for leaks at the inlet and outlet, a microscope camera (Moticam 5, Motic, Hong Kong) was focused at the critical level of the tubing connections. To asses watertightness between the ring and the cover, the chip was immersed in pure distilled water, which was visually checked for unwanted coloring.

The leakages tests were successfully carried out, showing a good usability of the system, and in addition no leakages.

Simulation-assisted validations Criteria (1), (2), and (3) were satisfied by design. Criteria (4), (5) and (6) remain to be checked. The high total volume of the microfluidic mode is

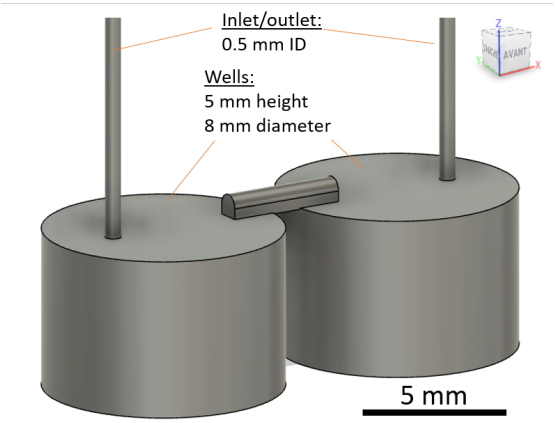

(A) CAD representation of the domain for the simulations of chip n°1 (presented in section 2.1.2.2), with dimensions (Internal Diameter (ID)). The dimensions of the channel between wells are provided in Fig. 2.5.

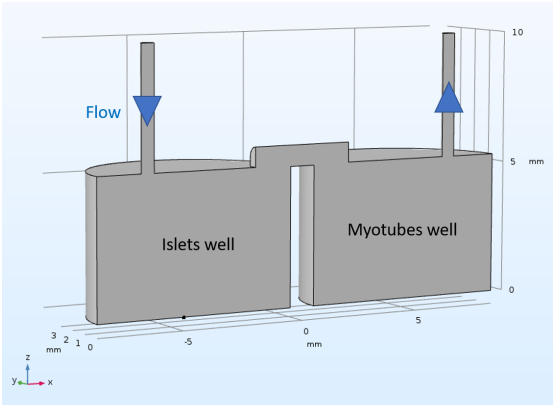

(B) Geometry used in COMSOL simulation; it is half of the chip, cut at the symmetry plane.

FIGURE 2.8: Geometry used for all simulations.

particularly to validate, checking they do not cause threatening slower dynamics and over-dilution of molecules below physiological ranges, as explained earlier.

For that matter, we used simulation tools that provide access to physical properties in the chip (shear-stress near the cells, steady-state concentrations of diluted species, concentration dynamics) that cannot be experimentally measured as precisely in space and time. These properties, further described below, were simulated using COMSOL Multiphysics with the Microfluidics module (license nbr. 8079902).

Description of the simulation design The future experiments using the MOoC will rely on changing the glucose concentration in the chip, switching from hypo to hyperglycemia conditions, and observe the regulation of the glucose concentration by cells interactions. Then the simulations observed the dynamics at the injection of a new glucose concentration, as well as the insulin concentration that can generate secreting islets in this chip. We also checked the fact the shear stress at the level of the cells is low.

To ease the study, 2 separated simulations were done: the first one predicts the dynamics of glucose when infused in the chip; the second one simulates the dynamics of insulin secreted by the islets. Note that shear stress only depends on fluid velocity and chip geometry; since these remained unchanged between simulations, the study of shear stress could be done in either insulin or glucose simulation.

The first step in setting simulations is to draw the domains where physical phenomena will be simulated. It corresponds to the volume of liquid in the chip described in section 2.1.2.2 p. 34, as represented in Fig. 2.8a (using Autodesk Fusion). As the geometry is symmetrical, only half of the geometry was simulated using COMSOL, using mirror symmetry to reduce model size and save computation time (see Fig. 2.8b). This *geometry*, is defined identically for insulin-, glucose-, and shear stress-oriented simulations.

For the physics, 2 physics interfaces were used: *Laminar Flow* and *Transport of Diluted Species*, both included in the Microfluidics module.

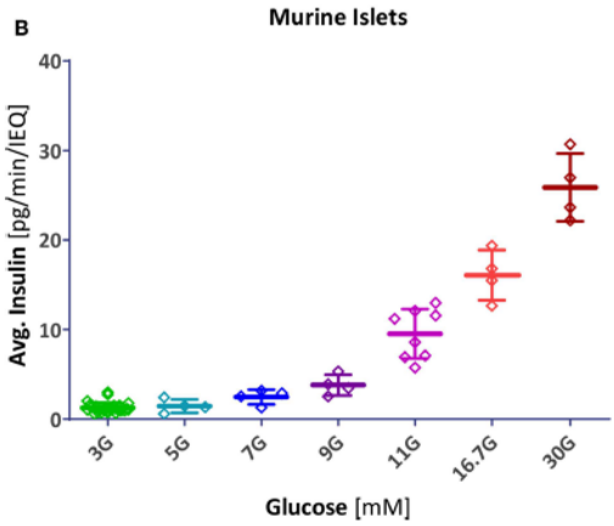

FIGURE 2.9: Original caption from [Alcazar and Buchwald, 2019]: "Scatter plot of insulin secretion in response to different glucose concentrations. Data points represent the average insulin secreted by each mouse islet sample (pg/min/IEQ; first- and second phase combined). Lines indicate group average and SD."

The *Laminar Flow* module set the physical equations for laminar flow in the system. In our simulations, it helped study the effect of inlet flow rates on molecule dynamics. A parametric analysis was performed at flow rates of 25 µl/min, 100 µl/min, 300 µl/min, 500 µl/min and 1000 µl/min. The values were chosen to span the range of low to high flow rates, relative to the volume of the chip (250 µl per well).

The *Transport of Diluted Species* was used to model molecule dynamics, and the following parameters were set:

- The **diffusion coefficients** used for insulin and glucose were respectively $1.50 \times 10^{-10} m^2.s^{-1}$ [Patel et al., 2021] and $4 \times 10^{-10} m^2.s^{-1}$ [L. Glieberman et al., 2019].
- The **initial concentration** of the system was 0 for insulin simulations, and 3 mM for the glucose simulations.
- For glucose simulations, an inflow of 11 mM glucose solution was set.
- Concerning insulin simulations, a point mass source was created at the bottom middle of the islet chamber to represent the insulin secretion of islets. The secretion rate of this point is defined by multiplying the secretion rate of a single islet by the number of islets studied. The secretion rate of a single islet was derived from [Alcazar and Buchwald, 2019], where islet secretion was measured in response to glucose steps (see Fig. 1.6). In this study, the results were used to build a complex COMSOL model taking into account oxygen and glucose effects on the islets, as well as biphasic insulin secretion. Since our simulations targeted to study steady-state behaviour, and that the average secretion rates actually almost corresponds to the second phase secretion rate, we used the average secretion rate to model our islets secretion (see Fig. 2.9). It is estimated at 10.4×10^{-12} $pg.min^{-1}.IEQ^{-1}$ for a step between 3 to 11 mM of glucose. Using 5 807.57 $g.mol^{-1}$ as insulin molar mass, the final average secretion rate used is 2.98×10^{-17} $mol.s^{-1}$.

Simulation results ***Simulation results of shear stress***

These simulations assess the shear stress in the chip, to validate criterion (4) and (7) p. 32. The shear-stress is post-processed from the velocity field of the fluid, as it is a quantitative marker of sharp velocity gradients. It is calculated using the following formula [L. Glieberman et al., 2019]:

$$\tau = \mu \times \nabla \vec{u} \tag{2.3}$$

otherwise written, in COMSOL syntax :

$$sqrt((d(spf.U,x)*mu)^2+(d(spf.U,y)*mu)^2+(d(spf.U,z)*mu)^2) \tag{2.4}$$

With *mu* a constant whose value was set to the dynamic viscosity of water ($0,69 \times 10^{-3}$ *Pa.s* at 37 °C).

The domain was cut into slices on which shear stress was represented by color/rainbow scale, as shown in Fig. 2.10. This revealed 2 types of shear stress distribution, depending on flow rate : below 300 µl/min (included), shear stress at the tubing and bridging channel is much higher than shear stress inside the well (see Fig. 2.10a panels (a) and (b)); above 500 µl/min, shear stress increased at the bottom, as visible in Fig. 2.10b panel (a), that shows a pronounced shear stress profile at 1000 µl/min. At these flow rates, the flow reaches the bottom of the well (see Fig. 2.10b, panel (c)) and splits bottom, which explains the ring-shaped distribution of the shear stress there (Fig. 2.10b panel (b)). Note that shear stress is present at flow rates below 300 µl/min (see Fig. 2.10a panel (c)).

To assess quantitatively shear stress near cells, it was measured along a segment, placed at the bottom of the wells, in the center (crossing the area of highest shear stress), as illustrated in Fig. 2.11a. The measured shear stress is shown in Fig. 2.11b, and the maximum shear stress values are summarized in Fig. 2.11c for every flow rate.

According to Fig. 2.11c, the limit shear stress for islets is only exceeded for a 1000 µl/min flow rate. Concerning the myotube well, shear stress is consistently lower than the islet well and never reaches the limit of tens of mPa.

In conclusion, this simulation showed that the chip geometry generated shear stress satisfying criterion (4) for flow rates below 500 µl/min (although the actual upper limit of flow rate may be higher, as shear stress near the islets is 3 mPa whereas the limit value is 6 mPa). Then high volumes reduce efficiently the shear stress.

However, even at flow rates below 500 µl/min (included), shear stress profile is not homogeneous inside either well. This is a limit of this geometry, as the cells will not be exposed to an homogeneous environment.

Simulation results about glucose concentration dynamics

The simulations reported below aim at validating criterion (5), stating that the concentration of a solution injected in the chip must stabilize rapidly (in under 10 min) and be homogeneously distributed near the cells in steady-state. To that end, the glucose turnover was simulated when a 11 mM glucose solution was injected in a chip resting at 3 mM glucose.

As for the shear stress, representations with 2D slices of the domain were made first to observe qualitatively the dynamics of glucose when a new medium at an other concentration was injected (see Fig. 2.12). Once more, we observe 2 types of dynamics depending on

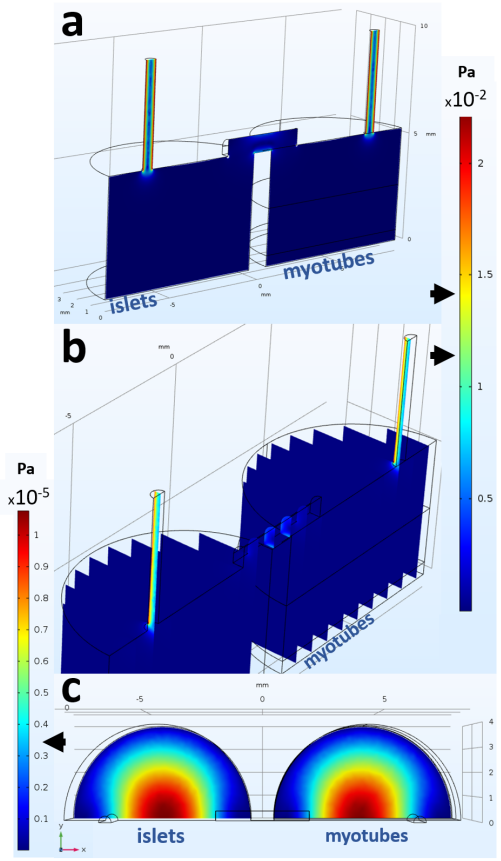

(A) (a) (b) and (c) shear stress at 25 µl/min (representative also for 100 µl/min and 300 µl/min), from different views. As expected the shear stress is greater in the tubings and the channel bridging the wells.

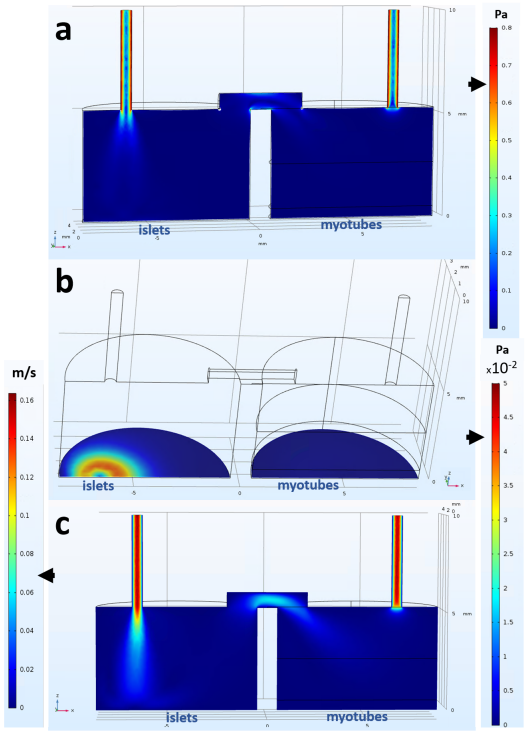

(B) (a) and (b) shear stress at 1000 µl/min (representative also for 500 µl/min). At those higher velocities, the shear stress is more important at the bottom of the well. The particular profile of (b) is explained by the velocity profile in (c).

FIGURE 2.10: Qualitative analysis of shear stress for chip design 1, with 2D slices representation, for the different flow rates explored.

the flow. The highest flows (500 µl/min and 1000 µl/min) show a quicker dynamic with a flux bringing the glucose toward the bottom of the well, while for the lowest flows (25, 100, 300 µl/min) the travel of the glucose sounds to be more diffusive as the progression of glucose is isotropic (meaning there is no privileged direction) in the well.

Then the glucose concentrations were studied quantitatively by assessing transient response of concentration at the bottom of each well. This evaluation was made using probes, placed at the bottom middle of each well (see Fig. 2.13a). The results measured by the probes are shown in Fig. 2.13b. The concentration is converging with a good amortisation, and the last 5% (from 10.5 mM to 11 mM) are greatly contributing to the transient time. Thus we consider the steady state as the first time the concentration is reaching 95% of the final value, that is 10.5 mM, called the 95% response time. Fig. 2.13c reports all response times for each well and every flow rate.

At highest flow rates (500 µl/min and 1000 µl/min), the final concentration was reached in less than 5 min. Concerning the lowest flow rates (25 µl/min and 100 µl/min), it was from 30 min to 90 min. This is too slow for the experiment, especially because this concerns the middle of the well where the final value is reached first. The maximum response time

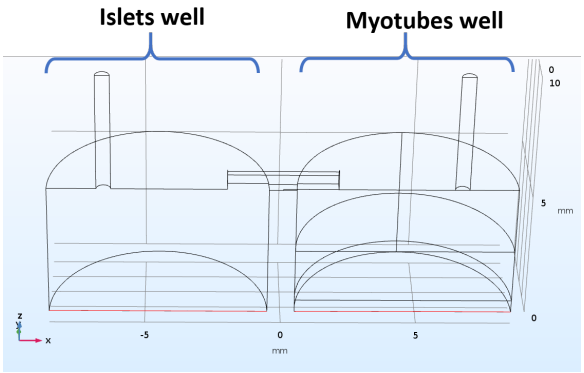

(A) Line (in red) along with the shear stress is calculated as in the Fig. 2.11b. This line is called a *Cut Line* in the COMSOL formalism.

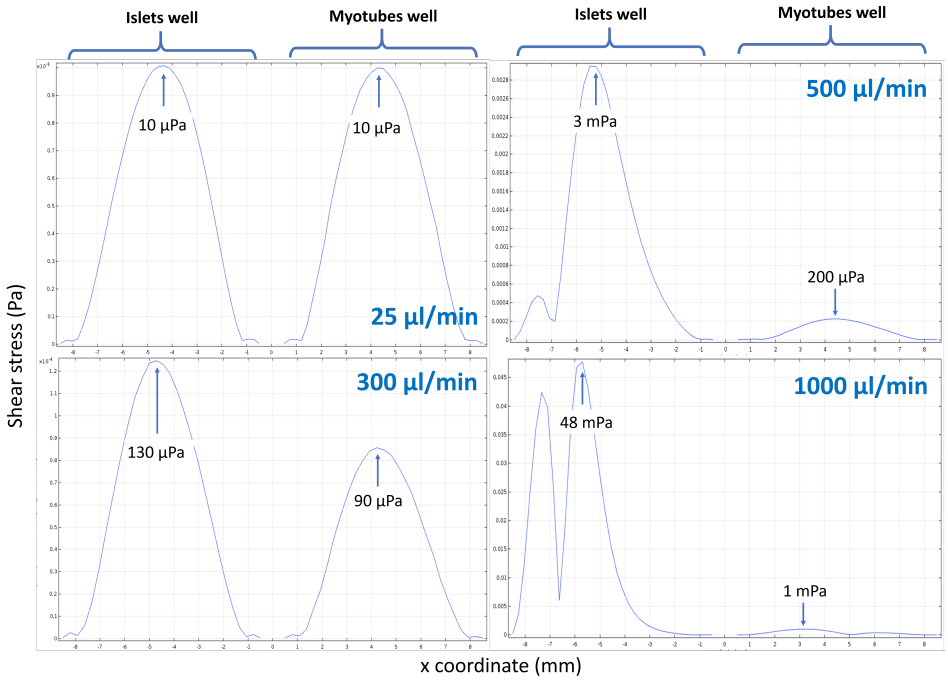

(B) Shear stress along the *Cut Line* defined in Fig. 2.11a, for the different flow rates.

Flow rate (µl/min)	Maximum shear stress	
	Islets well	Myotubes well
25	10 µPa	10 µPa
100	48 µPa	43 µPa
300	130 µPa	90 µPa
500	3 mPa	200 µPa
1000	48 mPa	1 mPa

(C) Table summarizing the maximum values of shear stress in both wells for the different flow rates of the study.

FIGURE 2.11: Shear stress results for chip design 1, calculated along a line at the symmetry plane of the geometry, at the level of the cells, for the different flow rates of the study.

set for the experiment (10 min) was reached at a 300 µl/min flow rate.

So for flow rates above 300 µl/min (included), the time to change the glucose concentration can be considered reasonable as full filling the requirement (5). However we see the concentration over the bottom surface of each well (near the cells) is not homogeneous, especially for cells bordering the well walls. This is a limitation that in intrinsic to the chip geometry and solving it would require a complete re-design.

Simulation results about insulin concentration and dynamics

In these simulations, we analyzed how the number of islets secreting insulin and flow rate influence insulin concentration in the device.

The targeted range of insulin concentration was between 300 pM to 1 nM, corresponding to the level after a meal for humans. We verified how many islets are required to attain the targeted concentration, thus checking they are in the 10-150 range defined in (6) p. 32. If a steady state can be reached at the target range of concentrations, we also need to verify the time needed to reach it (95% response time). This corresponds to the criterion (5).

First, stationary studies were conducted with different *(number of islets, flow rate)* couples, to assess *if* and *what* steady state concentrations can be reached. The flow rates tested were as previously (25 µl/min, 100 µl/min, 300 µl/min, 500 µl/min and 1000 µl/min) and we tested the extreme number of islets (10 and 150).

This time, to have an overview of insulin distribution in the chip, we represented isosurfaces of insulin (see Fig. 2.14a). Based on the presented results, insulin appears to mainly follow the flow going toward the myotube well. In the myotube well, insulin appears to preferably flow to the bottom, generating higher insulin concentration near the myotubes. This is a very favorable situation, as it maximises the chances to reach sufficient concentrations.

2D slices were plot at the bottom of the 2 wells to specifically study the concentration of insulin on the culture area. Upon comparing the 2 wells in Fig. 2.14b the insulin concentration appears higher near the islets than near the myotubes, which remains true for all flow rates. In a given well, the concentration is not homogeneous neither for flow rates between 25 to 300 µl/min included (see Fig. 2.14b). For example at 10 islets & 25 µl/min there is almost one order of magnitude between the extreme concentrations. However, when the flow rate is raised to 500 µl/min or 1000 µl/min, the concentration becomes homogeneous. This can be quantitatively verified using a domain probe sensing the concentration in the bottom 25 µl of the myotubes well (a 500 µm-high cylinder above the myotubes, representing their close environment), as well as a probe at the middle of the myotube well (see Fig. 2.15a). The Table in Fig. 2.15b shows the concentration in the 25 µl is the same as the concentration sensed by the probe at the middle of the myotube well for the highest flow rates, and the difference increases when the flow rate decreases.

If now we focus on the steady state values themselves of Fig. 2.15b, we see that despite high volumes, as few as 10 islets were able to produce higher than physiological concentrations at the probe. The simulations showed that it is possible, with different sets of *(number of islets, flow rates)*, to reach different levels of the physiological range. Indeed, with 10 islets, flow rates of 300 µl/min and 500 µl/min allows to reach respectively the high and the low limits of the physiological range. The flow rate can then be tuned between 300 and 500 µl/min to reach a precise target concentration. As the microfluidic setup can modulate flows rates as precisely as 1 µl/min, we have excellent resolution to tune the concentration.

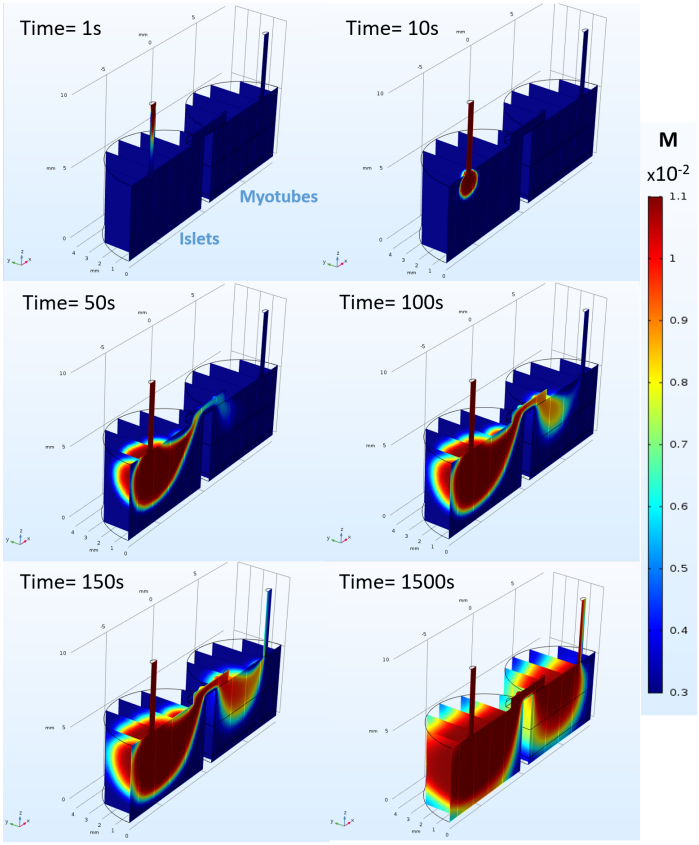

(A) Glucose concentration evolution at 25 µl/min (representative also for 100 µl/min and 300 µl/min).

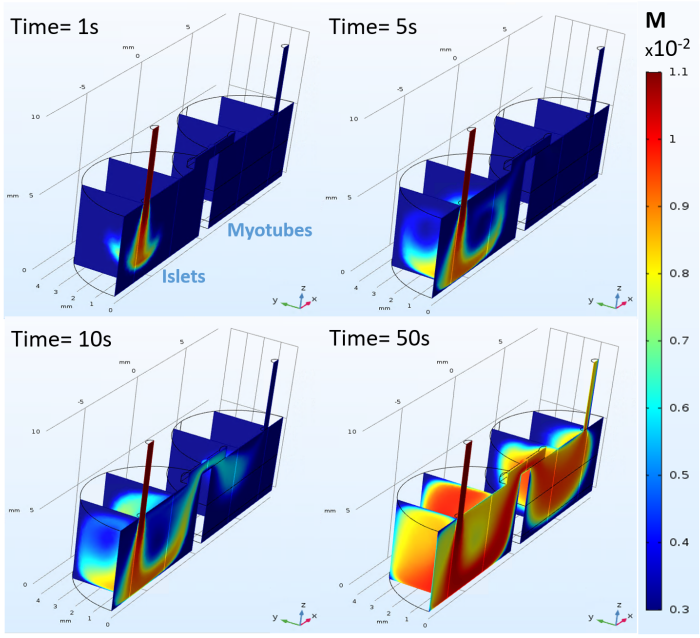

(B) Glucose concentration evolution at 1000 µl/min (representative also for 500 µl/min).

FIGURE 2.12: Qualitative glucose dynamics in the chip n°1 for the different flow rates of the study.

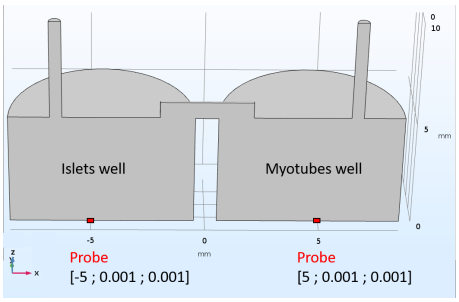

(A) Probes coordinates in the geometry, at the bottom of the 2 wells.

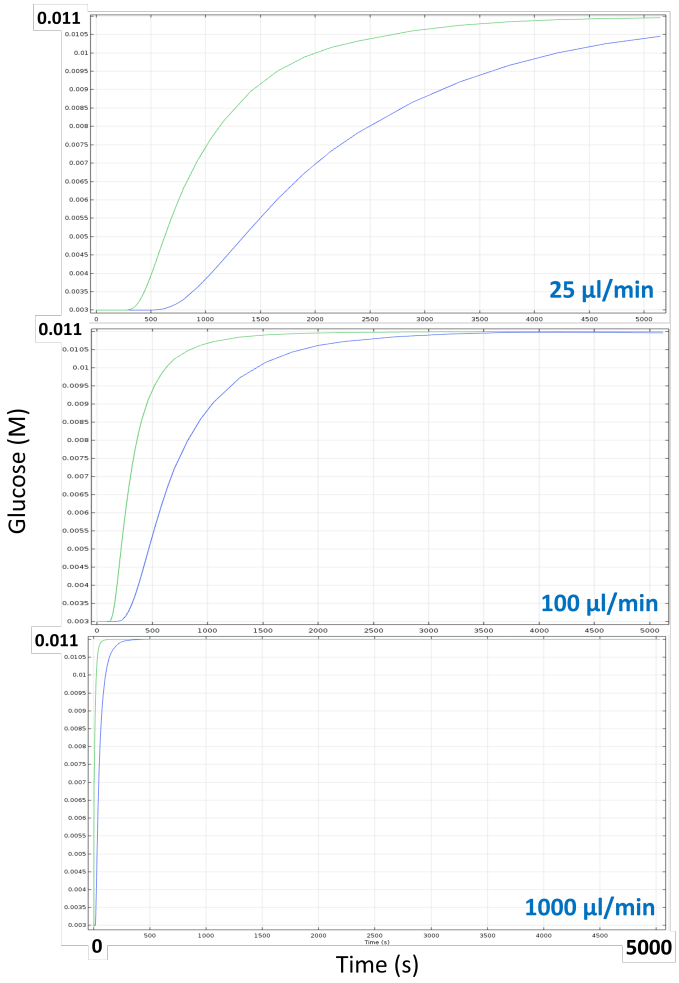

(B) Glucose concentration over time monitored by the 2 probes (green islets well, blue myotubes well), for 3 different flow rates studied.

Flow (µl/min)	t_{CV} islets chamber (s)	$t_{10.5mM}$ islets chamber (s)	t_{CV} myotubes chamber (s)	$t_{10.5mM}$ myotubes chamber (s)
25	6000	2800	>6500	5500
100	2500	850	4000	1850
300	900	180	2000	600
500	450	90	1000	300
1000	200	30	500	130

(C) Table summarizing the results of the probes monitoring glucose in the bottom of the 2 wells. The convergence is assess using 2 metrics: the time to reach the steady state, t_{CV}, and the time to reach 95% of the final value that is 10.5 mM, $t_{10.5mM}$.

FIGURE 2.13: Glucose concentration dynamics results for chip design 1, at probes placed at the bottom middle of the wells, for the different flow rates.

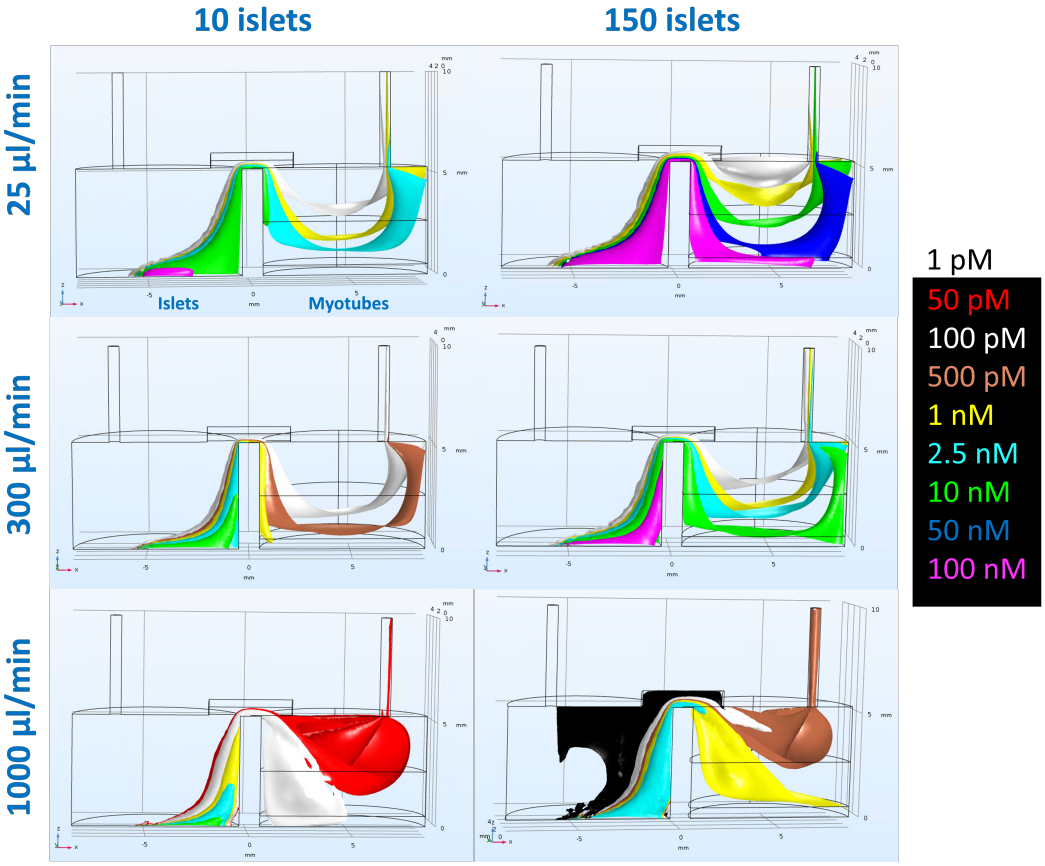

(A) Isosurfaces of insulin at steady state for several flow rates and number of islets.

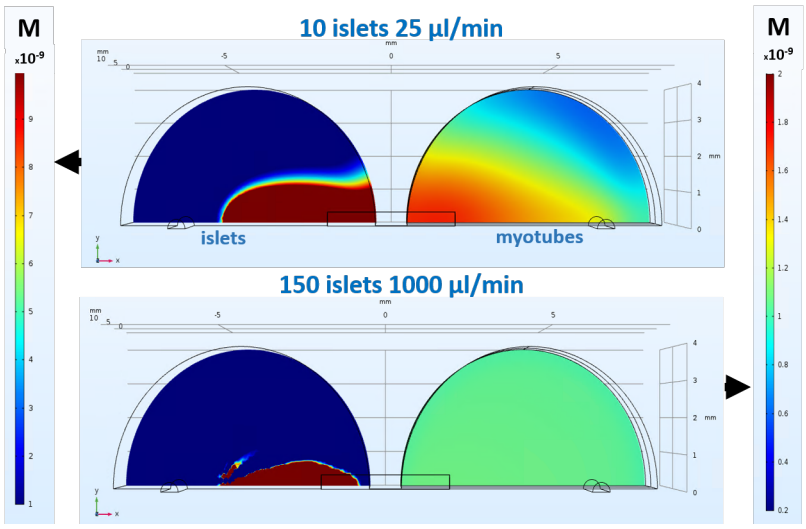

(B) Rainbow view showing the insulin concentration profile at the bottom of the 2 wells, with 10 islets & 25 µl/min (similar profile at 100 µl/min and 300 µl/min whatever the number of islets) and 150 islets & 1000 µl/min (similar profile at 500 µl/min whatever the number of islets).

FIGURE 2.14: Different representations of the profile of insulin concentration at steady state in the chip n°1.

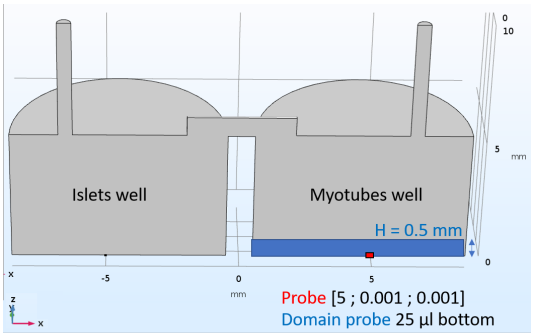

(A) Probes used in the quantitative study of insulin. A 25 µl domain is created at the bottom of the myotubes well to monitor the insulin in the neighborhood of the myotubes: it corresponds to the 500 µm height medium above the cells.

	Flow rate (µl/min)	25	100	300	500	1000
10 islets	Point probe myotubes chamber	7.3 nM	2.8 nM	880 pM	290 pM	99 pM
	25 µl domain probe myotubes chamber	5.6 nM	2.1 nM	740 pM	240 pM	94 pM
150 islets	Point probe myotubes chamber	109 nM	42 nM	13 nM	3.9 nM	1 nM
	25 µl domain probe myotubes chamber	84 nM	32 nM	11 nM	3.5 nM	1 nM

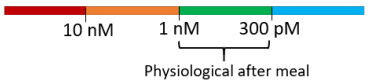

(B) Table summarizing the insulin concentration monitored by the 2 probes in the myotube well. The color corresponds to which range is situated the insulin concentration comparatively to the physiological range.

FIGURE 2.15: Insulin concentration study at steady state in the chip n°1, for the different couples of islets number islets and flow rate.

Now a critical point highlighted in the glucose simulations is the time to reach a steady state (95% rise time). Due to the extensive time and memory demands of these transient simulations, we opted to focus exclusively on the limited set of previously established parameters: 300 µl/min and 500 µl/min, with 10 islets. The probes used to record transient concentration were identical to those used in the stationary study.

As illustrated in Fig 2.16a, the system is not well dampened and exhibits overshoots and an oscillatory behaviour. Within the 5000 s window of the simulation, the concentration has not stabilized in any of the flow rates of interest. However the amplitude of the oscillations relatively small (less than 10% of the final value). Then the time of convergence is considered the first time the curve reaches the values found in the stationary study. The steady state concentration reached by the stationary simulations is less than 10% higher than the concentration range reached after 5000 s of transient simulations, therefore considered that both stationary and transient simulations concurred, and that the metric proposed was relevant to assess the performance of the system. Table 2.16b shows the resting value is first reached in 1400 s at 300 µl/min and in 1000 s at 500 µl/min. This satisfies the limit we set at 30 min.

Conclusions drawn from the simulation campaign

The simulations were intended to validate criteria (4), (5), (6) in the currently proposed chip, called chip n°1. The results of the simulations showed it satisfied most of the criteria, given the appropriate flow rate and number of islets. The shear stress constraint limits the flow below 1000 µl/min (excluded). To limit the transient time in glucose, the flow should be above 300 µl/min (included). In the remaining range of flow rates (from 300 µl/min to 500 µl/min), as few as 10 islets can generate insulin to reach the complete span of physiological concentrations.

However, even at these flow rates, the homogeneity constraint is not met (criteria (7)): the distribution of shear stress, glucose concentration between the 2 wells and inside one well, and insulin concentration between the 2 wells are inhomogeneous.

Experimental validation of simulated insulin secretion Before concluding the analysis of chip n°1, it is important to experimentally validate the simulations in order to ensure

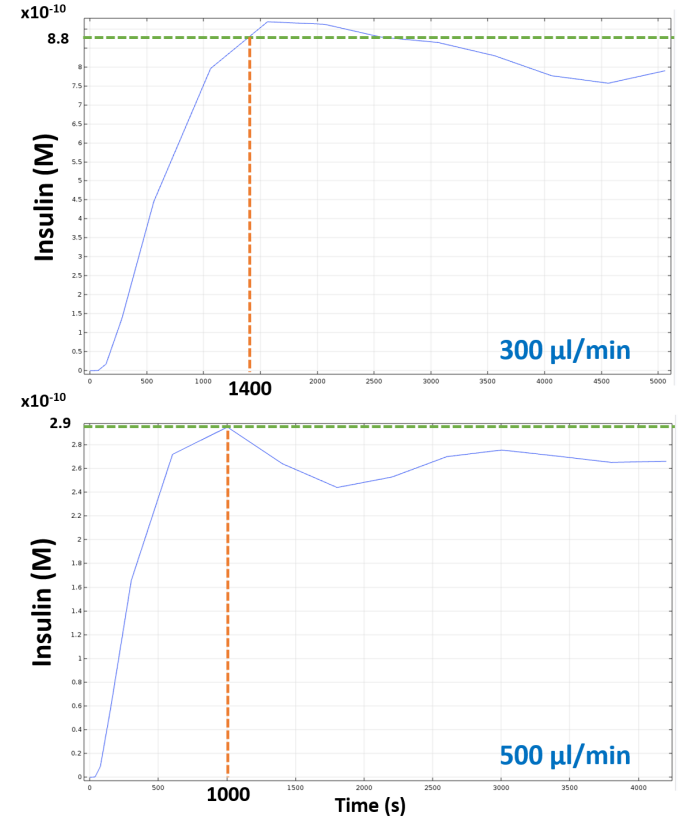

(A) Insulin concentration over time provided by the point probe at the bottom of the myotubes well. The way to determine the end of the transient time is drawn.

Flow rate (µl/min)	25	100	300	500	1000
10 islets	*Not relevant (Stationary study)*	*Not relevant (Stationary study)*	880 pM reached at **1400s**	290 pM reached at **1000s**	*Not relevant (Shear stress study)*
150 islets	*Not relevant (Stationary study)*	*Not relevant (Stationary study)*	*Not relevant (Stationary study)*	*Not relevant (Stationary study)*	*Not relevant (Shear stress study)*

(B) Table summarizing the time to reach the steady state, defined as the first time the stationary value determined in Table 2.15b is reached.

FIGURE 2.16: Transient results for 10 islets & 300 µl/min or 500 µl/min.

agreement between the simulation predictions and actual experimental results. Experimental validation of the simulation of islet secretion was especially important because islets in our culture conditions may have a different secretion rate than those used in [Alcazar and Buchwald, 2019].

Thus, we proposed an experimental validation of the insulin simulations. The aim was to assess if the insulin concentration in a prototype of the chip could reach, after a certain perfusion time, the same concentration as predicted by the simulation, for a given flow rate and number of islets.

This secretion experiment was conducted concurrently with the design of the simulations. It used C57Bl6J mouse islets, in a prototype of the chip described in section 2.1.2.2 whose fabrication is described in section 2.1.2.3 except that the substrate is a glass petri dish instead of MEA. In this instance, dissection yielded an unusually low number of islets, and 79 were seeded. The well was filled with 250 µl of islets medium (composition described in the section 2.1.3.2, in the Fig. 2.19 p. 54), and the islets cultured for 4 days. The day of the secretion experiment, the medium was replaced by a buffer described in 2.1.2.1 p. 32, with 3 mM of glucose to starve the islets for 45 min. This medium was supplemented with 0.2% BSA to prevent insulin adhesion to the surfaces of the tubings. When the 45 min were over, the chip was plugged to a microfluidic setup composed of a pump, pressure controller (MFCS-EZ series below 2 mbar) and flow rate meter (M size) (all from Fluigent), which has been previously coated with the future injected solution, which was the buffer at 11 mM of glucose and 0.2% BSA. The flow was maintained 30 min at 25 µl/min. After that duration, the flow was stopped to collect medium at the bottom of the myotube well, using an Hamilton Syringe. Collection was performed without opening the well, taking advantage of perforations in the cover inherited from former designs. A sample of 50 µl was collected for ELISA dosing of insulin (ref 10-1247-01, Mercodia, Uppsala, Sweden). This volume, larger than the minimum 10 µl required for a single measurement, ensured that multiple measurements could be performed at different dilutions (2, 1, 1/2, 1/4) that could maximize the odds of falling within the narrow measurement range of the ELISA assay.

As the simulations were not yet over at the time of this experiment, the number of islets and flow rate were chosen according to the availability of islets, and to maximise the concentration of insulin at the bottom of the myotube well. Indeed without simulations, it was already established that decreasing the flow increase insulin concentration. Once the simulation tool was ready, a simulation was run with identical experimental parameters (79 islets and 25 µl/min). A 50 µl domain was created at the bottom of the myotubes well to mimic collection volume, and a domain probe was attached to this domain to monitor insulin concentration over time.

The results provided by the simulations and the dosage are in accordance. At 1800 s after starting the flow, the insulin concentration in the bottom 50 µl of the myotube well was 4 nM in simulation (see Fig. 2.17), and 2.7 nM experimentally, as dosed by ELISA. Although this constitutes a 33% relative error compared to simulation and may seem prohibitive, this figure must be put into perspective with the amount of variability that occurs in biological systems; this is in fact very satisfactory as both measurements are within the same order of magnitude, and is enough to consider simulation as a viable scaling tool for MPS design.

2.1.2.5 Discussion

We demonstrated that simulations can viably reduce experimental assays, which usually are numerous to test several designs and repeat several times experiments to acquire significant results, while face usual delays of biological experiments (cell death and variable behaviour,

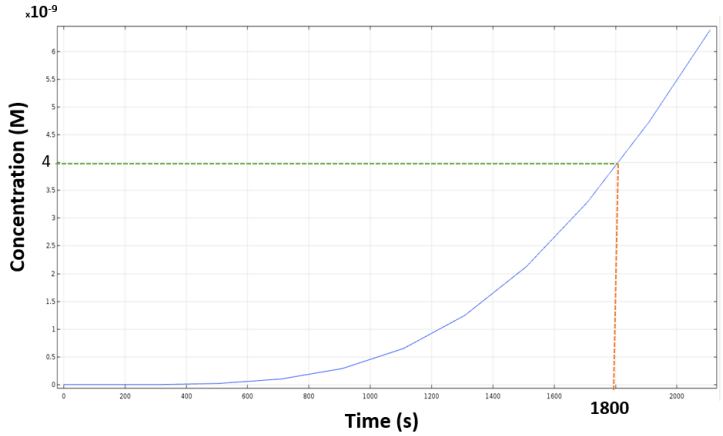

FIGURE 2.17: Insulin concentration over time in the 50 µl of the myotubes well bottom, when 79 islets are in the islets well and the flow rate is 10 µl/min.

practical issues). Simulation must however not be considered as a fully quantitative tool with exact predictive capabilities, as it is only a simplified model of both physics and biology.

The designed chip (chip n°1), can satisfy the criteria regarding usability and conditions of use (criteria (1), (2), and (3)), but also regarding physics and biology (criteria (4), (5), and (6)). The latter have been studied using a multiphysics simulation software, which was itself experimentally validated thanks to concurrent *in silico* and *in vitro* experiments. However there is a lack of spatial and temporal homogeneity in the chip (criteria (7), (8)), and precisely determining the acceptable delay or lag is challenging. As the objective of MPS is to control cell environment to relate it to cell behaviour, this lack of homogeneity is a serious limitation.

The range of glucose variations that the LHCN-M2 could provide in this chip has not been assessed in this study, due to the lack of glucose uptake model for the LHCN-M2 myotubes in the literature. It is a question of interest as a potential risk exists in the ability of myotubes to induce sufficient glucose variations. Indeed the flow rates of interest (300-500 µl/min) are significant relative to the volume of the chip (250 µl), and the volume of the chip itself is great. In addition the concentration variations are expected to be reduced by the higher velocities at the top of the well that induce a limiting phenomenon, where the medium flowing out from the chip is constituted by medium which has not been near the myotubes, as seen in Fig. 2.18. A solution to this could consist in lowering the outlet to the level of the myotubes, on the side wall of the well. However, the space left around the MEA ring by the MCS amplifier is insufficient to access side outlet (see Fig. 2.6). With no recourse to simulation due to the unavailability of uptake data in the literature, experiments with LHCN-M2 should be conducted to alleviate these concerns and assess to which extent they impact the system.

2.1.2.6 Concluding remarks on investigations about the chip design

In conclusion, **chip n°1 constitutes, according to *in silico* study, a well-performing candidate for the MOoC** in regards to the criteria defined in section 2.1.2.1 p. 32, despite the limitations listed in the discussion. The ***in silico* study has been validated by *in vitro* experiments** at the level of the insulin secretion. Experimental validations are still required with LHCN-M2 myotubes to assess the levels and dynamics of uptake. As the limitations of

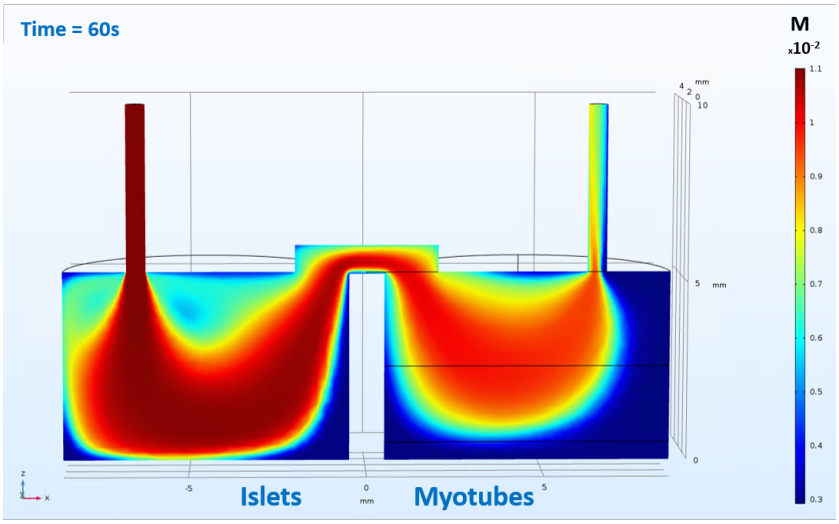

FIGURE 2.18: Glucose concentration 2D slice of the chip showing the medium at the outlet is constituted by mainly a solution from the islets well not passing by the myotubes environment.

the chip concern a lack of homogeneity in fluid parameters (species concentration at steady-state and shear stress), **chip geometry should be improved** in future iterations to promote homogeneity and dynamic control on cell environment.

The approach used in this section 2.1.2.4 of co-simulating physics and biology for MOoC scaling is not so common in the state of the art. In the context of MPS, we found 2 works that use insulin secreting islets simulations, based on the model in [Alcazar and Buchwald, 2019]: [Patel et al., 2021][L. Vanderlaan et al., 2023]. However these 2 works do not use the insulin secretion simulations in a *functional scaling*, as they are OoCs. They rather respectively confirmed the impact of hypoxia on secretion rate modification, or compared secretion profiles when the islets were encapsulated. This multiphysics approach may represent a powerful tool to reduce animal experimentation and to gain time by pre-selecting the experiments of interest.

2.1.3 Development of a co-culture medium

2.1.3.1 Introduction on culture media

Culture media are aqueous solutions, with an osmolarity and a pH close to the physiological values (300 mOsmol/l and 7.4, respectively). They are composed of a commercial solution, such as RPMI (Roswell Park Memorial Institute medium) or DMEM (Dulbecco's Modified Eagle Medium), supplemented with additives. These commercial solutions contain 4 types of elements that are required for cell survival and metabolism: inorganic salts, amino acids, vitamins and other components such as glucose and phenol red (providing a visual information on the pH of the solution). These commercial solutions are supplemented with different elements among which some are not specific to the cell type like serum, antibiotics or pH buffers and others are more specific like growth factors and hormones (e.i. insulin).

The composition of different culture media can differ very much in terms of presence or absence of some components, but also in terms of concentrations.

2.1.3.2 Comparison of islets medium and LHCN-M2 media

As a reminder, the LHCN-M2 myotubes require 2 media, the *KMEM* and the *KMEMdiff*, contrary to the primary islets. The *KMEM* is used for seeding, and maintains the cells at the relatively immature state of myoblasts and permits their proliferation; while the *KMEMdiff* induces the differentiation of myoblasts toward myotubes. To co-culture C57Bl6J mouse islets and LHCN-M2 myotubes, it was thus required to find a new culture procedure in one step. The other requirement was to find a co-culture medium replacing the *KMEMdiff* and the islets medium.

To find a co-culture medium, the composition of the media have been compared in order to point out their differences. The list of main components for each medium is provided in Fig. 2.19. It shows that the 2 media do not share the main components. However it is also required to compare the composition of the different "RPMI", "DMEM" and "Medium 199" used in the different media. To do so, the LHCN-M2 medium was simplified to 80% of DMEM and 20% of Medium 199, and the islets medium to 100% RPMI (Summary in Table A.1 in Appendix A). Briefly, this comparison highlighted again that these 2 media are very different in terms of presence/absence of some elements. In general the LHCN-M2 medium (when reduced to 80% of DMEM and 20% of Medium 199) has more elements.

The presence of each molecule and its concentration in each medium comes from empirical screening tests of the manufacturers or researchers, so it sounded hard to define what was a critical difference or not. If we take the example of the choice of RPMI 1640 for C57Bl6J islets medium, it comes from an article of 1978 [Andersson, 1978] where they compared the secretion of islets cultured in several media, based on either RPMI 1640, TCM 199, CMRL 1066, MEM-Eagle, HAM's F10. It was observed that the islets secrete more in the RPMI-based medium, thus leading the community to chose this base for their media. However the relevance/impact of each component of the RPMI was not studied as probably too laborious.

Despite that the full composition of the media cannot be analyzed, the groups working with C57Bl6J islets know some basic rules linked to the culture of islets, leading to the identification of 3 main points:

- (1) The insulin present in the LHCN-M2 differentiation medium, the *KMEMdiff*, cannot be kept for the culture of islets.
- (2) The glucose concentration in the LHCN-M2 medium is at 21 mM against 11 mM for islets, which is again supraphysiological and can negatively impact the islets' viability and function (glucotoxicity).
- (3) The *KMEMdiff* does not contain serum. It is usual for the differentiation medium of skeletal muscle cell lines, like the widely used C2C12. Indeed, the differentiation is supposed to be induced by removing the serum which is present in the proliferation medium. However, the islets require serum, as mentioned in [Andersson, 1978]. We can thus hypothesise that the presence of serum in the medium required for islets could be detrimental for LHCN-M2 myoblasts differentiation.

Those challenges are usually faced by trying to culture a cell type in the medium of the other, and/or to test different ratios of culture media [Leung et al., 2022]. The selection of candidate media is presented in the next section.

Components	C57B6J mouse islets	LHCN-M2 myoblasts (differentiation medium)
	Volume (ml)	
RPMI 1640 *from Sigma*	85.8	
SVF	10	
B-mercaptoethanol (5 mM)	1	
Pyruvate (500 mM)	0.2	
HEPES (1 M, pH 7.3)	1	
Pennicilin Streptomycin (1 M)	1	
Glutamin (1 M)	1	
DMEM 61965-026 *from Thermofischer*		40
Medium 199 4115-020 *from Thermofischer*		10
Human insulin I9278 (1.9 mM) *from Sigma*		0.05

FIGURE 2.19: Islets and LHCN-M2 media composition.

2.1.3.3 Screening experiments to select a candidate medium

General strategy for the selection of the media tested
The *KMEMdiff* had very few chances to be suitable for the islets because there is no serum, while it is mandatory of islets culture according to [Andersson, 1978]. Therefore the strategy was to test if the *islets medium* or different mixes between the *KMEMdiff* and *islets medium* was suitable for LHCN-M2 cells.

The 2 first media tested on muscle cells were:

- (1) The ***isleti medium***, an *islets medium* supplemented with 1.74 µM insulin (Insulin asparte, Novorapid), corresponding to the insulin concentration in *KMEMdiff*. Indeed, we considered that the insulin supplemented in the *islets medium* for the tests would come from islets in the future islet-muscle co-culture. Nonetheless, the fact that islets can provide enough insulin for myotubes survival and function had to be proven.
- (2) The ***50/50 mix medium***, composed of 50% *isleti* and 50% *KMEMdiff*, adjusted in glucose to have 11 mM. This medium was considered notably in the case the serum present in the *islets* medium, thus *isleti* medium, prevents the differentiation of myoblasts. Indeed, the serum would be divided by 2 in this 50/50 mix.

Assess the media toxicity on already formed myotubes

Material and Methods LHCN-M2 myoblasts were obtained from a culture flask after tripsinization. The cells were counted and seeded in plastic 6 wells plates (ref 140675, Thermofischer) at 830 $cells/mm^2$. As illustrated in Fig. 2.20, the usual culture protocol was followed to form myotubes in the 6 wells: 24 h in *KMEM* until reaching confluence, then 48 h in *KMEMdiff*. When large myotubes were formed, the media were replaced as follows: in 2 wells, the medium was replaced by *isleti*; in 2 others by the *50/50* medium; and in the 2 lasts, the *KMEMdiff* was simply renewed in a first one, and the *KMEMdiff* was replaced by *KMEM* to see if myotubes could persist longer in this medium than in *KMEMdiff*. Then, the shape of myotubes was observed during 1 week, taking bright field images.

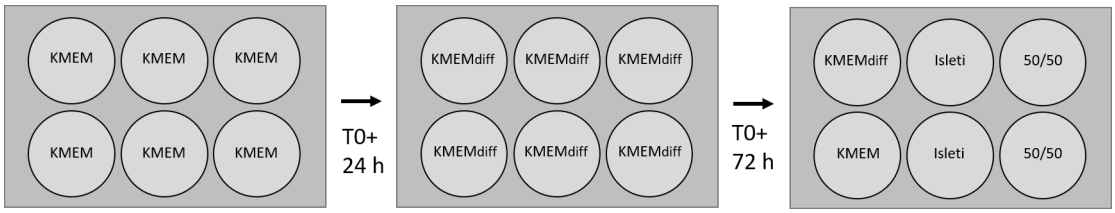

FIGURE 2.20: Protocol for the experiments assessing toxicity of the tested media on myotubes.

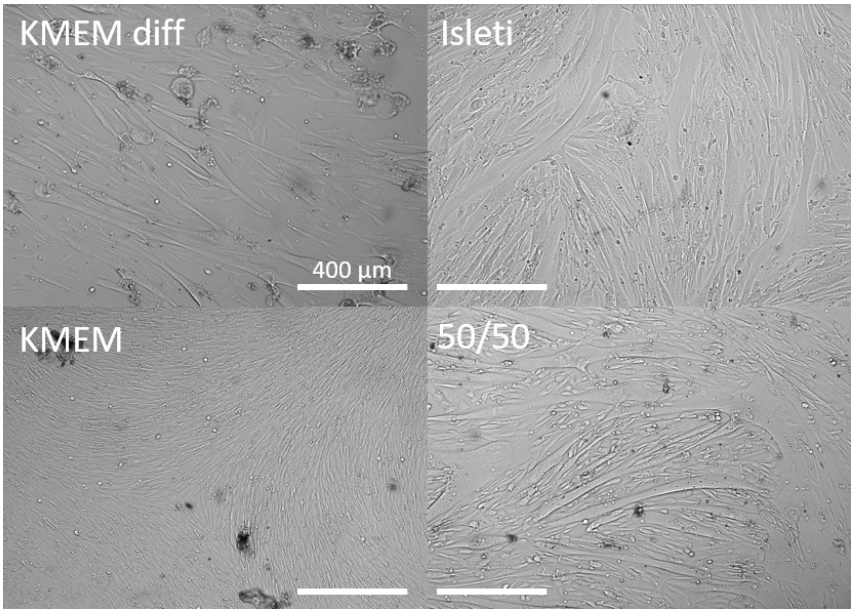

FIGURE 2.21: Bright field images of the LHCN-M2 myotubes 8 days after differentiation, and after 6 days in the different media tested. The *KMEM* well contained almost no myotube while large myotube areas remained in the *isleti* and *50/50* media. In the *KMEMdiff* well, the myotubes were severely detaching.

Results Myotubes are fragile cells easily detaching from the surface over time. After 7 days of culture, the wells with *isleti* and *50/50* showed clearly less detachment than the wells with *KMEM* and *KMEMdiff* media (see Fig. 2.21). Indeed, in *KMEM* and *KMEMdiff* wells, the detachment was visible without microscope, with quantity of floating myotubes. There were no observable differences between the cells treated with the *isleti* and the *50/50* media.

This pilot experiment showed that both medium candidates seemed to act as differentiation media since new myotubes fused and myoblasts stopped to proliferate.

Assess the possibility to form myotubes without the *KMEM* media

According to the last observation, the next step was to validate if differentiation could occur directly using the *isleti* or *50/50* media, without using *KMEM* and *KMEMdiff* media.

Material and Methods Plastic 12 wells plate were used here (same plastic as above, ref 150628, Thermofischer). The protocol of this experiment is illustrated in Fig. 2.22. The goal was to assess the formation of myotubes (differentiation) in the candidates media after 24h proliferation in *KMEM* medium (wells 5, 6, 9, 10), or without this proliferation phase (wells 7, 8, 11, 12). To have enough cell to reach confluence without the *KMEM* proliferation

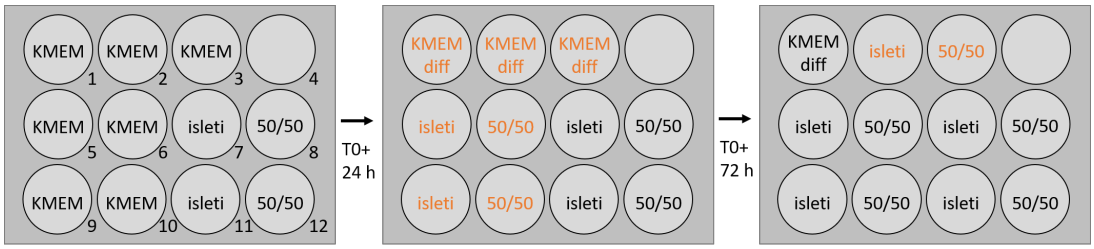

FIGURE 2.22: Protocol testing the capacity of the *isleti* and *50/50* media to differentiate the LHCN-M2 myoblasts, with and without proliferation step in *KMEM* medium.

step, the seeding density was doubled compared to the usual density (1660 $cells/mm^2$). Myoblasts cultured with the standard 2-steps protocol (*KMEM* followed by *KMEMdiff* media) were taken as control in well 1. Finally, wells 2 and 3 were dedicated to repeat the previous experiment (*KMEM* during 24h followed by *KMEMdiff* 48h, and then 7 days in either *isleti* or *50/50* medium). The cells were observed during 10 days and brightfield images were taken, until the myotubes of all the wells were detached.

Results We observed that the myotubes appeared similarly in all the wells. Three days after seeding, all the wells contained myotubes, and from day 4, the myotubes were large and numerous in all conditions. From day 7, the myotubes cultured with the standard 2-step protocol started to severely detach, while they remained until day 10 in the other wells. Note that the result of the previous experiment was confirmed (wells 2 and 3). Then the *isleti* and the *50/50* media are able to induce differentiation with or without a preliminary 24h *KMEM* step. We also observed a tendency of the myotubes to be present longer compared to the standard culture procedure.

However the bright field images do not constitute a proof of the viability and of the functionality of the myotubes formed in the candidates media, and with the new 1-step culture protocol. Moreover, it would be preferable to reduce the insulin concentration in the medium, as islets may not achieve to generate the 1.74 µM of insulin.

Therefore, to assess these crucial points, biochemical investigations were then performed and described in the next part. We focused on the most convenient of the 2 candidate media, that is the *isleti*. Indeed, if the insulin concentration could be removed, no experiments were required on the islets as the co-culture medium would be the *islets medium* itself.

2.1.3.4 Reduce insulin in the *isleti medium*

Therefore we explored the possibility to reduce the insulin concentration in the *isleti* medium, using the fusion index of myotubes as comparative marker. It is defined as the ratio between the number of nuclei inside myotubes over the total number of nuclei. It can be determined by staining nuclei with DAPI, and by marking troponin-T with an anti-body. Indeed troponin-T is expressed only in myotubes, thus it is possible to count the number of nuclei in myotubes and to compare it to the total number of nuclei (see the Fig. 2.23).

The fusion index after 4 days of differentiation in different *islets media* with different level of insulin were compared (0 nM, 1 nM, 100 nM, or 1.74 µM (last one is *isleti* medium)). As shown in Appendix A, in Fig. A.2, the fusion indexes were comparable whatever the insulin concentration.

Hence, insulin does not seem necessary for the myotubes formation. Therefore, the subsequent structural and functional investigations were performed with the ***islets medium*** without supplementation in insulin.

2.1.3.5 Structural and functional validation of the *islets medium* as co-culture medium

Introduction and method
In the literature, the myotube differentiation is studied through structural and functional investigations. Myotubes are polynucleated cells showing organised protein filaments as explained in section 1.1.2.2 in Fig. 1.7. To validate that myotubes possess these features of muscle cells, the presence and organisation of troponin-T and of α-actinin are usually studied by immunostaining: α-actinin is present at the early stages of differentiation, and troponin-T is a marker of myotube stage. The study is usually completed with the fusion index, previously used and defined.

The troponin-T and α-actinin immunostaining, as well as fusion index, were thus used for our **structural** investigations.

The response to insulin is the the most important **functional** feature of myotubes in the construction of this islet-muscle MOoC. The myotube response to insulin is studied by different means according to the literature. The increase in phosphorylated Akt, induced by insulin and leading to the GLUT4 mobilisation to the plasma membrane (see section 1.1.2.2), is often evaluated by western blotting. The presence of GLUT4 (the glucose transporter mediating insulin-induced glucose uptake) at the plasma membrane can be studied with immunostaining. Finally, the accumulation of glucose entered in the myotubes, or glucose uptake, can be observed with a fluorescent glucose, the 2-(N-(7-nitrobenz-2-oxa-1,3-diazol-4-yl)amino)-2-desoxyglucose (2-NBDG).

The protocols setting and their application have been established during the Master's degree internship of Dorian Chapeau and Bachelor's degree internship of Eleftheria Papasavva. The detailed *material and method* of the structural and functional investigations is provided in Appendix A.

Troponin-T, α-actinin, and fusion index Similarly to the classical 2-step protocol using *KMEM media*, the *islets medium* induced, after 4 days, the differentiation of LHCN-M2 myoblasts into large plurinucleated cells expressing both troponin-T and α-actinin (see Fig. 2.23).

The kinetics of myotube formation and then their detachment were evaluated over 14 days by calculating the fusion index. Since immunostaining is a destructive test, the kinetics were studied by cultivating myoblasts in 4 microwell slides in parallel, stopping each one either at day 4, 7, 10 or 14 after seeding, to perform the immunostaining. The Fig. 2.24 shows that fusion indexes were similar between myotubes cultured in the traditional way (2-steps, *KMEM/KMEMdiff* media, normal density (830 $cells/mm^2$)) compared to the condition with *islets* medium and high cell density (1660 $cells/mm^2$). The fusion index presented a better stability between day 4 to day 10 in the tested culture procedure compared to the classic culture, which is more optimal for investigations. A difference of fusion is present at day 14, where the myotubes in the traditional culture protocol are severely detached. It is interesting to note that in the preliminary experiments, the difference was present at day 7 instead. Thus the myotubes cultured in the classical protocol remained longer in these experiments, but still less than myotubes in the tested protocol.

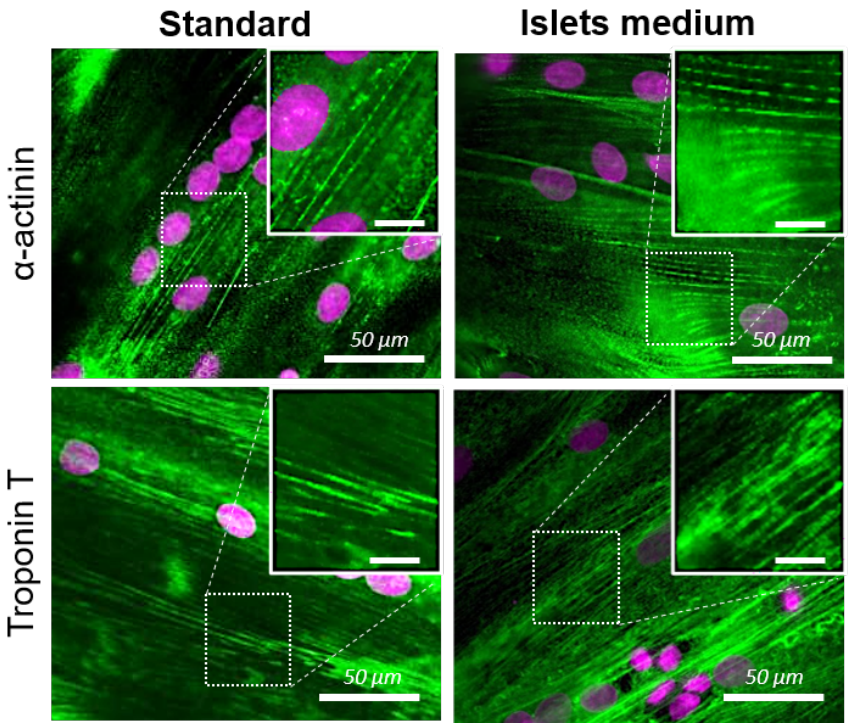

FIGURE 2.23: Troponin-T (green), α-actinin (green) and nuclei (pink) staining in LHCN-M2 myotubes cultured with the classical medium with the usual protocol (standard) or with the *islets medium* and single-step procedure, after 4 days of culture.

The presence of troponin-T and α-actinin, as well as similar or better fusion index, demonstrate that the single-step culture protocol with *islet* medium developed here is compatible with the culture of LHCN-M2 myotubes.

The second part of the investigations was studying insulin response at different levels of its signaling pathway. Whatever the experiment on this part, the following protocol, inspired from literature [Bala et al., 2021][Tsuchiya, Kanno, and Nishizaki, 2013][Navarro-Marquez et al., 2018] and from our preliminary tests was systematically applied after 4 to 6 days of culture:

- The myotubes were cultured according to the co-culture procedure (high cell density, 1660 $cells/mm^2$) at seeding, and direct differentiation using *islets* medium).
- The myotubes were starved by incubating them 3 hours in a medium derived from the *islets* medium. It is the same medium, but with low glucose level (3 mM), and 0.2% (v/v) BSA instead of serum, since serum could contain insulin and insulin-like proteins (proteins activating insulin receptors).
- The myotubes were then exposed to insulin during 15 min, at different concentrations (precised in each experiment), using the same islets medium derived solution.

These steps allow myotubes preparation prior to the investigation on insulin response.

pAkt/Akt ratio An increase of this ratio represents one of the first steps of insulin action on muscle cells. After the 3 steps described above, the medium was replaced for 30 min by the

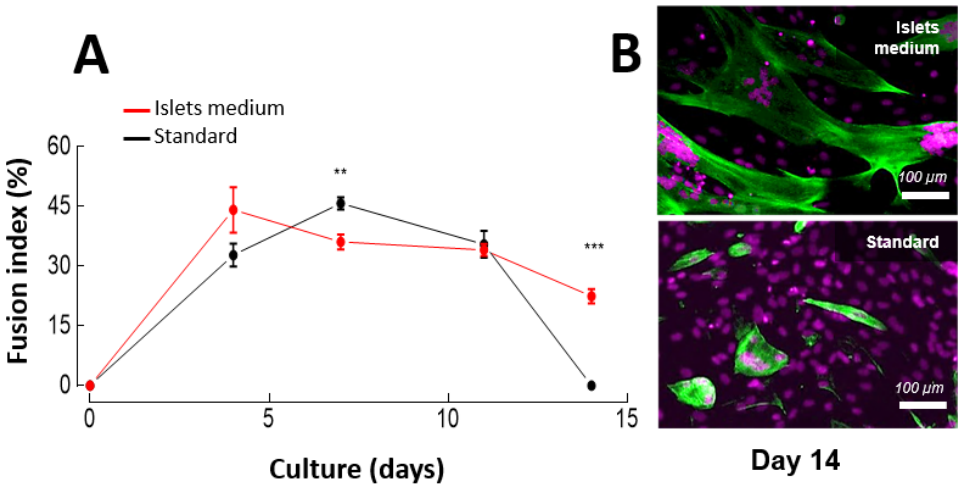

FIGURE 2.24: (A) Fusion index over time in LHCN-M2 myotubes cultured in the classical medium with the usual protocol (standard), and in myotubes cultured in *islets medium* with the single-step protocol. (B) Troponin-T (green) and nuclei (pink) staining of LHCN-M2 myotubes after 14 days of culture in both tested culture conditions. The troponin-T (in green) shows the presence of myotubes, their size as well as state of detachment. In the standard medium, troponin-T shows small and detached-like shape, while in *islet medium* large myotubes are still present.

islets medium without glucose and at different insulin concentrations: 0, 0.5, or 100 nM, the last being a widely used positive control [Bala et al., 2021][Tsuchiya, Kanno, and Nishizaki, 2013][Navarro-Marquez et al., 2018][Jeon et al., 2019]. Protein extract were prepared and the presence of phosphorylated forms or not of Akt detected in western blots using specific antibodies. The interest of studying the ratio pAkt to Akt is explained in section 1.1.2.2 p. 11.

The pAkt/Akt appeared superior in myotubes incubated with 500 pM and 100 nM of insulin than without insulin (see Appendix A, Fig.A.3), however the number of experiments (N=3) does not provide a statistical difference. More experiments might confirm this tendency. The pAkt/Akt ratio increase under insulin action might also be hidden by an elevated basal level of Akt phoshorylation in the cell lines like LHCN-M2. Indeed the Akt phosphorylation can be involved in other signaling pathways than insulin response, such as cell survival and proliferation, which are amplified in cell lines in comparison with primary cells.

GLUT4 immunostaining The 3 steps preparation protocol was used and ended with a 30 min incubation with the islets medium at 8.2 mM glucose and insulin at 0, 0.5 or 100 nM. The cells were then fixed and immunostained with an anti-GLUT4 antibody.

In the absence of insulin, GLUT4 was not observed in myotubes (see Fig. 2.25), while it was clearly observable in 0.5 nM and 100 nM of insulin. These results indicate that the myotubes cultured with the single-step protocol with islets medium mobilize the glucose transporter upon insulin for glucose uptake.

2-NBDG uptake The last part of the investigation consisted in verifying that the myotubes could effectively take glucose under the action of insulin, which is the most interesting event for the MOoC. The previous experiment proofed GLUT4 was mobilized, and this part aimed

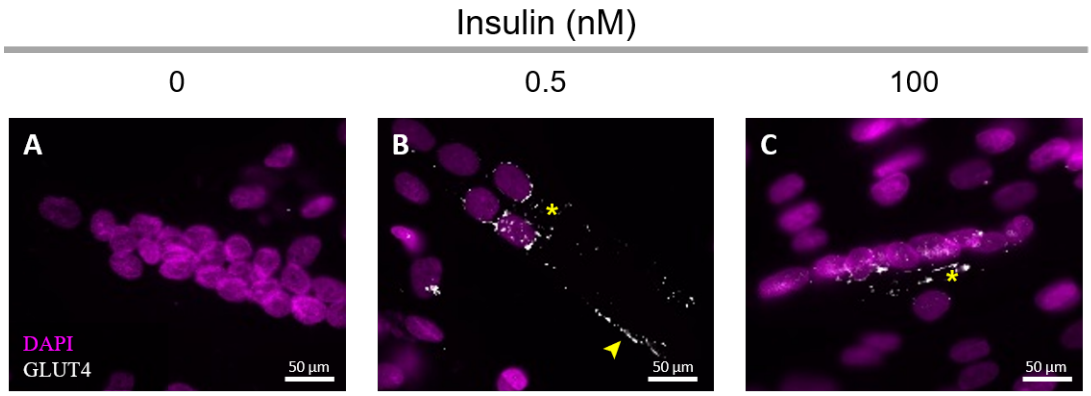

FIGURE 2.25: GLUT4 immunostaining after the described protocol, in the presence of insulin (0.5 nM or 100 nM) or not. The stars indicate GLUT4 at the vicinity of the nuclei, probably in trans-Golgi network or in cytoplasmic vesicles, and the arrows indicate GLUT4 at the vicinity of the plasma membrane.

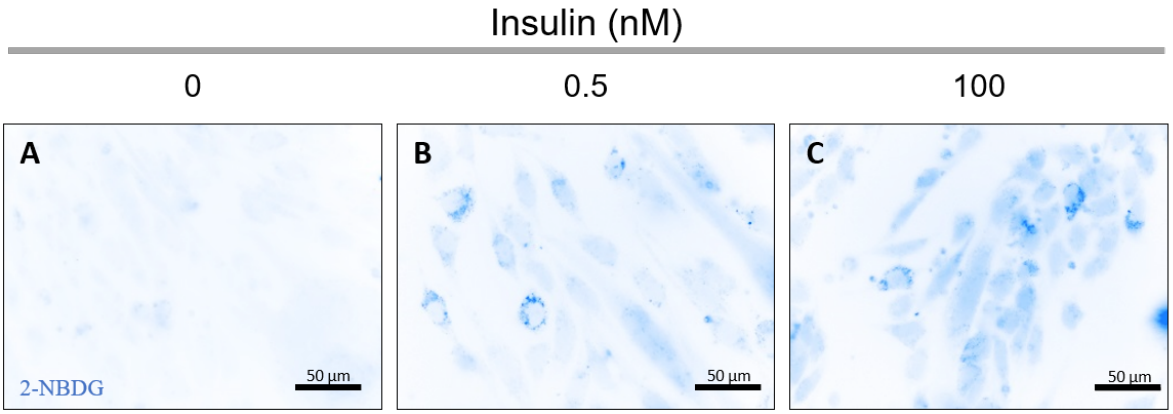

FIGURE 2.26: 2-NBDG fluorescence after a the described protocol with the presence of insulin (0.5 nM or 100 nM) or not.

at demonstrating it was situated at the plasma membrane and functional. This study used a glucose modified with a fluorochrom, called the 2-NBDG, to follow the accumulation of glucose that entered into the myotubes. The fact that this compound is not metabolized increases the chances to observe at intracellular level glucose uptake by widening the observation time window.

The myotubes followed the 3 steps procedure as described previously and then were exposed during 30 min to the islets medium without glucose and containing 0.4 µM of 2-NBDG [Bala et al., 2021] and different insulin concentrations: 0, 0.5 or 100 nM. The cells were then fixed and 2-NBDG fluorescence observed.

2-NBDG was not detected without insulin and clearly appeared upon insulin at both concentrations (see Fig. 2.26). It seemed the number of myotubes with 2-NBDG and fluorescence intensity was higher at 100 nM than at 0.5 nM of insulin, although this approach is not quantitative.

2.1.3.6 Concluding remarks on the co-culture medium development

To sum up, collectively these data show **LHCN-M2 myotubes can be generated with the single-step protocol using islets medium**, and that insulin, even at physiological concentrations, triggers GLUT4 translocation at the plasma membrane and glucose uptake. We also expect with more experiments to demonstrate that insulin triggers the phosphorylation of Akt too, as otherwise the 2 previous results could not have be found.

2.2 Cell adhesion defining the chip substrate

2.2.1 Introduction to cells adhesion and coating

In *in vivo* conditions, most of the cells are in an extracellular matrix (ECM) composed of proteins [K. Young and J. Beebe, 2010]. Adhesion is mandatory for observations in *in vitro* cell culture. The artificial culture substrates used, usually glass and organic polymers as polystyrene, are not always suitable for cell adhesion so that coatings are widely used [Hickman et al., 2016]. In addition to favor cell adhesion, coatings are used to emulate the cells micro-environment. Indeed the mechanical properties of the cells environment are required for some physiological processes such as differentiation in the case of myotubes [K. Young and J. Beebe, 2010][Toral-Ojeda et al., 2018].

These coatings are solutions or powders of single or mixed proteins, sometimes directly derived from the extracellular matrix of tissues. They are applied on the substrate prior to cell seeding.

In the future MOoC system, primary mouse islets and LHCN-M2 myotubes should adhere on a MicroElectrodes Array or MEA (introduced in section 1.1.2.1 p. 6). Indeed, both islets and skeletal muscles cells are electrogenic and using a MEA will allow to record their electrical activity or eventually stimulate muscle cells.

It was shown that the islets adhere on the surface of MEA provided by Multi Channel Systems (MCS) using a Matrigel coating [Jaffredo et al., 2021][Lebreton et al., 2015]. The LHCN-M2 muscle cells are reputed to easily adhere on classical culture substrates such as glass and PET plastic, without requiring coating. Nevertheless, to the best of our knowledge, the literature does not mention culture of the LHCN-M2 cells on MEAs. There are also few examples of culture of skeletal muscles on MEA [Molnar et al., 2007][Nagamine et al., 2011][Langhammer et al., 2013][Rabieh et al., 2016][Duc et al., 2021][Bailleul et al., 2022]. One essential step here for the development of our MEA-based chip was to test, and improve if necessary, the adherence of LHCN-M2. This is the first step essential to any co-culture.

2.2.2 Selection of the chip substrate

2.2.2.1 Culture without coating on MEAs from MCS (Silicon Nitride passivation layer)

The first tests of LHCN-M2 cell culture on MEA were conducted on 60MEA200/30iR-Ti MEA from MCS. Their surface is composed of electrodes in Titanium Black, and Silicon Nitride for the passivation layer that represents the main part of the surface.

As previously, LHCN-M2 myoblasts were obtained from a culture flask after tripsinization. They were seeded in these experiments in MEAs with the usual density ($8 \times 10^2 cells/mm^2$). The MEA chamber was then filled with 1 ml of proliferation medium according to their culture procedure.

Unfortunately, the myoblasts did not adhere after 48h as illustrated in Fig. 2.27a. Repeated tests confirmed this behaviour (N=12 considering all the negative controls of the

next experiments). Long term cultures (2 weeks) were then conducted to see if a kind of "natural selection" could occur over time as the myoblasts kept on proliferating despite the absence of adhesion. Re-seeding of a MEA with new cells after unsuccessful adhesion of a first seeding was also tried, but did not provide improvement. Indeed, such "pre-culture" are sometime used since some adhesion proteins secreted by the cells during a first seeding could enhance the adhesion of the second batch of cells.

As none of those trials led to myoblast adhesion, which is the prior step of any myotube formation, the introduction of a coating was then tested.

2.2.2.2 Coating tests on MEA from MCS (Silicon Nitride)

Briefly, no Matrigel coating (whatever the concentration), or Gelatin-Fibronectin, could provide sufficient adhesion. Even a coating poly-L-ornithin and laminin used in [Duc et al., 2021], with musculo-skeletal cells on a Silicon Nitride substrate, didn't allow the LHCN-M2 to adhere. For the last one, it is possible the adhesion of primary myoblasts was linked to the microgrooves made by drilling the passivation layer until the glass substrate.

The co-culture medium tests, described in details on section 2.1.3 p. 52, being conducted in parallel, an other set of coating experiments were playing between the traditional way to culture this cell line and the tested co-culture medium and culture procedure tested. In complement to those approaches, the presence of Matrigel in the medium was tested too. None of those approaches provided consistent adhesion. The only myotubes that appeared were not fully satisfying in terms of size and frequency. Most of all, they were obtained in conditions not satisfying for the future MOoC experiment: a base coating of Matrigel 5%, and the traditional culture procedure of the LHCN-M2 in 2 steps, with KMEM media supplemented with 2% Matrigel. It is not satisfying conditions as it is not the future culture procedure, and the presence of Matrigel in the culture medium could be a threat in the microfluidic system by adding viscosity to the flowing liquid.

The challenge to make the LHCN-M2 cells adhere on Silicon Nitride while they usually adhere easily led to try another type of MEA. An other supplier, MicroElectrodeDevices (Lausanne, Switzerland, MED), provides MEAs with a passivation layer based on a photoresist resin, the SU-8. Moreover, the islets have already been successfully cultured on this kind of substrate, in microfluidic conditions (Qwane company at the time of the article) [Perrier et al., 2018].

2.2.2.3 Culture with coating on the SU-8 passivation layer of MEA from MED

To test the hypothesis that passivation layer is responsible for the problem of cell adhesion, seeding experiments were repeated on MEAs from MED with Platinium Black electrodes. In this experiment, the conditions were chosen the closest ones to the future MOoC culture conditions, using the preliminary findings (the proliferation can be skipped, and isleti medium allows differentiation, see section 2.1.3). Therefore the LHCN-M2 myoblasts were seeded at high density on a MEA coated with Matrigel 2%, and with isleti medium (islets medium supplemented in insulin with the same concentration as the original KMEMdiff medium).

The formation of myotubes was similar to that obtained with usual culture substrates in terms of kinetics, frequency and size (see Fig. 2.27b). These data validate the use of SU-8-based MEA for the islet-muscle MOoC since it is a substrate on which both cell types can be cultured.

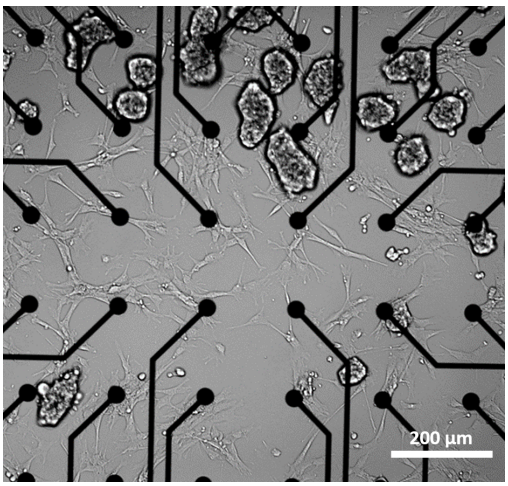

(A) Myoblasts not adhered and forming aggregates after 2 days of culture on 60MEA200/30iR-Ti MEA from Multi Channel Systems.

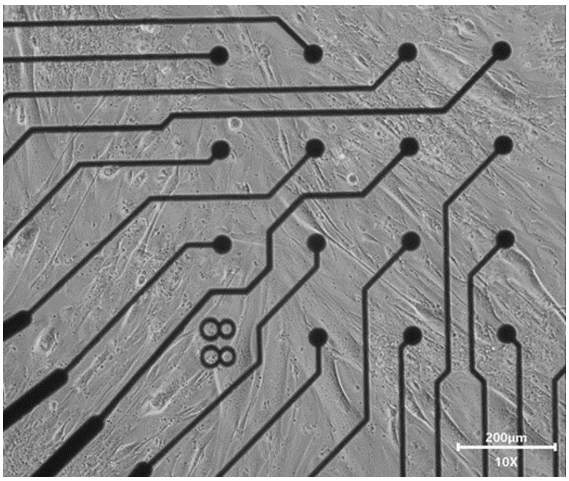

(B) Example of successful myotube formation after 3 days of culture on MEA60-200-30-PtB, from MED, with SU-8 passivation layer. The coating used is 2% Matrigel.

FIGURE 2.27: Results of LHCN-M2 myoblasts culture on different MEA of different passivation layers.

2.2.3 Concluding remarks on common culture substrate

Fig. 2.28 summarizes all the experiments conducted. With MCS MEA, no coating or culture protocol have induced LHCN-M2 myoblasts adhesion and differentiation. However **consistent results were obtained on MEAs with SU-8 passivation layer**. Knowing the islets can adhere on this substrate too, SU-8 was chosen as a common culture substrate for both LHCN-M2 cells and primary mouse islets.

2.3 Chip n°2 design

In this chapter, parallel works were described relative to the first challenges raised by a co-culture in a microfluidic chip: find a MEA substrate on which both cells types adhere, design a versatile chip for both static and microfluidic mode, and assess the possibility to have a co-culture medium. The 2 last points are related, as the dual-mode chip has been designed in perspective of the impossibility to do a co-culture.

The chip n°1 had limitations, but remained an asset for experiments in case co-culture is impossible: it was possible with this design to find a reasonable number of islet and flow rate reaching physiological levels of insulin, while exposing them to a low shear stress.

As a co-culture medium and protocol have been found, the limitations of the chip n°1 can be overcome by reducing the height of the wells and using geometry more directional to have a more controlled and homogeneous flow and environment. In this view, the second design (chip n°2) was composed of physically separated channels to prevent cells mixing during seeding and culture. These channels can be connected with a tubing (see Fig. 2.30).

It has been found that the MCS MEAs with Silicon Nitride passivation layer are not suitable for our chip substrate. As the design of chip n°1 is based on MCS MEAs, an important screening of coatings has been tried to solve the problem. Finally, only MEAs from MED provided consistent adhesion of LHCN-M2 cells. The MEAs from the 2 suppliers are very different (see Fig. 2.29, the chip n°1 design was not compatible with MED MEAs). Therefore

MEA passiva-tion layer	Medium/culture procedure	Coating	Adhesion after 72 h	Myo-tubes
Silicon Nitride	KMEM	No coating	No	No
		Matrigel 2%	No	No
		Matrigel 5%	No	No
		Matrigel 10%	No	No
		Gelatin+ Fibronectin mix	No	No
	1) KMEM +2% Matrigel 24h 2) KMEMdiff +2% Matrigel	No coating	Yes	Yes but small and few
		Matrigel 5%	Yes	Yes but small and few
		Gelatin+ Fibronectin mix	Yes	Yes but small and few
	1) KMEM +2% Matrigel 24h 2) Isleti	No coating	No	No
		Matrigel 5%	No	No
		Gelatin+ Fibronectin mix	No	No
	Isleti+ 2% Matrigel	No coating	Yes	No
		Matrigel 5%	Yes	No
	Isleti	No coating	No	No
		Matrigel 5%	No	No
		Laminin + Poly-L-ornithin double layers	No	No
SU-8	Isleti	Matrigel 2%	Yes	Yes
		Gelatin+ Fibronectin mix	Yes	Yes

FIGURE 2.28: Table summarizing all the experiments of adhesion combining different passivation layers, culture protocols, and coatings.

a chip n°2 was required, to define a compatible design with the MED MEAs, the second design with the 2 channels had to be contained in a PDMS block of 16×16 mm^2.

Finally Fig. 2.30 illustrates this new chip, called chip n°2, whose dimensions remain to be defined. The dimensions of islets channels are based on previous works of the team, where islets were cultured in a microfluidic channel of 10 mm length, 800 mm width and 500 mm height ([Jaffredo et al., 2021]). The channel in our design follows these dimensions, except the height, which is limited to 300 mm height due to fabrication limits of MED. The myotube channel has the same width. Its height and length have to be defined according to the metabolic objectives (level of insulin concentration to generate using islets, and level of glucose variations insulin induced with the LHCN-M2 myotubes), and the volume of the glucose sensor already identified at that time (the BST sensor described in section 4.2, requiring 6 µl). This work is developed in the Chapter 3.

2.4 Conclusion

In this chapter, we studied the culture requirements and co-culture possibility of our cell types to define a general chip design so called n°2. In case no co-culture was possible, a chip n°1 was designed and the multiphysics simulations set up for its study will benefit for the chip n°2 exploration and scaling, that will be discussed in next chapter.

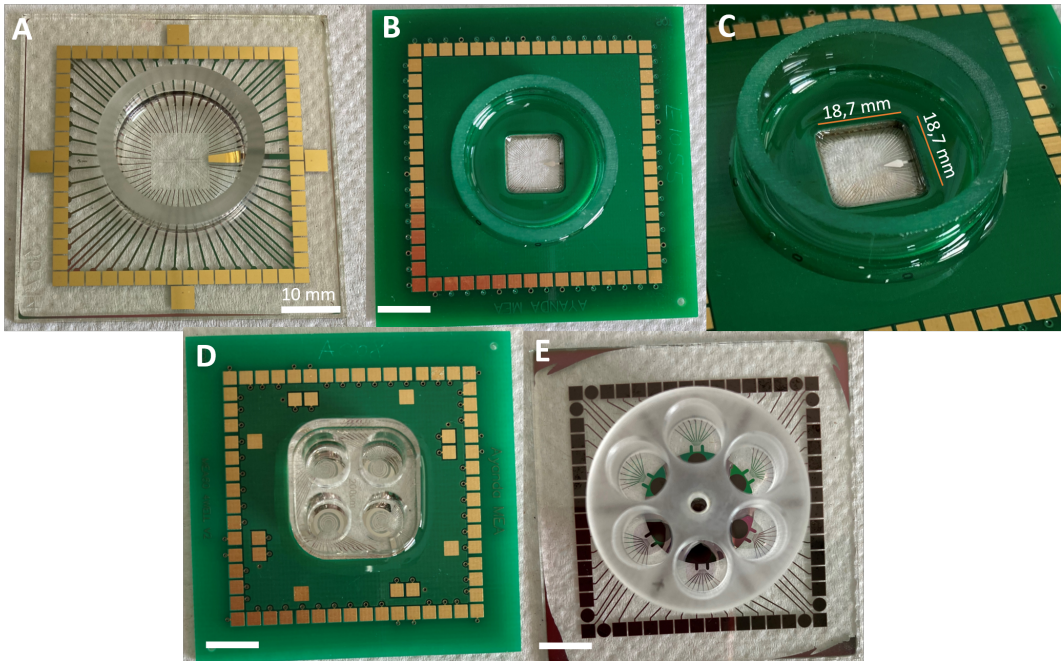

FIGURE 2.29: Comparison of the surface shape of MEAs from MCS and MED providers. (A) MEA from MCS with a flat surface. (B) and (C) MEA from MED without a completely flat surface. (D) Multi-well MEA from MED. (E) Multi-well MEA from MCS.

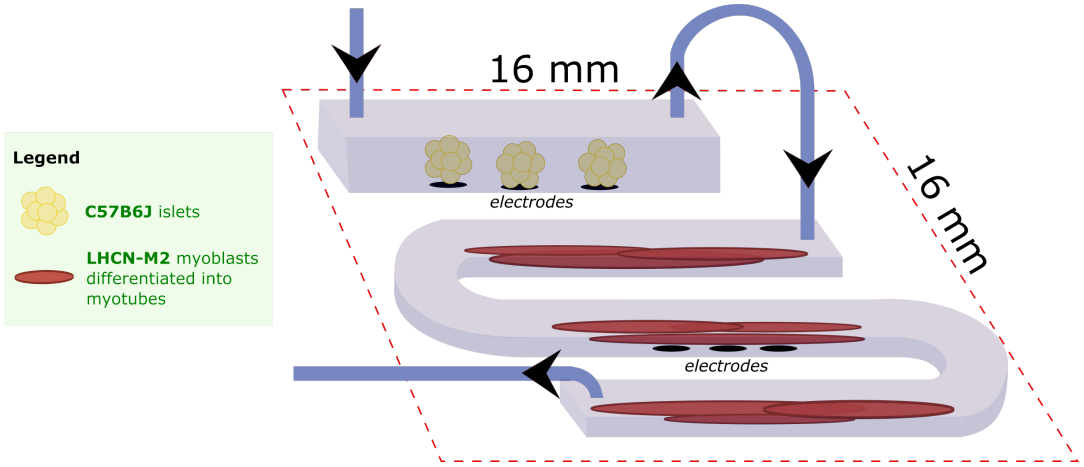

FIGURE 2.30: Schematic of the proposed chip n°2.

Chapter 3

Chip scaling

After conceptualization in the Chapter 1 of the targeted interaction to observe (represented by Fig. 3.1a), the Chapter 2 established general geometries and materials of the microfluidic chip (type of Micro-Electrode Array) dictated by the culture requirements of C57Bl6J islets and LHCN-M2 myotubes. The previous schematic can now be updated as in Fig. 3.1b.

The next challenge of the MOoC system design lies in mastering the glucose and insulin concentrations modified by biological sources (increasing concentrations) and sinks (reducing concentrations). This control is required for 2 different objectives in the MOoC: reproducing physiological concentrations for a relevant crosstalk, and ensuring measurable glucose variations linked to myotube metabolism. Indeed, the Chapter 2 conclusion rose this possibility in the previous chip design of an insufficient glucose variations by myotubes to be detected. Thus the system has to be correctly *scaled*.

This Chapter 3 describes how we scaled remaining features of the system according to the metabolic properties of the cells. Briefly, we reduce the organs to one main function: the islets are insulin sources and the myotubes glucose sinks. We target to match the cells activity (metabolism, hormone secretion, etc) to our objectives (physiological insulin concentration, detectable glucose uptake), which makes our scaling a *functional scaling*. Our scaling procedure involved combined *in vitro* and *in silico* experiments.

3.1 Introduction of the islet-muscle MOoC experimental protocol

The co-culture medium validation experiments (described in the section 2.1.3 p. 52) highlighted that, *in vitro*, myotubes conditioning is required prior to exposing them to insulin and study any response. Thus the schematic definition of the targeted MOoC experiment represented in Fig. 3.1 had to be precised. As the protocol used to validate the co-culture medium has successfully led to insulin-mediated myotube responses, the MOoC experiment was decided to be based on the co-culture medium validation procedure. We detail here the precised experiment planed to conduct with the MOoC to validate the islet-muscle interaction emulation.

Prior to studying the insulin response in a context of glucose elevation, the protocol starts with the fasting of myotubes in glucose and serum. This step must be compatible with the islets as well for the MOoC experiment. In the literature on islets, this concept of fasting process is also present [Jaffredo et al., 2021]. This is explained by the fact both cell types are cultured at high glucose concentrations compared to the physiology: 11 mM for islets like LHCN-M2 in this study (while 21 mM in the normal medium), whereas physiological concentrations are between 4 and 8 mM (physiological normoglycemia, see section 1.1.1 p. 3).

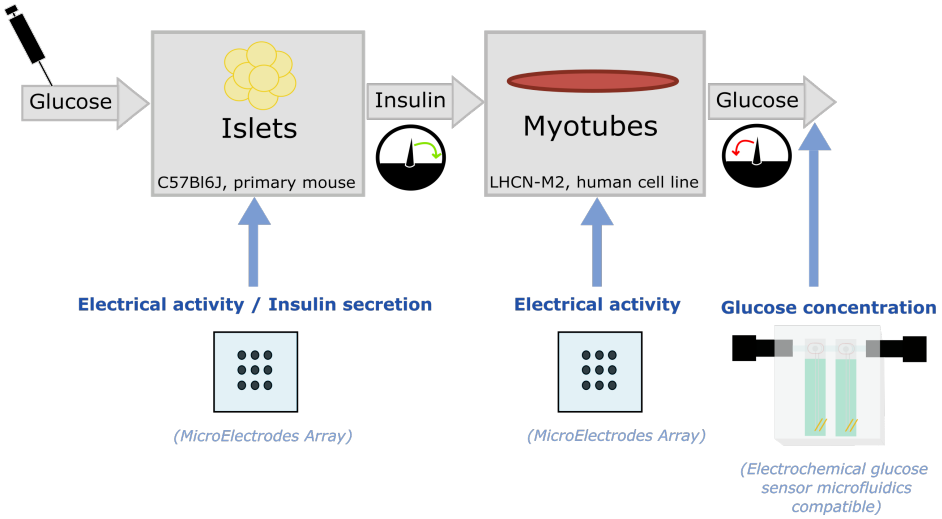

(A) Block diagram representing the targeted organs crosstalk, and the online sensors monitoring the molecules of interest.

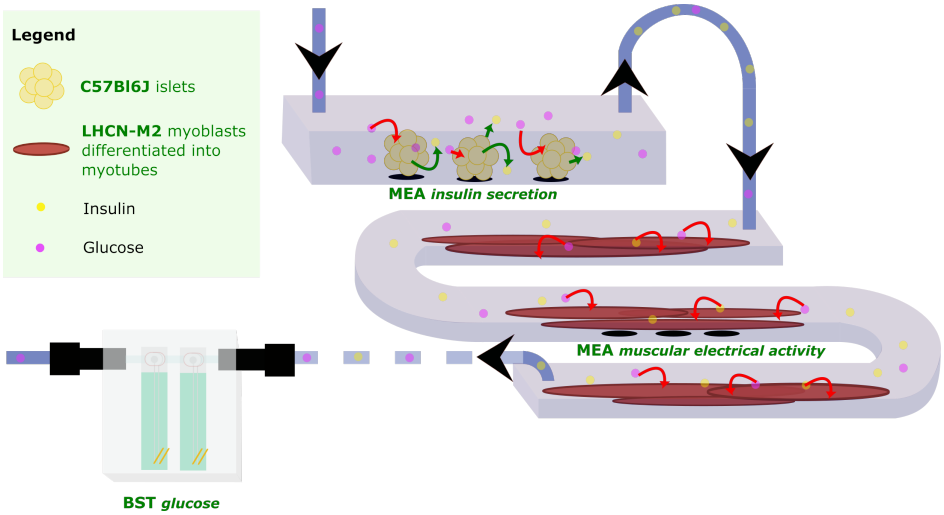

(B) Update of the block diagram 3.1a taking into account the geometry of the chip identified in Chapter 2.

FIGURE 3.1: Summary of the MOoC conceptualization and design achieved so far.

In the experiments of section 2.1.3, an additional intermediate step between the starvation and the high glucose exposure was used: that consisted in exposing myotubes to a starvation medium supplemented with high insulin concentration, in order to "prepare" myotubes to glucose increase. Such empirical pre-exposition to insulin cannot be kept in the MOoC experiment because it is not physiologically relevant: the islets are the insulin's source of the MOoC, and thus they cannot release high level of insulin at low glucose. We therefore had to validate that this intermediate step can be removed without affecting glucose uptake.

The next point to be considered in the protocol is the medium. Prior to the experiment, the cells are cultured inside the chip, in the validated co-culture medium (i.e. the islets medium, see section 2.1.3). When the cells are adhered, and differentiated, MOoC experiments can be conducted to test islet to muscle communication. The medium to use for this communication experiment, or MOoC experiment, can be either:

- A **minimalist medium** as introduced in section 2.1.2.1 p. 32. This physiological solution is composed of essential salts respecting physiological proportions, a pH buffer, glucose, but does not have serum (proteins) or amino-acids.
- A medium **closer to the co-culture medium** would be more physiological than the minimalist medium (notably containing essential amino-acids). Thus it can provide more relevant cell responses, closer to the *in vivo* situation. Such medium was used for the co-culture validation experiments in 2.1.3.5, where the functional tests studying insulin response used an islet medium derived solution, where serum was replaced by BSA (0.2%).

As the selected medium has to be preferably serum free to be compatible with microfluidics (it brings viscosity to the medium [Prill, Jaeger, and Duschl, 2014]), the serum-free version of the co-culture medium was chosen for the MOoC experiments, in addition to the fact it has a higher physiological relevance.

The last question regarding the experiment design was whether or not using continuous flow. The muscle is the organ taking the most glucose under insulin stimulation [Sylow et al., 2021]. It may be explained by 2 mechanisms: the volume of muscle is important compared to the other cells types, and the blood is recirculating. The glucose is then in contact with a great volume of cells conducting the uptake, and for a long time. Thus a MOoC system reproducing those mechanisms may provide high insulin-mediated glucose variation.

A recirculating loop was not considered yet at this proof-of-concept stage of the project. Indeed, we expect to work with volumes lower than a milliliter to obtain large insulin concentrations with a low quantity of biological material. But several milliliters are generally used in MOoCs integrating a recirculation loop, like those working with gravity driven recirculation [Oleaga et al., 2018] or peristaltic pumps and reservoir [Skardal et al., 2017] [Zhang et al., 2017].

To reproduce the long duration of the contact between glucose and muscle cells without recirculating loop, with a channel design introduced in Fig. 2.30 p. 63, there are 2 identified possibilities:

- The **length** has to be **large** and the **flow reduced**. The footprint of the microfluidic chip is limited to a square of 16 mm x 16 mm, which corresponds to the specifications of the MEA supplier (MicroElectrodeDevices or MED). This limits severely the channel length. The flow is also not a fully flexible parameter because it impacts the insulin concentration.

- Or the sample in which the myotubes take the glucose has to be **static**. This hinders the possibility of dynamic monitoring, but provides the highest uptake level possible.

Hence we propose on a first time a ***static*** MOoC experiment, where the flow is stopped at the step of myotube glucose uptake. This kind of experiment validates the presence of an interaction. Using the level of uptake measured in static, we are then able to simulate *in silico* the glucose variations induced by myotubes while playing on different parameters (flow, channels dimensions) to determine if a trade off exists to have a measurable glucose uptake under flow, respecting the footprint, the shear stress and insulin concentration (related to flow). The existence of a trade-off would allow ***dynamic*** MOoC experiments, with a continuous monitoring of myotubes response. This would also be the first step toward a recirculating closed loop system.

To conclude, according to the biological protocol determined in the co-culture medium investigations, and the choice of a *static* MOoC experiment on a first time, the scenario of the planned MOoC experiment is the following:

- Islets and myotubes are seeded on the electrodes of the MOoC chip and cultured in the co-culture medium (or islets medium) defined in Fig. 2.19 p. 54. The MOoC chips are placed in a pool, so that the chip can be covered by medium. The nutrients are expected to penetrate inside the channel by diffusion through the holes punched to plug inlet and outlet tubings.
- After islets adhesion and the myotubes formation, a fasting medium is injected as illustrated in Fig. 3.2a. It is based on the predefined co-culture medium, with the serum replaced by BSA as mentioned above. The concentration is simply elevated to 1%. Indeed in [Bala et al., 2021] they concluded that elevation of serum increases the overall glucose uptake (basal and insulin-driven), which would optimize chances to detect extracellularly the basal and insulin driven glucose uptake.
- After 3 hours in fasting conditions, the medium is changed to the serum-free derived co-culture medium, but at high glucose (8.2 mM), until the islets have generated the targeted insulin concentration in the myotube chamber as illustrated in Fig. 3.2b.
- The flow is stopped and the myotubes incubate with insulin-containing medium 1 hour as illustrated in Fig. 3.2c.
- The medium in the myotube channel is sent to the glucose sensor to determine the variation of glucose concentration before and after the incubation.

Note: In our functional investigations during the validation of the co-culture medium, the last step at high glucose was only lasting 30 min, and showed significant responses to insulin. For the experiments with the MOoC, we have chosen 1 hour of incubation with elevated glucose and insulin, which represents a more physiological time span and which increases the probability to measure significant glucose variations in the extracellular medium. Indeed, in terms of physiology [Woerle et al., 2003], the insulin is elevated for 1-1.5 hour after a standard meal prior to decrease, and the glucose decreases 1 hour after the insulin peak.

With this scenario, we hypothesize that the insulin concentration does not vary during the 1 hour incubation. Indeed, we consider the myotubes do not consume a significant level of insulin during the 1 hour incubation, regarding their very small volume in comparison with the total volume of the circuit. We also consider that after the flow stop, the islets still secrete, but the diffusion of insulin doesn't change the insulin concentration in the myotube channel.

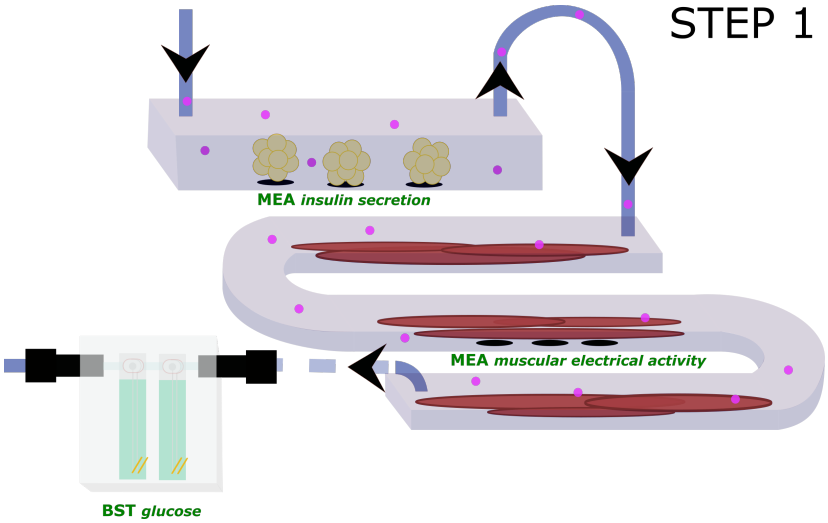

(A) After culture, the cells are starved in glucose and serum during 3 hours.

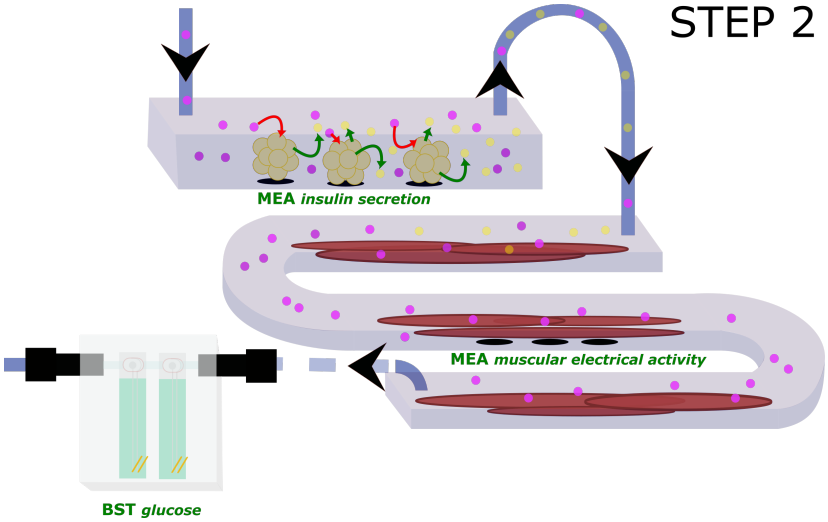

(B) After the starvation, high glucose medium is injected and the islets are generating the targeted concentration in the myotube channel.

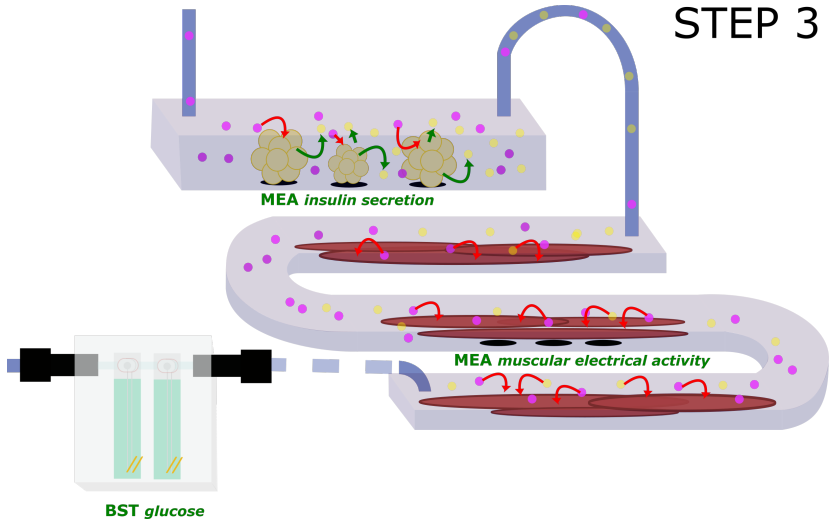

(C) When the desired concentration is reached, the flow is stopped to let the myotubes take glucose upon insulin action.

FIGURE 3.2: The main steps of our Glucose Uptake Assay (GUA) protocol.

3.2 MOoC scaling strategy

The goal of this MOoC is not only to observe a crosstalk, but also to observe it in relevant physiological conditions compared to *in vivo*. This differentiates our work from many MOoCs, as explained in the introduction (section 1.2.5.2 p. 24). It requires:

- (i) generating the proper insulin concentration in the myotubes channel, with islets as insulin source
- (ii) optimizing the insulin-dependent glucose uptake by myotubes to match the sensor capabilities

In line with the experimental scenario described in section 3.1, these 2 objectives correspond respectively to *Step 2* (see Fig. 3.2b), and *Step 3* (see Fig. 3.2c). For each *Step*, we will identify the leverages and specifications thanks to *in silico* and *in vitro* investigations.

3.2.1 A measurable glucose uptake

Obtaining a measurable insulin-driven glucose uptake was the driving factor in scaling the myotube channel. We considered the uptake capability per elementary surface of myotube as constant, and we expected the insulin-mediated uptake to be low. We then wanted to amplify these glucose changes with the microfluidic chip design, while preserving cell viability and function. This required a trade-off on the volume: the lower the volume, the highest the glucose variations for a given uptake; but it also opens possible change in cell function, viability, or gene expression due to a reduced contact with culture medium. Thus, the optimal volume is the **highest volume for which glucose variations are detectable by the dedicated sensor**. To find this optimal value, we had to determine the uptake capabilities of the LHCN-M2 in the co-culture medium, and then extrapolate the greatest volume possible to match the sensor capabilities while maximising culture medium volume. It also implies characterization from the glucose sensor, coming in Chapter 4.

Note that it is not possible to anticipate the insulin-induced glucose uptake from the literature:

- Myoblasts differentiation into myotubes is highly impacted by the **medium** [Lauritzen and Schertzer, 2010]. As we have cultured the LHCN-M2 cells differently from the literature (medium and protocol), it was mandatory to assess the glucose uptake in our conditions.
- The state-of-the-art experiments studying insulin-driven glucose uptake were conducted with supraphysiological insulin concentrations (as opposed to physiological concentrations in our MOoC) [Lee et al., 2019] [Houghton et al., 2019] [Bala et al., 2021] [Navarro-Marquez et al., 2018] and/or with other cell lines as C2C12 [Lee et al., 2019], a murine cell line.
- The same state-of-the-art, when not using fluorescence as metrics, generally normalised the glucose mass by protein mass [Houghton et al., 2019]. The absence of raw data prevents to reuse quantitative results. The only work found without this kind of normalisation and reusable data was [Lee et al., 2019] (see Fig. 3.3).

Taking these points in consideration, we had to conduct our own experiments of *Glucose Uptake Assay* (GUA) with our cells in our conditions. For these experiments, a microfluidic chip able to maximise glucose uptake was designed.

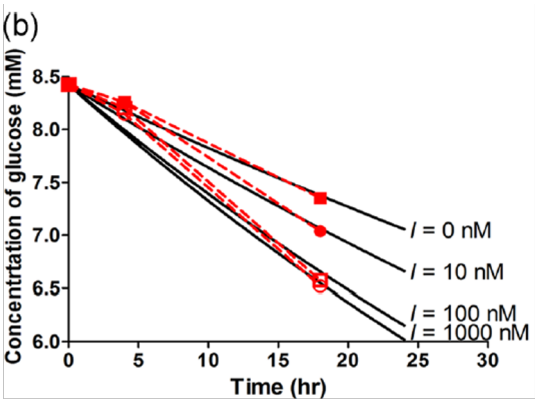

Glucose uptake by C2Cl2 muscle cells. Measured concentration profiles of glucose (dotted lines) in which C2C12 muscle cells were stimulated with different concentrations of insulin. A solid line depicts predicted profiles based on obtained parameters

FIGURE 3.3: Results of GUA conducted in [Lee et al., 2019] using C2C12.

The height of the chip is actually the only impacting dimension for glucose variations. Indeed, the volume increases proportionally with chip area, as does the uptake (under the assumption that a given surface of myotube has a constant uptake). As the variation of concentration is the ratio between the volume and uptake of glucose, increasing the surface will not increase concentration variations. This principle is illustrated in the Fig. 3.4. On the other hand, reducing chip height by 50% while keeping the same surface does not change the uptake but divides the volume by 2, doubling any variation in concentration.

According to this principle, GUA experiments were conducted in microfluidic chips with **100 µm height**. We hypothesize that this height is sufficient to maintain the cells, as it has already been used in previous work on skeletal muscle cells and non insulin-mediated glucose uptake [Zambon et al., 2014]. It is considered the minimum reasonable height, as the average diameter of a LHCN-M2 myoblast in suspension (non adhered to a surface) is 17 µm thus a fifth of the channel height.

Another adjustable parameter in our experiments could have been the number of myotubes: increasing them should increase glucose uptake for a given surface, in theory. However the formation of myotubes relies on the seeding of myoblasts reaching 80% of confluence when adhered. If too few or too many myoblasts are seeded, reaching less than 60% or more than 100%, respectively, they cannot fuse together in myotubes, as illustrated in the pictures of Fig. 3.5. Moreover, the final number and the size of myotubes cannot be controlled, whatever the number of seeded myoblasts. As a consequence, we did not consider the number or density of myotubes as a reliable leverage in our experiments.

To summarize, the intrinsic uptake capability of the 2D skeletal muscles culture was not a parameter we could reliably tune, whereas we could control the chips' height to amplify glucose variations induced by the uptake, and match with the glucose sensor capabilities. For these reasons, GUA experiments, which goal was to assess the glucose uptake capability of our model in our culture conditions, were conducted with the LHCN-M2 myotubes grown in chips containing 3 parallel channels of 100 µm height. This characteristic of the cell model can then be used to assess how far the height of the channel can be increased to find the proper trade-off in volume between detectable insulin-induced glucose uptake and cell's viability and function.

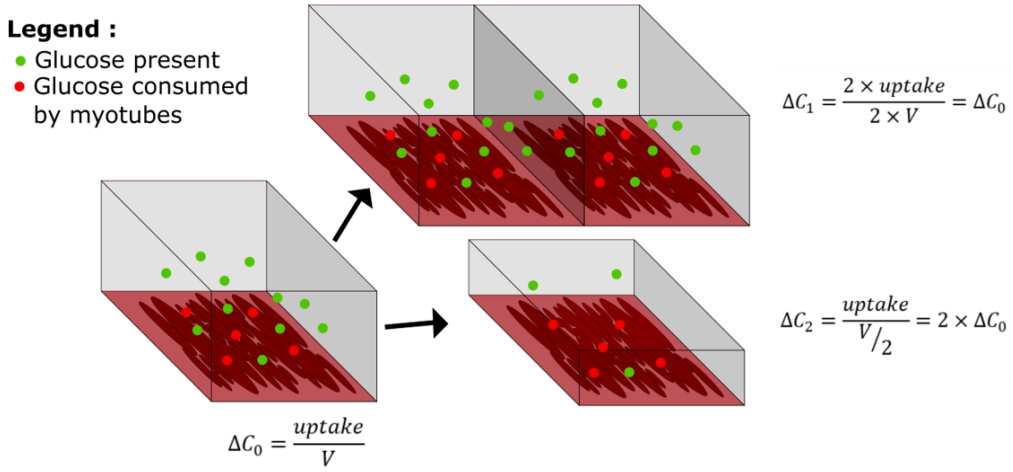

FIGURE 3.4: Illustration showing that the key point in the chip geometry to amplify the glucose variations myotubes-induced is the height. Left: reference chamber, where we consider the represented surface of myotubes takes 5 glucose molecules, named *uptake*. Top right: doubled surface which has no impact on concentration variations. Bottom right: half height, amplifying the concentration variations.

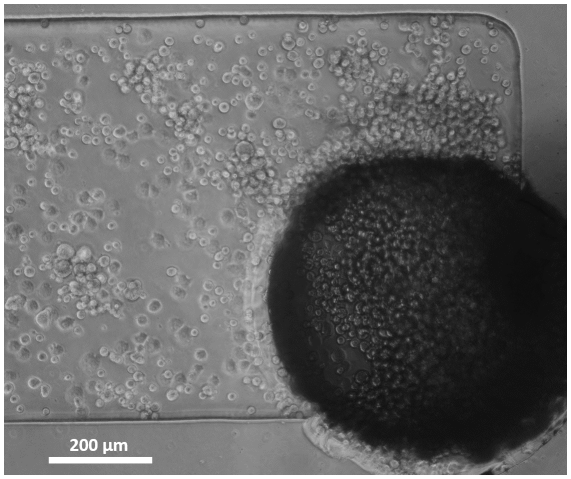

(A) LHCN-M2 myoblasts seeded too numerous.

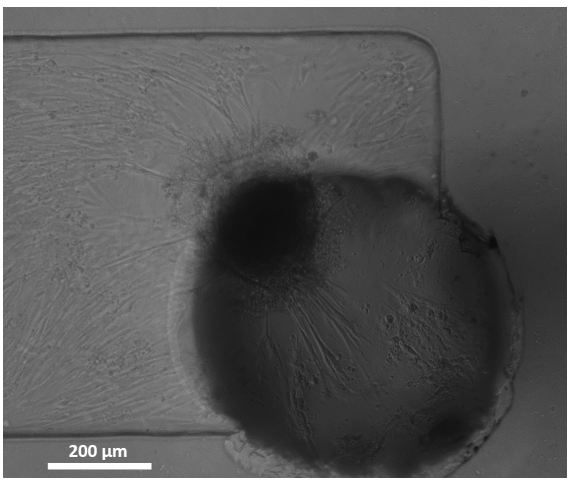

(B) After 4 days of culture, LHCN-M2 myoblasts have not well fused, and an aggregate of cells is formed.

FIGURE 3.5: Lack of fusion when too many LHCN-M2 myoblasts are seeded in a chip.

3.2.2 Generate physiological insulin concentration using a biological source

The other objective of the MOoC, as listed in the introduction of this section, is to generate insulin at physiological concentration in the myotube channel, with pancreatic islets as insulin source.

After a meal, the physiological insulin in human ranges between 300 pM and 600 pM according to previous works [Bhat et al., 2011][Woerle et al., 2003] [Singer et al., 1985][Lee and Woleve, 1998]; therefore the 300 pM to 1 nM range can be considered physiological. Within this range, we decided to target 500 pM for functional validation experiments (see section 2.1.3.5 p. 57). At this concentration, LHCN-M2 myotubes cultured in our co-culture medium showed a metabolic response. According to the literature, working in supraphysiological concentrations such as 100 nM insulin provides the maximum response, which makes it a usual positive control [Bala et al., 2021][Tsuchiya, Kanno, and Nishizaki, 2013][Navarro-Marquez et al., 2018][Jeon et al., 2019]. Positive controls are widely used in biology, thus we have used 100 nM for this purpose.

The insulin "generator" in our system are primary C57Bl6J mouse islets as explained in the Chapter 1 section 1.5.1. One of the main interest of this micro-organ model is the existence of an *in silico* model of C57Bl6J islets which has been developed by [Alcazar and Buchwald, 2019], a key point for our hybrid *in silico-in vitro* design methodology. Indeed we integrated a simplified islet model based on [Alcazar and Buchwald, 2019] work in the *in silico* MOoC model we investigate in section 3.3.

The MOoC *in silico* model was used to assessed the possibility of reaching the 2 targeted insulin concentrations (500 pM and 100 nM) in the system, while respecting the shear stress constraints described in Chapter 2 section 2.1.2.1 p. 32. This *in silico* MOoC also assessed the time required for islets to generate the targeted concentration in the myotube channel. This duration corresponds to the moment the flow has to be stopped in *Step* 2, to begin *Step* 3 (see Fig. 3.2 p. 71 for the schematic description of the MOoC experimental protocol).

3.2.3 Concluding remarks on setting the scaling strategy

After the determination of the 3 steps of the protocol on the MOoC (see Fig. 3.2), we have defined a **scaling methodology to identify the leverages (h, n, Q)** and characteristic of the system **(t)** to reach the target insulin levels and measurable glucose uptake. The MOoC schematics in Fig. 3.6 illustrate these leverages whose values are yet to determine. This is the objective of the 2 next sections.

3.3 Scaling the insulin generator

This section details how we scaled our insulin source, that is primary mouse islets, according to the strategy described in section 3.2.2. We used multiphysics simulation to explore the leverages controlling insulin concentration in the MOoC, and find proper sets of parameters while respecting biological limits. *In vitro* validation experiments were conducted on C57Bl6J mouse islets in a prototype of the MOoC chip to validate the simulations.

3.3.1 In silico experiments

3.3.1.1 Designing the simulation

The 3 parameters *expected* to mainly influence the steady state insulin concentration in a given myotubes chamber geometry are the flow rate, the insulin source rate, i.e. the number of islets, and the myotube channel section. Therefore, they were the subject of a simulation campaign with two primary objectives :

- find the couples of values *(Q,n)* of *flow rate* and *number of islets* for which the targeted insulin concentrations are reached in steady-state (500 pM as physiological value, 100 nM as positive control), and for which the shear stress constraint is met (below 6 mPa for islets, below tens of mPa for myotubes, see section 2.1.2.1),
- for the validated couples, measure the time needed to reach steady-state, to determine when the flow may be stopped *(t)* and the incubation process (Step 3) may start.

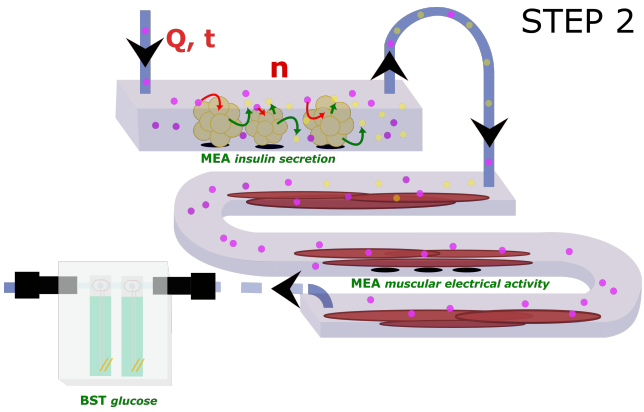

(A) Parameters to set the desired insulin concentration in the myotube channel, achieved in *Step 1*: 1) glucose solution flow rate *Q*; 2) duration of perfusion *t*; 3) the number of islets *n*.

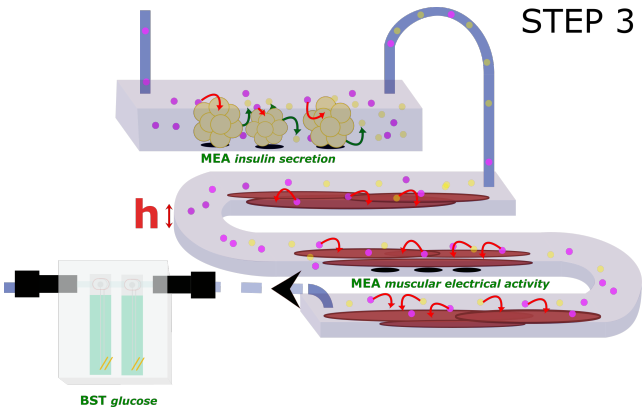

(B) Parameter to modulate the glucose variations induced by the insulin-dependent glucose uptake: the chamber height *h*.

FIGURE 3.6: Schematics representing the scaling leverages studied for the scaling, that appear in *Steps 2* and *3* of the MOoC interaction experiment.

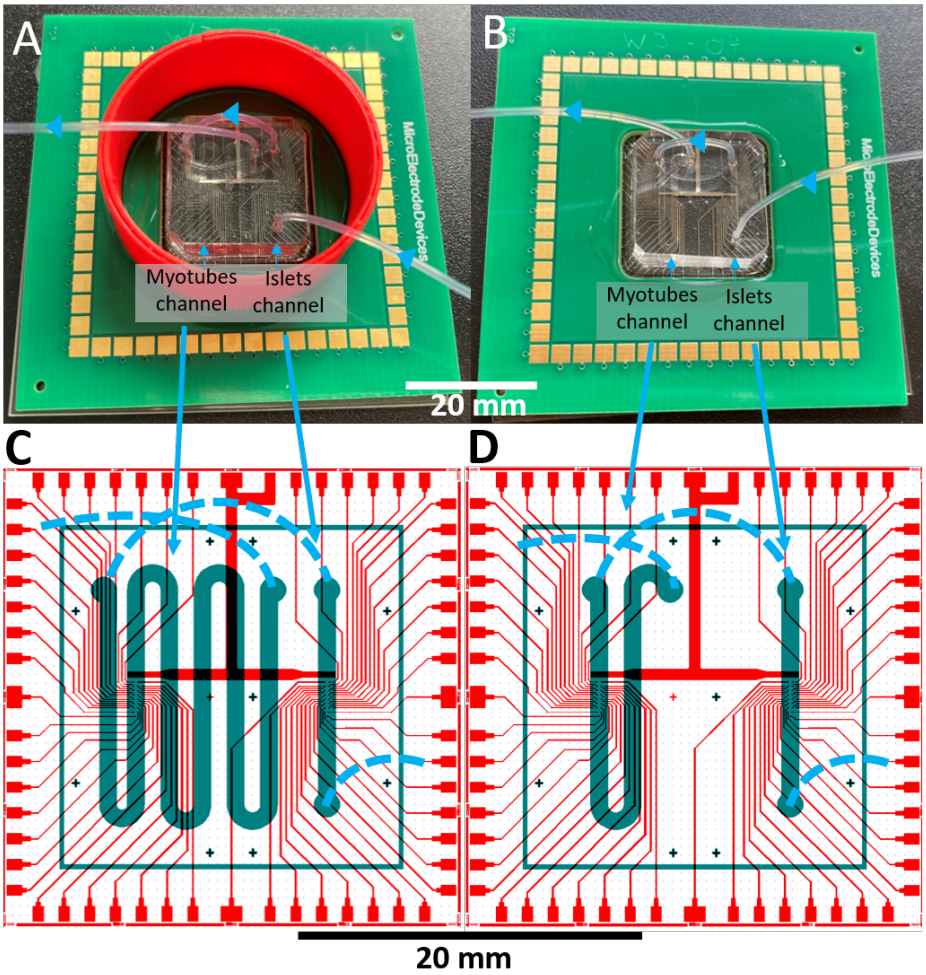

FIGURE 3.7: (A) the 100 µm height version of the chip with home made 3D printed ring (in red) bonded using PDMS, to create a culture pool; (B) the 300 µm height version of the chip as received from the supplier. (C) and (D) the corresponding CAD layouts of the MEA electrodes and contact pads (red), the aligned channels of the chip (blue/green) and tubings (dashed light blue).

As presented in section 3.2.1, the height of the myotube channel is to determine based on the GUA results from section 3.4. However GUAs being conducted in parallel, and due to fabrication constraints (supplier specifications, cost and timing), 2 heights were pre-selected to study the impact of the geometry in the simulations: the minimal height of 100 µm, and the maximal (according to supplier fabrication constraints) height of 300 µm. Thus simulations were conducted with 2 MOoC designs of extreme possible volumes, with a myotube channel of either 100 or 300 µm height. The length of the channel in those 2 designs varied so that the overall volume of the myotube channel was 6 µl (this volume was experimentally determined as the minimal compatible with the glucose sensor selected for the MOoC experiments (see section 4.2)). The 2 chips fabricated and delivered are shown in the Fig. 3.7, with photographs and CAD (Computer Assisted Design) layouts.

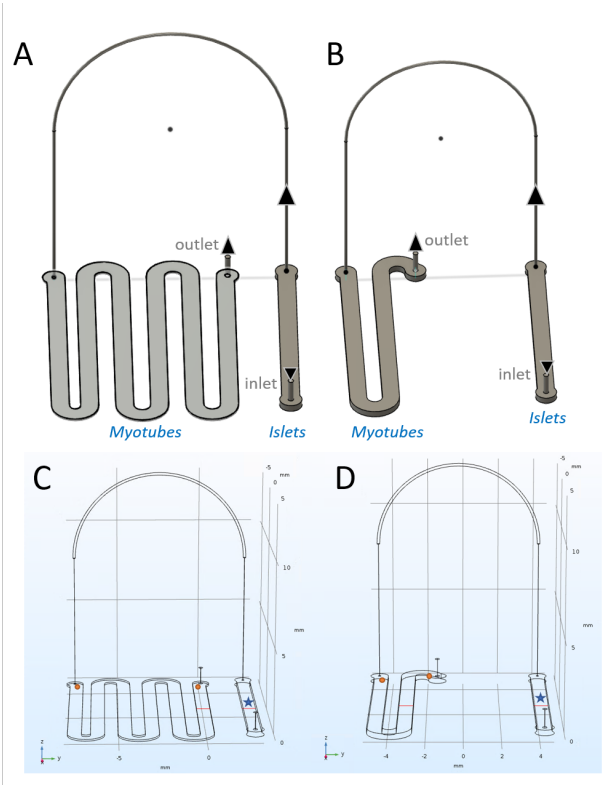

FIGURE 3.8: (A) and (B) CAD models (Autodesk Fusion) of the MOoC chip with the 100 µm or 300 µm height myotubes channel. (C) and (D) The 2 previous geometries used by COMSOL, with: the point of insulin source (blue star), the 2 probes measuring insulin concentrations at the inlet and outlet of the myotube channel (points), and the *Cut Lines* along with shear stress was calculated (red line).

3.3.1.2 Chip simulation description

The 3D geometry of the chip was drawn in COMSOL Multiphysics software (see Fig. 3.8). The islets were represented by a 1-D insulin source (see Fig. 3.8 panels (C) and (D)). The insulin source flow model was based on the work of [Alcazar and Buchwald, 2019], as already used in the previous chapter (see section 2.1.2.4 p. 39). COMSOL *probes* were placed at the inlet and outlet of the myotube channel to monitor insulin concentration over time (see Fig. 3.8 panels (C) and (D)).

Stationary simulations were conducted to find the flow rate and islets number allowing to get both the correct insulin concentration in the myotube chamber, and a shear stress within the specified limits. The simulated shear stress was recorded along a *Cut line* normal to the direction of the flow, as represented in Fig. 3.8 (C) and (D). The transient time, defined as the time to reach the plateau value, was assessed using a transient simulation. Table 3.1 provides the physics modules and the values of the parameters used for the simulations, as well as the post-processing expressions.

3.3.1.3 Results

To maintain the shear stress level in the islets channel below the 6 mPa limit (see Fig. 3.9), the flow was limited to 5 µl/min maximum. The dynamics of the system showed that insulin

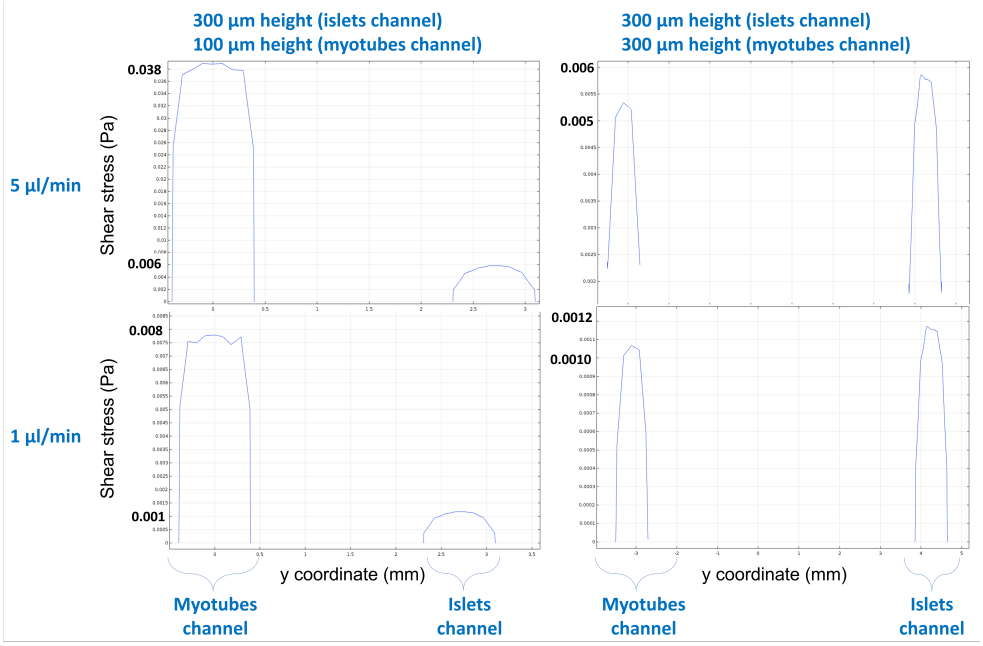

FIGURE 3.9: Shear stress plots at the bottom (z = 5 µm) of islets and myotubes channels, obtained in the 4 different configurations of geometries and flow rates given in Table. 3.11.

Parameter	Value/expression	Reference
Insulin diffusion coefficient in water	$1.50 \times 10^{-10}\ m^2.s^{-1}$	Patel et al., 2021
Glucose diffusion coefficient in water	$4.00 \times 10^{-10}\ m^2.s^{-1}$	L. Glieberman et al., 2019
Insulin secretion rate of 1 islet exposed from 3 mM glucose to 8 mM of glucose	$9.5 \times 10^{-18}\ mol.s^{-1}$	Alcazar and Buchwald, 2019
Shear stress expression in the results	d(spf.U,Z)*mu: derivative of speed toward z axis as main direction of speed variation, multiplied by the dynamic viscosity of water (0.000692 $kg.m^{-1}.s^{-1}$)	
Islet secreting	Point mass source ; in Transport of diluted species library	
Microfluidics	Laminar inflow library	
Molecule transport	Transport of diluted species library	

TABLE 3.1: COMSOL formalism and parameters with their reference.

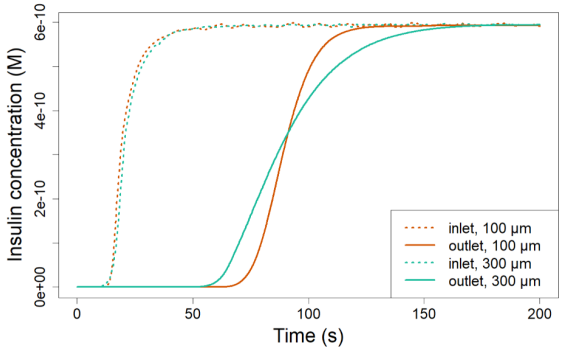

(A) Insulin concentration profile over time at the inlet and outlet of the myotube channel, depending on the myotube channel height, with 5 islets and 5 µl/min. Target insulin level is for 500 pM, actual plateau values is 590 pM.

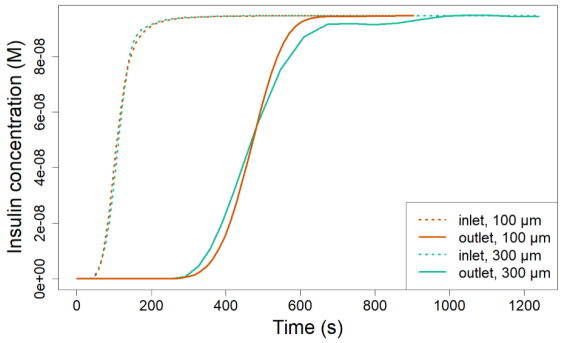

(B) Insulin concentration profile over time at the inlet and outlet of the myotubes channel, depending on the myotubes channel size, with 160 islets and 1 µl/min. Target insulin level is for 100 nM, actual plateau values is 94 nM.

FIGURE 3.10: Dynamic insulin profiles in the myotubes channels of different heights, for the targeted insulin concentrations (500 pM and 100 nM).

concentration reached a steady state with the 2 pre-selected geometries (see Fig. 3.10). Flow rates associated to specific numbers of islets were found to achieve the desired steady states in insulin concentration. As presented in Fig. 3.11, for both designs, selecting 5 islets and 5 µl/min provided a concentration at 590 pM in the myotubes channel; selecting 160 islets and 1 µl/min provided 94 nM. Interestingly the variation of myotube channel section did not appear to impact the steady state concentration. Moreover, we observed a convenient proportional impact of the flow or of the number of islets on the final insulin concentration, which fast forwarded the parameters research: increasing the number of islets proportionally increases insulin levels, while increasing the flow rate has the opposite effect.

Concerning the transient time, we observe for a given couple of parameters (n, Q) that the concentration rising slope is different according to the geometry: at the lowest height the concentration starts to rise later but converges earlier, while at the highest height the slope is lower and the concentration increases earlier but converges later (see Fig. 3.10). When the number of islets/flow rate is higher, the difference of slope is less important and the actual convergence time was found the same in the case of the 160 islets at 1 µl/min (or 100 nM targeted). The transient time found to reach 500 pM are finally 140s or 200s for respectively chambers of 100 and 300 µm, and 900s to reach 100 nM.

Design	Flow (µl/min)	Number of islets	Final insulin concentration in myotube chamber	Shear stress in islets chamber (mPa)	Shear stress in myotubes chamber (mPa)	Transient regim (s)
Channel + Serpentine of 100 µm height	5	5	590 pM	6	40	140
	1	160	94 nM	1.2	8.1	900
Channel + Serpentine of 300 µm height	5	5	590 pM	6	5	200
	1	160	94 nM	1.2	1.1	900

FIGURE 3.11: The different sets of parameters reaching the targeted insulin concentration and shear stress.

3.3.1.4 Discussion

Referring to the Fig. 3.6a in section 3.2.3 p. 76, the simulations allowed to determine the couples of parameters (n, Q) to reach the targeted insulin concentrations (respecting the shear stress constraint) in the 2 extreme possible MOoC chips. The simulations demonstrated the great versatility of the system: we found physically possible couples (n, Q) to reach the 2 targeted concentrations, even if the targeted concentrations were separated by a factor 200. When 100 nM is targeted, 160 islets are required, which is a slight and acceptable overflow compared to the 150 islets limit (defined in constraint (6) in section 2.1.2.1 p. 32). Indeed the criteria was set corresponding to the usual lowest number of islets collected with a mouse dissection, and it is possible to collect until about 400 islets. The flow rate required of 1 µl/min is technically possible when using appropriate flow rate meter (in Fluigent, the XS reference suits well). The number of islets found to reach 500 pM is this time less acceptable, as 5 islets is below the estimated 10 islets required to limit the biological variability of individual islets and provide statistically repeatable results. However the number of islets can be easily increased by design modification. Indeed, reaching 500 pM with more islets would require to increase the flow rate (above 5 µl/min). But the flow rate is already at the higher limit with the current channel geometry, due to the shear stress constraint. So to be able to increase the flow rate, the shear stress has to be decreased in the islet channel. This is possible by increasing the height of the channel, as increasing the channel section results in decreasing the flowing fluid velocity responsible for the shear stress. In this work it was limited to 300 µm due to supplier fabrication constraint, but it is possible to realize microfluidic channel of 500 µm height using lithography [Ugrinic et al., 2023] or 3D printing.

Therefore with the 2 extreme possible MOoC designs (myotube channel at 100 µm or 300 µm), it is possible to conduct experiments respecting the shear stress constraint. **A design modification in the islets chamber is requested to increase the number of islets over the limit of 10 islets in the case of 500 pM targeted**.

The transient time of these scaling simulations provided the t, that is the duration of *Step 2* in the MOoC experiment as presented in Fig. 3.6a in section 3.2.3 p. 76. This represents the time required for islets to generate the appropriate insulin concentration when high glucose is injected. **The values of t are informative in these simulations, and their suitability can only be discussed in regards to results of GUA experiments**. Indeed, the glucose uptake is measured in the volume of medium that incubated 1 hour, at *Step 3* (Fig. 3.6b p. 76), and any uptake occurring during the *Step 2*, with flow of duration t, is not taken into account in the measure. Therefore if the uptake is low and/or mostly occurs at the beginning of the insulin exposition, the transient time t must be short enough to not hide the acute insulin effects.

3.3.2 In vitro validation

3.3.2.1 Introduction and objectives

Our objective was to experimentally validate the simulations, and define if correction factors have to be applied between *in silico* and *in vitro*. One possible source of drift identified is the difference of medium used between the *in vitro* experiments used in [Alcazar and Buchwald, 2019], compared to the medium intended to be used for the MOoC experiments, derived from the co-culture medium, and that we will name hereafter the *GUA medium* (defined in section 3.1 p. 67). It is known that the secretion is different between a poor buffer containing only electrolytes like in [Alcazar and Buchwald, 2019] and a richer medium like our medium [Zhu et al., 2019].

The *in silico-in vitro* comparison is made on 2 features: the insulin concentration steady state and the time to reach the steady state.

3.3.2.2 Validation procedure

Briefly, the experiment consisted in cultivating C57Bl6J mouse islets in the islets channel of a MOoC fabricated by the supplier MED. At that time, only one design had been fabricated and was usable (2 chips): the MOoC with a myotube chamber at 100 µm height. The secretion of insulin in response to glucose was then determined by ELISA after collecting samples flowing out from the chip while high glucose was perfused. The experiment was conducted with buffer-type medium and GUA medium. The value and dynamics of insulin were then compared between the simulation and the real experiment.

We experimentally validated simulations with other (n, Q) than the ones found for the MOoC scaling, due to the ELISA detection range and to minimize the use of biological resources (primary mouse islets). Indeed, ELISA detection range is 34 pM to 1 nM according to the datasheet, and the lower limit is even considered to be 140 pM by the biologists (the concentrations below are poorly discriminated). Therefore 500 pM was too close to the lower limit of the assay: if the secretion was more than 3 times smaller than predicted, we would be in the less precise detection range or below the detection range. Regarding 100 nM, that required 160 islets, we decided to target a lower insulin concentration steady state to use less islets. Indeed, the validation of simulations does not require to work at such high insulin concentration. Therefore it was preferable to validate experiments with less islets and targeting less insulin concentration steady state to limit the use of the precious biological resource.

Using the proportional relationship found between the parameters and the final insulin concentration, we found 10 islets and 1 µl/min as a good compromise. The expected final concentration is 6 nM according to the simulation. A simulation confirmed 10 islets with 1 µl/min allows to reach a final insulin concentration at 5.9 nM in 800 s (taking into account the tubing used at the outlet of the chip to collect the samples). However the first experiment (data not shown), led us to consider to use more islets. Another set of experiments was also conducted with 50 islets and 1 µl/min, where the steady state predicted was 30 nM in 880 s.

3.3.2.3 *In vitro* experiment material and method

Microfluidic chips The 2 MOoC chips (MED n°1 and n°2) with a myotube channel of 100 µm height were supplied by MED without ring. A home made MOoC with glass substrate (Glass substrate) was also fabricated: a PDMS block was molded on a 3D printed mold fabricated by Protolab (description in section 3.4.1.1 and bonded on a glass substrate. For both types of chips, a culture ring was 3D printed in PLA filament, using MakerBot replicator 2 printer, to create the pool for medium (see panel (A) of Fig. 3.7).

Islets culture The primary mouse islets were collected from C57Bl6J according to the procedure in [Pedraza et al., 2015]. They were maintained in petri dish in the incubator (37 °C, 5% CO2) in culture medium 2 days prior to seed them in the sterilized islet channel of the MOoC. Sterilization of the MOoC was done by UV (30 min, 5,000 J), followed by plasma (hydrophilizing the surface too) 2 min at 9.83 $W.L^{-1}$ (Femto type B, electronic Diener, Ebhausen, Germany). Within 20 min a coating of 5% Matrigel was injected in the islet channel and let 1 hour at room temperature. Drops of Matrigel were applied at the inlet and outlet to prevent the Matrigel from complete drying during this hour. Depending

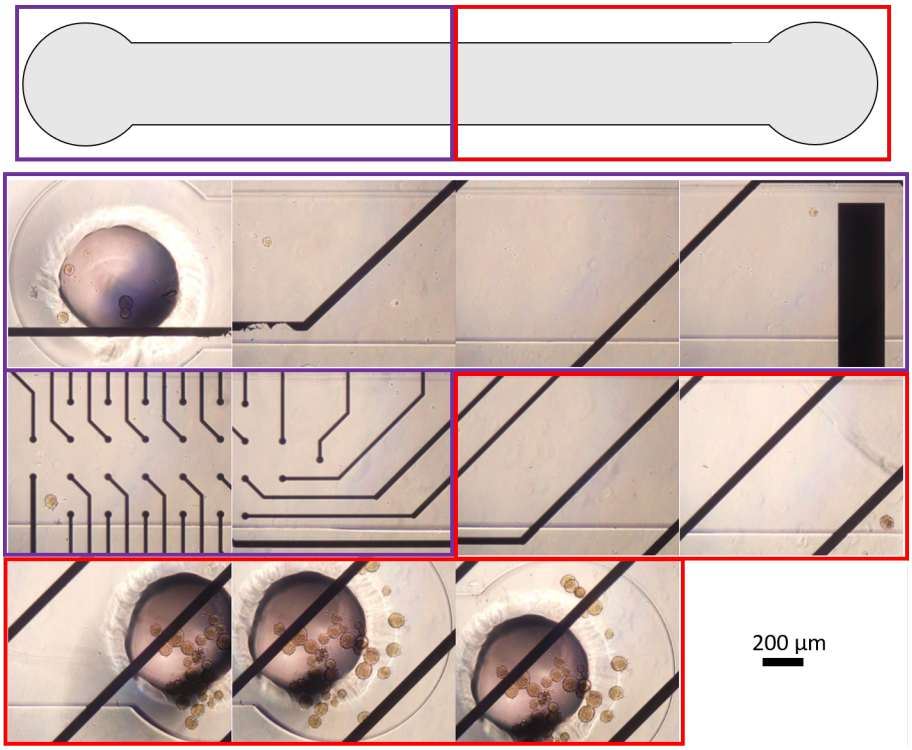

FIGURE 3.12: Bright field images of the seeded islets in the islet channel. The images from left to right and top to down correspond to the channel from left to right, as represented on the top scheme with the 2 colored frames.

on the experiment, 10 or 50 islets were seeded by injecting them using a P10 directly in the channel with Matrigel, after removing the drops. The seeded islets in the chip are visible in the Fig. 3.12. Culture medium was added in the pool of the chip, so that the level of liquid was above the chip and nutrients/oxygen can penetrate by diffusion by the inlet and outlet of the chip, as well as by the PDMS. After 3 days, the medium was renewed in the pool.

Secretion experiment The experiment was carried out the 5^{th} day after seeding, with the protocols illustrated in Fig. 3.13. The chip was firstly submitted to the protocol illustrated in Fig. 3.13a, and then to the one illustrated in Fig. 3.13b. The difference between the protocols is the medium: in the first protocol, the medium was the ***GUA medium***, and in the second protocol it was a buffer similar to the one used by [Alcazar and Buchwald, 2019], named ***EPHYS medium***, whose composition is provided in section 3.1 p. 67. Those 2 conditions were separated by 1 hour during which the islets recovered in the culture medium.

As illustrated in Fig. 3.13, the beginning of both protocols was similar: islets were perfused 45 min at low glucose (3 mM), followed by 54 min at high glucose (8.2 mM). The protocol with the GUA medium stops after the high glucose condition, while in the EPHYS medium protocol, the high glucose medium was replaced by EPHYS supplemented with 16.7 mM of glucose and Forskolin at 1 µM. Forskolin (Fsk) is a potent stimulus usually used as control to test the capacity of secretion of the islets. This control has been introduced after the first experiment showing extremely low secretion: the final concentration was 60 times lower than simulation (data not shown).

Samples of 6 µl were collected 12 minutes and 6 minutes before the end of the starvation step, and then every 6 minutes at high glucose (and during the stimulation with Forskolin

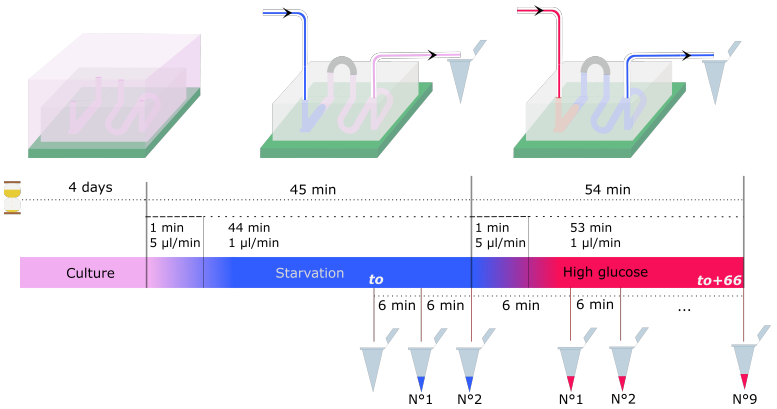

(A) Protocol for the experimental validation of simulations, with the GUA medium.

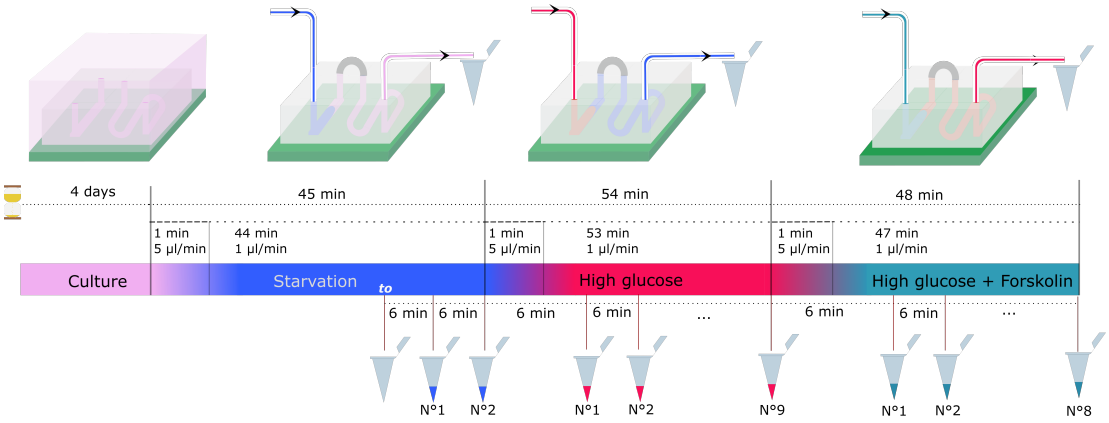

(B) Protocol for the experimental validation of simulations, with the EPHYS medium.

FIGURE 3.13: The 2 protocols applied subsequently on each chip: (A) with GUA medium (B) with EPHYS medium. Note that the second one has a supplementary control with Forskolin.

when EPHYS medium was used). To remove potentially detached cells that would contain insulin and distort the results, 5 µl of the samples were taken and supplemented with 5 µl of the corresponding medium. After centrifugation (5 min, 0.8 rpm, at 4 °C), 7 µl of the supernatant were collected. The 6 min sampling interval is a trade-off between having the highest sampling frequency and delivering the minimum volume required for ELISA (i.e. 5 µl).

The 5 experiments performed are listed with their respective parameters (chip, number of islets, medium) in Table 3.2. Note that the experiment made with Glass substrate chip used islets from the same pancreas as MED n°2 to compare substrate impact on the secretion.

Insulin quantification The volume of the samples was only allowing 1 measure with ELISA, which is a destructive test. This implied that the appropriate dilution factor must be chosen directly without possibility to measure a second time the sample.

Therefore, as a first estimate of the insulin steady-state concentration, the concentration of the last sample in the high glucose step (n°9, at t_0+66 min) was measured in each experiment with a first ELISA (mouse ELISA insulin kit, ref 10-1247-01, Mercodia, Uppsala, Sweden). We consider that at t_0+66 min, the steady state of concentration is guaranteed as it

Experiment name	Chip name	Number of islets	Medium
a	MED n°1	10	EPHYS
b	MED n°1	10	GUA
c	MED n°2	50	EPHYS
c	Glass substrate	50	EPHYS
d	MED n°2	50	GUA

TABLE 3.2: List of experiments and their respective conditions. MED chips had myotube chambers with 100 µm height. Glass substrate is a chip with the same microfluidic design but the PDMS was bonded on a glass slide. Note that the 2 experiments with MED n°1, as well as the 2 experiments with MED n°2, were conducted the same day then with the same islets. The experiment with Glass substrate chip had islets coming from the same pancreas as the experiments with MED n°2.

corresponds to more than 3 times the simulations prediction. Generally a second sample was measured during this dosage at t_0+60 min or t_0+72 min depending on the experiment. The results of this first ELISA could then indicate better dilution factor to apply to the remaining samples. The dilution factor of these first samples was chosen according to simulation results and considering half less secretion than expected.

3.3.2.4 Results

The kinetics of insulin secretion obtained during the 5 experiments listed in Table 3.2 were reported in Fig. 3.14.

Fsk control and validation of experiments In the EPHYS experiments (**a** and **c**), the Fsk control in the experiment with 10 islets did not provided reliable increase in insulin concentration between 72 min to 120 min (frame of Fsk perfusion). An effect of Fsk was detectable in the 2 experiments with 50 islets. In these 2 experiments, even if a part of the points were in the less reliable range, the difference between the concentration at the end of the high glucose step (60 min) and at the end of the Fsk step (114 min) was sufficiently consistent to consider an increase in insulin secretion. Therefore, we will not take into account the experiment with 10 islets in the case of EPHYS (**a**), and the other experiment conducted with these islets, in GUA (**b**), must be interpreted carefully.

Comparing the insulin concentration at steady state The experimental results to compare with the simulations are the concentrations measured at high glucose step. We focus here on the experiments with EPHYS as the perfusion medium was closest to the experiments used to set the model in [Alcazar and Buchwald, 2019] as previously explained.

After excluding **a**, we consider only the 2 experiments at 50 islets in EPHYS (**c**). The first ELISA (conducted to assess the dilution factor for the remaining samples) was erroneous and led to over dilute the remaining samples: the first dosage measured samples at about 12 nM while they should have been at about 700 pM according to the second ELISA. The Fsk point at 4 nM was probably the only reliable point of the first dosage, as it corresponds to the kinetics of the slope.

After excluding these outliers, the steady state concentration was at around 700 pM in the 2 experiments with 50 islets in EPHYS, whereas the simulations predicted 30 nM. Even if the 700 pM are not quantitatively fully reliable (points in orange), the repeatability between results in the 2 experiments in EPHYS suggests that the order of magnitude is consistent.

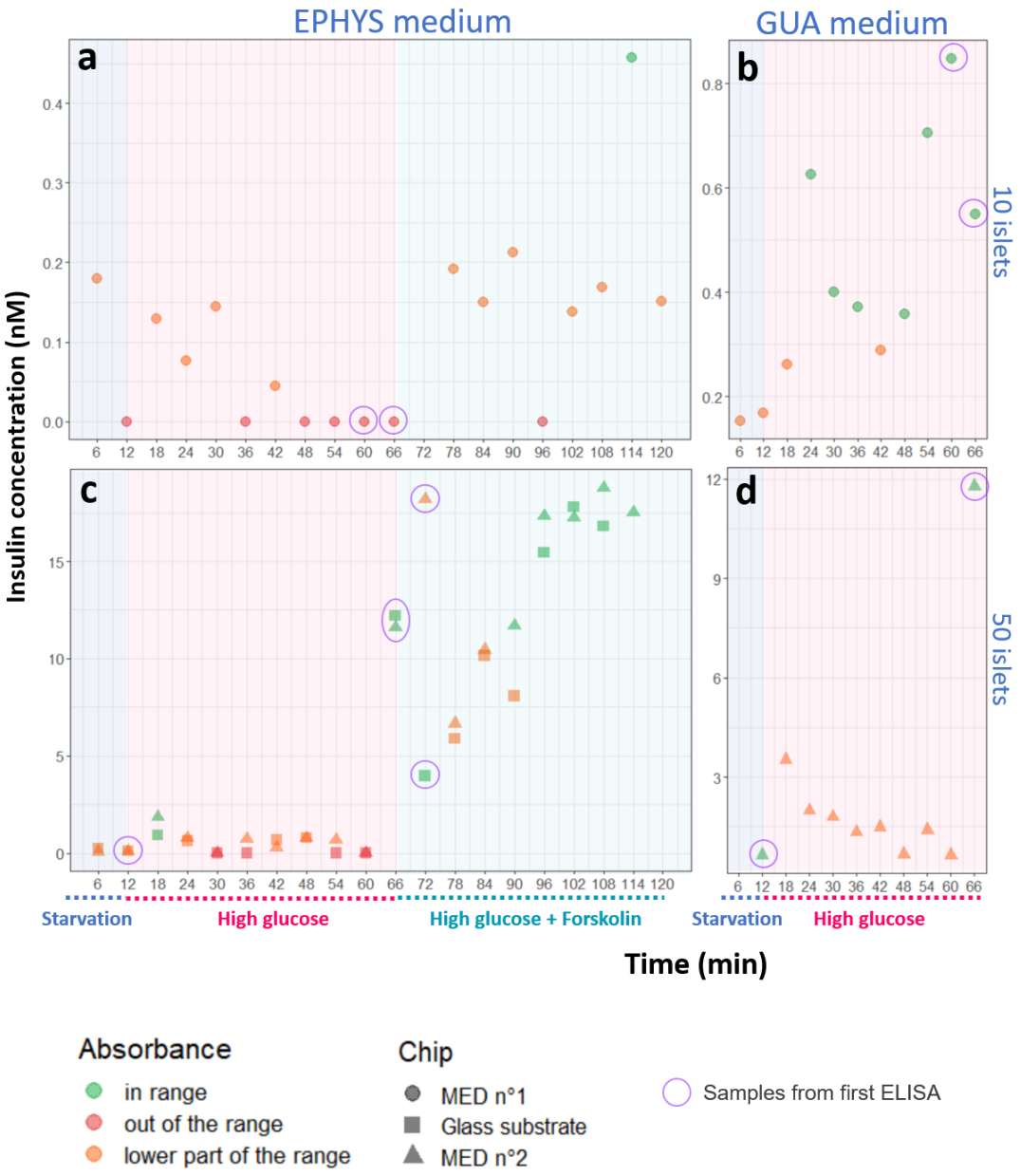

FIGURE 3.14: Insulin concentration over time in the 5 experiments listed in Table 3.2. There are 4 graphics, as the experiments were sorted by the number of islets used and by medium, thus the 2 experiments with 50 islets in EPHYS were plotted on the same graph (**c**). In all plots, the 3 different chips used can be distinguished by the shape of the point. Finally, the color of the points indicates if the absorption was in the reliable detection range of the ELISA (green), or out of the range (red, point plotted at 0 nM) or in the lowest part of the detection range thus not considered fully reliable (orange, absorbance below 0.1 but above the minimum of detection range). The correspondence between the time and the step in the protocol (starvation, high glucose, and high glucose and Fsk if the medium was EPHYS) is indicated by a colored background in the graphs.

Moreover, a factor 40 cannot be due to measure imprecision. Then the steady state concentration of *in vitro* results in EPHYS do not correspond to the simulation predictions.

Impact of the medium on the concentration at steady state The GUA medium was introduced in these experiments to know whether an eventual difference of secretion due to the different composition of the media can change the final insulin concentration. For 50 islets, in the experiment GUA (**d**), the concentration oscillates between 0.6 nM and 1.5 nM. The maximum of the oscillations is the double of the steady state value obtained in the EPHYS experiments with 50 islets (**c**).

Even when dropping out the 10 islets experiment in EPHYS (**a**), we can observe that the concentration was higher too in the GUA medium (**b**). Indeed, the same dilution factors were applied in both EPHYS and GUA medium experiments, and almost all concentrations were in the best part of the detection range with the GUA medium, contrary to the EPHYS experiment.

As the islets secreted more in GUA medium, the multiplying factor between the steady state concentration *in vitro* and *in silico* is lower. For 50 islets in GUA medium (**d**), the factor is 30 (1 nM in average vs 30 nM) while it is 40 with EPHYS medium (**c**). In the case of 10 islets in GUA medium (**b**), the factor is around 8 (if considering 700 pM vs 5.9 nM).

Deduction of the couples "number of islets / flow rate" from the *in vitro* results Other couples sets of (n, Q) parameters were deduced from *in vitro* data, using cross multiplication: we determined the number of islets required to reach either 500 pM or 100 nM, with 1 µl/min; if the number of islets was not in the acceptable range (10-150), the flow rate was modified (between 0.1 µl/min to 5 µl/min, to respect technical limits and shear stress limits) to try to reach this range. The results are summarized in the Table 3.3.

Targeted insulin concentration	Couple from simulation results	Couple from *in vitro* results with EPHYS medium	Couple from *in vitro* results with GUA medium
500 pM	5 islets 5 µl/min	36 islets 1 µl/min (and others)	14 islets at 2 µl/min (and others)
100 nM	160 islets 1 µl/min	7143 islets 1 µl/min, or 142 islets 20 nl/min	1429 islets 1 µl/min, or 286 islets 200 nl/min

TABLE 3.3: Table summarizing, for each targeted insulin concentration, the (n, Q) values found by simulation, and some possible couples possible using the *in vitro* results either in EPHYS or GUA medium.

We can see that other couples can be found for the physiological concentration (500 pM), however, it is impossible to find satisfying couples when 100 nM is targeted. Either the number of islets is not satisfying, or the flow rate. We conclude that it is not possible to set up a MOoC experiment targeting 100 nM of insulin with the current design and with islets secreting at the level found in these *in vitro* experiments.

Comparing the dynamics One objective of the experiments was also to analyse the insulin concentration dynamics. On Fig. 3.15, we zoom on the insulin concentration during the starvation and high glucose steps (experiments b, c, d, also see Table 3.2).

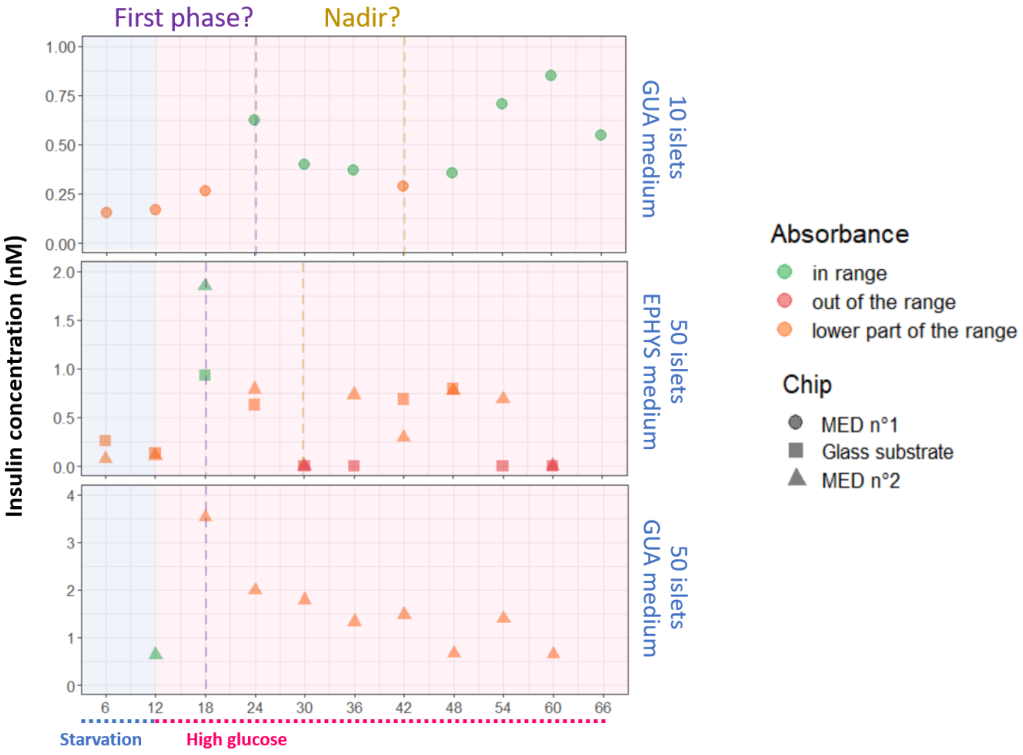

FIGURE 3.15: Focus on the results in the starvation and high glucose steps. On each graph, the potential first phase and Nadir are represented (notions introduced in section 1.1.2.1.)

In all 4 experiments, we observe a peak in concentration from 6 min to 12 min prior to the beginning of high glucose, similar to what is reported for the first phase of insulin secretion *in vitro*, notably in [Alcazar and Buchwald, 2019] (see Fig. 1.6 in section 1.1.2.1 p. 9). A Nadir can be observed in 3 of the 4 experiments. The fact that we did not observe it in the GUA experiment with 50 islets might be due to a desynchronization of the islets that did not have their Nadir at the same time.

The potential observed Nadir induced a delayed steady state compared to the simulations (see Fig. 3.16). With 50 islets, the measured steady state occurred 10 min after what was determined by simulation (36 min vs 26 min). Concerning the experiment at 10 islets in GUA medium, the Nadir was very delayed and the shift between the steady state of simulation and the measured one were separated by 24 min (54 min VS 30 min).

3.3.2.5 Discussion

These experiments were challenging, as ELISA requires high volumes compared to the chips' volumes and flow rates used. Thus the sampling frequency was low compared to expected dynamics (sampling every 6 min), and the samples could only be measured once. This required the dilution factor to be accurately chosen, but with dynamic evolution of insulin concentration, a narrow detection range, and erroneous results, the measures were mostly in the less detectable part of the technique. In almost all experiments the steady state in the high glucose step was in the lowest part of the detection range or out of it.

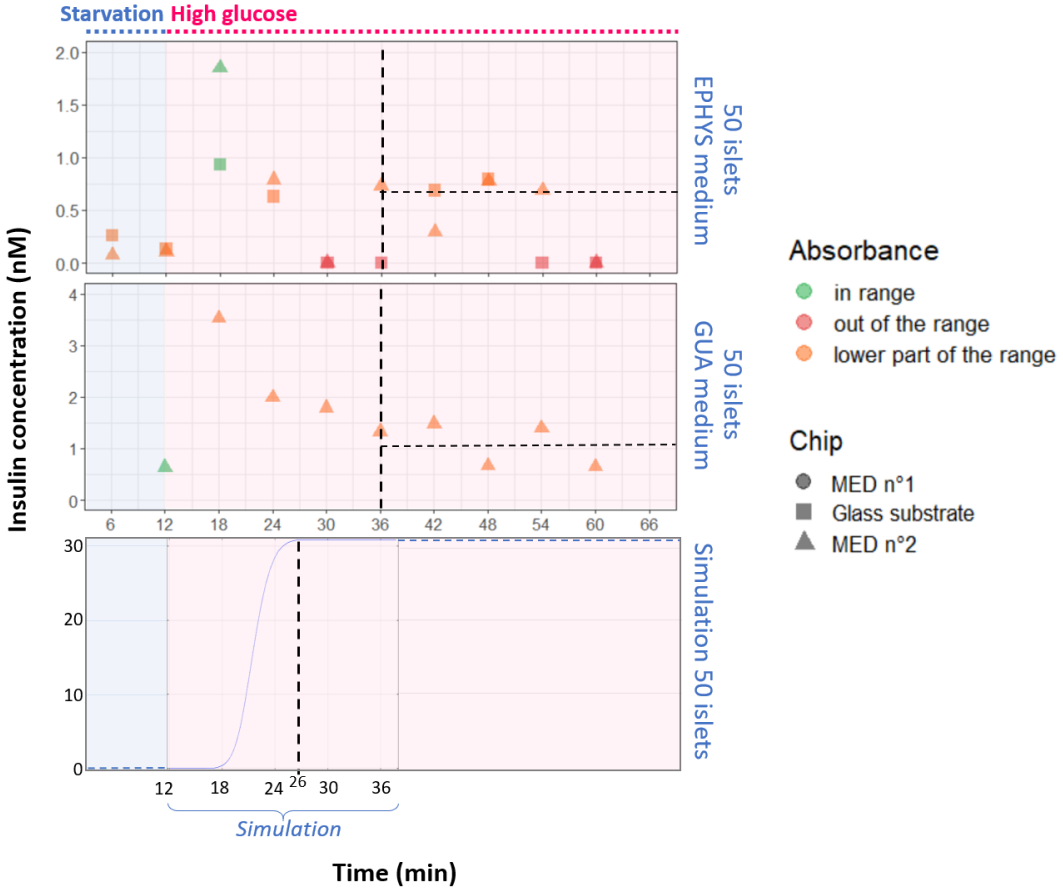

(A) Graphical comparison of the transient time in simulation and *in vitro* experiments using GUA and EPHYS media (50 islets with 1 µl/min).

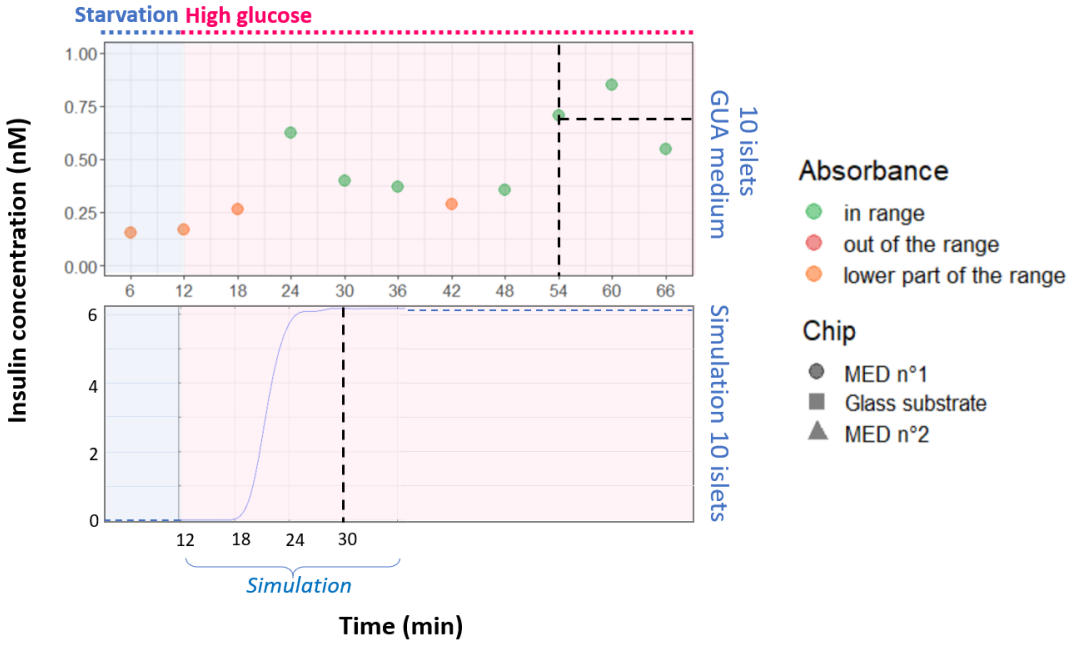

(B) Graphical comparison of the transient time in simulation and *in vitro* experiment using GUA medium (10 islets with 1 µl/min).

FIGURE 3.16

However, even if we cannot precisely determine the steady state concentration, there is a repeatability in the results confirming the order of magnitude around 1 nM in all experiments except **a**. Therefore, despite the lack of precision in the measurement, we can conclude that the steady state of insulin concentration *in vitro* does not match with the simulation. As expected, the GUA medium seems to amplify insulin secretion, by about a factor 2 but it would require to be confirmed by other experiments with proper dilutions.

To address the issue of the large difference between the insulin concentration steady state between simulations and experiments, we have to take into account the results of secretion experiment with the first MOoC chip design (see section 2.1.2.4), which shown a consistent similarity between *in vitro* and *in silico* (respectively 2.7 nM and 4 nM). We therefore hypothesize that the origin of the issue is not the simulation but the experiment.

The difference between the secretion experiments in chip n°1 and n°2 could not be due to the culture substrate (glass substrate in experiment with chip design n°1). Indeed, the 2 experiments with 50 islets in EPHYS medium were conducted with the same chip design but either with SU-8 substrate or glass substrate, and they showed similar results, as shown in the Fig. 3.14.

However the volume of culture was different between the initial secretion experiment and this one: the islets in chip n°1 were cultured in 250 µl while here the chip volume was approximately 6 µl (taking into account the channel volume and estimating the inlet and outlet volumes from the puncher diameter). Moreover, between the GUA medium experiments with 10 and 50 islets (see **b** vs **d** in Fig. 3.14) we do not find a factor 5 in the steady state concentrations. This means the average secretion per islet was lower with 50 islets than 10 islets. The steady state in these experiments was less pronounced so the difference may come from approximation in the estimation, but we propose that it comes from the number of islets which is too large for the size of the channel.

Concerning the transient time, we observed a delay of 10 min in 3 over 4 experiments. This seems to correspond to the duration of the first phase and Nadir that were neglected in the simplified secretion modelling in the simulation. Considering our low sampling frequency, our simplified *in silico* islet model demonstrates the relevance for prototyping chips, as we suggest to simply increment the *in silico* time of convergence by 10 min to take the first phase and Nadir into account. This model allows faster computation time than the complete model of [Alcazar and Buchwald, 2019].

According to this result, and to the *in silico* transient time results found in the section 3.3.1.3, illustrated in Fig. 3.10 p. 80, we can consider that, **between the moment the insulin enters the myotube channel and the moment the insulin is at the final value at the outlet of the myotube channel**, **12 min elapse for 500 pM** (we consider the concentration dynamic at 100 µm and 300 µm height equal for this order of magnitude study), and **25 min for 100 nM**.

3.3.3 Concluding remarks on scaling the insulin generator

The **scaling simulations were successfully set up** and provided couples of parameters Q and n respecting the shear stress constraint and allowing to reach the desired concentrations. ***In vitro* experiments exhibited an insulin response, although the resting concentration measured was much lower than that predicted by the *in silico* model**. This was surprising considering a first secretion experiment was in agreement with *in silico* results. More experiments analyzing islets viability in microfluidic chips are necessary to assess our hypothesis of an incompatibility between the number of islets and the channel size: the

diffusion of nutrients and metabolic waste inside the channel may be sub optimal. An interesting test would be to validate the oxygen availability in the chip using a fluorescent probe to detect hypoxia in islets (BioTracker 520 Green Hypoxia, Sigma Aldrich), as used in the MPS in [L. Vanderlaan et al., 2023].

According to our secretion measurements, albeit much lower than expected, **chip scaling remains possible to reach physiological insulin concentrations**. However, reaching the control concentration (supraphysiological, 100 nM) is inachievable due to the excessive amount of islets required or too low flow rate.

The duration of the transient time t has been determined from simulations, and was shorter than the one determined in the *in vitro* experiments. This is probably due to the simplification of the secretion model which is not taking into account the first phase peak and Nadir. However the shift was repeatable over experiments considering the sampling frequency, and the delay respecting a reasonable order of magnitude, therefore **the transient time approximation seems relevant for prototyping, and can be incremented by 10 min.** For further precision, the complete model of [Alcazar and Buchwald, 2019] could be implemented.

The discussion about the compatibility of the *in vitro* transient time value requires the inputs from dedicated GUAs, coming in the next section, as mentioned in the discussion of section 3.3.1.4 p. 81.

3.4 Scaling the myotube channel

This section describes the method implemented to determine the glucose uptake capabilities of LHCN-M2 myotubes grown in our co-culture medium and in microfluidic chips. For that purpose we designed GUA experiments and GUA chips.

3.4.1 Material and Method

3.4.1.1 Microfluidic chip

GUA were conducted with a specific chip, named here *GUA microfluidic chip*, consisting of a glass microscope slide on which a piece of channel-shaped PDMS was bonded (Fig. 3.17 B). Each chip was composed of 3 channels of 0.8 mm width, 10 mm length and 100 or 300 µm high. The pieces of PDMS (ratio 10:1 silicone/curing agent, w/w ; SYLGARD Dow) were casted on a 3D printed mold fabricated by Protolabs (Le Bourget du Lac, France), based on a layout designed with Autodesk Fusion software (see Fig. 3.17 A). The PDMS was heated 3 hours at 50°C before being removed from the tin and cut. Inlets and outlets were punched with a 2 mm puncher (ref D 69036-10, Delta microscopie). Bonding on the glass slide was obtained by oxygen plasma (O2 30 sccm, RF 100W, FLRIE 300C). For *insulin-induced GUAs* (see 3.4.2.3), prior to the 3 hours starvation and all along the GUAs, 2 cm length FEP tubings of 1/32" OD 0.25 mm ID were plugged into the inlets and outlets (Fig. 3.17 C) to ensure a normalization of chip volumes. Indeed, inlets and outlets volumes can vary, due to uncontrolled PDMS thickness and to the use of a puncher (variable diameter). Therefore these tubes, with their precise dimensions, ensured a normalized chip volume, required for a reliable comparison of glucose variations between different chips.

3.4.1.2 Glucose sensor and its characterization

During GUA experiments, glucose concentration had to be determined in the samples of medium coming from the chips. Glucose concentration of the samples was determined

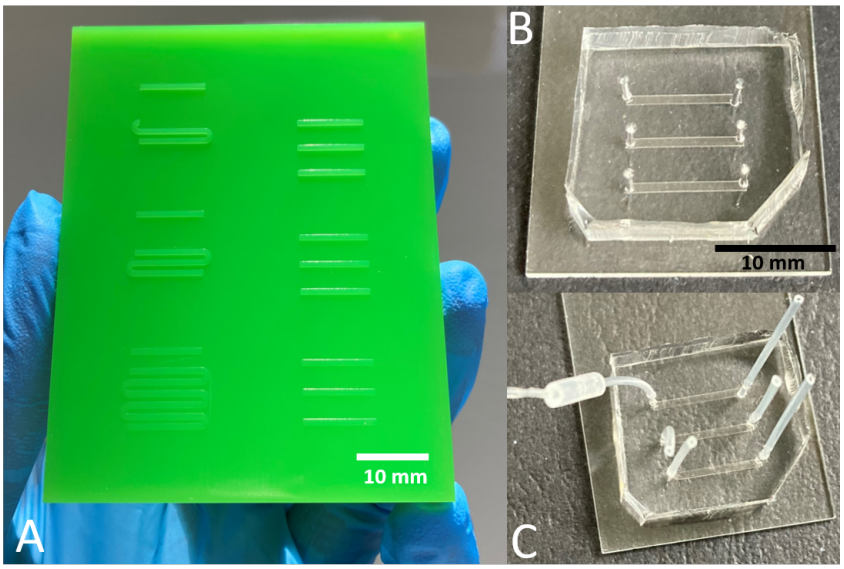

FIGURE 3.17: (A) 3D printed mold for the GUA microfluidic chips. (B) GUA microfluidic chip with 3 parallel channels. (C) GUA microfluidic chip with its tubes, to normalize the volumes during insulin-induced GUA.

by a commercial glucose monitoring device, used in clinics with its dedicated single use test strips (Contour Plus, ASCENCIA Diabetes Care, Neuilly-sur-Seine, France). This off-line sensor was used for the GUA experiments as these experiments did not require online sensing, but provided rather low volume samples, compatible with this sensor that only requires 0.6 µl. However, this sensor is dedicated to the analysis of blood droplets, so we had first to characterize its response to glucose in the GUA media.

Experiments were conducted with GUA media at 3, 5, 7, or 9 mM of glucose, supplemented or not with 500 nM insulin. The objective was to detect a potential impact of supraphysiologic insulin concentration on measurement, like the 500 nM used in some experiments. Prior to the GUA, glucose concentrations in the solutions were measured with an enzymatic glucose kit (GOD-PAP, Biolabo), considered as our gold standard. The results showed that the Contour Plus presents, in our media, a response linearly proportional to the actual glucose concentration, with an offset and a gain as presented in Fig. 3.18a. The offset does not impact our study, as the glucose variations we study in the GUA experiments are the difference between 2 measures using the Contour Plus: the initial concentration of the solution injected and the concentration after incubation in the channel. But the gain is magnifying the variations by 47% according to the regression, which has to be considered when discussing the GUA results. Result in Fig. 3.18a also showed that the insulin at 500 nM did not interfere with the glucose measures; for the rest of the study, we therefore considered that the Contour plus measurements are robust to insulin, at least for concentrations below 500 nM.

The standard deviation were evaluated, and provided in Table 3.18b. The Contour Plus accuracy decreases over glucose concentration increase. The standard deviation associated with 8.2 mM, the glucose concentration for GUA experiments (see next section 3.4.1.3), is between 0.17 mM and 0.46 mM.

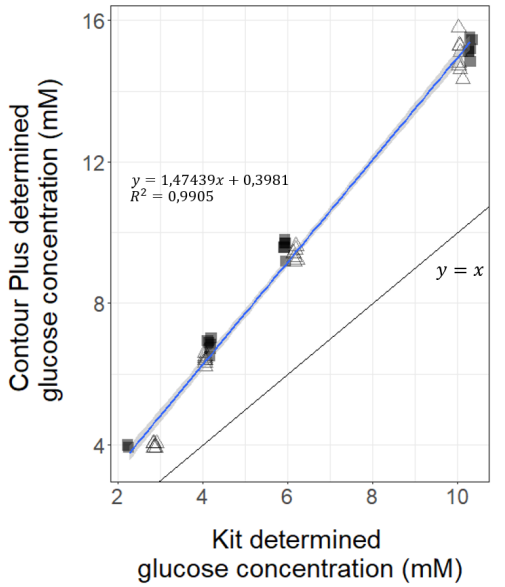

(A) Contour Plus characterization using GUA media with different glucose concentration, supplemented or not with insulin.

Glucose concentration (mM)	Standard deviation (mM)
3	0.06
4	0.12
6	0.17
10	0.46

(B) Standard deviation of the glucose concentrations measured using Contour Plus, depending on the actual glucose concentration of the solution.

FIGURE 3.18: Characterization of the Contour Plus glucose sensor.

3.4.1.3 Basal protocol of GUA in microfluidic chips

For the validation of the co-culture medium, we have developed a protocol of GUA where LHCN-M2 myotubes present a metabolic response to insulin (see section 2.1.3.5).

This protocol has been adapted for microfluidics, and is illustrated in Fig. 3.19: (i) the GUA microfluidic chips, seeded or not with myoblasts depending on the experiment, were placed in a petri dish filled with co-culture medium until the level was higher than the top of the chips for nutrients diffusion (see Fig. 3.19). The chips were let in culture for 4 days, so that the myoblasts differentiate inside the chip into myotubes. (ii) Then the chips were removed from the petri dish, and a starvation medium was injected to replace the culture medium inside the channel. This starvation medium was the co-culture medium with 1% of Bovine Serum Albumin (BSA) instead of serum, and 3 mM glucose instead of 11 mM. (iii) After 3-hour incubation, the starvation medium was renewed by the same medium, supplemented or not with insulin (Sigma Aldrich I9278) depending on the experiment, and let incubate during 15 min. (iv) The medium was replaced by the starvation medium with elevated glucose (8.2 mM) for 1 hour incubation, supplemented or not with insulin. (v) The samples were extracted from the channels with a micropipette, and their glucose concentration was measured with the Contour Plus.

Fluid renewal was achieved by infusing medium 2 min at 5 µl/min, thanks to the microfluidic setup illustrated in Fig. 3.20. These duration and flow are optimal according to microfluidic simulations (data not shown) to ensure media renewal and respect the shear stress limit. After each injection, the tubings of the microfluidic setup were removed prior to place in incubator while waiting for the next step of the protocol.

This GUA protocol is called "basal" hereafter, as different sub-protocols based on it have been implemented.

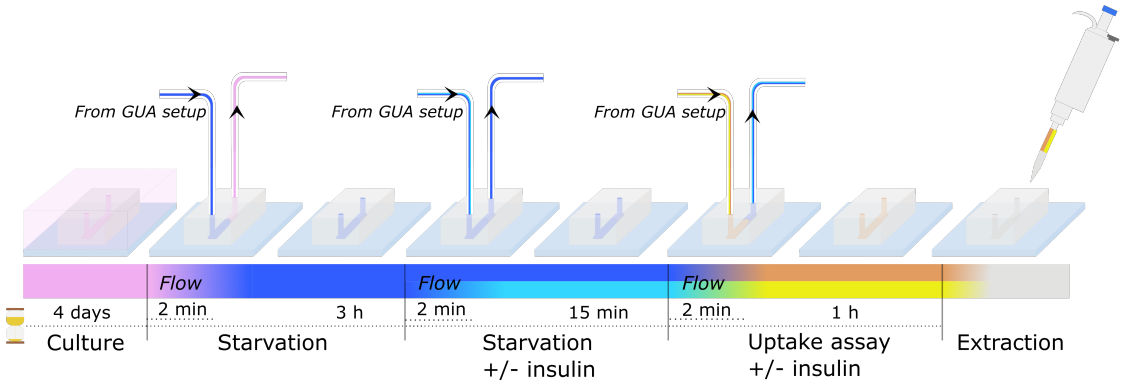

FIGURE 3.19: Schematic representing the steps of the basal GUA protocol (dark blue and orange for solutions without insulin, light blue and yellow for solutions with insulin). Note in this schematic, and in all the following ones, the chip is represented with 1 channel but each chip had 3 channels in reality.

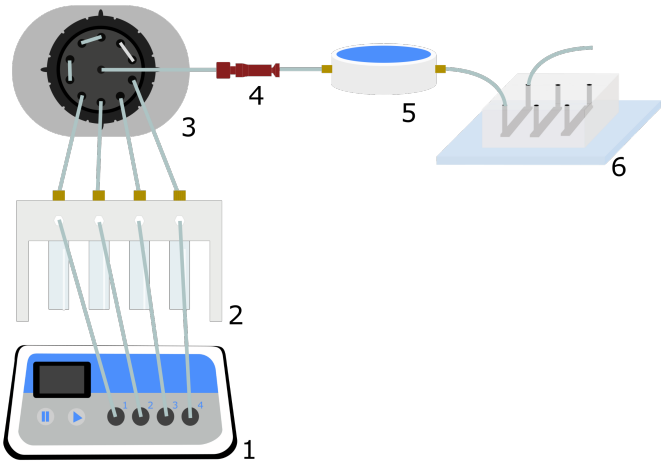

FIGURE 3.20: Microfluidic setup for the GUA experiments: 1. Pressure controller, 2. Reservoirs, 3. 10-to-1 switch, 4. 1/16" to 1/32" fitting, 5. Flow meter, 6. GUA chip (3 parallel channels), sequentially perfused.

3.4.2 Experiments

3.4.2.1 Insulin-independent glucose uptake

A first protocol of GUA was realized to assess the insulin-independent glucose uptake of LHCN-M2 myotubes. The experiment was based on the basal protocol of glucose uptake described in section 3.4.1.3, using insulin free media. This protocol, illustrated in Fig. 3.21, was repeated twice on each of 4 GUA chips, with and without myotubes (the same chip was used as its own control to avoid skewing results due to chip volume variability). The difference of glucose variations in the presence or not of myotubes is represented in Fig. 3.23a. We observed a larger decrease of glucose concentration in chips with cells (statistically significant, paired Wilcoxon test). Interestingly, we also observed an increase in glucose in the condition without cells, which shows that, beyond the myotubes, the device itself impacts the results. We hypothesized a release of glucose accumulated in the PDMS chip during the

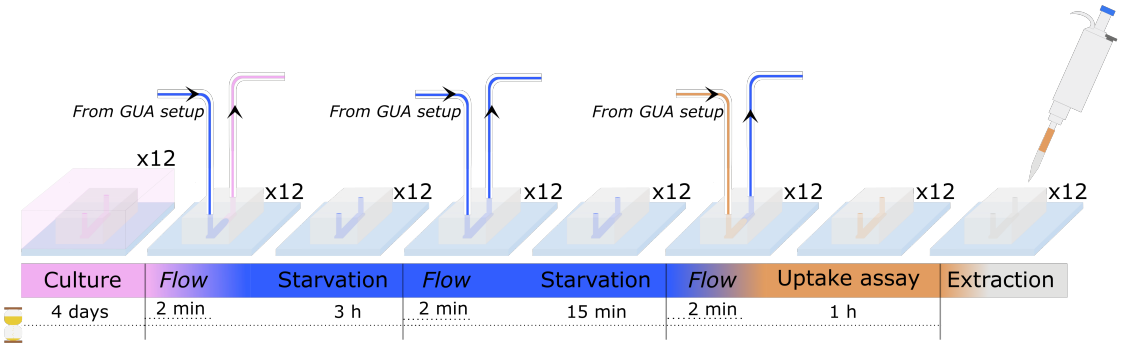

FIGURE 3.21: Protocol for insulin-independent glucose uptake. The protocol was repeated 2 times, with chips seeded with or without myoblasts. As the experiment was repeated 4 times with 4 chips, this represents 12 channels infused (3 channels per chip).

culture. Indeed the culture medium contains 11 mM of glucose (Culture step in Fig. 3.21), while the solutions used in the GUA are at 3 and 8.2 mM.

3.4.2.2 Glucose release from PDMS

We further investigated our hypothesis of glucose release from the PDMS during the culture step. In addition to altering the glucose concentration, it may also threaten the efficacy of the 3-hour starvation step: that step presents the highest glucose gradient between the medium in the channel (3 mM glucose), and the PDMS (potential remains of the 11 mM glucose medium). We performed experiments using 100 and 380 µm GUA microfluidic chips, the latter only used in these experiments. The experimental protocol, based on the basal GUA protocol described in 3.4.1.3, is illustrated in Fig. 3.22: the chips, without cells, were cultured alternately in 3 and 11 mM glucose media. Media samples from the chips were collected after the 3 hours starvation step. The chips cultured in 3 mM of glucose had a variation of glucose concentration almost null, whatever the chip volume, see Fig. 3.23b. However, when the same chips were cultured in the medium at 11 mM, an increase of glucose concentration after the 3 hours incubation was observed. The chips with higher volume had an average increase of concentration at 0.75 mM while the chips with lower volumes had an average release at 2 mM. This demonstrates the validity of our hypothesis, i.e. the presence of a glucose release from the chips.

A second experiment was conducted to determine the dynamic of this GUA. The protocol was very similar to the previous one. The same GUA microfluidic chips were incubated with the co-culture medium during 4 days, then the starvation medium was infused. The medium incubated in the channel was collected every 30 min and a new starvation medium infused. Using the Contour Plus, the variation of glucose concentration was measured between the infused medium and the samples. The Fig. 3.24a compares the release in the previous experiment (continuous 3 hours incubation) to the new experiment (successive 30-min incubation during 3 hours). Results show that the cumulated releases every 30 min over 3 hours is higher than the release during uninterrupted 3 hours. This could be explained by the gradient-driven release: in the case of a 3-hour uninterrupted incubation, the glucose concentration increases in the channel, so the gradient of glucose and the flux of glucose from the PDMS to the medium in the channel decreases over time; while in the case of 30-min successive renewals, the glucose gradient is periodically reset to its maximum value. The average glucose release per channel in 30 min plotted in Fig. 3.24b, shows a consistent

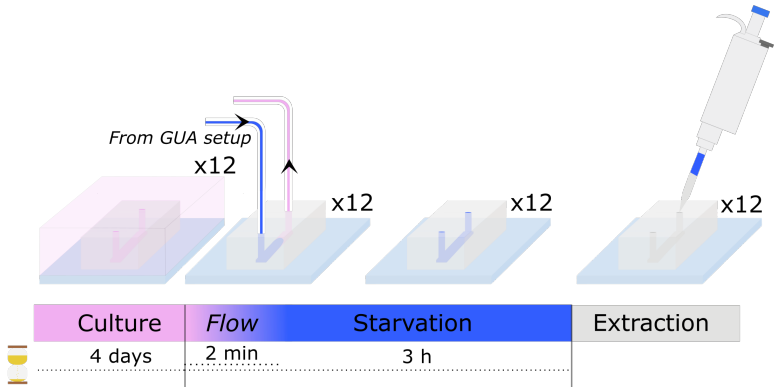

FIGURE 3.22: Protocol to measure the glucose released by PDMS after the starvation step. The protocol was repeated 2 times for each chip, which are alternately cultured in 11 mM and 3 mM co-culture medium. The protocol was performed on chips with 100 and 380 µm height.

average release for a given chip dimension. The average release during 30 min in channels of 100 µm height is around 0.6 mM, while the release for the 380 µm chips is around 0.2 mM. The ratio between these release values is in the range of the 3.8 volume ratio between the chips (respectively about 0.8 µl and 3 µl). We then wondered whether the release in 30 min decreases over time, due to the "disgorgement" of glucose in the PDMS after several medium renewals in the channel. The Fig. 3.24c represents the evolution of the 30 min release over the 3 hours. It is impossible to extract a tendency in the release profile. We therefore considered the PDMS, in the scale of our experiment, as an infinite source of glucose, impossible to "clean".

The last investigations consisted in evaluating the average glucose release during the 1-hour incubation in the Uptake Assay step. The basal protocol described in section 3.4.1.3 was conducted on 7 chips empty of cells. The variation of glucose quantity in medium after the final 1-hour incubation is represented on Fig 3.25.

The average glucose release is similar in 2 groups of chips: from chip 5 to 9 the average release is at $3.25^{-9}mol$; from chip 11 to 13 the average release is at $1.1^{-8}mol$. The chips 11 12 and 13 with the highest release correspond to the 3 chips with the highest volumes (due to higher thickness, thus longer inlet and outlet). Therefore we continued the GUA with PDMS, considering to use GUA chips of same thickness, and using tubings at the inlet and outlet as described in section 3.4.1.1. In addition this implied that the results obtained in the next section were not quantifying the glucose uptake, but assessing the presence of a difference, as the results were containing a part of glucose release.

3.4.2.3 Insulin-dependent glucose uptake

A final protocol of GUA was conducted to evaluate insulin-dependent glucose uptake by LHCN-M2 myotubes in our setup. The procedure, using the protocol described in section 3.4.1.3 was performed on chips seeded with myoblasts, as illustrated in Fig. 3.26. The difference lies in step (iii) in the GUA basal protocol (renewal of the starvation medium) that was skipped since data (not shown) suggested that this step does not influence the results. In the last 1-hour uptake step, the chips were infused and incubated with a solution supplemented or not with insulin. The experiment was repeated in the same medium supplemented either with 500 pM insulin (physiological) or 100 nM (supraphysiological, positive control).

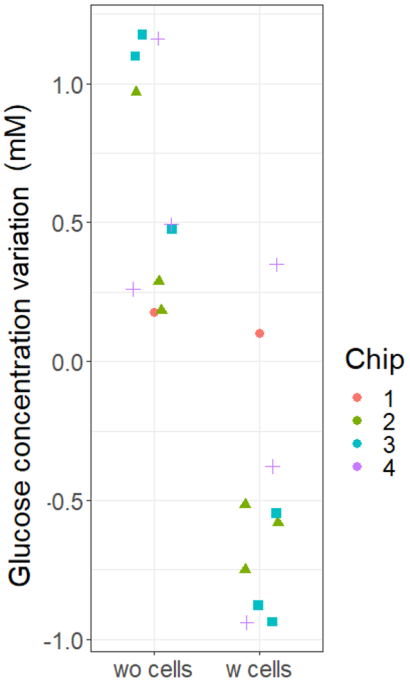

(A) Comparison of the glucose variation in 4 GUA chips with (right) and without (left) myotubes. Each chip has 3 channels except chip n°1, due experimental issues.

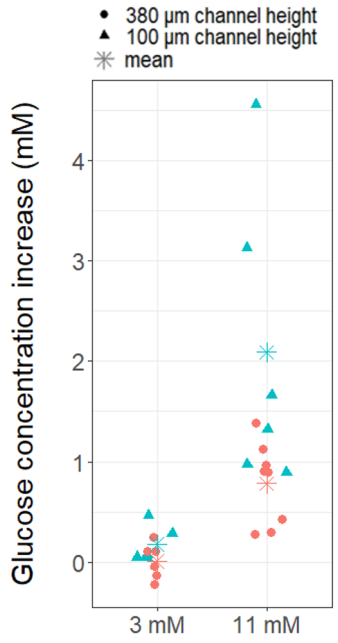

(B) Glucose concentration variation of starvation medium (3 mM glucose originally) after 3-hour incubation in 4 GUA chips (2 with 100 µm height and 2 with 300 µm height), "cultured" 4 days in either in 3 mM or 11 mM co-culture medium.

FIGURE 3.23: Insulin-independent glucose uptake and demonstration of a glucose release by PDMS.

Contrary to the 2 previous GUA experiments, a same chip was not reused to test both with and without insulin conditions. Indeed we had observed that myoblasts fusion was reduced in reused chips in comparison with "new" chips. A normalization of the chip volumes was performed as explained in 3.4.1.1 p. 91, with tubings used in the inlets and outlets, that allowed comparison of glucose concentrations between chips. This was also potentially reducing the glucose release at the level of the inlets and outlets, with the tubing isolating the liquid from the PDMS. A t-test on the results represented in Fig. 3.27a shows that the insulin had a significant effect on glucose uptake: the glucose concentration decreased more when the myotubes were exposed to 500 pM insulin than without insulin; and the glucose concentration increased with 100 nM insulin compared to without insulin.

It seems incoherent as 100 nM is supposed to be the positive control, thus providing the strongest uptake, and providing an uptake if the tested concentration (500 pM) provided an uptake. Moreover, the fact they provide a glucose release instead is not possible, as healthy skeletal muscles cannot release glucose [Jensen et al., 2011]. Therefore the statistical significance in the case of the 100 nM could be related to another phenomenon than the insulin response of myotubes. Another surprising phenomenon is the fact the uptake was similar between channels where the myotubes were not visually healthy (as in Fig. 3.27b) and the ones with visually healthy myotubes (see Fig. 3.27a). As visual aspect is not a proof of their inability of taking glucose in response to insulin, this observation has to be considered carefully.

So the results are questionable despite a statistical significance. They are discussed in more details in section 3.4.2.4.

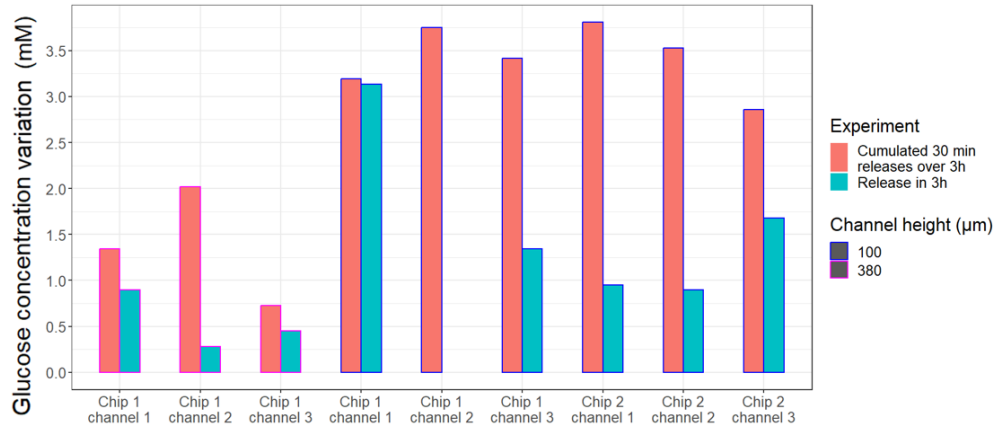

(A) Glucose release after 3 hour-incubation in GUA chips "cultured" 4 days in 11 mM glucose medium VS cumulated glucose releases every 30 min over 3 hours of the same chip also cultured in 11 mM glucose medium.

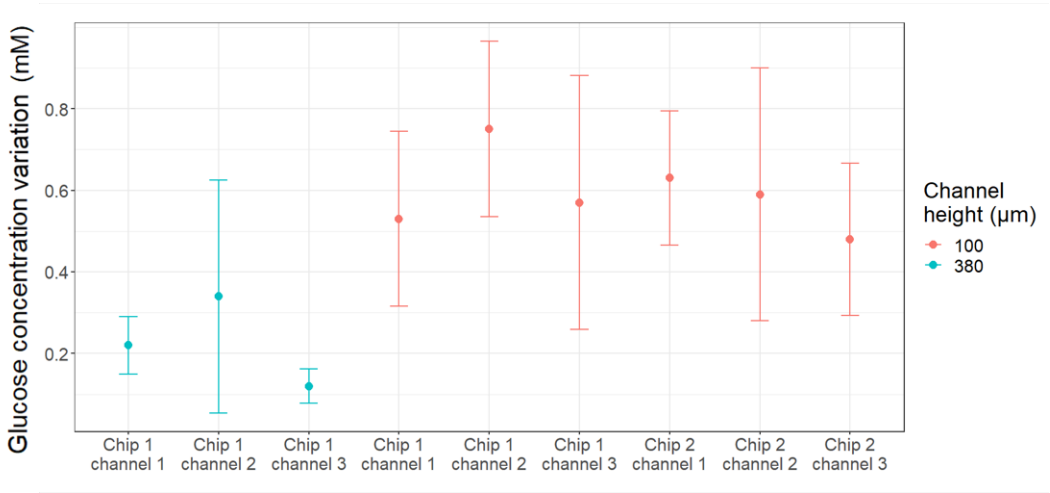

(B) Average glucose release each 30 min, for each channel of 3 chips of 2 different channel height (100 µm and 380 µm). Error bars represent standard deviation.

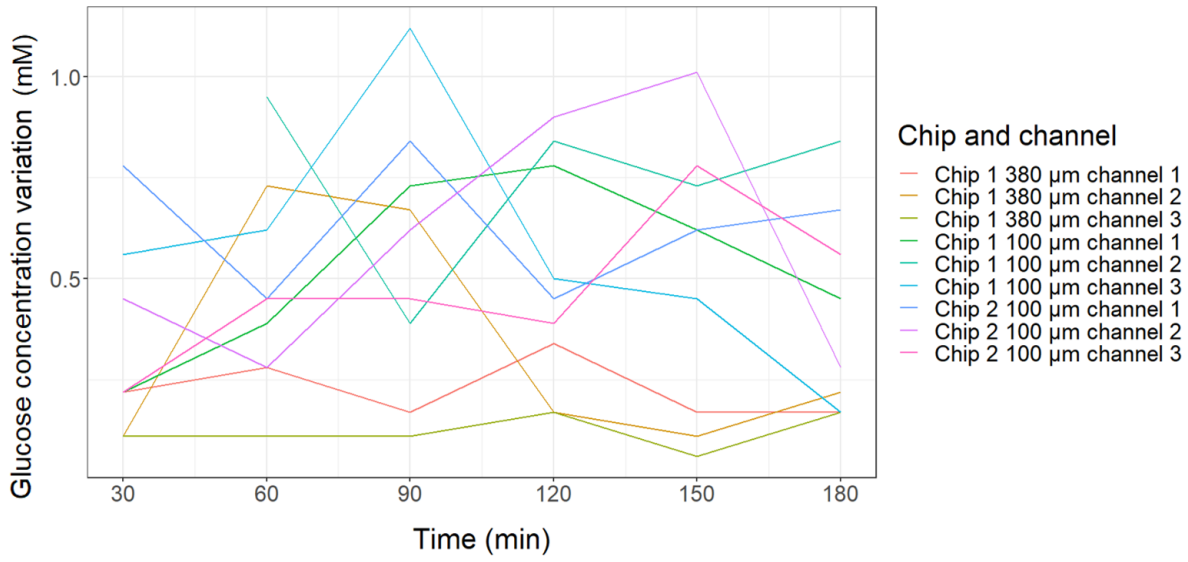

(C) Glucose release in 30 min over the 3 hours, for the 2 channel heights.

FIGURE 3.24: Study of the glucose release by PDMS.

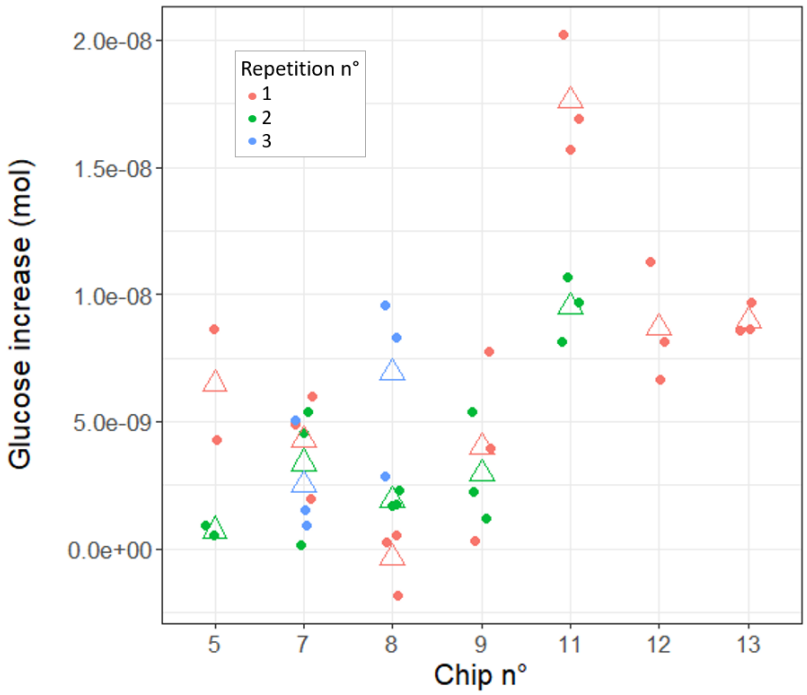

FIGURE 3.25: Glucose release during the last step of the basal protocol, in 7 chips empty of cells. The release has been normalised by the volume of the corresponding chip. Each chip has 3 channels, thus each experiment has maximum 3 points. The average of an experiment is represented by a triangle. The protocol was repeated several times with some chips, and the experiments are distinguished by the color.

Note that intermediate experiments were conducted prior to these results, testing the impact of changing the duration of the Uptake Assay step and insulin concentration. Indeed, shorter glucose uptake duration was tried with the hypothesis that the insulin response could be stronger shortly after the stimulation. In such case, a too long incubation could hide acute effect of insulin. The same protocol as the insulin-dependent experiments was conducted, but at 500 nM, and with a couple of chip with 1 hour uptake step and another with 20 min. No significant difference between with and without insulin was measured in both cases, therefore increasing insulin concentration or decreasing the duration of Uptake Assay do not provide statistically more glucose uptake.

3.4.2.4 Discussion

When testing our hypothesis that insulin has an effect on glucose uptake in our chips, we have found statistical significance for the following results:

1. At 500 pM insulin, the **glucose uptake** is increased compared to the basal uptake without insulin.

2. At 100 nM insulin, a **glucose *release*** appears compared to a basal uptake without insulin.

Despite their statistical significance, these results are questionable as mentioned previously in section 3.4.2.3. To explain the apparent and unexpected glucose release observed with the positive control (100 nM), 2 hypotheses are considered:

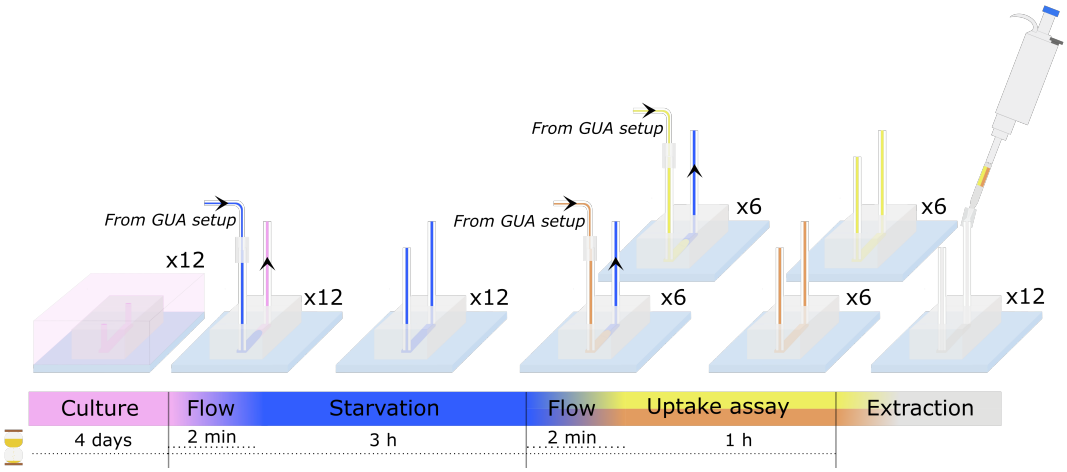

FIGURE 3.26: The protocol of GUA to evaluate the insulin-dependent myotube response. During the uptake assay step, the chips were split into 2 groups tested with or without insulin (orange and yellow).

1. **Our positive control may not have properly worked**. In the co-culture medium validation in section 2.1.3.5, 100 nM confirmed to be a positive control with more glucose uptake than without insulin. However in these experiments, the experimental volume and the duration of the Uptake Assay step were different (200 µl vs 2.8 µl in the present one; 30 min vs 1 hour in the present one). A long duration may have an impact on the insulin sensitivity, as at this concentration, insulin also activates other receptors (e.g. IGF receptors) and other pathways. If applied in a prolonged manner, it can induce the internalization of insulin receptors and the alteration of the insulin signaling pathway, resulting in lower glucose uptake. The glucose release by PDMS may therefore have exceeded the level of uptake and the overall glucose variation in the chip became a release.

2. Another hypothesis is that the **positive control worked** but its result was hidden by an exterior factor. **PDMS glucose release** could have not been similar between the chips with myotubes exposed to insulin compared to those not exposed to insulin. In the experiment with 100 nM insulin, we are confident in the glucose release values measured without insulin, as they fit those measured without insulin in the experiment at 500 pM (see Fig 3.27a, conditions without insulin in both experiments). The 2 experiments were conducted at 2 different days with different cells passage (thus different culture), therefore the experiments were independent. We can thus hypothesize that the usually stable glucose release has been for an unknown reason higher in the chips with myotubes exposed to 100 nM insulin, hindering the insulin-induced uptake.

From these hypotheses, we are unable to confirm whether the positive control (performed only once) worked properly or not. If the hypothesis of an unstable PDMS glucose release was to be confirmed, it could impact all GUA experiments results, including the 500 pM ones.

These observations did not completely sweep away the results. However we could not expressly validate them. Investigations were required to define leverages to strengthen the results of this complex experiment with materials, biology, and sensing challenges.

To summarize, two main questions arised from our previous remarks:

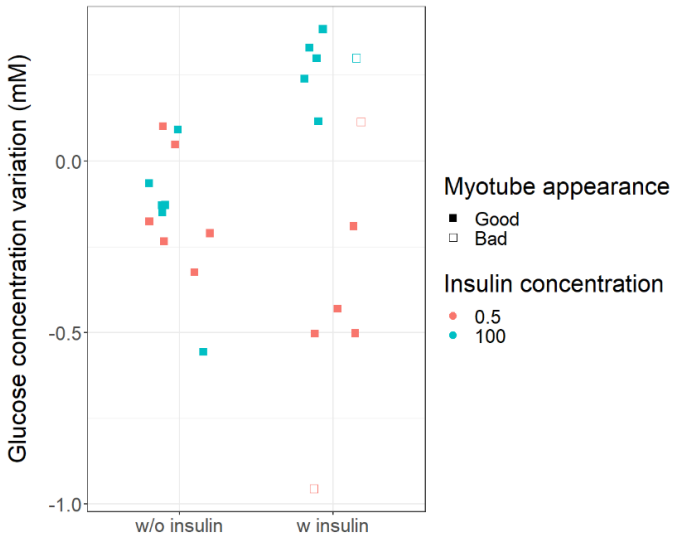

(A) Glucose concentration variations upon 500 pM and 100 nM insulin. The results for channels where the myotubes were not considered optically satisfying are also plotted.

(B) Example of a channel where the differentiation to myotubes is considered not satisfying (visual aspect). There are few potential myotubes as they are thin, and not regular probably due to some detachment.

FIGURE 3.27: Study of insulin-dependent glucose uptake.

- ***(A)*** Are the LHCN-M2 myotubes able to respond to insulin when cultured in our conditions, in microfluidic chips?
- ***(B)*** How can we increase the level of glucose uptake to exceed largely the PDMS glucose release and the Contour Plus sensor limitations?

(A) This first question still makes sense despite our previous validation of glucose uptake by LHCN-M2 myotubes upon insulin in the co-culture conditions. Indeed, scales were different in the GUAs experiments: we observed extracellular glucose concentration while previously it was intracellular one, and the culture volumes were different. Therefore the precedent experiments do not constitute a proof of feasibility of the actual GUA experiments in microfluidic chips. We then carried a more detailed analysis, following 2 tracks: is the LHCN-M2 response to insulin sufficient to produce measurable glucose extracellular variations? Are the LHCN-M2 myotubes cultured in our chip functional enough to respond to insulin?

In extracellular medium, the level of glucose uptake induced by insulin could be much smaller than the insulin-independent one, and thus hard to detect. Indeed, in [Forterre et al., 2014], the authors have characterized the C2C12 myotubes (mouse skeletal muscle cell line), and they concluded that insulin-dependent glucose uptake is hard to study in this cell line. The authors performed a proteomic analysis to compare C2C12 and mouse primary skeletal muscle cells. They found out that the glucose transporter responsible for the insulin-dependent glucose uptake, GLUT4, is much less present in C2C12 cell line than in the primary skeletal muscles. Moreover, while in skeletal muscle cells GLUT4 is more present compared to GLUT1 (the insulin-independent glucose transporter), it is the opposite in the cell lines: GLUT1 is 60 times more abundant in cell lines than in primary cells. Therefore in C2C12 myotubes, the insulin-independent glucose uptake is predominant. Although LHCN-M2 is a different cell line, it may present a similar tendency. This phenomenon in cell lines has also been pointed out in [Prill, Jaeger, and Duschl, 2014], in which the authors could not observe a glucose related phenomenon in their cell line (HepG2). A counter example of this argue would be the work in [Lee et al., 2019], in which a glucose uptake

was measured with C2C12 myotubes to scale an *in silico* MOoC. However we can wonder whether the glucose uptake in this study was due to insulin response or to cells stress due to long exposure (18 hours) to supraphysiological insulin concentrations (10 nM, 100 nM, and 1000 nM).

Similar to [Lee et al., 2019], we tried to measure the extracellular glucose uptake of LHCN-M2 myotubes with our GUA protocol (with an uptake assay step at 30 min), in the classical culture substrate used in section 2.1.3.5 (µ-Slide 8 Wells (80826, Ibidi): microscope slides with 8 separated wells of 200 µl each), using the Contour Plus sensor. The experiment results are shown in Fig. 3.28. Note that results related to several physiological concentrations in the [0.1 nM; 1 nM] were gathered to obtain a sufficient number of experiments to perform statistical analysis. These results show a measurable glucose uptake - at the limit of the Contour Plus precision (standard deviation between 0.17 mM to 0.46 mM, see section 3.4.1.2 p. 91) - increasing when the insulin concentration was raised to 100 nM. If we consider that, in both the GUA chip and the µ-Slide 8 Wells, the myotubes are monolayered and cover all the available surface, and that the uptake in 30 min is half of the uptake over 1 hour, we can approximate the expected glucose uptake for our GUA chip:

$$R_{slides} = \frac{volume_{medium}}{surface_{culture}} = \frac{200[\mu l]}{100[mm^2]} = 2 \quad \text{and} \quad R_{chips} = \frac{2.8[\mu l]}{8[mm^2]} = 0.35 \tag{3.1}$$

So

$$Uptake_{chips} = \frac{R_{slides}}{R_{chips}} \times Uptake_{slides} = 5.7 \times Uptake_{slides} \tag{3.2}$$

Glucose uptake in the GUA chip should be 5.7 times the glucose uptake in the slides, representing of about 6 mM at 500 pM and 9 mM at 100 nM. Of course this extrapolation does not include the PDMS glucose release, which cannot be exactly known. However we can assess an order of magnitude from the experiments in section 3.4.2.2. Considering the glucose release level at $1 \times 10^{-8} mol$, which corresponds to similar chip thickness, it would represent a glucose concentration increase of 1.5 mM. Note that, as tubings were plugged inside the inlet and outlet chips used for the insulin-dependent glucose uptake assays, the actual surface of PDMS in contact with the medium is lower and then the actual PDMS release should be lower than 1.5 mM. Despite this majored PDMS release, the expected glucose uptake levels are largely above what was measured: 4.5 mM in case of 500 pM insulin or 7.5 mM in case of 100 nM insulin. This large uptake difference suggests that myotubes in the microfluidic chips were not fully functional.

To investigate further this hypothesis, we have tried to assess the quality of the culture in the microfluidic GUA chip: the LHCN-M2 myoblasts looked correctly fused in bright field, nevertheless this did not necessarily mean that they were properly functional. The 100 µm height for the myotubes chamber has been chosen according to the results of [Zambon et al., 2014]. But they studied myoblasts, not myotubes, and the C2C12 cells used in this study produce smaller myotubes. The human myotubes may require more nutrients than what the diffusion can provide. It has also been observed during the experiments that myoblasts differentiate less easily in microfluidic chips than in macro volumes, notably if the density is a bit high. We have used an immunostaining validation protocol similar to section 2.1.3.5: troponin-T and GLUT4 immunostainings, for structural and functional validation, respectively. Only the fluorescence of the DAPI, staining the nuclei, was observable through the PDMS (and with a halo). In turn, the troponin-T fluorescence was only observed through the hole of the puncher. Based on these observations we hypothesized that the PDMS was diffusing too much the fluorescence, decreasing its intensity. Still, immunostaining in microfluidic chips has already been published before. A fellow biologist, Dr. Pauline Duc from

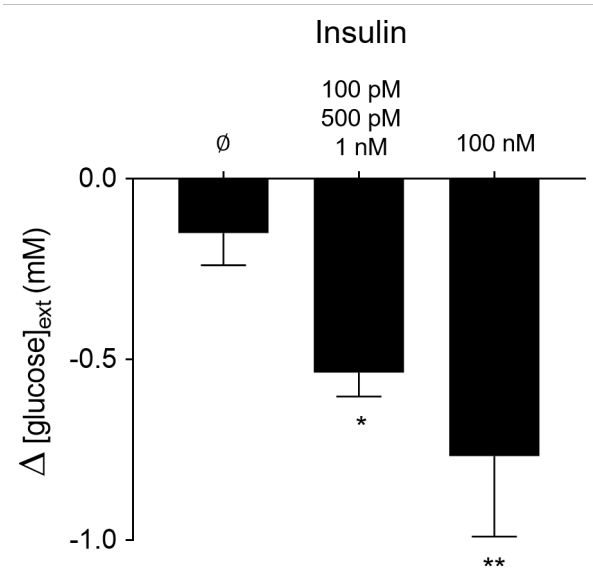

FIGURE 3.28: Extracellular glucose uptake of LHCN-M2 myotubes in µ-Slide 8 Wells, depending on insulin concentration. Mean ± SEM, one-way ANOVA, posthoc Bonferroni's multiple comparison test, *p<0.05 **p<0.01.

IGMM laboratory (Montpellier), who conducted immunostaining on myotubes in microfluidic chips, confirmed that the PDMS as well as the glass substrate were compatible with immunostaining. The main difference between our respective experiments was the fact our chip is fully immersed in the culture medium, as opposed to the microfluidic chip in this study which has reservoirs at the inlet and the outlet. The full immersion induces a blurring of the PDMS, compatible with bright field observation but penalizing for immunostaining, which therefore cannot be used as a reliable culture validation technique in our chips. We were not able to bring further these investigations, but the perspectives would be: (i) to conduct investigations *ex situ* by removing myotubes from the chip and use other characterization techniques (Western blot to study troponin-T and GLUT 4 expression, or study transcription factors); (ii) or to prevent PDMS blurring by perfusing medium into the channel for the cell culture prior to experiments, instead of incubating the chips in petri dish filled of medium as done in the present work.

(B) In the case the myotubes actually uptake glucose upon insulin in the chips, we should focus on reducing uncertainties on glucose uptake. We identified 2 strategies: reduce or remove the PDMS glucose release, or use a more precise glucose sensor.

The glucose release from PDMS reduces the measurable glucose uptake either by reducing the effectiveness of the starvation step, or by interfering with the uptake induced by myotubes at the Uptake Assay step of our GUA protocol. Starvation under flow would have been a relevant solution to reduce the impact of PDMS glucose release. However, all our experiments were made with several channels in parallel in each chip, to obtain a statistical significance in a reasonable amount of experimental time. Therefore a starvation under flow would have required the use of a splitter and the injection of all the channels in parallel. As we used 3 or 4 chips in parallel, with 3 channels each, starvation under flow would have required from 9 to 12 injection lines, while the usual splitters available have a maximum of 8 ways. Furthermore, having a proper control on each channel flow rate and thus shear stress would also require 9 to 12 flow rate meters. Starvation under flow is definitely very

demanding in terms of equipment, and we had - and still have - no possibility to implement it.

The best and most radical option would be to get rid of the PDMS. PDMS is widely used in the OoC field, even if it is known to absorb small hydrophobic molecules [Radisic and Loskill, 2021]. Indeed, so far no material is clearly rising to replace the PDMS, with its interesting features like oxygen permeability, biocompatibility, diversity of possible designs, and low fabrication cost. A possible replacement material is PMMA (PolyMethyl MethAcrylate), but this polymer manufacturing requires specific fabrication facilities and the cells below PMMA need to be continuously perfused to ensure oxygen renewal. In [Dornhof et al., 2022], the authors observed that when the flow is stopped, the cells are able to consume in 30 min all the oxygen in the chip.

Finally, a more *accurate* glucose sensor would improve the glucose uptake deciphering and its quantification (the latter being the objective of the GUA experiments, in order to scale the MOoC myotube channel). The Contour Plus was characterized in section 3.4.1.2 and its standard measurement uncertainty (or standard deviation) at 8.2 mM was between 0.17 mM to 0.46 mM. On the other hand, the BST sensor described in the next Chapter 4 presented a low level of error, and standard measurement uncertainty of 0.0385 mM, when used with *Air* protocol (further detailed in next Chapter). The BST had then improved accuracy, which was promising for glucose uptake quantification.

3.4.3 Concluding remarks on myotube channel scaling

The main conclusions we can draw from the GUA experiments are:

- LHCN-M2 myotubes are able to generate measurable extracellular glucose concentration changes in macro volumes.
- LHCN-M2 myotubes have been obtained in the microfluidic chips (GUA chips), but their level of maturity remains to be studied.
- The LHCN-M2 myotubes cultured in the GUA chips showed a significant glucose uptake without insulin.
- Glucose uptake was significantly higher in the presence of insulin at physiological level, while the positive control at supraphysiological concentration showed a statistically significant glucose release. To confirm the results, further investigations studying the myotube state and function in chip are required, as well as attempt to limit glucose release by PDMS.
- The results obtained are not quantitative, due to the Contour Plus gain that is not taken into account as not fully repeatable. We can assess the presence of uptakes, but they may all be decreased of between 30 to 50% according to the observed Contour Plus gains. This does not change our qualitative conclusions. The perspective to use the BST sensor described in the next chapter, with appropriate calibration prior to each experiment, will allow more quantitative experiments to characterize the uptake.
- The presence of a glucose release from the PDMS has been demonstrated. Its value has been observed as stable with similar PDMS chip thickness, allowing to pursue experiments. However the replacement of PDMS is preferable to improve the results robustness.

3.5 Conclusion

Firstly, the MOoC experiment emulating the islet to muscle communication in response to glucose elevation has been defined, considering islet and myotube *in vitro* culture requires specific pre-treatment prior to observing their respective response in terms of glucose and insulin. We have then decomposed the protocol in 3 *Steps* (see Fig. 3.2 p. 71). The last 2 *Steps* correspond each to one cell type (islets and myotubes) and one objective (respectively physiological insulin concentration, and measurable glucose variations); therefore, the scaling methodology presented in section 3.2 was **separated in 2 main streams: one islet-oriented, the other one myotube-oriented**.

In the first islet-oriented investigations, the **simulations provided sets of solutions for the flow rate and number of islets (n, Q)** to attain the targeted insulin concentrations (500 pM and 100 nM), however the ***in vitro* experiments were not in agreement regarding the level of insulin**. The islets secreted much less insulin than expected, which challenged the possibility to scale up the system in order to reach 100 nM insulin. The **discrepancy between simulations and experiments should be further investigated**, as former experiments of insulin secretion (section 2.1.2.4) showed an agreement between *in silico* and *in vitro* data.

In the second part of the investigations addressing the myotubes, we **successfully observed myoblast fusion in microfluidic chips**. To our knowledge, this is the first time LHCN-M2 has been cultured in microfluidic chips. Their **insulin-independent glucose consumption was repeatedly measured**, but the observed **insulin-dependent glucose uptake** (only at physiological insulin concentration) **requires further investigations**. The fact **insulin-driven glucose uptake has been observed in bigger volumes** (using culture plates) is encouraging and provides insights regarding the glucose variations expected in microfluidic chips. All these results also suggest a lack of proper functionality of the cells within the microfluidic chip, although our testing could not demonstrate it due to technical and time limitations. In any case, using a material other than PDMS could be beneficial, as we demonstrated for the first time to our knowledge, that **PDMS could release glucose in the medium**.

Discussion on the transient time (t) in *Step* 2 was started in section 3.3.1.4 p. 81, and was supposed to be completed based on GUA experimental results.

As a reminder, the time (t) required for islets to generate the targeted insulin concentration in the myotube channel (see Fig. 3.2b, p. 71) was estimated from *in silico* experiments (see Fig. 3.10 p. 80), and was adjusted considering the observations of *in vitro* experiments: **between the moment the insulin enters the myotube channel and the moment the insulin concentration is at the final value at the outlet of the myotube channel, 12 min and 25 min respectively elapse for 500 pM and 100 nM MOoC experiments**. Considering the following Uptake Assay step, or *Step 3*, which lasts 60 min, this transient time represents a not negligible increase of total insulin exposition of myotubes (they would be exposed to 72 min and 85 min for respectively 500 pM and 100 nM experiments). As no glucose uptake could be confirmed yet in the microfluidic chips, we could not test the difference of uptake on 15 min, 30 min, 60 min, 90 min to assess the uptake dynamic, and validate the possibility to detect glucose variations during 60 min after previous 12 min or 25 min of early glucose uptake. A possibility would be to conduct these GUA experiments in culture plates (opened system with bigger volumes).

Our strategy for this 3-year PhD was to use *in silico* simulation as an accelerator for

an informed design of an islet-myotube MOoC, in addition to *in vitro* characterization and validation experiments. This scaling methodology hopefully stopped us prior to perform static interaction experiments with islets and myotubes in the MOoC chip, where no or irrelevant interaction would have been observed. We could identify unexpected sub optimal cell function (level of insulin secretion and glucose uptake) from islets and myotubes, where culture volumes are likely to be incriminated.

This echoes the Chapter 2, where the chip n°1 design, with its dual mode, looked for a trade off in volumes. The design n°1 required at the end large volumes (250 µl per cell chamber) compared to the design n°2 (about 6 µl), impacting the performances in terms of transient time and homogeneity. The reduction of volumes through the design n°2 drastically improved the performances on these levels, however on the other hand the cells function seems modified too. We hypothesize that the culture procedure of islets and myotubes prior to experiments, consisting in a static incubation of the chips in a petri dish full of medium, is critical. Even if the level of medium is largely above the top of the chip during the culture, the diffusion of nutrients and metabolic waste inside the channel may be sub optimal, **not inducing to cell death but lower functionality**.

Chapter 4

Glucose sensing integration

In section 1.2.5.1 of the introducing chapter, the stakes of online sensing in MPS have been presented. Positioning sensors inside the microfluidic chip, close to the cells, is needed for accurate spatial and temporal monitoring, which is essential for validating culture and studying cell behaviour. However, this causes chip design to be closely related to sensor design. As demonstrated in the two previous chapters, the chip design was already highly constrained by biological considerations (cell culture in Chapter 2 and scaling in Chapter 3). Thus, to alleviate constraints, a physically distinct device (that could connect to the outlet of the MOoC) was deemed preferable.

The first part of this Chapter dives deeper into electrochemical sensors working principle in case of glucose sensing. The second part deals with the sensor selection and characterization to define its usability in the context of the MOoC developed here. The third part deals with microfluidics integration: we studied using multiphysics simulation the sample distortion along its transport toward the sensor due to the microfluidic phenomena. Even if the sensor was not yet integrated inside the microfluidic chip hosting cells, a custom potentiostat has been set up in the perspective of a MOoC hosting both cells and several electrochemical sensors in a same chip, requiring a custom integrated electronic acquisition system. This work is treated in a fourth part.

4.1 Introduction to electrochemical biosensors

4.1.1 Biosensors

Biosensors rely on a 3-step sensing pathway, starting from the **recognition** of the molecule of interest (analyte), followed by **transduction** to a signal (electrical), which can finally be **detected** by an acquisition system [Cargill, 2016][Sabu et al., 2019]. They are termed "biosensors" because analyte recognition is handled by a biological recognition element, or bioreceptor, which is specific to the analyte. Examples of bioreceptors include enzymes, antibodies, DNA (or aptamers), and whole cells [Grieshaber et al., 2008][Sabu et al., 2019]. Recognition by the bioreceptor generates a physico-chemical signal, that is then converted to an electrical signal by a transducer (either electrochemical, optical, thermometric, magnetic, or piezoelectric). The electronic detection system is a *potentiostat*, whose role is described later in this part.

4.1.2 Enzymatic electrochemical biosensors for glucose monitoring

Electrochemical biosensors are frequently used in the context of online sensing for MPS, as introduced in section 1.2.5.1. In this work we focus more particularly on the sensors using enzymes as bioreceptor (enzymatic electrochemical biosensors), as they are the preferred technology for glucose monitoring [Vashist et al., 2011].

These sensors utilize an immobilized enzyme that interacts chemically with the analyte to detect. In the case of glucose detection, the enzymes used are the Glucose Oxidase (GOx) or Glucose DeHydrogenase (GDH) [Vashist et al., 2011] (the latter is a generic name encompassing several enzymes [Prévoteau, 2011]). These enzymes catalyze glucose oxidation or, in other words, enhance the reaction of glucose with oxygen to product gluconolactone (later hydrolysed as gluconic acid). In the case of GOx, the most widely used enzyme for glucose sensors, the reaction is allowed by the Flavin Adenine Dinucleotide (FAD), the enzyme redox center [Prévoteau, 2011]. The oxidation of glucose induces the reduction of this center to $FADH_2$. The enzyme is re-generated once $FADH_2$ is oxidized back to FAD, and oxygen reduced to hydrogen peroxide (H_2O_2). This reaction is formalized in the following equations:

$$GOx(FAD) + glucose \rightarrow GOx(FADH_2) + glucanolactone$$
$$GOx(FADH_2) + O_2 \rightarrow GOx(FAD) + H_2O_2$$

The enzyme is immobilized on a metallic electrode (generally platinum) termed the **Working Electrode** (WE). In a second redox reaction, this electrode oxidises the hydrogen peroxide (H_2O_2) produced, which generates electrons. The generated electrons are transferred to the platinum electrode and constitute a detectable current, making the WE the biosensor's transducer. The full electrochemical reaction is represented as follows:

$$glucose + O_2 \xrightarrow{GOx} glucanolactone + H_2O_2$$
$$H_2O_2 \xrightarrow{Pt} O_2 + 2H^+ + 2e^-$$

To maximize the hydrogen peroxide oxidization response [Li et al., 2017], the electrical potential of the WE is set relative to a Silver/Silver Chloride (Ag/AgCl) **Reference Electrode** (RE) [Vashist et al., 2011]. This is called the polarization of the sensor. The current generated between WE and RE varies with the concentration of glucose in the solution. A schematic of a glucose sensor is presented in Fig. 4.1, summarizing all the concepts introduced so far, from the structure of the 2-electrode enzymatic glucose sensor to the chemical reactions involved (using the usual formalism found in the literature).

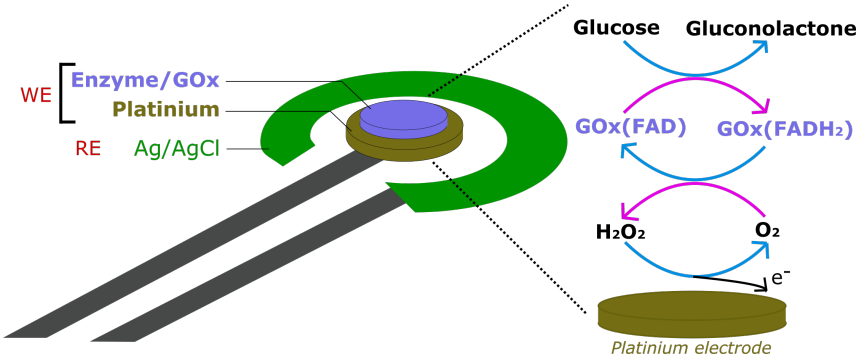

FIGURE 4.1: Schematic of the different parts of a 2-electrodes enzymatic glucose sensor of first generation, and the reaction occurring in the different parts. The blue arrows represent oxidation, and the pink ones reduction. WE, Working Electrode; RE, Reference Electrode.

The electronic instrumentation used to both polarize the WE and acquire the current variations is called a **potentiostat**. It is used in **Chronoamperometry**, or **Amperometry** mode when the potential is fixed and the current variations measured. The potentiostat is

an instrument capable of performing other types of acquisition for different electrochemical techniques: Voltametry (an amperometry but with varying potentials over time), Potentiometry, Coulometry, Impedance Spectroscopy [Grieshaber et al., 2008].

The enzymatic detection principle described above is not the only principle, and has varied with sensor generations. The differences are not always clearly and explicitly described in the literature. The explanations above are relevant for the *first generation* of enzymatic sensors (second generation sensors differ as they use a redox mediator to address O_2 dependence in the chemical reaction; third generation use a specific enzyme to allow direct electron transfer to the electrode without depending on a secondary redox reaction [Prévoteau, 2011]). Moreover, in first generation sensors, detection was originally based (Clark-type sensors, [Clark Jr. and Lyons, 1962]) on the *decrease* in O_2 reduction on the platinum electrode due to the presence of glucose oxidation consuming O_2. The detection of H_2O_2 oxidation corresponds to a second version.

Among first generation sensors, we can find 2-electrode or 3-electrode sensors. The latter is most widely used as it remedies a severe limitation of the 2-electrode version. In [Li et al., 2017] a detailed explanation is provided, and summarized on the Fig. 4.2.

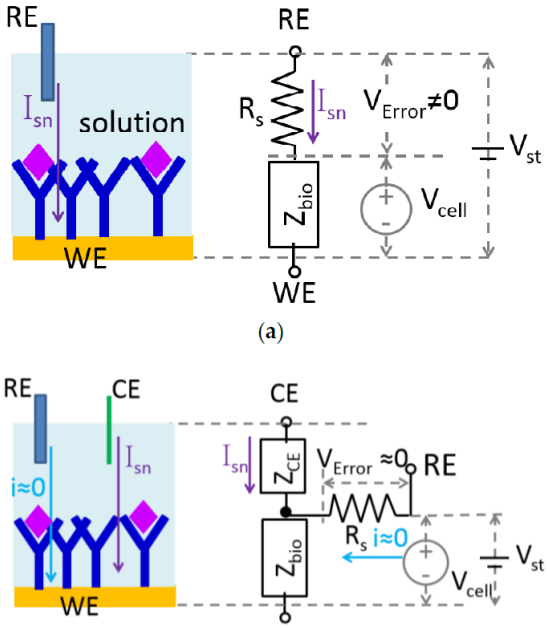

FIGURE 4.2: Comparison of the 2- and 3-electrode systems using an equivalent circuit. In the 2-electrode system, current I_{sn} passes between RE (Reference Electrode) and WE (Working Electrode), which generates a parasitic voltage V_{error} modifying the actual voltage applied between the RE and WE: V_{cell} is the desired voltage to apply and V_{st} the actual one. This parasitic voltage being dependent on current, the real voltage V_{st} varies and is not known, which decreases measurement precision. The third electrode introduced in the 3-electrode system is the *Counter Electrode* (CE). The current now passes between WE and CE and not RE anymore, thus V_{error} is almost null. Z_{bio} and Z_{CE} are respectively the impedance of the electrode-electrolyte interface, and impedance between RE and CE.

The online glucose sensor used in this work (Bio Sensor Technolgy (BST) ref. 560 000000) is a 2-electrode first-generation sensor, whose working principle aligns closely to the explanations provided above. The motivations behind the choice of this sensor are further explained in section 4.2 below.

4.2 Glucose sensor selection

4.2.1 Specifications

The MOoC system designed in this work requires a glucose sensor as defined in the introduction 1.4. The glucose is indeed one of the 2 main molecules of interest in the islet-muscle MOoC to both validate injected glucose concentrations and monitor cell interactions. Considering its role is to measure glucose concentration and its variations induced by the myotubes in response to insulin, we define the following specifications to select the glucose sensor:

- **(1) The sensor's linearity range should go up to minimum 11.1 mM**. Indeed the experiments with the MOoC intend to reproduce normoglycaemic conditions (4-8 mM), but also pathological conditions, and 11.1 mM is a critical value in diabetes diagnostic. Diabetes is diagnosed for a patient presenting at least one of those the following conditions [Mathew, Zubair, and Tadi, 2023]: (i) 2 hours after ingestion of 75 g of glucose, the venous blood glycaemia is at or above *11.1 mM* ; (ii) during a random test, venous blood glycaemia is at or above *11.1 mM* ; (iii) for 2 or more tests, fasting blood glucose is at or above 7 mM.
- **(2) if possible, the sensor's measurement range should extend to 30 mM** as blood glucose can reach 30 mM in diabetic patients [Robinson et al., 1992].
- **(3) The sensor should be compatible with a microfluidic setup**. We defined in the introduction of the current chapter, p. 107 that the glucose sensor should be placed outside of the microfluidic chip with cells, to simplify chip design. Therefore the selected sensor requires to be online, compatible with a microfluidic setup, and compatible with acquisition interfaces.

4.2.2 Technological choices

4.2.2.1 Choosing enzymatic sensors over optical sensors

As introduced in Chapter 1.2.5.1, there are 2 main techniques used for glucose sensing: electrochemical biosensors and optical biosensors.

Optical sensing requires expensive equipment that the IMS and CBMN laboratories did not possess. Optical access was also limited due to the MCS amplifier (shown in section 1.1.2.1 Fig. 1.5): the only access is a hole visible at the bottom of yellow metallic plate. On the contrary, the CBMN team possessed a potentiostat, and a team of electrochemists is present at CBMN, the *Spectroscopie et Imagerie de Peptides Actifs sur les Membranes* team.

The electrochemical technology appeared then as the most suitable for the MOoC project considering the environment.

4.2.2.2 Choosing commercial sensors over in-house sensors

Application-specific enzymatic sensors, especially for MPS, can be custom-made as this facilitates later integration. According to the literature, the fabrication process requires little

specialized equipment and follows the subsequent steps [Misun et al., 2016][Dornhof et al., 2022]:

- deposition of the metallic electrodes on the substrate
- Ag/AgCl reference electrode fabrication by silver deposition and silver chloride transformation using a bath of potassium chloride (KCl)
- working electrode functionalization with an hydrogel hosting enzyme, deposited using a pipette
- deposition of a membrane over the hydrogel

While collaborators were identified who had both the know-how and the facilities to realize the above described steps, they were located in different cities, and a collaborator was missing to know the precise design rules that appeared complex through patent literature [Hoss et al., 2013][Hoss and Budiman, 2017][Hoss et al., 2014]. Therefore custom-fabrication constituted too great a risk in terms of reliability.

On the other hand, commercial glucose sensors compatible with microfluidics are available, and generally exhibit greater reliability. For microfluidics use, these rely on a *flow cell*, which is a fluidic chamber with a slot that ensures contact between the sensor and a flowing liquid. Tubings are used to connect such system to a microfluidic setup.

4.2.3 Commercially available enzymatic sensors for microfluidics

A very cited sensor in the literature is the GLUKOMETER PRO strips from Bio Sensor Technology (BST) used with their in-house flow cell [**noauthor_organ_nodate**][Zhang et al., 2017][Fuchs et al., 2023]. These have been used in a project of liver-on-chip [Bavli et al., 2016][Prill, Jaeger, and Duschl, 2014][Ezra et al., 2015], and are the only sensors highlighted by the ORCHID consortium in their state of the art of the commercially available online sensors.

However, other suppliers exist and propose similar products. A list of the providers for microfluidics-compatible enzymatic sensor is given in Table 4.1.

Among the identified providers, Micrux was excluded from consideration for the MOoC, as they do not provide functionalized sensors. Sensors from Rusens and BVT Technologies

Supplier	Glucose sensor strip reference	Flow cell reference	Linear range	Commentaries
Micrux Technologies	Not Applicable	All-In-One Drop Cell-Add-on	Not Applicable	Sensor strips available but not functionalized
Rusens	No reference	Wall-jet cell	1 µM - 1 mM	/
BVT Technologies	AC1.GOD	FC2.TL.* PMMA	0.001 mM - < 10 mM	/
Jobst Technologies	B.LV5	B.LV5	0.05 - 25 mM	Several analytes possible with the same sensor: lactate, pyruvate, glutamine, glutamate
Bio Sensor Technology	art. 560 000000	art. 1410 000000	0.5 - 15 mM [Prill, Jaeger, and Duschl, 2014]	No datasheet available. Publications in the context of organ-on-chips: [Bavli et al., 2016][Ezra et al., 2015][Prill, Jaeger, and Duschl, 2014]

TABLE 4.1: Commercial glucose sensors and their compatible flow cell.

were also ruled out because they have an insufficient linear range. The two remaining options (sensors from Jobst technologies and Bio Sensor Technologies) both meet the requirements of our MOoC.

Based on their prior use in organs-on-chips, the **sensor and flow cell from Bio Sensor Technology (BST) were selected for the MOoC**.

4.2.4 Selected sensor information : BST biosensor and flowcell

The BST company provides several electrochemical sensors, meant for clinical applications. Amongst their products, the GLUKOMETER PRO and LAC PRO devices measure glucose and lactate respectively in a patient's blood drop. These devices operate with removable sensors, which are not single use contrary to the usual glucose sensors for self monitoring. According to BST, the lifetime of either sensor is 30 days (with an undefined usage frequency).

BST developed a PMMA flow cell on research purpose (art. 1410 000000), compatible with the sensors of the GLUKOMETER PRO (art. 560 000000) and LAC PRO. The flow cell accommodates one sensor but can be extended to host two, allowing simultaneous measurement of glucose and lactate. BST does not provide an acquisition system and software for the flow cell: a generic potentiostat must be used and connected to the electric contacts available on the flow cell. A picture of the flow cell and sensor is shown in Fig. 4.3.

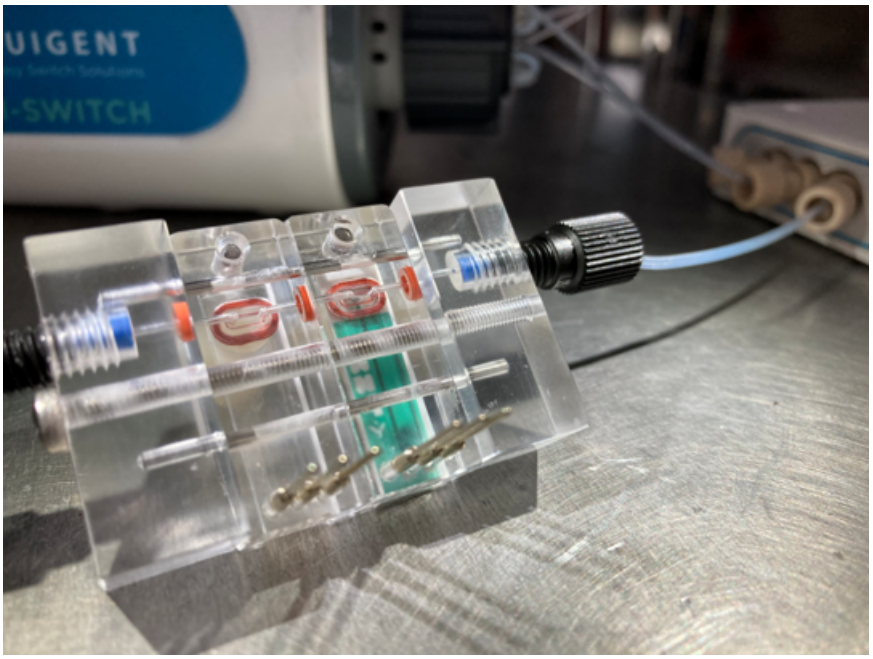

FIGURE 4.3: BST flow cell with 2 compartments, one hosting a glucose sensor strip. The sensor is connected to a microfluidic setup.

The glucose sensor provided by BST is a 2-electrode sensor. According to [Colburn et al., 2021], this particular sensor has sufficient precision even compared to a 3-electrode equivalent thanks to the micro-scale of its electrodes. Indeed, the small parasitic current that appears in 2-electrode sensors (see 4.1.2) is considered to have negligible effects on the polarization at such a small scale.

BST does not provide technical specifications for the sensor, but instead encourages users to characterize their sensors according to the operating conditions desired. Indeed, sensor response is highly dependent on parameters specific to experimental conditions, such as:

- Solution composition
- Solution injection protocol

The primary source of information regarding the BST sensor came from publications related to Fraunhofer Institute's liver-on-chip project. They used the BST flow cell to detect glucose and lactate in a study of mitochondria activity of HepG2 hepatocytes [Prill, Jaeger, and Duschl, 2014][Ezra et al., 2015][Bavli et al., 2016]. Their first publication on the subject mainly characterized the sensor and showed the proof of concept of cell metabolism monitoring [Prill, Jaeger, and Duschl, 2014]; the second presented a microfluidic platform for automatic injection of the samples [Ezra et al., 2015]; and the last one integrated the previous results and added an oxygen sensor to the system [Bavli et al., 2016]. Mainly, their work provided :

- An estimation of sensor performance in use conditions similar to ours (with cell culture medium and in cellular biology context): a linear range until 15 mM, a current in the order of the hundreds of nanoamperes, a response time below 100 s)
- The polarization voltage for the sensor (+450 mV compared to reference electrode potential)
- The flow cell volume (26 µl total volume for two modules, and one chamber in contact with the electrodes is only 2 µl)

These publications by the Fraunhofer team also provided valuable insight regarding measurement protocols. They suggested an elaborate one (illustrated in Fig. 4.4), made possible by their custom microfluidic platform: each measurement of a sample was preceded by a calibration, and a buffer solution was injected between each calibration and measurement to preserve electrode longevity; all solutions were separated by air to ensure a sharp chemical gradient between conditions [Prill, Jaeger, and Duschl, 2014].

4.3 Characterization

Sensor response greatly depends on the method used to inject a sample in the flow cell: even beyond flow rates, the introduction of intermediary conditions can enhance sensor performance. The required sensor specification in terms of usage conditions was not known at the time of these investigations (medium used, volume of the sample to analyze, MOoC experiment with Uptake Assay in static or dynamic), as the work in Chapter 3 was not conducted yet. Therefore 3 injection patterns were designed and characterized to have a general overview of the BST possible condition of use, to select later the proper injection protocol depending on results providing specifications (hence the investigations of Chapter 3).

We defined several injection protocols (illustrated in Fig. 4.5, left part), that explore the impact of isolating the sample for the measurements:

- **Continuous injection** - In the case of our work, the most convenient would be a sensor directly connected at the outlet of the MOoC. The medium to analyte would then be directly injected to the sensor. This protocol is hereafter termed *Continuous*.

- **Air-separated injection** - To test how far the strong chemical gradient notified by [Prill, Jaeger, and Duschl, 2014] while using air can enhance performance. This protocol consisted in adding air bubbles to discretize the sample into smaller samples. Compared to the *Continuous* protocol, the microfluidic setup is more complex with routing accessories to introduce air in the stream. This protocol is hereafter termed *Air-separated*, abbreviated as *Air*.

- **Buffer-separated injection** - As exposing continuously the sensor to glucose could reduce its lifetime, a third protocol was considered, selecting either to inject in the sensor the medium flowing out from the chip, either a buffer without glucose as in [Prill, Jaeger, and Duschl, 2014]. This last protocol is hereafter termed *Buffer-separated*, abbreviated as *Buffer*.

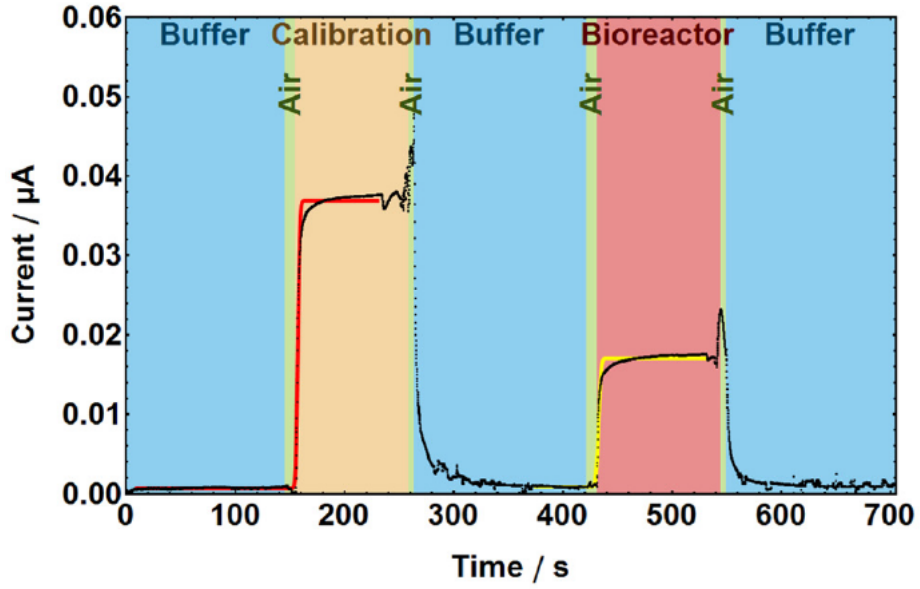

FIGURE 4.4: Microfluidic injection protocol used in the set of publications of the Fraunhofer institute with the BST glucose sensor, adapted from [Prill, Jaeger, and Duschl, 2014].

Another question regarding these injection protocols was whether the sample should be static or flowing during the measurement:

- **Static** measurements refer to the sample being still (i.e. the flow is stopped) *during measurement*, as was done in [Prill, Jaeger, and Duschl, 2014]. Note that the flow is intermittently re-started to replace the sample, and stopped to perform another measurement.

- **Dynamic** measurements refer to the sample being permanently flowing.

All 3 injection protocols are compatible with static and dynamic measurements (as shown in Fig. 4.5, right part) and as such must be characterized to determine the benefits and drawbacks of those operating conditions.

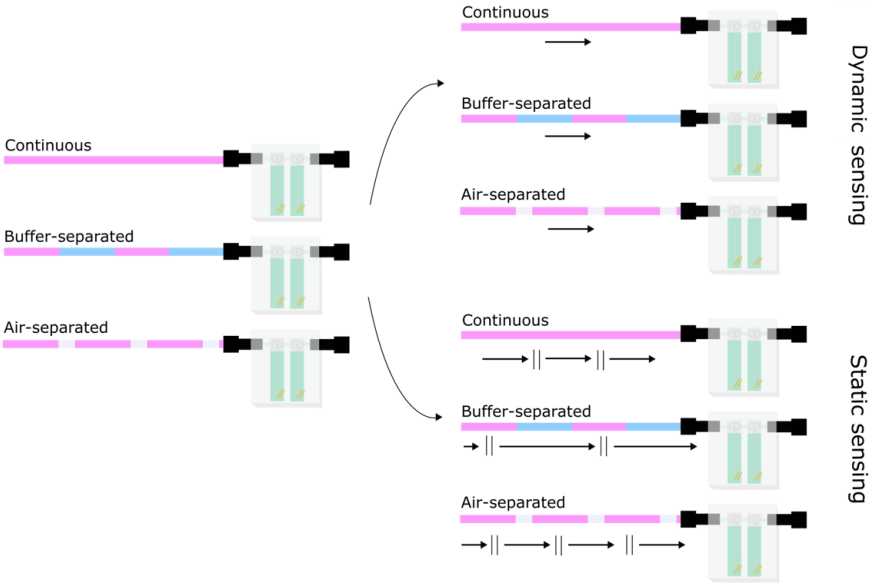

FIGURE 4.5: **Left** illustration of the different injection protocols with samples and separators (if relevant). **Right** illustration of the possible kinetics of injection: for the 3 top ones, the flow is permanent (represented by arrows); for the 3 bottom ones, the flow brings the sample to the sensor (arrow) and is stopped for measurement (parallel lines for breaks).

4.3.1 Characterization strategy

Defining operating conditions The first tests aimed at determining if the flow cell and sensor supported both static and dynamic measurements.

Characterization Then, the sensors were characterized to estimate the following performance metrics:

- Linear range
- Rise time
- Measurement error
- Absence of insulin interference (or insulin bias)

The first 3 metrics are illustrated in Fig. 4.6. Insulin interference tests were performed to validate that supraphysiological concentrations of insulin did not interfere with glucose measurement. Indeed, BST sensor strips are designed for clinical use; they are therefore graded for physiological insulin concentrations only. These tests were motivated by necessity for GUA experiments to have a positive control at supraphysiological insulin concentration (100 nM) according to the literature.

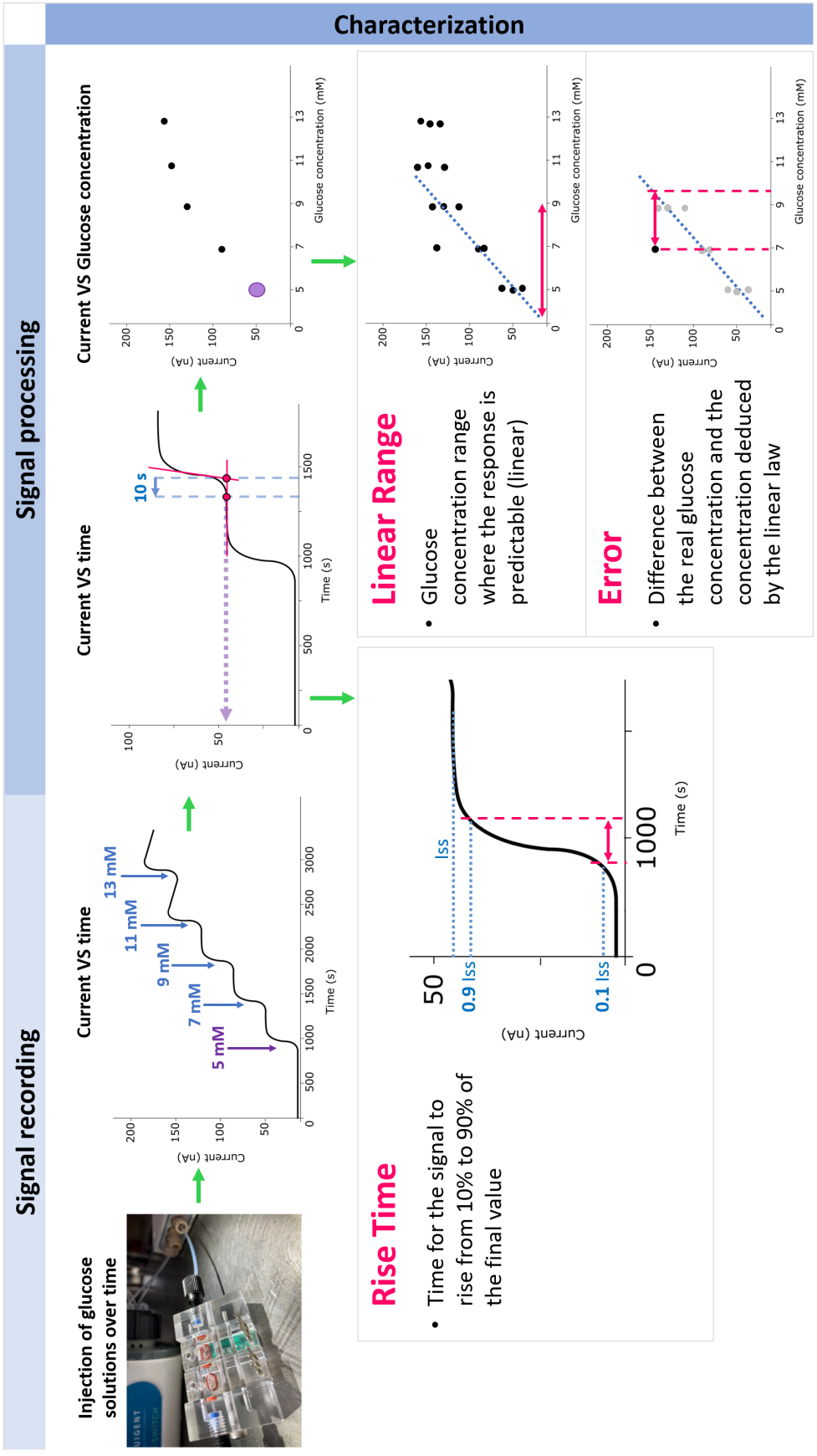

FIGURE 4.6: Sensor characterization processes and metrics.

4.3.2 Materials and Methods for characterization

Characterisation solutions Characterization was conducted in the same buffer solution as previously used in Chapter 3, that we termed EPHYS, and whose exact composition is provided in section 3.1 p. 67.

For glucose-dependent experiments, the EPHYS buffer was supplemented in glucose (D-(+)-Glucose, G8270, Sigma-Aldrich) to reach the desired set of glucose concentrations, as indicated in the results.

For insulin bias experiments, EPHYS solutions of different glucose concentrations were prepared, and then split into 2 solutions: one remaining without insulin and the second one supplemented with 100 nM insulin (Insulin asparte, Novorapid).

Acquisition setup The output current of the sensor was measured using the PalmSens EmStat 3+ potentiostat in *Chronoamperometry* mode. Inputs *Counter* and *Reference* were connected together on the potentiostat, since the BST sensor is a 2-electrode sensor.

The acquisition software provided by PalmSens, PS Trace 5.9, was used to control the potentiostat and record data. The polarization voltage was set at +450 mV, as described in [Prill, Jaeger, and Duschl, 2014], and sensor response was monitored in real-time and saved for further processing.

Before experiments, the sensor was left polarised in the EPHYS buffer solution for 2 hours, for the output current to stabilize. To validate sensor functionality before recording, a 3 mM glucose solution was used as a control (chosen as it yielded the most repeatable results).

Signal processing The different signal processing and characterization steps described here are graphically represented on Fig.4.6.

The output current of the sensor was processed in Python, and all graphical representations were made using R Studio (version 2022.12.0+353).

Timestamps of experimental condition changes were manually marked on the recorded signals (placed at the crossing of two tangents surrounding each step response, see Fig.4.6). As first step of signal processing, steady-state current values were collected 10 s prior to each condition change, as represented on Fig.4.6. *Rise time* (time for the step to rise from 10% to 90% of the deviation between steady-state values) was measured for each condition change. Steady-state current values were plotted against glucose concentration, and the *characteristic curve* of the sensor was obtained through linear regression (least squares method) for every injection protocol. Finally, the measurement *error* was calculated as the absolute difference between the reference glucose concentration and that derived from the characteristic curve.

Microfluidic setup The setup used in all characterization experiments is illustrated in Fig. 4.7. The buffer solution and air used 2 of the 4 reservoirs available in one rack. They were not only used in the injection protocols *Buffer separated* and *Air separated*, but also in the general management of the sensor (cleaning, polarization, removing bubbles). To extend the number of glucose solutions tested, a second 4-reservoir rack was added. As only one 4-channel pressure controller was available, pressure channels were switched to the desired solution during the experiment. This way, up to 6 glucose solutions could be tested.

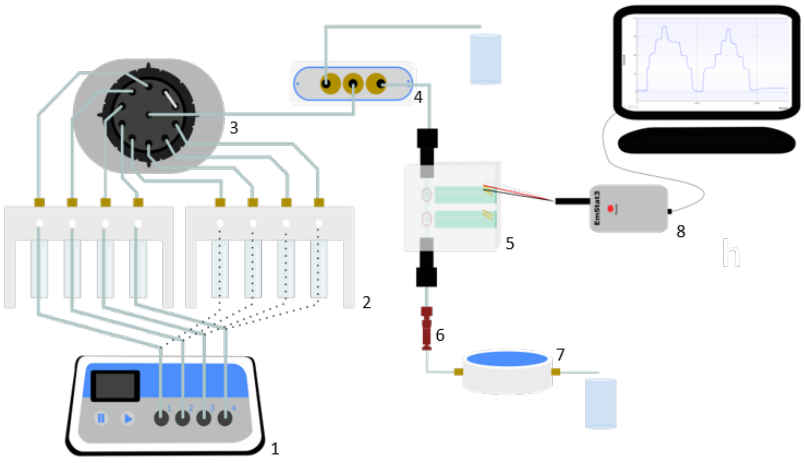

FIGURE 4.7: Microfluidic setup used for sensor characterization. **1.** Pressure controller, **2.** Solution reservoirs, **3.** 10-to-1 switch, **4.** 2-to-1 switch, **5.** BST glucose sensor, **6.** 1/16" to 1/32" fitting, **7.** Flow meter, **8.** Potentiostat.

The microfluidic setup for each protocol was operated as follows:

- ***Continuous* injection** - glucose solutions were switched successively. The pattern of injection followed successive increases and decreases of glucose concentrations (as illustrated in Fig. 4.8a) to test for hysteresis in glucose measurement (difference of glucose sensor response at a given glucose concentration depending if the glucose concentration was increased or decreased).

- ***Buffer separated* injection** - The EPHYS buffer solution was injected between glucose solutions by switching to the buffer reservoir, until sensor response stabilization at basal level. This minimized the effect of previous measurements on the sensor, as it was brought back to basal state (0 mM glucose) between experimental conditions. Therefore this protocol was not tested for hysteretic behaviour (increases only). The protocol is illustrated in Fig. 4.8b.

- ***Air separated* injection** - Air was injected between glucose solutions by switching to a pressurized (800 mbar) empty reservoir for 2 s. This process generated approximately a 2 cm-long air section between samples, which is a suitable length to prevent diffusion between isolated samples. The protocol is illustrated in Fig. 4.8c.

To assess insulin bias, only *Continuous* injection was used, as we considered that the injection method had no influence on insulin interference. *Continuous* injection was preferred over the two other methods since it comparatively allowed more repetitions in an experiment. The insulin bias protocol consisted in (as illustrated in Fig. 4.8d):

1. 2 repetitions of increasing and decreasing series of glucose steps without insulin,

2. the sensor is brought to basal state and let in EPHYS without glucose. Meanwhile, the reservoirs and tubings were emptied and refilled with a second set of solutions of identical glucose concentrations, with added insulin (100 nM),

3. same as 1 (2 repetitions of increasing and decreasing series of glucose steps) with 100 nM insulin.

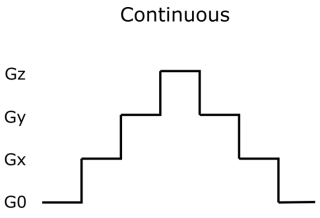

(A) Injection protocol in the *Continuous* mode.

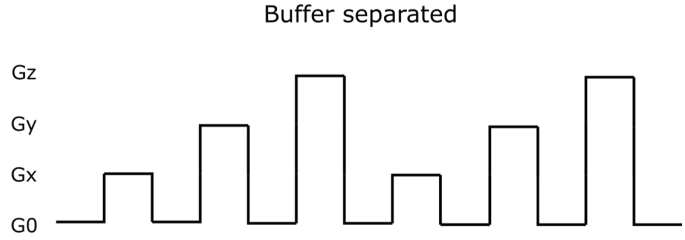

(B) Injection protocol in the *Buffer separated* mode.

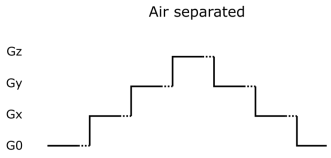

(C) Injection protocol in the *Air separated* mode.

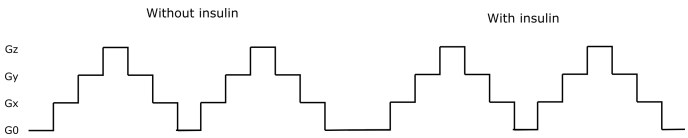

(D) Injection protocol for insulin bias experiments.

FIGURE 4.8: Injection protocols used in all the experiments. The time scale is not defined here as, in earlier experiments, glucose solutions were only switched once the sensor's output current had stabilized. Based on the general stabilization duration observed, later experiments were set to switch between solutions every 6 min.

In earlier experiments, glucose solutions were only switched once the sensor's output current had stabilized. Based on the observed duration to stabilize, later experiments were set to switch between solutions every 6 min.

4.3.3 Results

4.3.3.1 Measurements in static VS dynamic

The results reported here helped assess the difference between glucose measurements performed statically (in a still solution) and dynamically (under flow); in other words, they helped assess the impact of flow on glucose measurement. The *Buffer* injection protocol was used as it minimized the effect of past conditions on the sensor. Glucose solutions were either injected permanently at a constant flow rate of 40 µl/min (dynamic), or injected at 40 µl/min and left still during signal rise (static). The effects of flow rate value were also tested.

As shown in Fig. 4.9a, in static, the signal had poor repeatability: the sooner the interruption of flow, the lower the plateau. Artifacts (peaks) were also observed in the current soon after the flow was switched back on: the sooner the flow had been interrupted, the greater the artifact. A steady-state was expected but never appeared: after the flow was stopped, the current kept increasing with a constant slope. The expected stabilization only appeared when measurement was performed under flow (dynamic sensing). When the flow was stopped close to the signal stabilization, the signal presented once more a continuous increase and no steady state.

Then, the effects of flow rate were tested for dynamic sensing. The initial 40 µl/min flow rate used in characterization experiments was likely to be above the flow in further MOoC experiments. The expected flow rate for those was 10 µl/min, therefore comparative tests

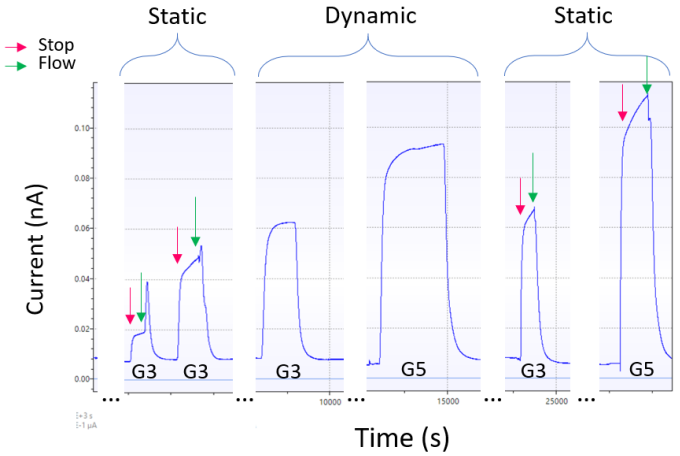

(A) Comparison of the glucose sensor's output current over time, in dynamic and static, with 3 mM (G3) and 5 mM (G5) glucose solutions.

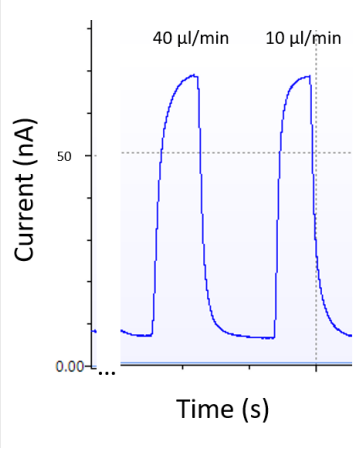

(B) Comparison of the glucose sensor's output current at 40 µl/min and 10 µl/min flow rates, measuring a 3 mM glucose solution.

FIGURE 4.9: Effects of flow on the glucose sensor's output current.

were performed for glucose measurements when solutions were injected at 40 µl/min and 10 µl/min. It did not reveal any difference, as visible on the Fig. 4.9b.

In agreement with Stéphane Arbault, senior researcher in electrochemistry in the *Spectroscopie et Imagerie de Peptides Actifs sur les Membranes* team at CBMN, measurements in static were considered inconsistent and **all further experiments were conducted in dynamic, under flow**. The characterization was made at 40 µl/min, and then 30 µl/min to reduce the consumption of solutions which was critical.

4.3.3.2 Performance metrics of the injection protocols

The results in this section provide a comparative study of sensor performance (linearity, measurement error, rise time) in all 3 injection methods, with dynamic sensing according to the previous result. In addition we verified the absence of insulin interference. The glucose concentrations tested ranged between 0 to 15 mM, and Fig. 4.10 (left) shows the sensor's output current relative to the glucose concentration, for each injection protocol. Every experiment is assigned a different color, and each experiment is constituted of generally 3 repetitions of the tested protocol.

Linear range Based on the spread of points in the *Continuous* protocol, it appeared that saturation occurred between 9 mM and 11 mM. This is especially noticeable above 9 mM glucose in experiments using sensor 12 and using sensor 13 (green squares and grey crosses in Fig. 4.10 (left), or hereafter named experiments *e* and *f* in Fig. 4.12).

In the *Buffer* protocol, saturation also appeared at 15 mM in experiments using sensor 6 (purple in Fig. 4.10 (left), or hereafter named experiment *a* in Fig. 4.11). Additionally, in Fig. 4.10 (right) representing the linear laws, measurements in the *Buffer* protocol appear less repeatable: the experiments with the largest 95% interval confidence were experiments testing concentrations from 11 mM.

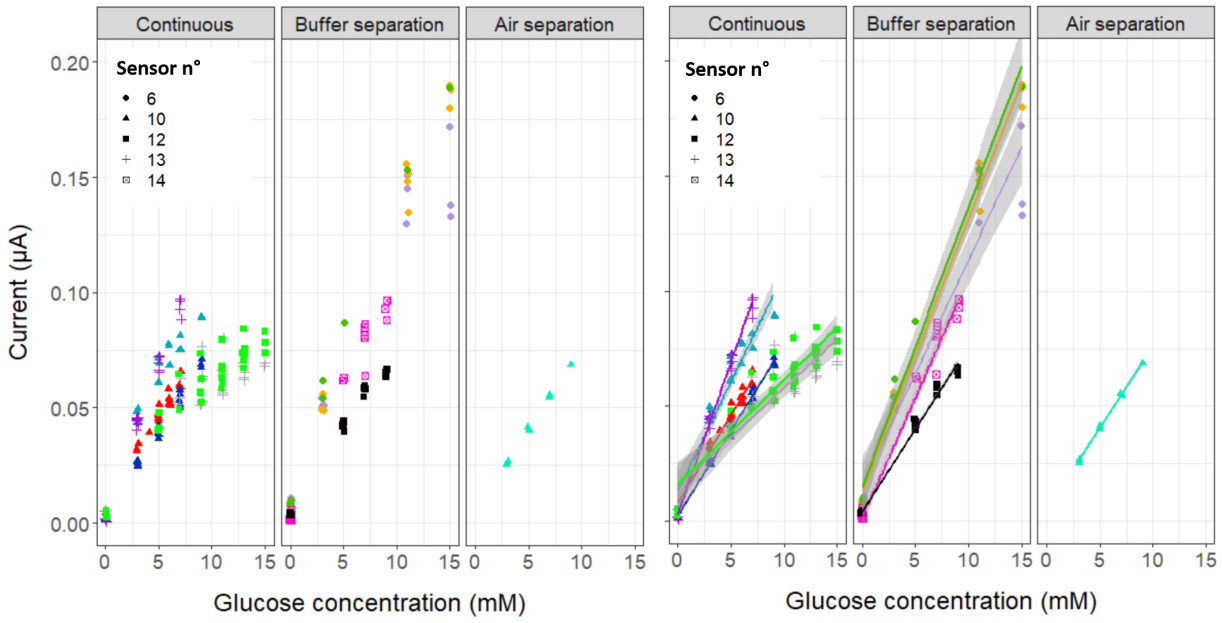

FIGURE 4.10: Current response of the BST sensor to glucose concentrations, for the 3 injection protocols tested. Every experiment is assigned a color. Each experiment involves replicates of the tested protocol, that are all represented. **Left**: raw results; **Right**: linear characteristics calculated for each experiment. The grey area surrounding the curves indicates the 95% uncertainty interval.

The *Air* protocol was tested in only one experiment between 0-9 mM glucose, and linearity was achieved in the whole range of concentrations. It is however possible that the actual linear range is wider than the tested range.

Based on these observations :

- In *Continuous* protocols, the linear range identified experimentally was 0-9 mM.
- In the *Buffer* protocol, the linear range identified was 0-15 mM, as the occurrence of saturation could not be reproduced. However, a decreased precision in measurement was observed above 11 mM.
- In the *Air* protocols, the linear range identified was 0-9 mM, although it could be wider.

Hysteretic behaviour In the *Continuous* protocol, the experiments which previously showed saturation (experiments *e* and *f*, or green and grey in Fig. 4.10) also exhibited a phenomenon similar to hysteresis. Each continuous experiment has been plot separately in Fig. 4.12 to better highlight the phenomenon. Over the 6 experiments, all except "d" had at least one staircase cycle where increasing current plateaus were different than decreasing current plateaus.

In general, output currents measured in decreasing glucose concentrations were lower than those increasing, and the hysteresis observed was greater in the first staircase cycle (red) than in later ones. The largest hystereses were present in experiments testing glucose concentrations of 0-11 mM ("e","f"). The experiments testing concentrations of 0-9 mM ("b","c") exhibited a smaller one, and the ones testing 0-7 mM ("a","d") did not systematically exhibit it (only experiment "a", repetitions 1 and 2).

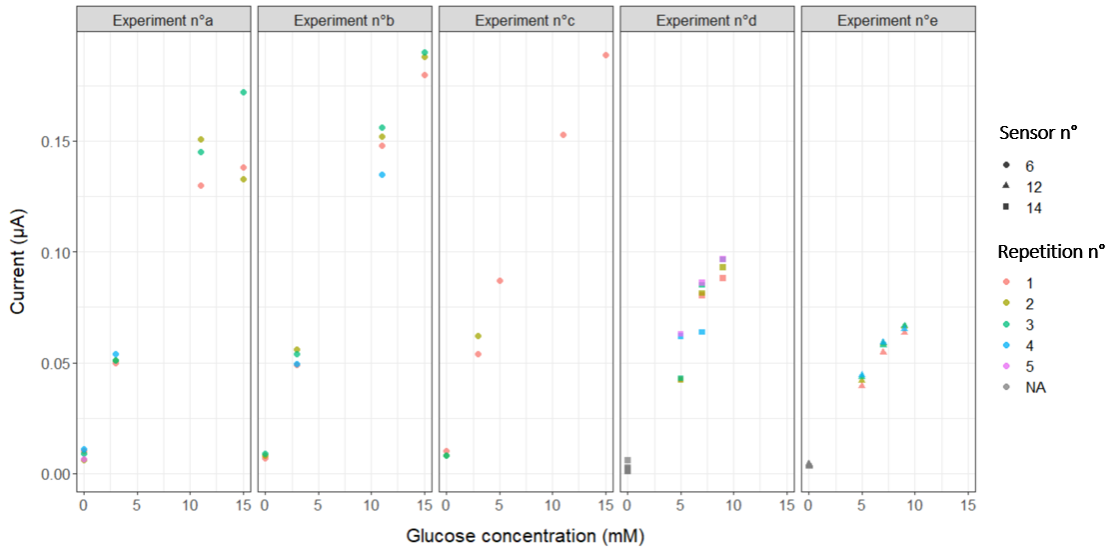

FIGURE 4.11: Glucose sensor response when using the **Buffer separated** protocol. Each frame is an experiment, where the protocol was repeated several time, corresponding to each color. The shape of the points distinguishes the sensor used.

In the literature of enzymatic sensors, the hysteresis phenomenon is rarely described [Matthews et al., 1988][Nien et al., 2023], which at first suggested that the observed hystereses were in fact sensor drift or an artifact from signal processing. Indeed, during processing, steady-state detection could overshoot or undershoot the actual plateau value. This hypothesis was however excluded as this would imply currents during glucose increase would be measured lower than those during decrease, but the opposite was observed. Sensor drift also could not produce this phenomenon as it would imply that the currents during glucose decrease would have been higher than those during the next increase; again, this was not the observed behaviour.

Considering the experimental results, the hysteresis phenomenon cannot be excluded. For the rest of the analysis, experiments "e" and "f" with the largest hysteresis were withdrawn, as the sensor was thus not used in proper operating conditions. For the other experiments ("a" to "d"), the small phenomenon was considered as measurement error.

Absolute error The results in this paragraph quantify the absolute error, as defined in section 4.3.2. It was calculated for all measurements obtained with the 3 injection protocols. The absolute error of all experiments in the different protocols is shown in Fig. 4.13a. Numerical values are reported in Table 4.2.

Protocol	Min	q1	Median	Mean	q3	Max
Continuous	0.001	0.103	0.195	0.208	0.251	0.703
Buffer separated	0.003	0.057	0.110	0.331	0.566	1.13
Air separated	0.042	0.054	0.065	0.082	0.111	0.138

TABLE 4.2: Statistical summary of the **absolute error** in mM for the different protocols (q1 for first quartile; q3 for third quartile).

To compare sensor performance between injection protocols, the maximum absolute error measured could provide a robust indication of sensor precision. However, outlying

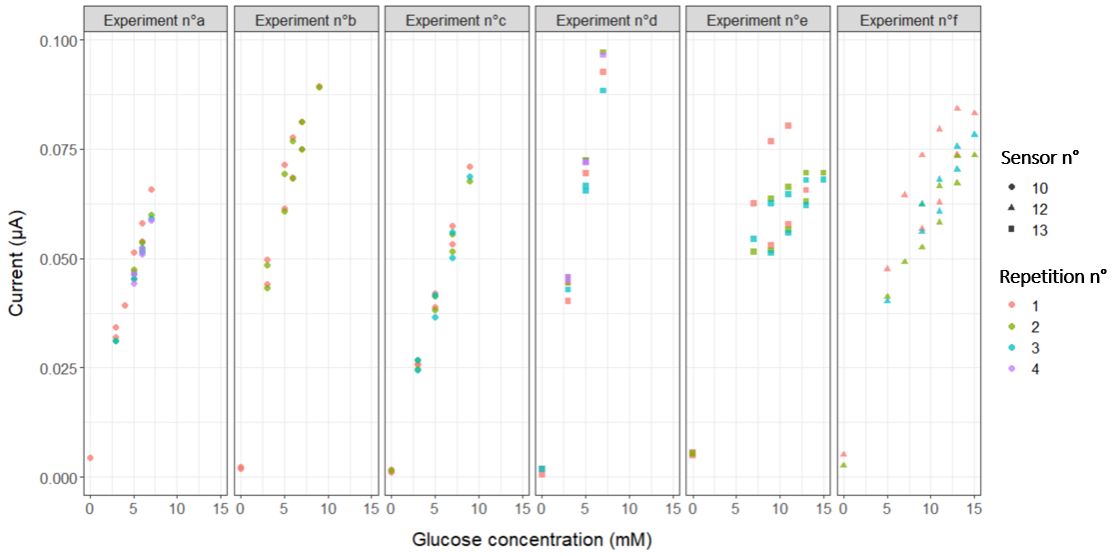

FIGURE 4.12: Glucose sensor response when using the **Continuous** protocol. Each frame is an experiment, where the protocol (increase and decrease of concentration) was repeated several times, corresponding to each color. The shape of the points distinguishes the electrodes used.

observations could lead to an over-estimation of statistically-relevant measurement error. For that reason, sensor precision was assessed based on the third quartile absolute error, as it indicated the maximum error of 75% of the observations.

Using the third quartile (q3) as metrics to compare the error, the *Air* protocol was considered the most accurate with a q3 error of 0.111 mM, followed by the *Continuous* at 0.251 mM, and finally by the *Buffer* separation at 0.566 mM.

Rise time Fig. 4.13b shows the distribution is regular, thus we can compare the protocols using the average. We see that **rise time was minimized (with a large factor) with *Air*, while *Buffer* was slightly better than *Continuous* injection**. On average, the rise time was 1.67 seconds only when *Air* was used, whereas it was 129 seconds when the protocol was *Continuous* and 105 seconds when the protocol *Buffer*-separated (see Table 4.3).

Protocol	Min	q1	Median	Mean	q3	Max
Continuous	34	109	129	129	146	246
Buffer separated	46	89	105	108	126	185
Air separated	1	1.25	2	1.67	2	2

TABLE 4.3: **Rise time** in second for the all 3 injection protocols. q1: first quartile; q3: third quartile.

Insulin interference testing The results shown below helped asses the absence of insulin interference in glucose measurements. In this experiment, 3 glucose solutions (3 mM, 5 mM, 7 mM, within the sensor's linear range) were tested with and without 100 nM insulin present. Fig.4.14 shows there was **no noticeable effect of insulin** (at suprapysiological concentration) on glucose measurement.

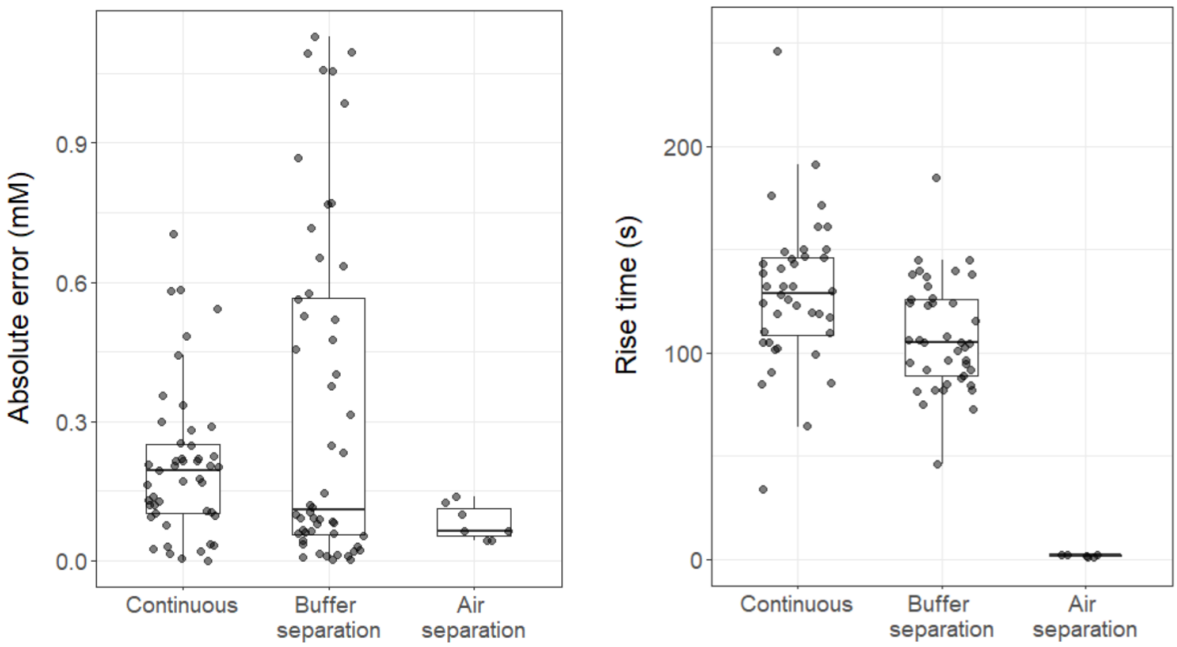

(A) (B)

FIGURE 4.13: Results of the characterization of the BST glucose sensor in all 3 injection protocols. The boxplots represent the first quartile, median, and third quartile values. The whiskers are 1.5 times the inter-quartile range. **(A)** Absolute measurement error (difference between real concentration and measured concentration as deduced by the linear law). **(B)** Rise time (time to reach from 10% to 90% of the final value).

4.3.3.3 Discussion and comparison of protocols performance for the MOoC

Injection kinetics The experiments about dynamic VS static sensing concluded the sensor **must be used with a dynamic sensing** (see section 4.3.3.1).

This was surprising considering in [Prill, Jaeger, and Duschl, 2014] they mentioned measurement in static ("stationary"). After completing the characterization of the 3 protocols, we hypothesise that they considered their measure static as they used air to isolate the sample, that we saw provides fast rise time (2 s maximum in our experiments).

Therefore we can consider the *Air* injection protocol as an almost static protocol as the perfusion time is very low (about 2 s). Considering the rise time measured for the *Continuous* and *Buffer* injection protocols (respectively 246 s maximum, and 185 s maximum), and the volume of sample in the myotube channel (6 µl), the sample should be injected at a maximum of 1.5 µl/min and 2 µl/min respectively. This is technically achievable in the MOoC setup, although further validation is required to assert that sensor response at these flow rates is similar to the one observed at 30 µl/min in our characterization.

Linear range The constraints posed by the MOoC experiments validating myotube response to islet-secreted insulin only required a glucose measurement range extending to 8.2 mM, as it aimed at measuring glucose consumption in a 8.2 mM solution. Therefore, any injection protocol has sufficient linear range (the smallest linear range, with the *Continuous* protocol, extended up to 9 mM). However, this may not translate to further experiments in pathophysiological conditions: only the *Buffer separated* and *Air separated* protocols may

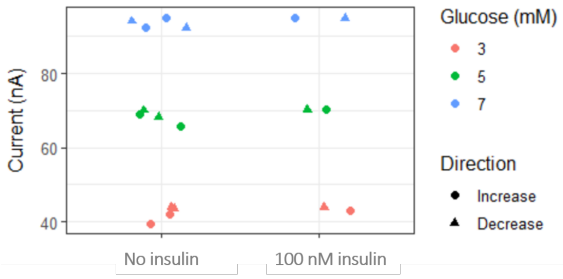

FIGURE 4.14: Output current of the BST sensor at 3 mM, 5 mM, 7 mM glucose, with and without 100 nM insulin.

have sufficient linear range. Note the *Buffer* protocol has less reliable linear range at higher concentrations than the *Air* protocol.

The linear range is variable between sensors and during the sensor life. Indeed, as seen in Fig. 4.10, different sensors yielded different characteristics entirely; however, sensors, when re-used, had characteristics with near equal slopes and an offset. Therefore, to ensure maximum measurement accuracy in the MOoC experiments, each new sensor required full calibration, and those re-used would require at least 1-point calibration. The calibration impacts the microfluidic setup in the perspective of an automated MOoC, and the suggested minimal setup required is illustrated in Fig. 4.15, allowing the 1-point calibration. If the first calibration of a new sensor is desired to be made with the same setup, a pressure controller should be added to use at least 3 glucose solutions.

Rise time and error The best performance in terms of rapidity and accuracy were obtained with *Air* protocol. However the results require to be confirmed with more experiments. The retained values of error to provide inputs for the scaling strategy were respectively 0.111 mM, 0.251 mM and 0.566 mM (*Air*, *Continuous*, *Buffer*). Indeed, we can consider this error as the minimum level of glucose variations we should try to achieve using MOoC scaling in order to have reliable measurements of glucose concentration variations. In the perspective of automated experimentation, the maximum rise time gives an indication regarding the shortest possible time interval between measurements: in *Continuous* injection, two consecutive measurements of a given sample cannot be separated by less than 246 s, 185 s for *Buffer*, and 2 s for *Air*.

The enhanced performance of the *Air* injection protocol probably comes from the sharp chemical gradient air creates between the samples [Prill, Jaeger, and Duschl, 2014]. Indeed, with the use of buffer between the solutions or when the liquids are injected continuously, there is a mixing of solutions due to the non uniform velocity field toward the section of the tubings (see section 2.1.2.1)). Thus the concentration arriving to the sensor increases slowly, while the presence of air breaks the parabolic velocity profile and prevents any diffusion between samples.

The injection of air provides the best results for sensing, however it has some limitations to consider:

- The microfluidic setup and driving is more critical. Indeed, the flow is less smooth with air in the tubings, and air bubbles could easily get stuck in the enzyme chamber of the sensor, leading to undesirable interference. The automated control of the microfluidics are a challenge, to prevent stuck bubbles, and to ensure precise displacement of the sample. However, solutions have already been developed in other works

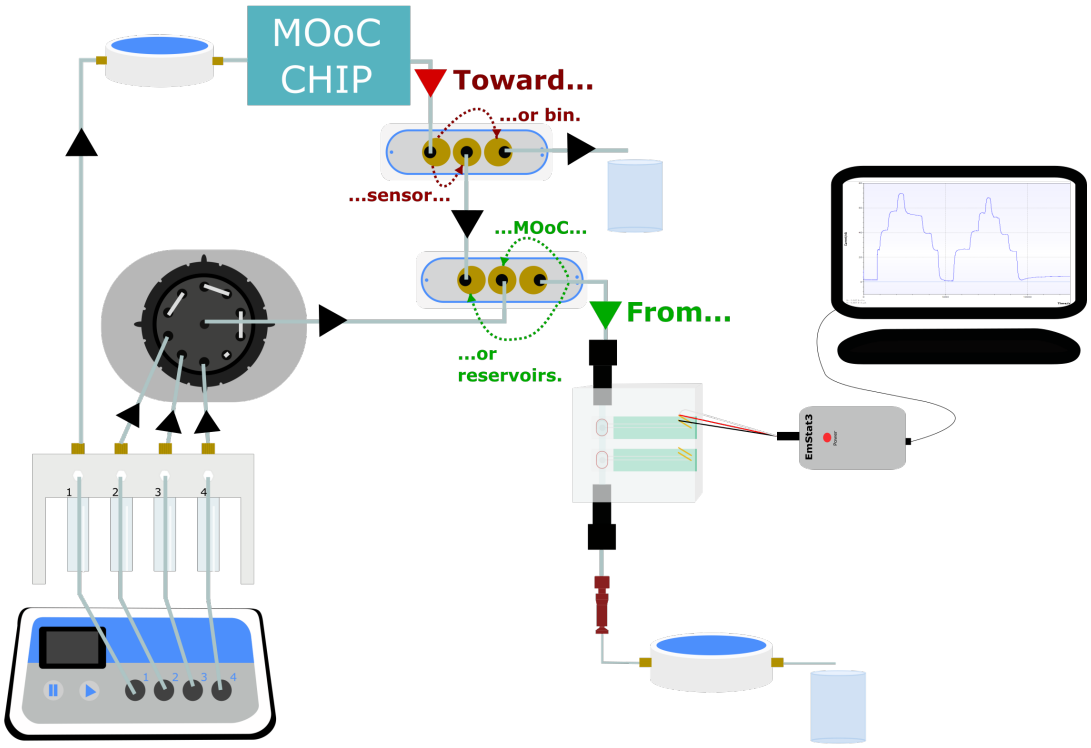

FIGURE 4.15: Minimal microfluidic setup required to use the BST sensor in the different injection protocols. Reservoir 1 for culture medium, 2 with air 3 with buffer and 4 with a calibration glucose solution.

[Sassa, Chandra Biswas, and Suzuki, 2020] than [Prill, Jaeger, and Duschl, 2014], suggesting its feasibility. Moreover, a custom flow cell with improved design could limit the prevalence of bubble issues (eg. the chamber could be designed with a progressive opening).

- The *Air* protocol, as tested with a sample preceded and followed by an air bubble, would imply with the MOoC design n°2 to generate an air bubble in the microfluidics circuit *before* the cell chambers. This exposition to air could harm the cells, preventing repeated experiments. A possible solution, which requires further experimentation, would consist in generating an air bubble prior to the sample, but injecting buffer to "push" the sample. The chemical gradient of the front of the sample would then be kept for the sensor performance, but the cells preserved.

4.3.4 Concluding remarks on sensor characterization

We found **3 usable protocols for the BST sensor**, which all respect the linear range for the current MOoC experiments: they operate linearly below 9 mM of glucose. However for experiments in pathological conditions (glucose above 11 mM, not tested here), the *Continuous* protocol is not suitable (presence of saturation), and the *Buffer* protocol may not be sufficiently reliable (error increase with concentration): **the *Air* protocol is the most promising one in terms of both rise time and absolute error**. Some further experiments with *Air* protocol are required to validate sensor linearity above the current 9 mM tested. An alternate *Air* protocol should also be tested, using a liquid (buffer) as separator before the sample (thus

before the microfluidic chip with the cells) to preserve cells from exposition to air, allowing for multiple experiments.

As *Air* protocol implementation is much more technically demanding, **the other two protocols remain strong candidates** with acceptable performance, especially for physiological experiments.

4.4 Microfluidic integration for the *Buffer* and *Continuous* protocols

The work reported in this section was conducted after the BST characterization under 3 injection protocols, and after the identification of the experimental scenario with the MOoC described in section 3.1. The static experiment that was planned in a first time implied small samples to analyse with the BST.

This static, thus low volume, step was critical for the *Continuous* or *Buffer* protocols, that had low rise time. Depending on the lowest flow rate allowed by the BST sensor for the measure, larger samples could be required than the 6 µl. A limited volume could be critical too from the microfluidics point of view, during the transport of the sample from the chip (with cells) to the flow cell supporting the sensor. Indeed, the medium in the myotube channel, when pushed toward the BST sensor for measure, could mix with the surrounding liquid in these 2 protocols due to diffusion and due to its parabolic velocity profile. These phenomena could not occur in the case of the *Air* separated protocol.

In this section, using multiphysics simulations, the fluid mixing was analyzed in a simple case study of the *Continuous* protocol. The impact of flow and internal diameters were then studied to highlight dependencies and define microfluidic design rules to integrate the sensor in the case of the protocols with liquid-liquid interfaces, that is the *Continuous* and *Buffer* protocols.

4.4.1 Simulation: quantitative impact of the parabolic profile

A simulation was conducted in a simple geometry representing a channel chip of 300 µm height and 1 cm length, with 20 cm of 0.254 mm ID output tubing followed by the inlet of the glucose sensor, that is a 15 mm tubing with 0.8 mm ID. This inlet was the portion of tubing inside the flow cell that drives the liquid to the chamber with the enzyme. The initial conditions of the simulation were as follows: the glucose concentration in the channel was at 4 mM (to reflect the myotubes glucose uptake), while the rest of the system was at the initial 8.2 mM. Then a flow at 45 µl/min (comparable to the one used in the glucose sensor characterization experiments) was applied for the *transport* of the sample.

The objective was to check how the information (glucose concentration) is distorted when the sample reaches the sensor.

The geometry as built in COMSOL is illustrated in Fig. 4.16a. Briefly, the geometry was separated in 3 domains where the initial conditions were different for the *Transport of Dilutes Species*: in the MOoC channel the concentration was at 4 mM, and the rest of the setup was at 8.2 mM of glucose. The flow rate used for the *Laminar Flow* was 45 µl/min. The glucose concentration was evaluated on a slice crossing the geometry in its middle (Fig. 4.16b), as well as over a line (or *Cut Line*) placed at the center of the microfluidic path (see Fig. 4.17 (A)).

The colored scale, or rainbow view, in Fig. 4.16b shows the travelling of the sample from the channel to the glucose sensor inlet. The parabolic profile impacts the sample at the first

second, where the front of concentration becomes a gradient (before and after the sample). The length of the gradients surrounding the sample is growing over time, until they reach the "body" of the sample and increase its concentration ($t = 14\ s$). Prior to the glucose sensor inlet, the concentration increased from 4 mM to 5.25 mM (see Fig. 4.17). The inlet of the glucose sensor has a higher diameter, which induces a length decrease of the gradient of glucose (see in Fig. 4.17 (B) the difference between $t = 14\ s$ and $t = 20\ s$). This change of diameter seems to exacerbate the "body" concentration increase: in the first 10 mm of the glucose sensor inlet, the concentration increased by 0.75 mM while on the 10 mm of the sensor inlet the increase is 1.25 mM.

In conclusion, the sample concentration varies significantly while traveling to the glucose sensor, as the concentration seen at the channel output does not go below 6 mM when 4 mM is presented at the input.

4.4.2 Explorations of the geometrical parameters

To test how geometrical parameters influence this phenomenon, and if it was possible to reduce it, the simulation was repeated with 2 other flow rates (5 µl/min and 25 µl/min), and with 2 other tubing diameters (0.15 mm ID and 0.5 mm ID).

To compare the distortion of the glucose concentration depending on these parameters (flow rate, tubing ID), 2 metrics were used:

- the average glucose concentration circulating in a section of tubing 5 mm before the inlet of the sensor, plotted over time
- the average glucose concentration circulating through the outlet of the geometry (thus the solution arriving to the glucose sensor chamber), plotted over time

The sections on which the averages were calculated are represented in Fig. 4.18. The average concentration over time was calculated in the COMSOL nod *Derived values*. The surface selected to calculate the average of the variable corresponding to concentration was the boundary of the outlet (see Fig. 4.18 (A)), and a *Cut Plane* created in the *Data Set* nod (see Fig. 4.18 (B)).

Parametric analysis on flow rate Prior to the inlet of the glucose sensor, we observe that the sample concentration increases with the flow. The increase is similar at 45 µl/min and 25 µl/min, however 5 µl/min shows a better preservation of the sample (increase of 11%, compared to an increase of 27% and 31% for 25 µl/min and 45 µl/min). But after passing the sensor inlet, the samples are distorted to a similar level and reach 6.4 mM at 5 µl/min and 6.7 mM at 25 µl/min and 45 µl/min. This represents an increase of 53% and 60% respectively compared to the original concentration of the sample (4 mM).

Note an oscillatory behaviour of the average concentration prior to the sensor inlet, in the case of a 25 µl/min flow rate.

Parametric analysis on tubing internal diameter In a second time the tubing diameter impact on the sample distortion was studied. The standard tubing internal diameters (ID) are 0.15 mm, 0.254 mm and 0.5 mm. So far the diameter considered was 0.254 mm; the following simulations were performed with the 2 other diameters, with the medium flow rate at 25 µl/min.

Results shows (see Fig. 4.20) that an increase of the tubing ID increases the distortion occurring prior to to the sensor inlet or chamber entrance; an ID decrease minimizes the distortion. Indeed the sample glucose concentration reaches 7 mM when the tubing is increased

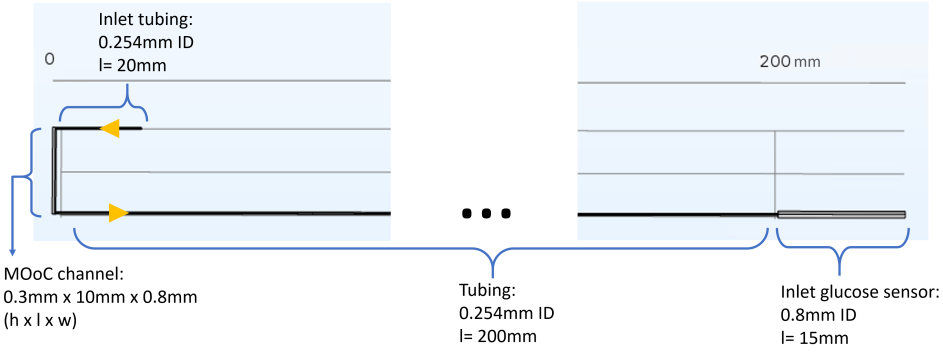

(A) Geometry of the simulation.

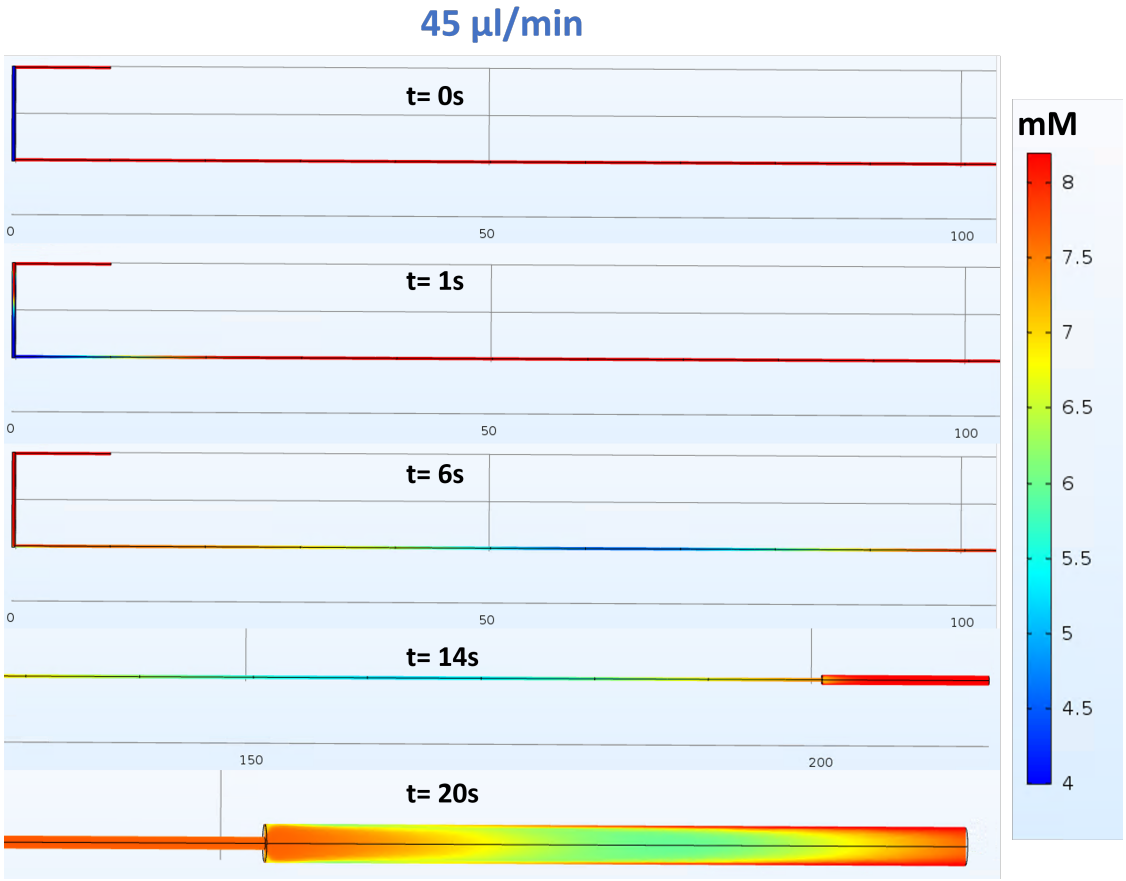

(B) Distortion of the sample glucose concentration while flowing toward the glucose sensor inlet.

FIGURE 4.16: Illustration of sample mixing issues induced by the parabolic velocity profile.

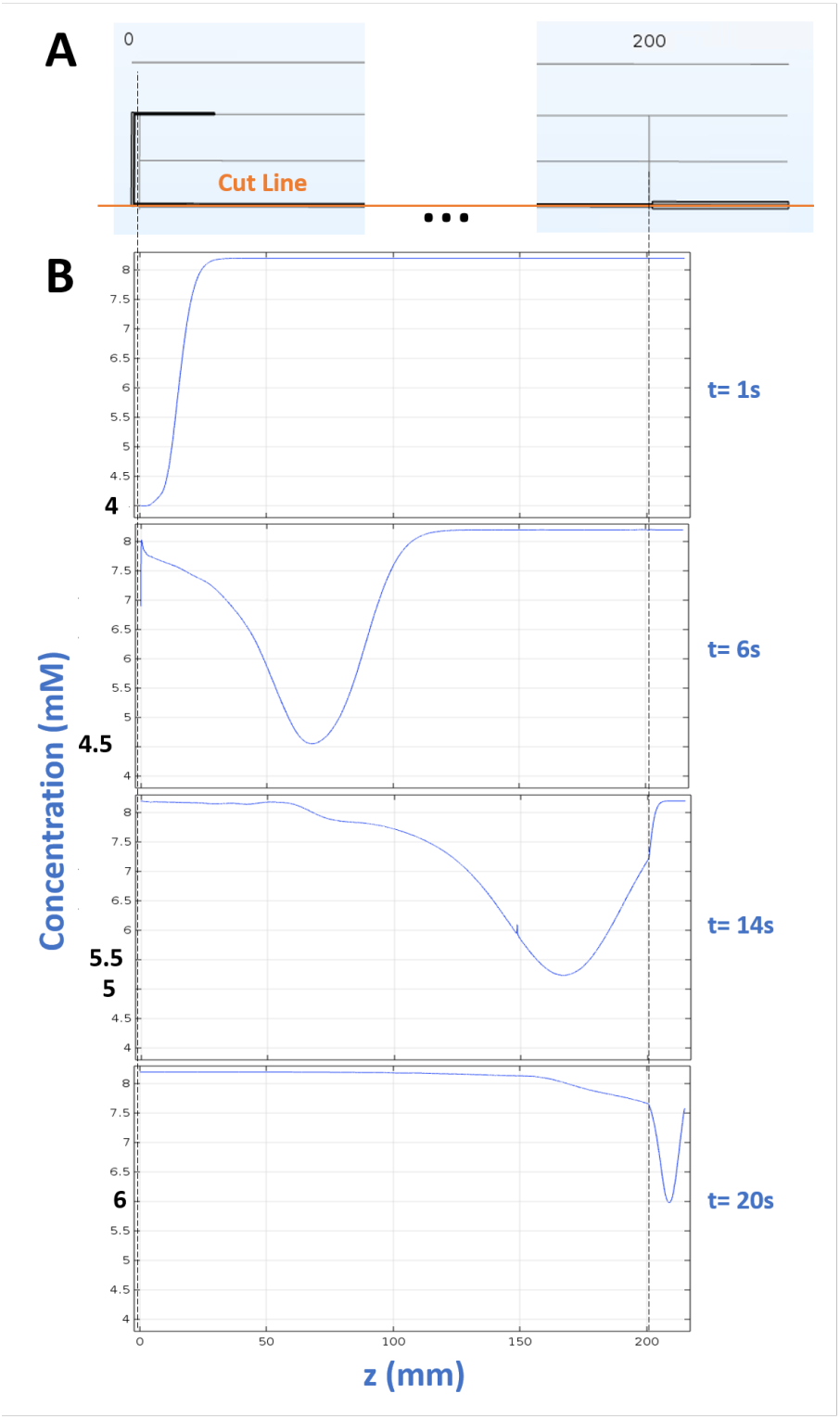

FIGURE 4.17: (A) Cut Line and associated glucose concentration represented in a 2D plot, at different times (B).

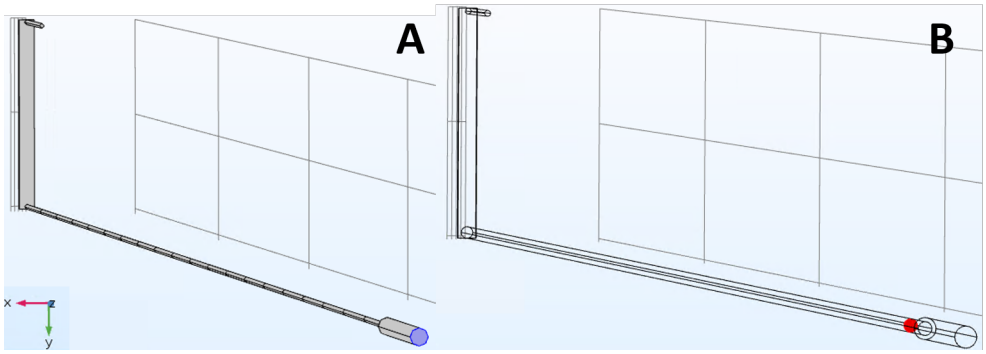

FIGURE 4.18: Representation of the sections on which the average glucose concentration was calculated over time: in (A) the blue section corresponds to the end of the glucose sensor inlet, or the inlet of the chamber with the enzyme; in (B) the red section corresponds to 5 mm prior entering the sensor inlet.

to 0.5 mm while it remains at 4 mM when the tubing diameter is decreased to 0.15 mM. Note the gradient before and after the sample still exists (the transitions between 8.2 mM and the minimum concentration is progressive). With the 0.5 mm tubing, the sample concentration is only increased by 0.2 mM between the sensor inlet and the sensor chamber, while it is increased by 1.5 mM in the case of 0.254 mm and by 3.7 mM in the case of 0.15 mm.

4.4.3 Concluding remarks on the integration of injection protocols

In the simulated microfluidic circuit, the parabolic velocity profile could drastically affect sample concentration while travelling to the sensor for analysis. The **impacting factor is the difference in tubing diameters between the tubing coming from the chip and the sensor inlet**. Indeed, even if the reduction of the flow rate and the tubing's internal diameter could preserve sample concentration, the benefits were erased in the case of a significant diameter difference between the tubing and the sensor inlet.

In either *Continuous* or *Buffer* protocols, the inlet diameter found to best preserve the original sample concentration was 0.15 mm. To ensure a constant inner diameter in the microfluidic circuit, the ID of all other components should be 0.15 mm as well. However, the flow cell for BST sensors has an ID of 0.8 mm, and no other model was commercially available. Likewise, no switches with an ID of 0.15 mm were found (our switches from Fluigent are 0.8 mm, and the only other reference found at Elveflow is 0.5 mm). Therefore, bespoke flow cell and switches were required.

It should be noted that the numeric recommendations discussed above are prone to re-adjustments, since the simulated geometries were those of the GUA setup instead of the MOoC setup (a linear channel instead of a serpentine). Indeed, the simulations were designed in perspective of replacing the Contour Plus with the BST Sensor and flow cell in GUA experiments.

The observations made are usefull in designing the routing between the chip and the sensor in the MOoC microfluidic setup, in either *Continuous* or *Buffer* injection protocols.

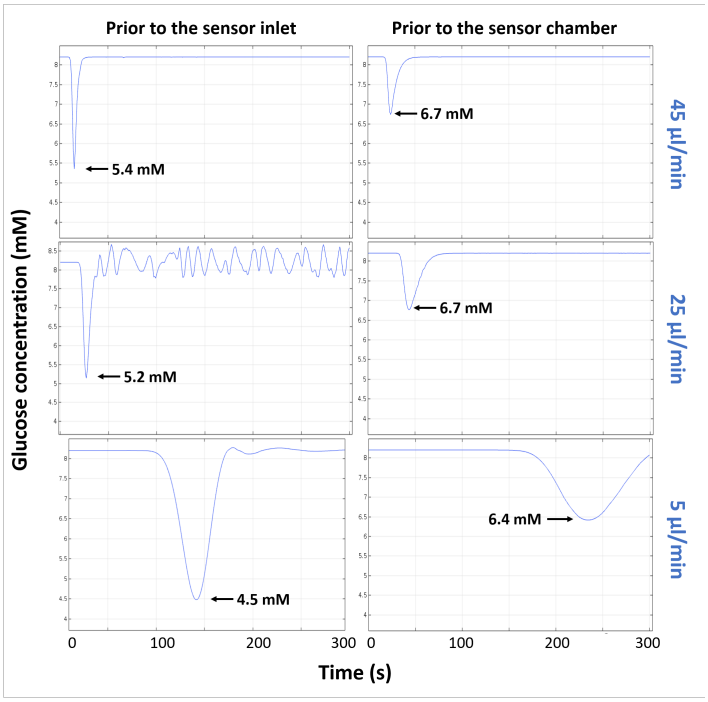

FIGURE 4.19: The average concentration crossing the section 5 mm prior to the glucose sensor inlet (left), and the average concentration going out of the system (right), for the 3 flow rates (45 µl/min, 25 µl/min, 5 µl/min), with 0.254 mm ID tubing.

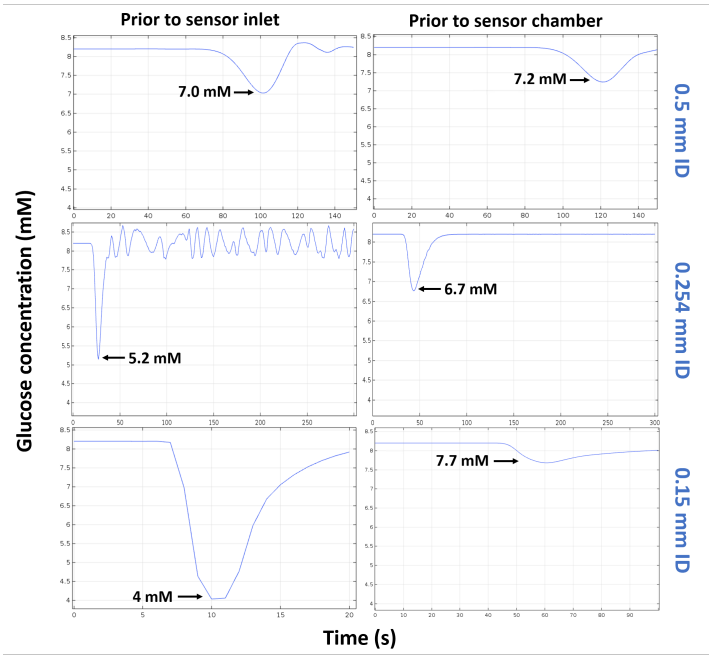

FIGURE 4.20: The average concentration crossing the section 5 mm prior to the glucose sensor inlet (left), and the average concentration going out of the system (right), for the 3 tubing ID (0.15 mm, 0.254 mm, 0.5 mm), with a flow rate at 25 µl/min.

4.5 Custom Potentiostat

This work has been realised with the active support of Gilles N'Kaoua, (CNRS Research Engineer at IMS), as well as Amandine Seroussi during her Master's engineering degree internship.

4.5.1 System requirements

There are different commercial potentiostats available, and two noticeable suppliers are *PalmSens* and *Biologic*. Potentiostats can be large instruments (HCP-803 Potentiostat, Biologic, 50x50x25 cm), but smaller ones exist like the EmStat3+ (7x6x3 cm) from PalmSens that was used in the BST characterization experiments (see section 4.3.2). PalmSens provides other models, from the stand-alone electronic chip (Emstat Pico Core) to modules with integrated communication ports and acquisition front end, but without housing (Emstat Pico Module).

However, we needed a **full bespoke** potentiostat, positioned as close as possible to the sensor to limit noise addition. It also has to be versatile enough to follow future development of the MOoC (organs and sensors addition, recirculating loop): a MOoC modification can change the Input/Output interface and the required performance of the potentiostat. Moreover, in the case sensors of different natures are implemented, a custom potentiostat can be upgraded to a multi-port system processing sensors outputs in parallel.

The potentiostat also has a footprint constraint, as it has to fit in a dry incubator, alongside the microfluidics equipment.

4.5.2 Glucose sensor output: signal profile

To design the potentiostat board, the profile and scale of the sensor signal (a current) have to be anticipated. The work accomplished in [Prill, Jaeger, and Duschl, 2014], with the characterization curve presented in Fig. 4.21, provided precious information: the current to detect is expected to range from a few nA to hundreds of nA, and the signal is low frequency, in the order of Hz.

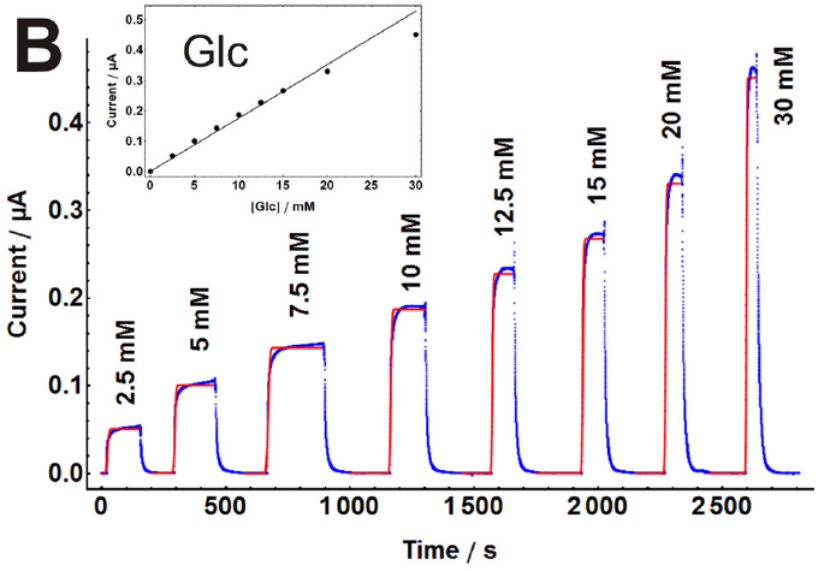

FIGURE 4.21: Sensor response (blue curve) to different glucose concentrations (red curve), extracted from [Prill, Jaeger, and Duschl, 2014].

Like in any electronics environment, we expected electromagnetic noise addition on the sensor signal. The main noise source is generally related to the main electrical power lines, at 50 Hz in Europe and 60 Hz in the USA. Fig 4.22 illustrates the impact of a periodic noise on the sensor response. From left to right, the signal aspect is transformed by the addition of parasitic signals at different frequencies (50 Hz and 200 Hz were selected for illustration).

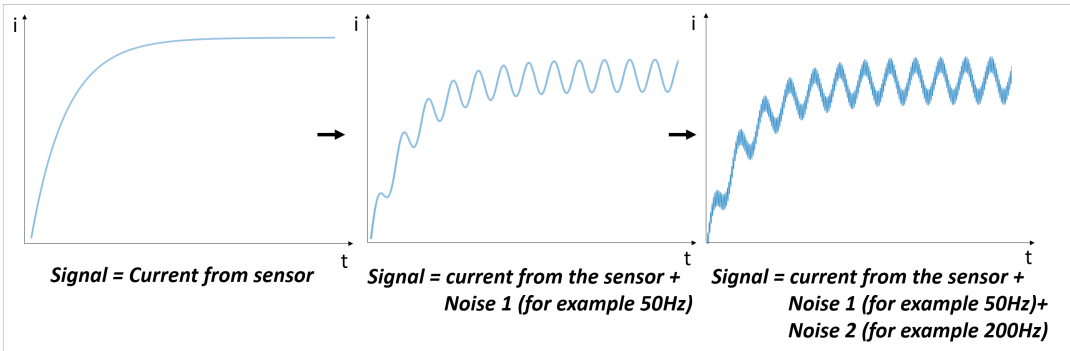

FIGURE 4.22: Impact of the addition of sine waves of different amplitudes and frequencies, simulating the addition of noise.

4.5.3 Final measurement system and potentiostat

The designed potentiostat is presented on Fig. 4.23. The sensor is polarized and its output current measured through its 2 electrodes WE and RE, connected to an analog acquisition front-end, which output voltage is sent to an Arduino UNO R3 board featuring an Atmega328P microcontroler with a 10-bit ADC. The Arduino also has DC pins that can supply voltage (5 V DC) to the potentiostat circuit. The Arduino board itself is powered by a computer through a USB port. This avoids the use of a separate power supply (respecting the requirement defined in 4.5.1). The Arduino sends the digitized signal by the USB port to the laptop, to be recorded and plotted in real-time, under the control of a Labview (National Instruments) program.

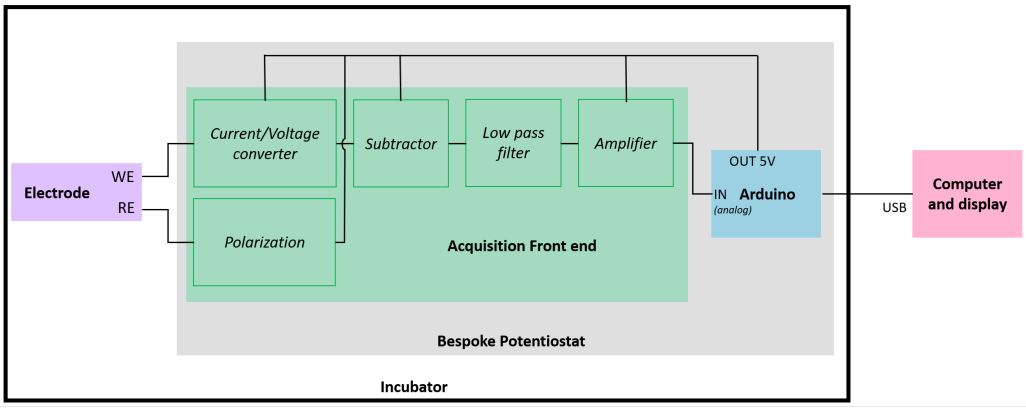

FIGURE 4.23: Architecture of the sensing system.

The schematic and stages of the acquisition front-end are shown in Fig. 4.24. This section details the stages circuitry, designed to fulfill the following objectives: allow amperometric detection, minimize noise, condition the signal to fit the Arduino ADC converter specifications. The role of each stage is graphically illustrated in Fig 4.25, and are explained in more details in the following sections.

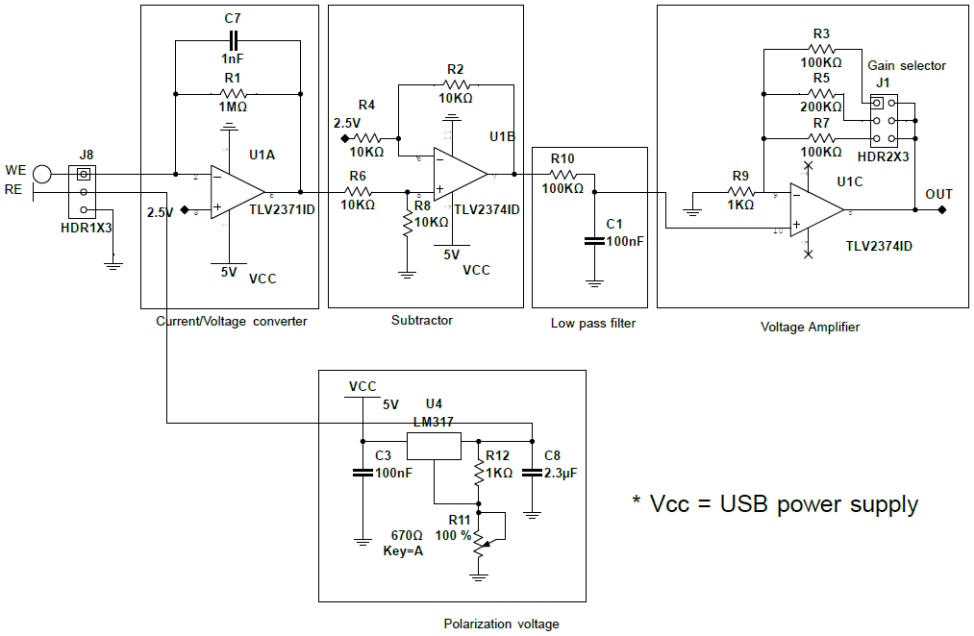

FIGURE 4.24: Schematic of the acquisition front end circuit.

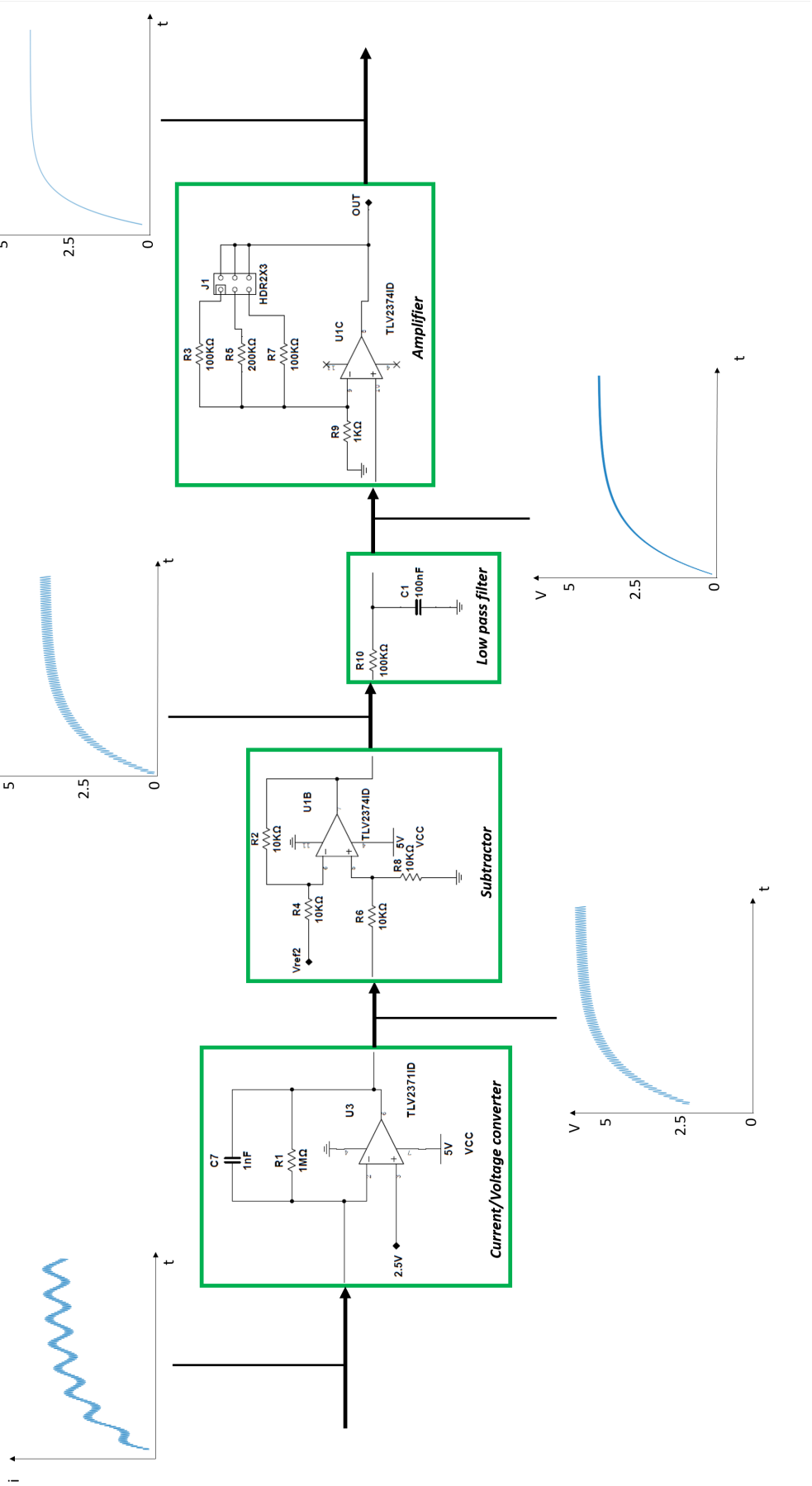

FIGURE 4.25: Acquisition front-end: signal processing decomposed per stage

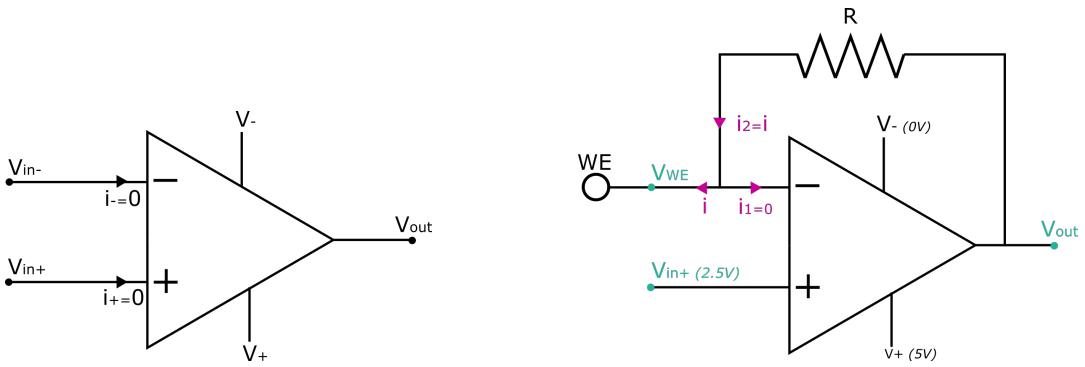

(A) Operational Amplifier symbol and inputs/outputs

(B) Schematic of a AOP-based current/voltage converter.

FIGURE 4.26

4.5.3.1 Amperometric detection

As described in section 4.1.2, the role of the potentiostat is, in the case of 2-electrode sensor, to set a polarization voltage between RE and WE, and to measure the current passing through WE. This is performed respectively by the stages *Polarization Voltage* and *Current/Voltage Converter* (or *transimpedance amplifier*) of Fig. 4.23 and Fig. 4.24.

Current/Voltage Converter The aim of this block is to acquire a signal carried by an electrical current, and convert it into a measurable voltage, proportional to the current. This conversion is required because the signal digitization, required for further processing in a computer, is performed by an analog-to-digital converter (ADC, see section 4.5.3.2) that only supports voltage inputs.

Current/Voltage conversion also allows to introduce a gain, intrinsic to the conversion. This helps raising the signal immunity to noise [Colburn et al., 2021], which is particularly prevalent in currents of such small magnitudes (hundreds of nA).

To understand briefly the principle of this important block in the circuit, the paragraph below explains basic principles of the Operational Amplifier (Op Amp), the component presented in Fig. 4.26a. This component is central in this stage, but also to several others within the board (see Fig. 4.24).

This component has 2 inputs ($+$: non-inverting input; $-$: inverting input), 2 power supplies (V_+ and V_-) and one output. Some rules govern this component:

(1) the inputs impedance (between $+$ and $-$) is so high that we can consider no current can enter the Op Amp

(2) the output voltage (V_{out}) is comprised between V_- and V_+

The schematic in Fig. 4.26b represents the Current/Voltage Converter connected to the WE pin. The input current i is measured based on the Ohm's law relating the current and the difference of voltage across the resistor R:

$$V_{out} - V_{WE} = R \times i \tag{4.1}$$

$$\text{Thus} \qquad i = \frac{V_{out} - V_{WE}}{R} \tag{4.2}$$

For a proper functioning, the following conditions have to be fulfilled:

- The leakage of current from WE to the $(-)$ entry of the Op Amp should be negligible, as only the current crossing R are taken into account in the Ohm's Law (see Fig. 4.26b, $i_1 = 0$). This is guaranteed by the principle 1 of Op Amp.
- The potential at WE, V_{WE}, has to be known. This is allowed by the feedback applied on the inverting input, that ensures the input voltages (V_{in+} and V_{in-}) are equal (the Op Amp operates in linear mode). As V_{in+} is connected to a voltage source of constant value (here 2.5 V,justified later), V_{in-} or V_{WE} is set.

Note on Fig. 4.24 the presence of a capacitor in parallel to the resistance. This does not influence the conversion principle explained above, but filters out undesirable high frequencies noise components (the signal is supposed to be low frequency, according to section 4.5.2). Noise filtering is developed later in section 4.5.3.3.

Using the numerical values provided in Fig. 4.24, the gain of the Current/Voltage Converter, also named transimpedance amplifier, is 1 V/µA.

The Op Amp principles described above correspond to an ideal component, whereas in actual devices the Op Amp current is not null and labelled as the *Current bias*. The TLV2371 Op Amp from Texas Instrument has been selected for this stage as it has a very low current bias of $\pm$ 10 pA (loss of 1/100 of current in the worst case, as we expect the lowest current to be of a few nA, see section 4.5.2).

Polarization The other requirement of an amperometric sensor is to set the voltage between WE and RE at a fixed value, here 450 mV (according to investigations in [Prill, Jaeger, and Duschl, 2014]). The WE potential has to be set at 2.5 V as explained later, thus the potential at RE is set at 2.05 V. To set the potential at 2.05 V, an adjustable regulator (LM317 NoPB from Texas Instrument) is used, with appropriate resistors (see Fig. 4.24). The regulator output voltage is provided by the following formula according to the component datasheet: $V_{out} = 1.25 \times (1 + \frac{R_{12}}{R_{11}})$, with R_{12} and R_{11} the names of corresponding resistors in our circuit. R_{11} is a trimmer resistor adjusted to precisely set the voltage to 2.05 V, using a voltmeter.

RE also supplies the current produced by the flow of electrons [Li et al., 2017]. Therefore the regulator selected to set the potential has also been selected as it can supply up to 100 mA, which is well above the expected currents (see section 4.5.2).

So far, we saw how the sensor is polarized, and the current passing through the WE is converted to voltage by the acquisition board.

4.5.3.2 Analog to digital conversion

The 10-bit Arduino analog-to-digital converter (ADC) converts voltages ranging from 0 to 5 V, with a resolution of 5 mV (5 V divided by 2^{10}). Considering the *Current/voltage* conversion operated in the first stage, and the lowest gain of the *Amplification* stage, 5 mV represent a current of 0.1 nA. This is a sufficient resolution considering the order of magnitude of expected currents (nA to hundreds of nA).

To benefit from the maximum ADC resolution, the voltage signal must be scaled between 0 to 5 V, and use this dynamic as much as possible (see Fig. 4.27, illustrating this concept). Therefore, according to the principle 2 of Op Amp, the power supplies of Op Amp are all at 0 V and 5 V (see Fig. 4.24) so that the output voltages are from 0 to 5 V.

As a general rule, the potential that is imposed at the $(+)$ input of Op Amp has to be symmetrical. This means it has to be at the center of the power supply range, thus 2.5 V in

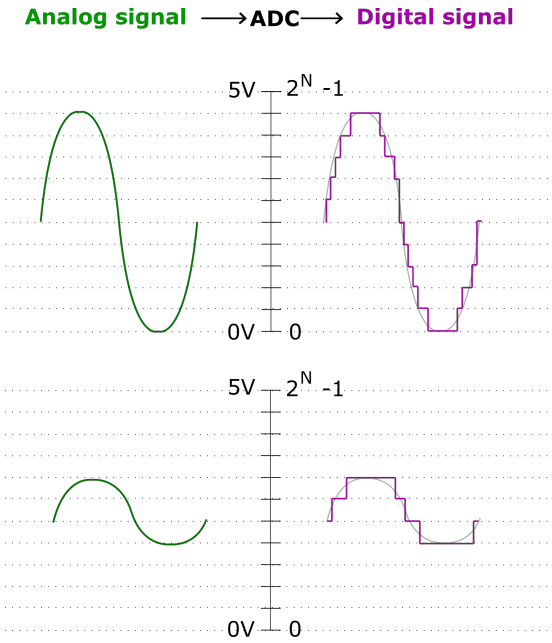

FIGURE 4.27: Graphical explanation of the interest to scale the input signal to match with the full ADC dynamic range.

our case. This 2.5 V represents the "zero" of the system, called the virtual mass. This explains why the WE potential was set to 2.5 V in the Current/Voltage Converter stage.

Therefore the signal path from the first stage to the ADC is the following: the voltage at the output of the *Current/Voltage Converter* varies from 2.5 V to 5 V ($V_{out} = 2.5 + R \times i$); the signal is then translated between 0 to 2.5 V by the *Subtractor* stage, and *Amplified* to reach the ADC full scale, that is 0 to 5 V (see Fig. 4.23, without considering yet the *Low pass filter* stage). Note that despite the Op Amp of the Current/Voltage converter is *rail to rail*, the actual dynamic of the signal cannot reach 0-5 V due to the existence of a 10 mV voltage drop (actual voltage range: 0.01-4.99 V).

The Subtractor and Voltage Amplifier stages presented in Fig. 4.24 are briefly explained in this paragraph. They have a transfer function stages between input and output potentials as expressed in the following equations (their explanation can be easily found in electronic engineering books for interested readers). Considering the notation of resistors in Fig. 4.24:

- **Subtractor**: $V_{out} = \frac{R_4+R_2}{R4}\frac{R_8}{R_6+R_8}V_+ - \frac{R_2}{R_4}V_-$
- **Voltage Amplifier**: $V_{out} = V_+ \times \frac{R_{eq}}{R_9}$ (with R_{eq} the equivalent resistor depending on the resistors selected by the user)

For the Subtractor, as all resistors are selected equals (see Fig. 4.24), the output potential is simply the potential coming from the Current/Voltage Converter stage, to which 2.5 V are subtracted. For the Voltage Amplifier, R_{eq} is determined by the resistor or combination of resistors selected by the user (through jumpers). As an example if R_7 is selected, the gain is $\frac{100E3}{1E3} = 100$, according to the resistors values. The selected resistors depend on the expected current range to measure, which is related to the glucose concentration: the lowest the glucose concentration the lowest the current (and the lowest the equivalent voltage through to the Current/Voltage Converter), and the highest the gain to select. The range of gain of this stage is from 40 to 200.

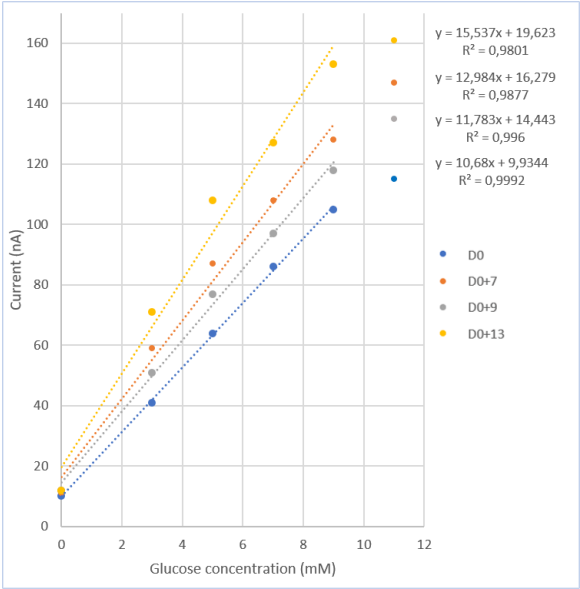

FIGURE 4.28: Current vs glucose concentration, obtained with the custom potentiostat and BST sensor. The sensor strip has been reused several time.

4.5.3.3 Noise reduction

A low-pass filter is implemented for high frequency noise reduction before amplification (Fig. 4.23). As can be seen on Fig. 4.24, it is composed of a resistor and a capacitor, and attenuates the frequency components higher than the cut-off frequency ($f_c = \frac{1}{2\pi RC}$). The signal of interest is considered at low frequency (around Hz, see section 4.5.2), thus the resistor and capacitor were selected to cut signal components at frequencies higher than 15 Hz (10 dB rejection at 50 Hz).

Note the capacitor in the Current/Voltage Converter also creates a low pass filter to pre-filter the signal (Cut off frequency at 156 Hz).

4.5.4 Validation experiments

Electrical tests and validations were performed (not detailed here) after fabrication of the potentiostat board. Then it was validated in a basic setup without the flow cell, thus without microfluidic (Fig. 4.29 (A)). The BST electrode was connected to the custom potentiostat thanks to the SPE Connector 2 mm from PalmSens, compatible with BST electrodes. Several Phosphate Buffered Saline (or PBS -/-) solutions (Ref 20012-019 Gibco) were supplemented with glucose and placed in beakers. The sensor was dipped successively in the different beakers.

Our custom potentiostat output is coherent with the signal obtained using the EmStat3+ potentiostat in the characterization experiments in section 4.3.2, with a *Continuous* protocol. The same linear range has been found using glucose concentrations from 0 to 11 mM, with a better linearity between 0 and 9 mM (see Fig. 4.28). This validates the potentiostat function.

4.5.5 Multi-potentiostat

The potentiostat described and validated in the above sections is presented in Fig. 4.29 (A). The acquisition front-end board is connected on top of the Arduino board (Fig. 4.29 (B)).

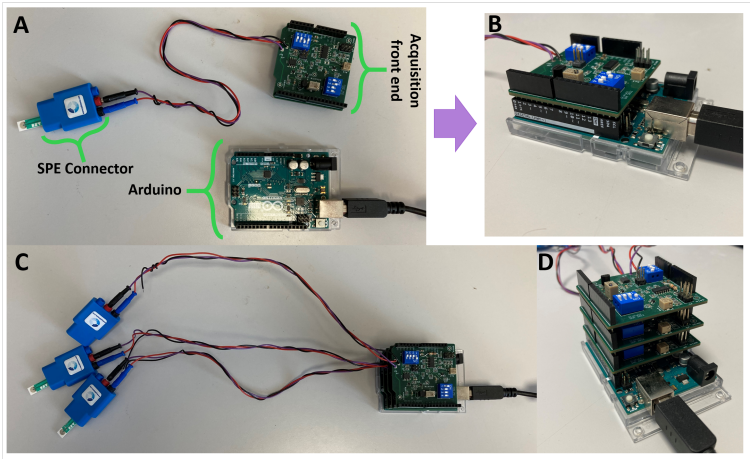

FIGURE 4.29: (A) A BST sensor plugged into a PalmSens connector, itself connected to the acquisition front-end, which can be stacked on the Arduino as in (B). By stacking several acquisition front-end boards, up to 4 biosensors can be used ((C) top view and (D) side view).

The Arduino's ADC possesses 4 different analog inputs, thus 4 acquisition front-end boards can be connected to process in parallel 4 biosensors' signals. The acquisition front-end boards are designed to be stacked up, and a switch system connects each board analog output to one of the 4 ADC analog input (Fig 4.29 (C and D)). That configuration has not been tested yet.

4.5.6 Concluding remarks on the custom potentiostat

A bespoke potentiostat has been designed and validated. The design has been optimized for 4 sensors running in parallel, turning the system into a multi-potentiostat, which remains to be validated. This set-up is very convenient at this stage of the project where the sensors are not fully specified. Still, the overall system footprint could be easily reduced, notably by replacing the Arduino by a customized microcontroller chip or board. In the future, a fully integrated multi-potentiostat including the digital front-end could then be designed based on FPGAs and/or ASICs.

4.6 Conclusion

For use with the BST sensor, 3 injection protocols (*Continuous*, *Buffer-separated*, and *Air-separated*) have been **designed and characterized, with experiments and multiphysics simulations**. The investigations specified the operating conditions of the different protocols: linear range, repeatability[1] and reproducibility[2], rapidity to get a measure, absence of insulin interference in supraphysiological concentrations (100 nM). For *Buffer* and *Continuous* protocols, microfluidic requirements were also defined. A **metric has also been proposed to characterize the measurement error** in each injection protocol.

[1]Measurement precision with the same sensors in a short period of time (a day in our case) [*ISO/IEC Guide 99:2007(fr), Vocabulaire international de métrologie — Concepts fondamentaux et généraux et termes associés (VIM)* 2007]

[2]Measurement precision with different sensors and different experimental days [*ISO/IEC Guide 99:2007(fr), Vocabulaire international de métrologie — Concepts fondamentaux et généraux et termes associés (VIM)* 2007]

However, **decisive GUA results are necessary** to define the specifications for glucose measurement, **to select one of the three injection protocols**. Indeed, the GUA would provide:

- the **sample volume**, depending on the ability of myotubes to generate sufficient insulin-induced glucose variation. As discussed in section 4.3.3.3 p. 124, if the BST sensor cannot reliably conduct measure at 2 µl/min or less, the *Continuous* and *Buffer* protocols would require, due to their high rise time, more than the 6 µl available with the current MOoC designs. The increase of this 6 µl is only possible if the level of uptake allow to increase the channel height to more than 100 µm height. Indeed, at 100 µm height channel, the myotube serpentine is at the maximum length possible due to the chip footprint (see Fig 3.7 panel (C) p. 77). The *Air* injection protocol, as considered static, does not require more than the 6 µl already reached in the smallest myotube channel.
- the acceptable level of **absolute error** of the sensor to assure proper detection of glucose concentration variations. As defined in the error results, we consider the associated error to the different protocols (respectively *Air Continuous* and *Buffer*): 0.111 mM, 0.251 mM, and 0.566 mM. After future successful GUA experiments, it would be possible to select the proper myotube chamber height to reach glucose variations above the sensor error and maximise successful experiments.

As the co-culture medium has been identified and validated, we need also to **verify the performance of the BST sensor using the modified co-culture medium instead of the buffer**. Note that once more the presence of 1% BSA in the co-culture medium for the experiments instead of 10% serum is convenient. This time it is not the fact it facilitates the flow by reducing viscosity, but it limits the sensor degradation by protein adhesion to the sensor.

An **ad hoc potentiostat has successfully been designed and validated**. The option to use it as multi-potentiostat has yet to be validated.

Conclusion

This manuscript summarizes three years of felling on the wide research field of MPS, to identify and implement a strategy to set the first islet-muscle MOoC deciphering islets to muscles communication. This work represents the first step of a larger project on which an ANR grant was obtained, DIAMOCHIP (2023-2026), to further develop the system toward a MOoC recapitulating the complete organ network involved in blood glucose regulation.

The thesis work focused on the **physiological relevance of the circulating insulin and glucose** concentrations, which is not a priority in many MOoCs, as well as the integration of online monitoring to provide a new vision of cellular interactions not allowed by *in vivo* and classical *in vitro* approaches. To do so, an interdisciplinary method has been conducted using both laboratories facilities to perform *in vitro* and *in silico* experiments. Each approach provided specifications to the various blocks composing our MOoC, which is a complex system to assembly.

1. Synthesis

MPS are sprawling projects, where it may be hard to define a starting point in the design strategy. The methodology we developed has been explained over this manuscript chapters, and the discussions and conclusions provide the main results and the perspectives. The scheme in Fig. 4.30 provides a comprehensive overview of this thesis work, that is both the projected methodology and its implementation, that went as far as possible in the allocated time.

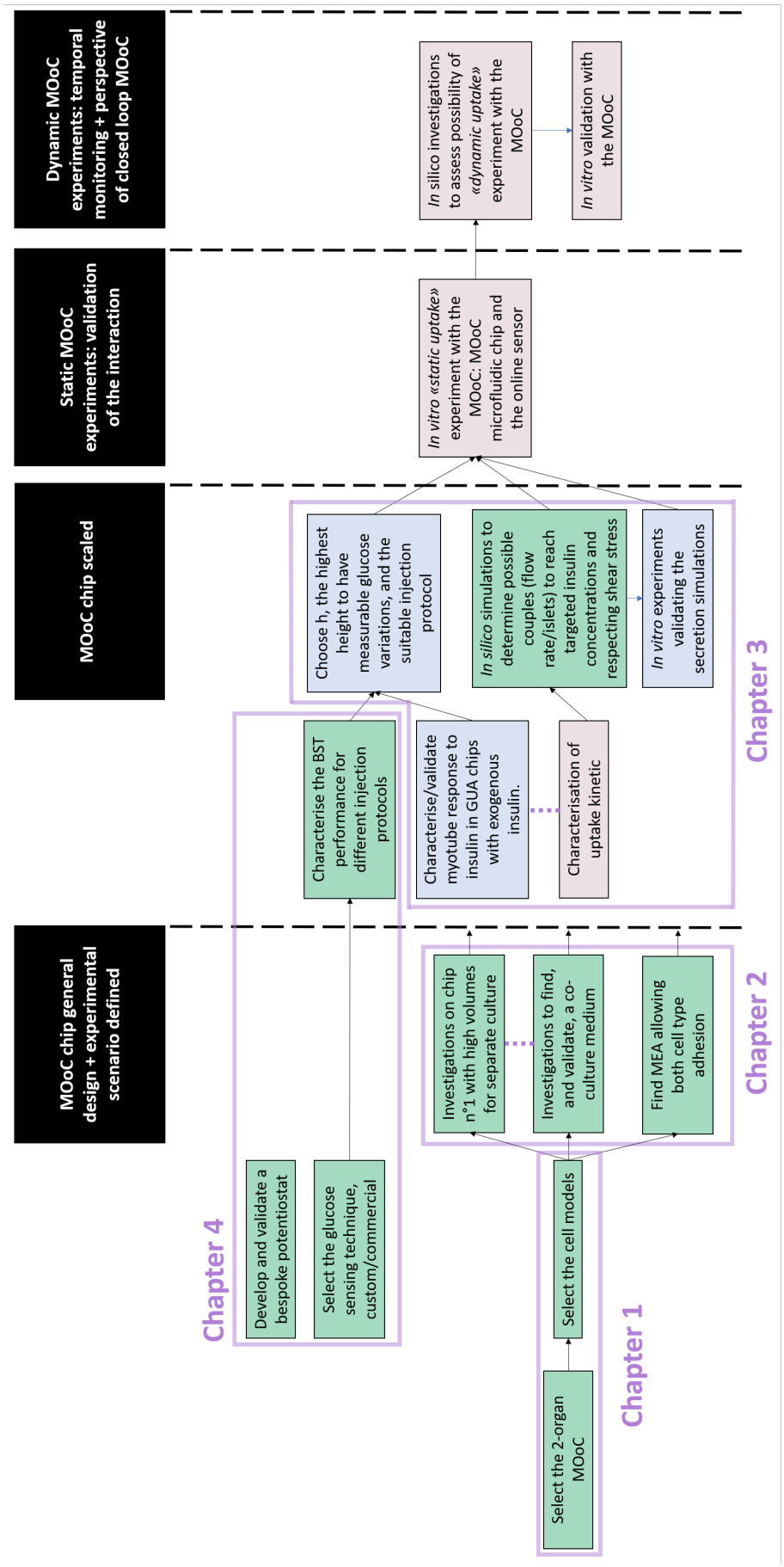

FIGURE 4.30: Thesis defined workflow and tasks achievement level: in black the main methodological steps, in green the achieved tasks, in blue the tasks partially finalized, in red the next tasks.

2. Perspectives

We propose here some perspectives for future work on the islet-muscle MOoC, notably following the discussions and conclusions in Chapter 3.

Improve the culture in chip n°2

The chapter 3 conclusion (see section 3.5 p. 105), highlighted the challenging search for a trade off in chip volumes, that had been investigated over chapters 2 and 3.

A possible perspective allowing to keep the benefits of both large and reduced volumes would be to achieve a culture of cells in a small-volume chip under flow, prior to experiments. In this way, the MOoC would present an optimal nutrients access and/or metabolic waste withdrawal, while keeping a reduced volume similar to the chip n°2. In addition to improve the cell culture quality, a culture under flow may be required in the perspective to replace PDMS. As explained p. 104, the current major substitute to PDMS (PMMA, glass) are generally not permeable to oxygen. Therefore the replacement of PDMS to prevent glucose release would impose to develop a MOoC where cell culture under flow is possible.

This solution seems feasible for myotubes based on our observations: myoblasts adhered strongly 30 min after seeding and, during experiments, no detachment due to the flow was observed. However this is more challenging for the islets. This was already attempted by a former PhD student in the CBMN team, Dr. Emilie Puginier: islets detached after 24h of perifusion at 1 µl/min, in a chip with a geometry similar to our chip n°2 except for the height that was about double, which resulted in a shear stress even lower than in our chip.

The use of membranes or hydrogel is a very attractive way to counteract these shear stress issues. This is more physiologically relevant than placing the cells inside a microfluidic channel, because, *in vivo*, the cells are separated from the flow by the endothelium and ECM. In the context of islet-on-chip more specifically, using a hydrogel implies a modified secretion profile, with delayed response to glucose and reduced amplitude first phase peak [Buchwald et al., 2018][L. Vanderlaan et al., 2023]. This profile may be more relevant, as it could mimic more accurately delays due to an ECM-like environment.

In this work the choice to place directly the cells inside the channel, as in most of the MPS, is related to:

- the complexity of hydrogel/membrane MPS in terms of fabrication and mostly characterization,
- the possible incompatibility of hydrogel-based solutions with MEA, or at least reduced electrical signal quality.

The complexity of characterization was the primary reason for which we did not make the choice of using hydrogels or membranes at the beginning of the thesis. Indeed, the diffusion of all the molecules of interest has to be known in the hydrogel, or through the membrane, to perfectly understand and master cells' environment: the hydrogel induces time lags, which impacts the interaction happening in the MoOc.

[Dornhof et al., 2022] tried such strategy: organoids were cultured in 75% Matrigel, contained in a channel delimited by pillars, and the medium was flowing on channels aside. The glucose, lactate and oxygen sensors were placed in the stream flow, and additional oxygen sensors situated in the area containing the Matrigel and organoids. Using diffusion coefficients found in the literature, they simulated with COMSOL the diffusion of H_2O_2 and Doxorubicin (chemotherapeutic drug) from the stream flow through the area with the cells

and Matrigel. They choose these 2 molecules to be representative substances for small and larger molecules. They found a good accordance between the simulation and the experiment in case of H_20_2, the only molecule they could measure with their electrochemical sensors. This encouraging result is to put into perspective with the fact that diffusion coefficients are "extremely challenging to measure", in addition to the fact that we cannot estimate the exact pericellular concentration during experiment, like for glucose.

Therefore the use of ECM-like hydrogels and membranes is still a great challenge but expectations are high for MPS in general, as well as for our project. Solving the hydrogel/membrane challenge requires an interdisciplinary approach: the use of multiphysics simulations is mandatory, as well as expertise on the ECM complexity and on *in vivo* dynamics.

Enhance cell models

The GUA experiments in chapter 3 raised some questions about the use of a muscle cell line in the context of a MOoC reproducing the glucose homeostasis. Indeed the cell lines have transformed phenotypes [C. Peterson et al., 2020], including for the management of glucose. This was raised by [Prill, Jaeger, and Duschl, 2014] for hepatic cell lines, and by [Forterre et al., 2014] in a proteomic comparison of C2C12 and primary skeletal muscle cells.

Replacing the cell lines by primary cells is a general tendency in MPS, but it seems to be even more desirable in MPS reproducing glucose homeostasis.

3. Drawn lessons for MOoC projects management and perspectives

MOoCs, simulators of a version of reality: method and challenges

This work evidences an interesting parallel between multiphysics simulation and MOoC design. A multiphysics simulation computes a simplified model of our complex physical reality; and MOoCs are simplified models of a complex human physiology. Simplification is a necessary process in modelling as **the full representation of reality would be tedious if even possible**, in addition to be **complex to analyze and interpret**. For example in the chip n°1 simulations, we described all the material of the chip in contact with the sample as simple walls, an inert limit, while the porous PDMS properties could have been implemented in the simulation to represent a potential liquid penetration; and the medium we used was considered as water (as in all MOoC simulations). Simplification choices are either related to the simulation cost (computational power and/or time) or to the lack of knowledge of model parameters: characterize all the PDMS and cell culture medium properties would require cumbersome work. The same observations apply to our MOoC, where we cannot represent yet a full pancreas with all cell types and architecture and we therefore focus on the cells of interest. At the systemic level, it is not possible yet to design a MOoC gathering all the organs and tissues impacting glucose homeostasis: even bones appeared to have impact on insulin secretion [Liu, Mosialou, and Liu, 2018], not speaking about the nervous regulations.

Therefore simulations or MOoCs are representations of ***a version of reality***, whose relevance depends on the design choices. These choices are made not only to render the study feasible (less complex), but also because they are expected to have **no significant impact on the results**. In the above mentioned case of modelling a simple wall over a PDMS one, we were confident that the PDMS would need a long time of contact with medium so that penetration starts, and even though, it would represent a small portion compared to the full

volume of the chip. Cell culture media (used in microfluidics) are aqueous solutions basically, with a low percentage of serum or BSA bringing slight viscosity. However, in many cases, the impact of MOoc design choices is more complex to estimate.

Our conclusion is that, like simulations, as long as one respects basic principles (physics principles in simulation; cell survival, operating conditions of sensors in MOoC), a simulation or a MOoC always delivers a result. It is up to the designer to justify and validate that result consistency and scope.

The MOoc design field can benefit from its parallel with the simulation field by searching an inspiration in some of its methodologies. Like for simulations, or mathematical models, to be sure that MOoC results are relevant enough, it is mandatory to validate intermediate versions of the system, using different approaches to *confront expected results to what is actually obtained with the modeled system*. This is for example what we did when the insulin secretion determined with our *in silico* simulations did not fit with the corresponding *in vitro* experiments, which made us think that cells have sub optimal functionality inside the chip (after previous validation of the simulation relevance); or when confronting *in vitro* GUA in macro- and micro- volumes. This *in silico* vs *in vitro* confrontation is not easy in the MOoC context: this was done in this work thanks to the laborious work done by [Alcazar and Buchwald, 2019], which probably does not have an equivalent for many other cell types and models. Moreover, in MOoCs for glucose homeostasis and diabetes, we did not find a similar method to confront the level of secretion or uptake observed *inside the chip* to an expected level, previously determined *in silico* or *in vitro* evaluations. Possibly in these works, cells were validated with a biochemical assay prior to their placement in the MOoC [Bauer et al., 2017], or secretion was compared between monolayers and their 3D construction, but in well plates (macrovolumes) and not in the chip. This concept of results comparison by different methods was found in one OoC for diabetes: [L. Vanderlaan et al., 2023] used the *in silico* model of [Alcazar and Buchwald, 2019] and commercial perifusion machines as comparison.

The necessity of preliminary validation appeared clearly with our GUA experiments. Indeed, the validation of this "simple" block of the system consisted in trying to answer the question: do we observe an insulin response? We saw how complex the results interpretation and validation were. We can expect even more difficulties for the validation and analysis of the results obtained with a MOoC not properly characterized by preliminary experiments (for example without identifying the impact of glucose release by the PDMS).

We saw that the parallel between simulation and MOoC can suggest a methodology of validation by sub-blocks to improve the system relevance, but another matter should be considered: the *comparability* of the results between different MOoCs will be crucial in the next stages of MPS scientific life (and more specifically MOoCs) to prove their relevance. As we previously mentioned, each MOoC represents *a version of reality*, driven by the design choices, their comparison is hard and not really addressed in the current state of the art. Future work comparing and characterizing the different scaling methodologies could be a strategy to allow MOoC characterization, but also results comparison between different systems of different scaling.

Building a MOoC: block by block approach or systemic approach?

The first choice to make in this PhD was the system design approach:

- by blocks: each OoC and each sensor is separately developed, *without co-culture and interaction specifications yet*, and later they are assembled together in a MOoC by finding a common culture substrate, co-culture medium, and so on;
- or directly tackle the systemic level: find a co-culture medium, design a microfluidic chip comprising the 2 co-cultured organs, directly scaled for cell's interaction. This scaling made using functional results (e.g. insulin secretion or glucose uptake) from the cell's in the co-culture medium in "dummy" chips (our channel chips for example), and finally develop/characterize the sensor in the co-culture medium.

The first option may appear more time consuming, because the OoCs built may have volume, footprint, substrate/chip material satisfying for each organ scale alone, *but not for the MOoC*. Moreover the functional results obtained with the OoC, or the performance of the sensor, could change when up-scaled to the MOoC, and therefore may not be used directly for a functional scaling strategy. Indeed, the MOoC system uses a new culture medium, the co-culture medium, and may require a new cell culture protocol (as for the LHCN-M2 in this work), or need a new culture substrate (the MEA in our case). As a consequence, the cells response and activity can change with a different culture procedure, medium and substrate, as well as the sensor performances when changing the medium. Last but not least, the cell types selected for the OoC may not withstand a co-culture, therefore the cell model may have to be changed for the MOoC.

Therefore it appears that this approach requires a lot of development (thus time), that would have to be re-done at the time of the final MOoC design. This is what led us in this thesis to select the systemic approach.

However, after the 3 years of work, I think it would have been more *efficient* (more results per unit of time) to build our MOoC with a block by block strategy. I consider that the current issues identified in the project could have been tackled with the block by block strategy, as explained below.

The systemic strategy sounds definitely interesting (and realistic) when: (i) the cell model culture specifications in microfluidic chips can be deduced from the literature, covering a variety of microfluidic chips studying the same organs (different culture substrate tested, or chip volumes, and quantification of secretion/uptake in such conditions); (ii) when the biochemical assays protocols are already known and mastered amongst project partners. Indeed, the main issues I observed to construct this MOoC respecting a functional scaling were: (i) to ***find proper order of magnitudes*** in equivalent microscale muscle cells systems: there is no publication on muscle-on-chip insulin-dependent glucose uptake; (ii) to have sufficient ***time*** to ***develop*** and ***conduct*** all the ***biochemical assays*** to validate the different biological questions, like the cells functionality in either a new co-culture medium or in microfluidic chips. Indeed, rigorous biology requires to validate each question through several experiments (myotubes' insulin response validated through NBDG, Akt and GLUT4 experiments).

Both (i) (ii) are issues that impact the development **resources**: when order of magnitude are unknown, *in vitro* assays are mandatory to find them, which is laborious (the GUA experiments lasted about 8 months, and fortunately secretion assays were not required for islets); establishing a new biochemical assay protocols is time consuming, in addition to the fact they may not be *compatible with microfluidic* afterwards and require further development.

Therefore to build a MOoC like ours, with a cell type not integrated in the team routine and without much precedent in the scientific literature of OoCs, I would suggest a ***Ooc to MOoc*** **strategy**:

- build at first 2 OoCs independently of the co-culture perspective: an islet-on-chip to validate the glucose response in terms of insulin secretion, and a muscle-on-chip to validate the insulin response in terms of glucose uptake, each OoC being equipped with its relevant online sensor (the MEA for islets, and a glucose sensor for muscles)
- then reunite them only in a second time, with definition of a co-culture procedure, scaling of a chip, selection of materials.

This strategy might allow better **efficiency**. Indeed, by starting at OoC level, it is possible to:

- **acquire precious specifications** for the engineering investigations to design the MOoC system, like cell's functionality in chips, the required volume of culture, the chip material according to the functionality of the OoC (for example no PDMS for the muscle-on-chip to have robust glucose uptake experiments)
- **settle the biochemical investigations protocols suitable with microfluidic chips**.

Even if the specifications found with the OoC level **may change** (if the culture substrate or protocol or cell model change), the ***assays would be already set in this case***, and the ***order of magnitude assessed*** (functionality in microvolumes, suitable culture volume in chip), as they must be *similar despite changes of culture conditions or cell model*. These pre-estimated specifications can be used as ***first inputs to start informed engineering investigations*** like scaling, microfluidic chip and sensors design. This is a crucial time saving, as it allows at the beginning of the MOoC project a parallel work of engineering and biology (co-culture medium procedure, substrate), in addition to the fact the biological investigations are accelerated thanks to the previous microfluidic compatible assay protocols already set. In addition the OoC can be used as a more relevant characterization platform than the "dummy" chip.

To conclude, an interesting concept in this MOoC system design is the **different speed of development between engineering and biology**, that have to be correctly placed to optimize the project advancement. The first is sometimes said less complex than biology, but it is a confusion between time and complexity: fabrication in engineering can be *fast when repetitive*, but *design complexity is often underestimated*. The idea of a strategy *OoC to MOoC* is to **distribute the biological questions among 2 projects**, as well as **provide biological specifications** by a first OoC project that are then used in the next MOoC project. This allows engineering investigations (microfluidic chip and circuitry, sensors) to **start with pre-specifications**, and adjust the design according to the final specifications from **final biological investigations at the MOoC level**.

4. Personal perspectives

This thesis confirmed me the important role of a biomedical engineer - which I am - in extremely interdisciplinary projects. Being part of the life of two laboratories with very different cultures, attending a diversity of workshops and conferences of many fields, and setting up my own experiments whether it be in biology, microfluidics, electrochemistry or multiphysics simulations, I have developed an understanding of the cell culture, the challenges, the scientific context of a wide range of domains from engineering to life sciences. It allows me now, when meeting experts of all domains, to have a critical point of view and be source of proposal. This would have been hard without the initial pluridisciplinary skills and curiosity culture gifted by passionate teachers at the Institut Supérieur d'Ingénieurs

de Franche-Comté biomedical engineering school. The importance of such "orchestra conductors" should not be underestimated, and they should be systematically included in any interdisciplinary project. They help identify a common and coherent objective across all disciplines (a subtle issue identified progressively during this PhD), enhance the scientific emulation between thematics by mixing approaches and tools, ensure coherence of the scientific investigations to reach a proper system assembly that does not only *work* but also *makes sense* for end users.

The domain of MPS has been a wonderful discovery, as a cousin of biomedical engineering that I was more familiar with before my PhD. This topic is quite old but also new at the same time: pioneers have been exploring this intriguing idea to culture cells in microfluidic chips since the 80s, but it is only during the last decade that they achieved to create a vibrant community, as well as get support from industry and governments to fuel the research. It was a very exciting experience to be part of this nascent community, that is also interestingly impacted by *lobbies* and *political stakes*.

Appendix A

Co-culture medium validation supplementary results

A.1 Protocols

A.1.1 Cell culture

LHCN-M2 myoblasts have been provided by the platform for immortalization of human cells from the Center of Research in Myology (Dr Vincent Mouly, Paris, France). This cell line derived from immortalized human satellite cells of the pectoralis major muscle of a 41-year-old Caucasian heart transplant donor [Zhu et al., 2007]. Myoblasts were cultured in a skeletal muscle medium composed of one volume of Medium 199 (Gibco® by Thermo Fisher Scientific, Waltham, MA, USA), four volumes of Dubelcco's modified Eagle Medium (DMEM) with high-glucose and glutaMAX™ and without pyruvate (Gibco) supplemented with 20% fetal bovine serum (Eurobio scientific, Les Ulis, France), 50 g/mL gentamycin (Gibco) and a commercial mix of skeletal muscle cell growth medium supplements (ref C-39365; Promocell, Heidelberg, Germany), which includes 25 µg/mL fetuin, 5 ng/mL human recombinant epidermal growth factor, 0.5 ng/mL basic fibroblast growth factor, 5 µg/mL insulin, 0.2 g/mL dexamethasone.

According to the standard protocol, myotubes were obtained by cultivating 90% confluence myoblasts for one day in growth medium and three days in a differentiation medium, composed of the skeletal muscle medium supplemented only with 10 µg/mL insulin (ref I9278; Sigma-Aldrich, Burlington, MA, USA). The new procedure tested here consisted in cultivating 90% confluence myoblasts in the islet medium [Jaffredo et al., 2021] composed by Roswell Park Memorial Institute medium (RPMI 1640; Gibco) supplemented with 10 mM HEPES (Gibco), 100 U/mL penicillin-streptavidin (Gibco), 1 mM pyruvate (TOKU-E, Bellingham, WA, USA), 2 mM L-glutamine (Gibco), 50 µM ß-mercaptoethanol (Sigma-Aldrich), 10% foetal bovine serum (Eurobio scientific). Modified islet medium corresponded to islet medium supplemented with 10.5 µg/mL insulin (ref. I9278; Sigma-Aldrich). Multinucleated and elongated myotubes formation was monitored daily using the inverted microscope Olympus IX81 (Olympus, Waltham, MA, USA). All cell cultures were kept under standard conditions (37 °C, humidified atmosphere, 5% CO2/95% Air).

A.1.2 Immunocytofluorescence

1.1 or 1.7x104 cells were seeded in 8-well Ibidi-treat µslideTM (ref. 80826; Biovalley, Nanterre, France) and differentiated as described above. Cells were washed in Dulbecco's phosphate-buffered saline supplemented in calcium and magnesium (referred to hereafter as DPBS) and fixed in 4% paraformaldehyde in DPBS for 10 min at 4 °C, permeabilized with 0.1% triton X-100 in DPBS for 5 min, saturated for 30 min with 2% bovine serum albumin (BSA;

Thermo Fisher Scientific) in DPBS. The cells were incubated with primary antibodies, washed with DPBS supplemented with 2% BSA, incubated with secondary antibodies and washed again. Anti-α-actinin (ref. A7811; Sigma-Aldrich), anti-troponin T (ref. T6277; Sigma, Saint-Louis, MO, USA), anti-GluT4 (ref. G4048; Sigma-Aldrich) were used respectively at 1:250, 1:300 and 1:300 in DPBS supplemented with 2% BSA. The secondary antibodies used were Alexa-fluor-488-labelled goat anti-mouse IgG (ref. A11001; Thermo Fischer Scientific) and Alexa-fluor-546-labelled goat anti-rabbit IgG (ref. A11010; Thermo Fischer Scientific). Nuclei were stained using DAPI incubated 3 min. Immunolabelled cells were stocked at 4 °C in DPBS.

Fluorescence was examined using a fluorescence microscope (Olympus IX81) with the following filter combinations: filter cube U-MWU2 for observation in blue (band-pass 330-385 nm excitation filter, 400 nm dichromatic mirror, low-pass 420 nm emission filter), filter cube U-minIBA2 (band-pass 470-490 nm excitation filter, 505 nm dichromatic mirror, low-pass 510-550 nm emission filter) and filter cube U-MWG2 (band-pass 510-550 nm excitation filter, 570 nm dichromatic filter, low-pass 420-590 nm emission filter). Images were recorded with a XM10 cooled CCD monochrome camera (Olympus) and treated using ImageJ software.

A.1.3 Glucose Uptake Assays (GUA)

Functional assays were performed on myotubes obtained using the islet medium after 4 to 6 days of differentiation. The culture medium was replaced for the islet medium deprived of serum and red phenol, supplemented with 0.2% BSA (fraction V) [Navarro-Marquez et al., 2018] and low glucose (3 mM) for 3 hours. Myotubes were stimulated with different concentrations of insulin for 15 min (value specified in results; ref. I9278; Sigma-Aldrich).

The uptake of glucose was determined using either 8.2 mM glucose or 400 µM 2-(N-(7-Nitrobenz-2-oxa-1,3-diazol-4-yl)Amino)-2-Deoxyglucose (hereafter 2-NBDG, ref. N13195; Invitrogen™ by Thermo Fisher Scientific), a fluorescent non metabolizable analogue of glucose [Bala et al., 2021] for 30 min. After stimulation, the cells were washed with DPBS at 4 °C before fixation in 4% paraformaldehyde for 10 min on ice. From the myotubes stimulated with glucose, the supernatant was retrieved and its content in glucose was measured using a colorimetric reaction (Kit 80009; Biolabo, Maizy, France) and the fixed cells were immunolabelled against GluT4 as previously described. From the myotubes stimulated with 2-NBDG, the fluorescence was tracked using the filter cube U-MWU2 for observation in blue.

A.1.4 Western blot

10 µg protein extracts, which were obtained from myotubes stimulated or not with insulin, were separated on a 10% SDS-PAGE. Semi-dry electrophoretic transfer (Bio-Rad, Hercules, CA, USA) onto PVDF (polyvinylidene difluoride) membrane was performed for 1 h at 100 V. After blocking with 5% non-fat dry milk in tris-buffered saline with Tween-20 (TBST) at room temperature for 2 hours, the membranes were incubated overnight at 4 °C with primary antibodies against Akt (ref. 9272; Cell Signaling Technology, Danvers, MA, US) or p-Akt (ref. 4060; Cell Signaling Technology) diluted at 1:1000 and GAPDH (ref. G9545; Sigma-Aldrich) diluted at 1:20000. After washing, the blots were incubated with goat antibodies anti-rabbit IgG (ref. NA934; Cytiva™ by Sigma-Aldrich) at room temperature for 2 hours. The bands were revealed, after washing, using Opti-4CN™ Substrate kit (Bio-Rad) and the membranes scanned with the CanoScan 5600F device (Canon, Tokyo, Japan) and LabScan software. The bands intensity was quantified using Image J software.

A.2 Comparison of the components in islets and KMEMdiff media

	Muscles medium	Islets medium	Comparison
	(20% of Medium 199 41150. and 80% DMEM 61965)	(100% of RPMI 1640)	Ratio of the concentration for the islets medium compared to the myotubes medium
	Molar concentration (M)		Ratio
Amino Acids			
L-Alanine	0.0561798	0.0000000	
L-Alanyl-Glutamine	3.3148386	0.0000000	
L-Arginine (free base)	0.0000000	1.1481056	
L-Arginine hydrochloride	0.3848341	0.0000000	
L-Asparagine (anhyd)	0.0000000	0.3787879	
L-Aspartic acid	0.0451128	0.1503759	3.3
L-Cysteine hydrochloride-H2O	0.0001136	0.0000000	
L-Cystine 2HCl	0.1826890	0.2083067	1.1
L-Glutamic Acid	0.0908844	0.1360544	1.5
L-Glutamine	0.0000000	2.0547945	
Glycine	0.4533333	0.1333333	0.3
L-Histidine	0.1808381	0.0967742	0.5
Hydroxy-L-Proline	0.0152672	0.1526718	10.0
L-Isoleucine	0.7022901	0.3816794	0.5
L-Leucine	0.7328244	0.3816794	0.5
L-Lysine hydrochloride	0.7147541	0.2185792	0.3
L-Methionine	0.1812081	0.1006711	0.6
L-Phenylalanine	0.3503030	0.0909091	0.3
L-Proline	0.0695652	0.1739131	2.5
L-Serine	0.3676190	0.2857143	0.8
L-Threonine	0.6890756	0.1680672	0.2
L-Tryptophan	0.0725490	0.0245098	0.3
L- Tyrosine	0.3182320	0.0000000	
L-Tyrosine disodium salt dihydrate	0.0444444	0.1104598	2.5
L-Valine	0.6854701	0.1709402	0.2
Vitamins			
Ascorbic Acid	0.0000568	0.0000000	
D-Biotin (Thermofisher)	0.0000000	0.0008187	
Biotin (Thermofisher)	0.0000082	0.0000000	
Choline chloride	0.0235714	0.0214286	0.9
D-Calcium pantothenate	0.0067128	0.0000000	
Folic Acid	0.0072608	0.0022676	0.3
Menadione sodium bisulfate (Vitamin K3)	0.0000116	0.0000000	
myo-Inositol	0.0000000	0.1942718	
Niacinamide	0.0262705	0.0081967	0.3
Nicotinic acid (Niacin)	0.0000407	0.0000000	
Para-Aminobenzoic Acid	0.0000730	0.0072993	100.0
D-Pantothenic Acid•½Ca	0.0000000	0.0005224	
Pyridoxine hydrochloride / Pyridoxine•HCl	0.0155583	0.0048629	0.3
Pyridoxal hydrochloride	0.0000245	0.0000000	
Riboflavin	0.0008564	0.0005319	0.6
Thiamine hydrochloride	0.0095015	0.0029674	0.3
Vitamin A (acetate)	0.0000610	0.0000000	
Vitamin B12	0.0000504	0.0000037	0.1
alpha Tocopherol phos. Na salt	0.0000036	0.0000000	
i-Inositol	0.0320556	0.0000000	
Inorganic salts			
Calcium nitrate $Ca(NO_3)_2•4H_2O$	0.0000000	0.4237288	
Calcium chloride CaCl2 x 2H2O	1.7959183	0.0000000	
Ferric nitrate (Fe(NO3)-9H2O)	0.0005446	0.0000000	
Magnesium Sulfate (MgSO4-7H2O)	0.6504065	0.0000000	
Magnesium Sulfate (MgSO4) (anhyd.)	0.1626016	0.4070000	2.5
Potassium Chloride (KCl)	5.3333335	5.3333335	1.0
Sodium Bicarbonate (NaHCO3)	40.4761910	23.8095250	0.6
Sodium Chloride (NaCl)	111.7241368	103.4482700	0.9
Sodium Phosphate monobasic (NaH2PO4-2H2O)	0.9350317	0.0000000	
Sodium Phosphate monobasic (NaH2PO4) anhydrous	0.0000000	6.6677780	
Other Components			
D-Glucose (Dextrose) anhydrous	21.1111111	11.1111110	0.5
Glutathione (reduced)	0.0000326	0.0032573	100.0
Phenol Red	0.0425080	0.0140808	0.3
Guanine hydrochloride	0.0003191	0.0000000	
Hypoxanthine	0.0004412	0.0000000	
2-deoxy-D-ribose	0.0007463	0.0000000	
Adenine sulfate	0.0049505	0.0000000	
Adenosine 5'-phosphate	0.0001153	0.0000000	
Adenosine 5'-triphosphate	0.0003306	0.0000000	
Cholesterol	0.0001034	0.0000000	
Ribose	0.0006667	0.0000000	
Sodium acetate-3H2O	0.1220588	0.0000000	
Thymine	0.0004762	0.0000000	
Tween 80®	Infinity	0.0000000	
Uracil	0.0005357	0.0000000	
Xanthine	0.0003954	0.0000000	

FIGURE A.1: Composition of the 2 media when reduced to 20% of Medium 199 and 80% of DMEM for LHCN-M2 medium and 100% of RPMI for the islets.

A.3 Supplementary results

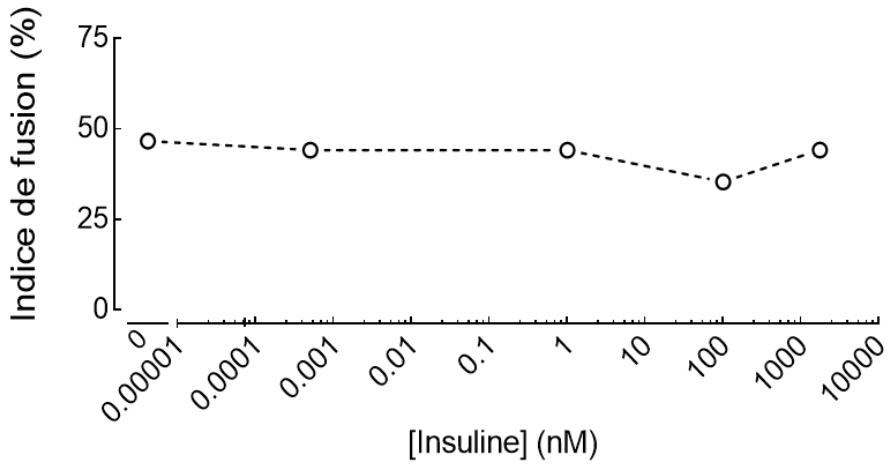

FIGURE A.2: Fusion index of myotubes at day 4 when cultured in islets medium supplemented in different concentrations of insulin. The fusion index was similar whatever the insulin concentration of the islet medium. Thus the insulin can be removed from the medium composition.

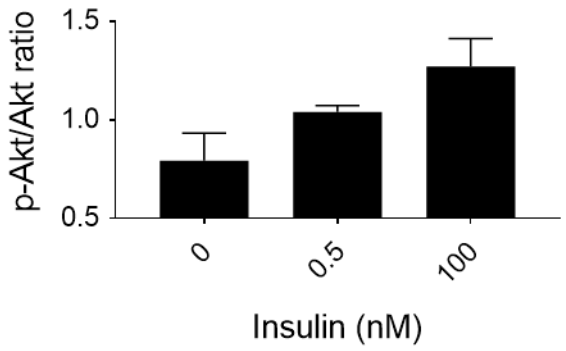

FIGURE A.3: Ratios of Akt and phosphorylated Akt in myotubes, cultured in islet medium, at day 4 when exposed to different insulin concentrations. The ratio was higher in myotubes exposed to insulin, meaning the metabolic pathways mediating GLUT4 translocation were amplified.

Bibliography

Aamodt, Kristie I. and Alvin C. Powers (2017). "Signals in the pancreatic islet microenvironment influence β-cell proliferation". In: *Diabetes, Obesity and Metabolism* 19 (S1). _eprint: https://onlinelibrary.wiley.com/doi/pdf/10.1111/dom.13031, pp. 124–136. ISSN: 1463-1326. DOI: 10.1111/dom.13031. URL: https://onlinelibrary.wiley.com/doi/abs/10.1111/dom.13031 (visited on 08/23/2023).

Abarkan, Myriam et al. (2022). "Vertical Organic Electrochemical Transistors and Electronics for Low Amplitude Micro-Organ Signals". In: *Advanced Science* 9.8, p. 2105211. ISSN: 2198-3844. DOI: 10.1002/advs.202105211. URL: https://onlinelibrary.wiley.com/doi/abs/10.1002/advs.202105211 (visited on 10/13/2023).

About - Hesperos Inc. - Leader in Organ-on-a-Chip Technology (Nov. 14, 2018). URL: https://hesperosinc.com/about/ (visited on 08/31/2023).

Akash, Sajidur Rahman, M. A. Jobayer Billah Arnob, and Md Jamal Uddin (2023). "FDA Modernization Act 2.0: An insight from nondeveloping country". In: *Drug Development Research* n/a (n/a). _eprint: https://onlinelibrary.wiley.com/doi/pdf/10.1002/ddr.22108. ISSN: 1098-2299. DOI: 10.1002/ddr.22108. URL: https://onlinelibrary.wiley.com/doi/abs/10.1002/ddr.22108 (visited on 08/28/2023).

Alcazar, Oscar and Peter Buchwald (2019). "Concentration-Dependency and Time Profile of Insulin Secretion: Dynamic Perifusion Studies With Human and Murine Islets". In: *Frontiers in Endocrinology* 10. Publisher: Frontiers. ISSN: 1664-2392. DOI: 10.3389/fendo.2019.00680. URL: https://www.frontiersin.org/articles/10.3389/fendo.2019.00680/full (visited on 01/12/2021).

American Diabetes Association (Dec. 16, 2013). "Diagnosis and Classification of Diabetes Mellitus". In: *Diabetes Care* 37 (Supplement_1), S81–S90. ISSN: 0149-5992. DOI: 10.2337/dc14-S081. URL: https://doi.org/10.2337/dc14-S081 (visited on 08/15/2023).

Andersson, A. (June 1978). "Isolated mouse pancreatic islets in culture: effects of serum and different culture media on the insulin production of the islets". In: *Diabetologia* 14.6. Number: 6, pp. 397–404. ISSN: 0012-186X. DOI: 10.1007/BF01228134.

Anene-Nzelu, Chukwuemeka George et al. (2013). "Scalable alignment of three-dimensional cellular constructs in a microfluidic chip". In: *Lab on a Chip* 13.20, p. 4124. ISSN: 1473-0197, 1473-0189. DOI: 10.1039/c3lc50730k. URL: http://xlink.rsc.org/?DOI=c3lc50730k (visited on 07/12/2022).

Artasensi, Angelica et al. (Jan. 2020). "Type 2 Diabetes Mellitus: A Review of Multi-Target Drugs". In: *Molecules* 25.8. Number: 8 Publisher: Multidisciplinary Digital Publishing Institute, p. 1987. ISSN: 1420-3049. DOI: 10.3390/molecules25081987. URL: https://www.mdpi.com/1420-3049/25/8/1987 (visited on 08/30/2023).

Bailleul, Alexia et al. (2022). "Bioimpedance Spectroscopy Helps Monitor the Impact of Electrical Stimulation on Muscle Cells". In: *IEEE Access* 10. Conference Name: IEEE Access, pp. 131430–131441. ISSN: 2169-3536. DOI: 10.1109/ACCESS.2022.3228479.

Bal-Price, Anna and Sandra Coecke (2011). "Guidance on Good Cell Culture Practice (GCCP)". In: *Cell Culture Techniques*. Ed. by Michael Aschner, Cristina Suñol, and Anna Bal-Price. Neuromethods. Totowa, NJ: Humana Press, pp. 1–25. ISBN: 978-1-61779-077-5. DOI: 10.

1007/978-1-61779-077-5_1. URL: https://doi.org/10.1007/978-1-61779-077-5_1 (visited on 08/28/2023).

Bala, Manju et al. (May 1, 2021). "Efficient and modified 2-NBDG assay to measure glucose uptake in cultured myotubes". In: *Journal of Pharmacological and Toxicological Methods* 109, p. 107069. ISSN: 1056-8719. DOI: 10.1016/j.vascn.2021.107069. URL: https://www.sciencedirect.com/science/article/pii/S1056871921001210 (visited on 01/17/2022).

Balasubramanyam, Ashok (2021). "Defining and Classifying New Subgroups of Diabetes". In: *Annual Review of Medicine* 72.1. _eprint: https://doi.org/10.1146/annurev-med-050219-034524, pp. 63–74. DOI: 10.1146/annurev-med-050219-034524. URL: https://doi.org/10.1146/annurev-med-050219-034524 (visited on 08/20/2023).

Balboa, Diego et al. (July 2022). "Functional, metabolic and transcriptional maturation of human pancreatic islets derived from stem cells". In: *Nature Biotechnology* 40.7. Number: 7 Publisher: Nature Publishing Group, pp. 1042–1055. ISSN: 1546-1696. DOI: 10.1038/s41587-022-01219-z. URL: https://www.nature.com/articles/s41587-022-01219-z (visited on 11/02/2023).

Barroso, Inês and Mark I. McCarthy (Mar. 2019). "The Genetic Basis of Metabolic Disease". In: *Cell* 177.1, pp. 146–161. ISSN: 00928674. DOI: 10.1016/j.cell.2019.02.024. URL: https://linkinghub.elsevier.com/retrieve/pii/S0092867419302065 (visited on 08/20/2023).

Bauer, Sophie et al. (Nov. 3, 2017). "Functional coupling of human pancreatic islets and liver spheroids on-a-chip: Towards a novel human ex vivo type 2 diabetes model". In: *Scientific Reports* 7.1. Number: 1 Publisher: Nature Publishing Group, p. 14620. ISSN: 2045-2322. DOI: 10.1038/s41598-017-14815-w. URL: https://www.nature.com/articles/s41598-017-14815-w (visited on 10/23/2020).

Bavli, Danny et al. (Apr. 19, 2016). "Real-time monitoring of metabolic function in liver-on-chip microdevices tracks the dynamics of mitochondrial dysfunction". In: *Proceedings of the National Academy of Sciences* 113.16. Number: 16 Publisher: National Academy of Sciences Section: PNAS Plus, E2231–E2240. ISSN: 0027-8424, 1091-6490. DOI: 10.1073/pnas.1522556113. URL: https://www.pnas.org/content/113/16/E2231 (visited on 12/18/2020).

Bhat, Sl et al. (Oct. 2011). "Plasma glucose and insulin responses to mixed meals: Impaired fasting glucose re-visited". In: *Diabetes and Vascular Disease Research* 8.4, pp. 271–275. ISSN: 1479-1641, 1752-8984. DOI: 10.1177/1479164111421036. URL: http://journals.sagepub.com/doi/10.1177/1479164111421036 (visited on 07/18/2023).

Buchwald, Peter et al. (2018). "Glucose-stimulated insulin release: Parallel perifusion studies of free and hydrogel encapsulated human pancreatic islets". In: *Biotechnology and Bioengineering* 115.1, pp. 232–245. ISSN: 1097-0290. DOI: https://doi.org/10.1002/bit.26442. URL: https://onlinelibrary.wiley.com/doi/abs/10.1002/bit.26442 (visited on 02/15/2021).

Cargill, Allison Anne (2016). "Development of an enzymatic glucose biosensor for applications in wearable sweat-based sensing". Pages: 11164936. Master of Science. Ames: Iowa State University, Digital Repository. DOI: 10.31274/etd-180810-5300. URL: https://lib.dr.iastate.edu/etd/15672/ (visited on 12/10/2020).

Carter, Steven and Thomas P. J. Solomon (Mar. 1, 2019). "In vitro experimental models for examining the skeletal muscle cell biology of exercise: the possibilities, challenges and future developments". In: *Pflügers Archiv - European Journal of Physiology* 471.3. Number: 3, pp. 413–429. ISSN: 1432-2013. DOI: 10.1007/s00424-018-2210-4. URL: https://doi.org/10.1007/s00424-018-2210-4 (visited on 01/07/2021).

Chandra, Rashmi and Rodger A. Liddle (Sept. 2009). "Neural and Hormonal Regulation of Pancreatic Secretion". In: *Current opinion in gastroenterology* 25.5, pp. 441–446. ISSN: 0267-1379. DOI: 10.1097/MOG.0b013e32832e9c41. URL: https://www.ncbi.nlm.nih.gov/pmc/articles/PMC2838392/ (visited on 08/30/2023).

Chen, Zhihong et al. (Dec. 1, 2007). "Graphene nano-ribbon electronics". In: *Physica E: Low-dimensional Systems and Nanostructures* 40.2, pp. 228–232. ISSN: 1386-9477. DOI: 10.1016/j.physe.2007.06.020. URL: https://www.sciencedirect.com/science/article/pii/S1386947707001427 (visited on 08/30/2023).

Clark Jr., Leland C. and Champ Lyons (1962). "Electrode Systems for Continuous Monitoring in Cardiovascular Surgery". In: *Annals of the New York Academy of Sciences* 102.1, pp. 29–45. ISSN: 1749-6632. DOI: 10.1111/j.1749-6632.1962.tb13623.x. URL: https://onlinelibrary.wiley.com/doi/abs/10.1111/j.1749-6632.1962.tb13623.x (visited on 10/31/2023).

Colburn, Alex W. et al. (2021). "Lifting the lid on the potentiostat: a beginner's guide to understanding electrochemical circuitry and practical operation". In: *Physical Chemistry Chemical Physics* 23.14, pp. 8100–8117. ISSN: 1463-9076, 1463-9084. DOI: 10.1039/D1CP00661D. URL: http://xlink.rsc.org/?DOI=D1CP00661D (visited on 03/31/2023).

C. Peterson, Norman et al. (2020). "Application of microphysiological systems in biopharmaceutical research and development". In: *Lab on a Chip* 20.4. Publisher: Royal Society of Chemistry, pp. 697–708. DOI: 10.1039/C9LC00962K. URL: https://pubs.rsc.org/en/content/articlelanding/2020/lc/c9lc00962k (visited on 10/12/2023).

Dornhof, Johannes et al. (2022). "Microfluidic organ-on-chip system for multi-analyte monitoring of metabolites in 3D cell cultures". In: *Lab on a Chip* 22.2. Publisher: Royal Society of Chemistry, pp. 225–239. DOI: 10.1039/D1LC00689D. URL: https://pubs.rsc.org/en/content/articlelanding/2022/lc/d1lc00689d (visited on 02/07/2022).

Duc, Pauline et al. (Oct. 26, 2021). "Human neuromuscular junction on micro-structured microfluidic devices implemented with a custom micro electrode array (MEA)". In: *Lab on a Chip* 21.21. Publisher: The Royal Society of Chemistry, pp. 4223–4236. ISSN: 1473-0189. DOI: 10.1039/D1LC00497B. URL: https://pubs.rsc.org/en/content/articlelanding/2021/lc/d1lc00497b (visited on 11/30/2021).

Ellingsgaard, Helga et al. (Sept. 2, 2008). "Interleukin-6 regulates pancreatic α-cell mass expansion". In: *Proceedings of the National Academy of Sciences* 105.35. Publisher: Proceedings of the National Academy of Sciences, pp. 13163–13168. DOI: 10.1073/pnas.0801059105. URL: https://www.pnas.org/doi/full/10.1073/pnas.0801059105 (visited on 08/23/2023).

Esch, Eric W., Anthony Bahinski, and Dongeun Huh (Apr. 2015). "Organs-on-chips at the frontiers of drug discovery". In: *Nature reviews. Drug discovery* 14.4, pp. 248–260. ISSN: 1474-1776. DOI: 10.1038/nrd4539. URL: https://www.ncbi.nlm.nih.gov/pmc/articles/PMC4826389/ (visited on 10/02/2023).

Essaouiba, Amal et al. (Dec. 15, 2020). "Development of a pancreas-liver organ-on-chip co-culture model for organ-to-organ interaction studies". In: *Biochemical Engineering Journal* 164, p. 107783. ISSN: 1369-703X. DOI: 10.1016/j.bej.2020.107783. URL: https://www.sciencedirect.com/science/article/pii/S1369703X20303375 (visited on 05/11/2021).

Ezra, Elishai et al. (Aug. 2015). "Microprocessor-based integration of microfluidic control for the implementation of automated sensor monitoring and multithreaded optimization algorithms". In: *Biomedical Microdevices* 17.4, p. 82. ISSN: 1387-2176, 1572-8781. DOI: 10.1007/s10544-015-9989-y. URL: http://link.springer.com/10.1007/s10544-015-9989-y (visited on 06/30/2022).

FDA (May 1, 2022). "Advancing Alternative Methods at FDA". In: *FDA*. Publisher: FDA. URL: https://www.fda.gov/science-research/about-science-research-fda/advancing-alternative-methods-fda (visited on 10/04/2023).

Fernández-Costa, Juan M. et al. (Jan. 1, 2021). "Bioengineered in vitro skeletal muscles as new tools for muscular dystrophies preclinical studies". In: *Journal of Tissue Engineering* 12. Publisher: SAGE Publications Ltd STM, p. 2041731420981339. ISSN: 2041-7314. DOI: 10.1177/2041731420981339. URL: https://doi.org/10.1177/2041731420981339 (visited on 06/08/2022).

Fernández-Costa, Juan M. et al. (Aug. 23, 2022). "Training-on-a-Chip: A Multi-Organ Device to Study the Effect of Muscle Exercise on Insulin Secretion in Vitro". In: *Advanced Materials Technologies*, p. 2200873. ISSN: 2365-709X, 2365-709X. DOI: 10.1002/admt.202200873. URL: https://onlinelibrary.wiley.com/doi/10.1002/admt.202200873 (visited on 11/21/2022).

Forterre, Alexis et al. (Jan. 2, 2014). "Proteomic Analysis of C2C12 Myoblast and Myotube Exosome-Like Vesicles: A New Paradigm for Myoblast-Myotube Cross Talk?" In: *PLOS ONE* 9.1. Publisher: Public Library of Science, e84153. ISSN: 1932-6203. DOI: 10.1371/journal.pone.0084153. URL: https://journals.plos.org/plosone/article?id=10.1371/journal.pone.0084153 (visited on 06/08/2022).

Frontera, Walter R. and Julien Ochala (Mar. 1, 2015). "Skeletal Muscle: A Brief Review of Structure and Function". In: *Calcified Tissue International* 96.3, pp. 183–195. ISSN: 1432-0827. DOI: 10.1007/s00223-014-9915-y. URL: https://doi.org/10.1007/s00223-014-9915-y (visited on 08/22/2023).

Fuchs, Stefanie et al. (Oct. 1, 2023). "Optical glucose sensor for microfluidic cell culture systems". In: *Biosensors and Bioelectronics* 237, p. 115491. ISSN: 0956-5663. DOI: 10.1016/j.bios.2023.115491. URL: https://www.sciencedirect.com/science/article/pii/S0956566323004335 (visited on 08/15/2023).

Gerich, J. E. (2010). "Role of the kidney in normal glucose homeostasis and in the hyperglycaemia of diabetes mellitus: therapeutic implications". In: *Diabetic Medicine* 27.2. _eprint: https://onlinelibrary.wiley.com/doi/pdf/10.1111/j.1464-5491.2009.02894.x, pp. 136–142. ISSN: 1464-5491. DOI: 10.1111/j.1464-5491.2009.02894.x. URL: https://onlinelibrary.wiley.com/doi/abs/10.1111/j.1464-5491.2009.02894.x (visited on 09/04/2023).

Grieshaber, Dorothee et al. (Mar. 2008). "Electrochemical Biosensors - Sensor Principles and Architectures". In: *Sensors* 8.3. Number: 3 Publisher: Molecular Diversity Preservation International, pp. 1400–1458. DOI: 10.3390/s80314000. URL: https://www.mdpi.com/1424-8220/8/3/1400 (visited on 02/07/2021).

Hart, Nathaniel J. and Alvin C. Powers (Feb. 1, 2019). "Use of human islets to understand islet biology and diabetes: progress, challenges and suggestions". In: *Diabetologia* 62.2, pp. 212–222. ISSN: 1432-0428. DOI: 10.1007/s00125-018-4772-2. URL: https://doi.org/10.1007/s00125-018-4772-2 (visited on 08/30/2023).

Hickman, Graham J. et al. (Feb. 8, 2016). "The Importance and Clinical Relevance of Surfaces in Tissue Culture". In: *ACS Biomaterials Science & Engineering* 2.2. Number: 2 Publisher: American Chemical Society, pp. 152–164. DOI: 10.1021/acsbiomaterials.5b00403. URL: https://doi.org/10.1021/acsbiomaterials.5b00403 (visited on 02/15/2021).

Hoffmann, F. A. and P. Langerhans (Oct. 1, 1869). "Ueber den Verbleib des in die Circulation eingeführten Zinnobers". In: *Archiv für pathologische Anatomie und Physiologie und für klinische Medicin* 48.2, pp. 303–325. ISSN: 1432-2307. DOI: 10.1007/BF01986370. URL: https://doi.org/10.1007/BF01986370 (visited on 08/23/2023).

Hoss, Udo and Erwin Satrya Budiman (May 2017). "Factory-Calibrated Continuous Glucose Sensors: The Science Behind the Technology". In: *Diabetes Technology & Therapeutics* 19

(S2). Num Pages: S-50 Publisher: Mary Ann Liebert, Inc., publishers, S–44. ISSN: 1520-9156. DOI: 10.1089/dia.2017.0025. URL: https://www.liebertpub.com/doi/full/10.1089/dia.2017.0025 (visited on 09/14/2023).

Hoss, Udo et al. (Sept. 1, 2013). "Continuous Glucose Monitoring in the Subcutaneous Tissue over a 14-Day Sensor Wear Period". In: *Journal of Diabetes Science and Technology* 7.5. Publisher: SAGE Publications Inc, pp. 1210–1219. ISSN: 1932-2968. DOI: 10.1177/193229681300700511. URL: https://doi.org/10.1177/193229681300700511 (visited on 09/14/2023).

— (Jan. 1, 2014). "Feasibility of Factory Calibration for Subcutaneous Glucose Sensors in Subjects With Diabetes". In: *Journal of Diabetes Science and Technology* 8.1. Publisher: SAGE Publications Inc, pp. 89–94. ISSN: 1932-2968. DOI: 10.1177/1932296813511747. URL: https://doi.org/10.1177/1932296813511747 (visited on 09/14/2023).

Houghton, Michael J. et al. (2019). "Gut microbiome catabolites as novel modulators of muscle cell glucose metabolism". In: *The FASEB Journal* 33.2, pp. 1887–1898. ISSN: 1530-6860. DOI: 10.1096/fj.201801209R. URL: https://faseb.onlinelibrary.wiley.com/doi/abs/10.1096/fj.201801209R (visited on 06/13/2021).

Huh, Dongeun et al. (June 25, 2010). "Reconstituting Organ-Level Lung Functions on a Chip". In: *Science* 328.5986. Publisher: American Association for the Advancement of Science, pp. 1662–1668. DOI: 10.1126/science.1188302. URL: https://www.science.org/doi/full/10.1126/science.1188302 (visited on 08/28/2023).

IMPSS BY-LAWS (n.d.). International MPS Society. URL: https://impss.org/about-us/ (visited on 08/29/2023).

Ingber, Donald E. (Aug. 2022). "Human organs-on-chips for disease modelling, drug development and personalized medicine". In: *Nature Reviews Genetics* 23.8. Number: 8 Publisher: Nature Publishing Group, pp. 467–491. ISSN: 1471-0064. DOI: 10.1038/s41576-022-00466-9. URL: https://www.nature.com/articles/s41576-022-00466-9 (visited on 10/12/2023).

Ino, Kosuke and Hitoshi Shiku (2019). "Electric and Electrochemical Microfluidic Devices for Cell Analysis". In: *Frontiers in Chemistry* 7.

ISO/IEC Guide 99:2007(fr), Vocabulaire international de métrologie — Concepts fondamentaux et généraux et termes associés (VIM) (2007). URL: https://www.iso.org/obp/ui/#iso:std:iso-iec:guide:99:ed-1:v2:fr (visited on 11/01/2023).

Jaffredo, Manon et al. (Jan. 19, 2021). "Dynamic Uni- and Multicellular Patterns Encode Biphasic Activity in Pancreatic Islets". In: *Diabetes* 70.4, pp. 878–888. ISSN: 0012-1797. DOI: 10.2337/db20-0214. URL: https://doi.org/10.2337/db20-0214 (visited on 04/16/2023).

Jensen, Caleb and Yong Teng (2020). "Is It Time to Start Transitioning From 2D to 3D Cell Culture?" In: *Frontiers in Molecular Biosciences* 7. ISSN: 2296-889X. URL: https://www.frontiersin.org/articles/10.3389/fmolb.2020.00033 (visited on 08/28/2023).

Jensen, Jørgen et al. (Dec. 30, 2011). "The Role of Skeletal Muscle Glycogen Breakdown for Regulation of Insulin Sensitivity by Exercise". In: *Frontiers in Physiology* 2, p. 112. ISSN: 1664-042X. DOI: 10.3389/fphys.2011.00112. URL: https://www.ncbi.nlm.nih.gov/pmc/articles/PMC3248697/ (visited on 10/19/2023).

Jeon, Ja Young et al. (Sept. 1, 2019). "GLP-1 improves palmitate-induced insulin resistance in human skeletal muscle via SIRT1 activity". In: *International Journal of Molecular Medicine* 44.3. Publisher: Spandidos Publications, pp. 1161–1171. ISSN: 1107-3756. DOI: 10.3892/ijmm.2019.4272. URL: https://www.spandidos-publications.com/10.3892/ijmm.2019.4272 (visited on 07/18/2023).

Jiwlawat, Nunnapas et al. (Apr. 11, 2018). "Current Progress and Challenges for Skeletal Muscle Differentiation from Human Pluripotent Stem Cells Using Transgene-Free Approaches". In: *Stem Cells International* 2018. Publisher: Hindawi, e6241681. ISSN: 1687-966X. DOI: 10.1155/2018/6241681. URL: https://www.hindawi.com/journals/sci/2018/6241681/ (visited on 08/23/2023).

Jones, Ian L. et al. (Mar. 1, 2011). "The potential of microelectrode arrays and microelectronics for biomedical research and diagnostics". In: *Analytical and Bioanalytical Chemistry* 399.7, pp. 2313–2329. ISSN: 1618-2650. DOI: 10.1007/s00216-010-3968-1. URL: https://doi.org/10.1007/s00216-010-3968-1 (visited on 08/30/2023).

"Organs-on-chip monitoring" (2018). "Organs-on-chip monitoring: sensors and other strategies". In: *Microphysiological Systems*. Ed. by Tugba Kilic et al. DOI: 10.21037/mps.2018.01.01.

Kim, Joeng Ju et al. (Mar. 9, 2023). "Pathophysiological Reconstruction of a Tissue-Specific Multiple-Organ On-A-Chip for Type 2 Diabetes Emulation using 3D Cell Printing". In: *Advanced Functional Materials*, p. 2213649. ISSN: 1616-301X, 1616-3028. DOI: 10.1002/adfm.202213649. URL: https://onlinelibrary.wiley.com/doi/10.1002/adfm.202213649 (visited on 04/05/2023).

K. Young, Edmond W. and David J. Beebe (2010). "Fundamentals of microfluidic cell culture in controlled microenvironments". In: *Chemical Society Reviews* 39.3. Publisher: Royal Society of Chemistry, pp. 1036–1048. DOI: 10.1039/B909900J. URL: https://pubs.rsc.org/en/content/articlelanding/2010/cs/b909900j (visited on 07/10/2022).

Lambert, Samuel A. et al. (Feb. 2018). "The Human Transcription Factors". In: *Cell* 172.4, pp. 650–665. ISSN: 00928674. DOI: 10.1016/j.cell.2018.01.029. URL: https://linkinghub.elsevier.com/retrieve/pii/S0092867418301065 (visited on 08/25/2023).

Lang, Jochen (1999). "Molecular mechanisms and regulation of insulin exocytosis as a paradigm of endocrine secretion". In: *European Journal of Biochemistry* 259.1, pp. 3–17. ISSN: 1432-1033. DOI: 10.1046/j.1432-1327.1999.00043.x. URL: https://onlinelibrary.wiley.com/doi/abs/10.1046/j.1432-1327.1999.00043.x (visited on 08/30/2023).

Langhammer, Christopher G. et al. (Feb. 2013). "A topographically modified substrate-embedded MEA for directed myotube formation at electrode contact sites". In: *Annals of Biomedical Engineering* 41.2. Number: 2, pp. 408–420. ISSN: 1573-9686. DOI: 10.1007/s10439-012-0647-8.

Langlois, Allan et al. (2022). "Crosstalk Communications Between Islets Cells and Insulin Target Tissue: The Hidden Face of Iceberg". In: *Frontiers in Endocrinology* 13. ISSN: 1664-2392. URL: https://www.frontiersin.org/article/10.3389/fendo.2022.836344 (visited on 04/24/2022).

Lauritzen, Hans P. M. M. and Jonathan D. Schertzer (Aug. 2010). "Measuring GLUT4 translocation in mature muscle fibers". In: *American Journal of Physiology-Endocrinology and Metabolism* 299.2. Publisher: American Physiological Society, E169–E179. ISSN: 0193-1849. DOI: 10.1152/ajpendo.00066.2010. URL: https://journals.physiology.org/doi/full/10.1152/ajpendo.00066.2010 (visited on 03/09/2023).

Leal, Fischer Karen et al. (2021). "Cellules α et β du pancréas - Meilleures ennemies ou partenaires pour la vie ?" In: 37.

Lebreton, Fanny et al. (June 1, 2015). "Slow potentials encode intercellular coupling and insulin demand in pancreatic β cells". In: *Diabetologia* 58.6, pp. 1291–1299. ISSN: 1432-0428. DOI: 10.1007/s00125-015-3558-z. URL: https://doi.org/10.1007/s00125-015-3558-z (visited on 07/18/2023).

Leclerc, Eric, Yasuyuki Sakai, and Teruo Fujii (June 1, 2003). "Cell Culture in 3-Dimensional Microfluidic Structure of PDMS (polydimethylsiloxane)". In: *Biomedical Microdevices* 5.2,

pp. 109–114. ISSN: 1572-8781. DOI: 10.1023/A:1024583026925. URL: https://doi.org/10.1023/A:1024583026925 (visited on 10/04/2022).

Lee, Bm and Tms Woleve (Dec. 1, 1998). "Effect of glucose, sucrose and fructose on plasma glucose and insulin responses in normal humans: comparison with white bread". In: *European Journal of Clinical Nutrition* 52.12, pp. 924–928. ISSN: 0954-3007, 1476-5640. DOI: 10.1038/sj.ejcn.1600666. URL: https://www.nature.com/articles/1600666 (visited on 07/18/2023).

Lee, Dong Wook et al. (Dec. 2019). "Construction of pancreas–muscle–liver microphysiological system (MPS) for reproducing glucose metabolism". In: *Biotechnology and Bioengineering* 116.12. Number: 12, pp. 3433–3445. ISSN: 0006-3592, 1097-0290. DOI: 10.1002/bit.27151. URL: https://onlinelibrary.wiley.com/doi/10.1002/bit.27151 (visited on 10/04/2021).

Leung, Chak Ming et al. (May 12, 2022). "A guide to the organ-on-a-chip". In: *Nature Reviews Methods Primers* 2.1. Number: 1 Publisher: Nature Publishing Group, pp. 1–29. ISSN: 2662-8449. DOI: 10.1038/s43586-022-00118-6. URL: https://www.nature.com/articles/s43586-022-00118-6 (visited on 06/07/2022).

Li, Haitao et al. (Jan. 2017). "CMOS Electrochemical Instrumentation for Biosensor Microsystems: A Review". In: *Sensors* 17.1. Number: 1 Publisher: Multidisciplinary Digital Publishing Institute, p. 74. DOI: 10.3390/s17010074. URL: https://www.mdpi.com/1424-8220/17/1/74 (visited on 07/19/2021).

Li, Xian and Tian Tian (2018). "Recent advances in an organ-on-a-chip: biomarker analysis and applications". In: *Analytical Methods* 10.26. Publisher: Royal Society of Chemistry, pp. 3122–3130. DOI: 10.1039/C8AY00970H. URL: https://pubs.rsc.org/en/content/articlelanding/2018/ay/c8ay00970h (visited on 08/28/2023).

Liu, Dong-mei, Ioanna Mosialou, and Jian-min Liu (2018). "Bone: Another potential target to treat, prevent and predict diabetes". In: *Diabetes, Obesity and Metabolism* 20.8. _eprint: https://onlinelibrary.wiley.com/doi/pdf/10.1111/dom.13330, pp. 1817–1828. ISSN: 1463-1326. DOI: 10.1111/dom.13330. URL: https://onlinelibrary.wiley.com/doi/abs/10.1111/dom.13330 (visited on 11/02/2023).

Lu, Shusheng, Colleen E. Dugan, and Robert T. Kennedy (Apr. 17, 2018). "Microfluidic Chip with Integrated Electrophoretic Immunoassay for Investigating Cell–Cell Interactions". In: *Analytical Chemistry* 90.8. Number: 8 Publisher: American Chemical Society, pp. 5171–5178. ISSN: 0003-2700. DOI: 10.1021/acs.analchem.7b05304. URL: https://doi.org/10.1021/acs.analchem.7b05304 (visited on 02/12/2021).

L. Glieberman, Aaron et al. (2019). "Synchronized stimulation and continuous insulin sensing in a microfluidic human Islet on a Chip designed for scalable manufacturing". In: *Lab on a Chip* 19.18. Number: 18 Publisher: Royal Society of Chemistry, pp. 2993–3010. DOI: 10.1039/C9LC00253G. URL: https://pubs.rsc.org/en/content/articlelanding/2019/lc/c9lc00253g (visited on 11/17/2020).

L. Vanderlaan, Emma et al. (2023). "Islet-on-chip: promotion of islet health and function via encapsulation within a polymerizable fibrillar collagen scaffold". In: *Lab on a Chip* 23.20. Publisher: Royal Society of Chemistry, pp. 4466–4482. DOI: 10.1039/D3LC00371J. URL: https://pubs.rsc.org/en/content/articlelanding/2023/lc/d3lc00371j (visited on 10/16/2023).

Mandenius, Carl-Fredrik (Sept. 2018). "Conceptual Design of Micro-Bioreactors and Organ-on-Chips for Studies of Cell Cultures". In: *Bioengineering* 5.3. Number: 3 Publisher: Multidisciplinary Digital Publishing Institute, p. 56. DOI: 10.3390/bioengineering5030056. URL: https://www.mdpi.com/2306-5354/5/3/56 (visited on 11/02/2020).

Mastrangeli, Massimo (2019). "Building blocks for a European Organ-on-Chip roadmap". In: *ALTEX*, pp. 481–492. ISSN: 1868596X. DOI: 10.14573/altex.1905221. URL: https://www.altex.org/index.php/altex/article/view/1289 (visited on 05/23/2022).

Mathew, Thomas K., Muhammad Zubair, and Prasanna Tadi (2023). "Blood Glucose Monitoring". In: *StatPearls*. Treasure Island (FL): StatPearls Publishing. URL: http://www.ncbi.nlm.nih.gov/books/NBK555976/ (visited on 09/12/2023).

Matthews, D. R. et al. (1988). "An Amperometric Needle-type Glucose Sensor Tested in Rats and Man". In: *Diabetic Medicine* 5.3, pp. 248–252. ISSN: 1464-5491. DOI: 10.1111/j.1464-5491.1988.tb00978.x. URL: https://onlinelibrary.wiley.com/doi/abs/10.1111/j.1464-5491.1988.tb00978.x (visited on 09/22/2023).

Matthiesen, Isabelle et al. (Oct. 2022). "Metabolic Assessment of Human Induced Pluripotent Stem Cells-Derived Astrocytes and Fetal Primary Astrocytes: Lactate and Glucose Turnover". In: *Biosensors* 12.10. Number: 10 Publisher: Multidisciplinary Digital Publishing Institute, p. 839. ISSN: 2079-6374. DOI: 10.3390/bios12100839. URL: https://www.mdpi.com/2079-6374/12/10/839 (visited on 08/29/2023).

Misun, Patrick M. et al. (June 6, 2016). "Multi-analyte biosensor interface for real-time monitoring of 3D microtissue spheroids in hanging-drop networks". In: *Microsystems & Nanoengineering* 2.1. Number: 1 Publisher: Nature Publishing Group, pp. 1–9. ISSN: 2055-7434. DOI: 10.1038/micronano.2016.22. URL: https://www.nature.com/articles/micronano201622 (visited on 01/08/2021).

Modena, Mario M et al. (2018). "Smart Cell Culture Systems: Integration of Sensors and Actuators into Microphysiological Systems". In: *ACS Chem. Biol.*

Molnar, Peter et al. (2007). "Photolithographic Patterning of C2C12 Myotubes using Vitronectin as Growth Substrate in Serum-Free Medium". In: *Biotechnology Progress* 23.1. Number: 1 _eprint: https://aiche.onlinelibrary.wiley.com/doi/pdf/10.1021/bp060302q, pp. 265–268. ISSN: 1520-6033. DOI: https://doi.org/10.1021/bp060302q. URL: https://aiche.onlinelibrary.wiley.com/doi/abs/10.1021/bp060302q (visited on 02/01/2021).

Moraes, Christopher et al. (Sept. 19, 2013). "On being the right size: scaling effects in designing a human-on-a-chip". In: *Integrative Biology* 5.9, pp. 1149–1161. ISSN: 1757-9708. DOI: 10.1039/c3ib40040a. URL: https://doi.org/10.1039/c3ib40040a (visited on 08/29/2023).

M. Maoz, Ben et al. (2017). "Organs-on-Chips with combined multi-electrode array and transepithelial electrical resistance measurement capabilities". In: *Lab on a Chip* 17.13. Publisher: Royal Society of Chemistry, pp. 2294–2302. DOI: 10.1039/C7LC00412E. URL: https://pubs.rsc.org/en/content/articlelanding/2017/lc/c7lc00412e (visited on 10/09/2023).

M. Walker, Glenn, Henry C. Zeringue, and David J. Beebe (2004). "Microenvironment design considerations for cellular scale studies". In: *Lab on a Chip* 4.2. Number: 2 Publisher: Royal Society of Chemistry, pp. 91–97. DOI: 10.1039/B311214D. URL: https://pubs.rsc.org/en/content/articlelanding/2004/lc/b311214d (visited on 02/18/2021).

Nagamine, Kuniaki et al. (2011). "Spatiotemporally controlled contraction of micropatterned skeletal muscle cells on a hydrogel sheet". In: *Lab on a Chip* 11.3. Number: 3 Publisher: Royal Society of Chemistry, pp. 513–517. DOI: 10.1039/C0LC00364F. URL: https://pubs.rsc.org/en/content/articlelanding/2011/lc/c0lc00364f (visited on 02/01/2021).

Naskar, Sharmistha, V. Kumaran, and Bikramjit Basu (June 12, 2017). "On The Origin of Shear Stress Induced Myogenesis Using PMMA Based Lab-on-Chip". In: *ACS Biomaterials Science & Engineering* 3.6. Publisher: American Chemical Society, pp. 1154–1171. DOI: 10.1021/acsbiomaterials.7b00206. URL: https://doi.org/10.1021/acsbiomaterials.7b00206 (visited on 08/28/2022).

Navale, Archana M. and Archana N. Paranjape (Mar. 1, 2016). "Glucose transporters: physiological and pathological roles". In: *Biophysical Reviews* 8.1, pp. 5–9. ISSN: 1867-2469. DOI: 10.1007/s12551-015-0186-2. URL: https://doi.org/10.1007/s12551-015-0186-2 (visited on 08/30/2023).

Navarro, Fabrice et al. (Dec. 2021). "P.171: Long-term Study of Vascularized Pancreas-on-chip". In: *Transplantation* 105.12, S72. ISSN: 0041-1337. DOI: 10.1097/01.tp.0000804728.22916.26. URL: https://journals.lww.com/transplantjournal/Fulltext/2021/12001/P_171__Long_term_Study_of_Vascularized.116.aspx?context=LatestArticles (visited on 08/29/2023).

Navarro-Marquez, Mario et al. (May 1, 2018). "Herpud1 impacts insulin-dependent glucose uptake in skeletal muscle cells by controlling the Ca2+-calcineurin-Akt axis". In: *Biochimica et Biophysica Acta (BBA) - Molecular Basis of Disease* 1864.5, pp. 1653–1662. ISSN: 0925-4439. DOI: 10.1016/j.bbadis.2018.02.018. URL: https://www.sciencedirect.com/science/article/pii/S0925443918300759 (visited on 07/18/2023).

NETRI - Digitizing human biology (June 5, 2023). URL: https://netri.com/ (visited on 11/02/2023).

Nien, Yu-Hsun et al. (2023). "Application of Non-Enzymatic Lactate Sensor Modified by Graphitic Carbon Nitride/Iron–Platinum Nanoparticles and Combined With the Low Power Consumption Instrumentation Amplifier and Calibration Readout Circuit". In: *IEEE TRANSACTIONS ON INSTRUMENTATION AND MEASUREMENT* 72.

Noto, Rachel E., Logan Leavitt, and Mary Ann Edens (2023). "Physiology, Muscle". In: *StatPearls*. Treasure Island (FL): StatPearls Publishing. URL: http://www.ncbi.nlm.nih.gov/books/NBK532258/ (visited on 08/22/2023).

Nunemaker, Craig S. et al. (Sept. 15, 2006). "Glucose Modulates [Ca2+]i Oscillations in Pancreatic Islets via Ionic and Glycolytic Mechanisms". In: *Biophysical Journal* 91.6. Publisher: Elsevier, pp. 2082–2096. ISSN: 0006-3495. DOI: 10.1529/biophysj.106.087296. URL: https://www.cell.com/biophysj/abstract/S0006-3495(06)71924-5 (visited on 08/30/2023).

Oleaga, Carlota et al. (Dec. 14, 2018). "Long-Term Electrical and Mechanical Function Monitoring of a Human-on-a-Chip System". In: *Advanced Functional Materials*, p. 1805792. ISSN: 1616-301X, 1616-3028. DOI: 10.1002/adfm.201805792. URL: https://onlinelibrary.wiley.com/doi/abs/10.1002/adfm.201805792 (visited on 10/30/2020).

Olson, Harry et al. (2000). "Concordance of the Toxicity of Pharmaceuticals in Humans and in Animals". In.

Ong, Kanyin Liane et al. (July 2023). "Global, regional, and national burden of diabetes from 1990 to 2021, with projections of prevalence to 2050: a systematic analysis for the Global Burden of Disease Study 2021". In: *The Lancet* 402.10397, pp. 203–234. ISSN: 01406736. DOI: 10.1016/S0140-6736(23)01301-6. URL: https://linkinghub.elsevier.com/retrieve/pii/S0140673623013016 (visited on 08/21/2023).

Organ on Chip in Development, ORCHID Project, (2019). CORDIS | European Commission. URL: https://cordis.europa.eu/project/id/766884/results (visited on 08/15/2023).

Papoz, Anastasia et al. (Jan. 1, 2022). "[Generating pancreatic islets organoids: Langerhanoids]". In: *Medecine sciences* 38.1, pp. 52–58. ISSN: 1958-5381. DOI: 10.1051/medsci/2021244. URL: https://doi.org/10.1051/medsci/2021244 (visited on 08/28/2023).

Park, DoYeun et al. (Jan. 1, 2020). "Integrating Organs-on-Chips: Multiplexing, Scaling, Vascularization, and Innervation". In: *Trends in Biotechnology* 38.1. Number: 1, pp. 99–112. ISSN: 0167-7799. DOI: 10.1016/j.tibtech.2019.06.006. URL: https://www.sciencedirect.com/science/article/pii/S0167779919301556 (visited on 02/25/2021).

Patel, S. N. et al. (Feb. 1, 2021). "Organoid microphysiological system preserves pancreatic islet function within 3D matrix". In: *Science Advances* 7.7. Number: 7 Publisher: American

Association for the Advancement of Science Section: Research Article, eaba5515. ISSN: 2375-2548. DOI: 10.1126/sciadv.aba5515. URL: https://advances.sciencemag.org/content/7/7/eaba5515 (visited on 02/15/2021).

Pediaditakis, Iosif et al. (Aug. 2022). "A microengineered Brain-Chip to model neuroinflammation in humans". In: *iScience* 25.8, p. 104813. ISSN: 25890042. DOI: 10.1016/j.isci.2022.104813. URL: https://linkinghub.elsevier.com/retrieve/pii/S2589004222010859 (visited on 08/29/2023).

Pedraza, Eileen et al. (2015). "Guiding pancreatic β cells to target electrodes in a whole-cell biosensor for diabetes". In: *Lab on a Chip* 15.19. Publisher: Royal Society of Chemistry, pp. 3880–3890. DOI: 10.1039/C5LC00616C. URL: https://pubs.rsc.org/en/content/articlelanding/2015/lc/c5lc00616c (visited on 07/25/2023).

Perrier, R. et al. (Oct. 15, 2018). "Bioelectronic organ-based sensor for microfluidic real-time analysis of the demand in insulin". In: *Biosensors and Bioelectronics* 117, pp. 253–259. ISSN: 0956-5663. DOI: 10.1016/j.bios.2018.06.015. URL: https://www.sciencedirect.com/science/article/pii/S0956566318304469 (visited on 04/16/2023).

Picollet-D'hahan, Nathalie et al. (Aug. 1, 2021). "Multiorgan-on-a-Chip: A Systemic Approach To Model and Decipher Inter-Organ Communication". In: *Trends in Biotechnology*. Special Issue: Microphysiological Systems 39.8, pp. 788–810. ISSN: 0167-7799. DOI: 10.1016/j.tibtech.2020.11.014. URL: https://www.sciencedirect.com/science/article/pii/S0167779920303097 (visited on 05/18/2022).

Pirog, Antoine et al. (Oct. 2017). "A versatile electrode sorting module for MEAs: Implementation in a FPGA-based real-time system". In: *2017 IEEE Biomedical Circuits and Systems Conference (BioCAS)*. 2017 IEEE Biomedical Circuits and Systems Conference (BioCAS). Torino: IEEE, pp. 1–4. ISBN: 978-1-5090-5803-7. DOI: 10.1109/BIOCAS.2017.8325154. URL: http://ieeexplore.ieee.org/document/8325154/ (visited on 09/14/2023).

Prill, Sebastian, Magnus S. Jaeger, and Claus Duschl (May 1, 2014). "Long-term microfluidic glucose and lactate monitoring in hepatic cell culture". In: *Biomicrofluidics* 8.3. Number: 3 Publisher: American Institute of Physics, p. 034102. DOI: 10.1063/1.4876639. URL: https://aip.scitation.org/doi/abs/10.1063/1.4876639 (visited on 04/27/2021).

Prévoteau, Antonin (2011). "Électrodes enzymatiques à base d'hydrogels rédox en vue de l'oxydation du glucose". In: p. 237.

P. Wikswo, John et al. (2013). "Scaling and systems biology for integrating multiple organs-on-a-chip". In: *Lab on a Chip* 13.18. Number: 18 Publisher: Royal Society of Chemistry, pp. 3496–3511. DOI: 10.1039/C3LC50243K. URL: https://pubs.rsc.org/en/content/articlelanding/2013/lc/c3lc50243k (visited on 11/02/2020).

Quintard, Clément et al. (Apr. 15, 2022). "Microfluidic device integrating a network of hyperelastic valves for automated glucose stimulation and insulin secretion collection from a single pancreatic islet". In: *Biosensors and Bioelectronics* 202, p. 113967. ISSN: 0956-5663. DOI: 10.1016/j.bios.2022.113967. URL: https://www.sciencedirect.com/science/article/pii/S0956566322000069 (visited on 08/28/2023).

Rabieh, Noha et al. (Nov. 4, 2016). "On-chip, multisite extracellular and intracellular recordings from primary cultured skeletal myotubes". In: *Scientific Reports* 6.1. Number: 1 Publisher: Nature Publishing Group, p. 36498. ISSN: 2045-2322. DOI: 10.1038/srep36498. URL: https://www.nature.com/articles/srep36498 (visited on 01/08/2021).

Radisic, Milica and Peter Loskill (July 12, 2021). "Beyond PDMS and Membranes: New Materials for Organ-on-a-Chip Devices". In: *ACS Biomaterials Science & Engineering* 7.7. Publisher: American Chemical Society, pp. 2861–2863. DOI: 10.1021/acsbiomaterials.1c00831. URL: https://doi.org/10.1021/acsbiomaterials.1c00831 (visited on 07/18/2023).

Reardon, Sara (July 1, 2015). "'Organs-on-chips' go mainstream". In: *Nature* 523.7560. Number: 7560 Publisher: Nature Publishing Group, pp. 266–266. ISSN: 1476-4687. DOI: 10.1038/523266a. URL: https://www.nature.com/articles/523266a (visited on 08/28/2023).

Ren, Yufei et al. (Dec. 7, 2015). "A Simple and Reliable PDMS and SU-8 Irreversible Bonding Method and Its Application on a Microfluidic-MEA Device for Neuroscience Research". In: *Micromachines* 6.12, pp. 1923–1934. ISSN: 2072-666X. DOI: 10.3390/mi6121465. URL: http://www.mdpi.com/2072-666X/6/12/1465 (visited on 05/24/2022).

Rigal, Sophie (2023). "Diseased human pancreas and liver microphysiological system for preclinical diabetes research". In: *bioRxiv*. DOI: 10.1101/2023.07.03.547412.

Robinson, M R et al. (Sept. 1, 1992). "Noninvasive Glucose Monitoring in Diabetic Patients: A Preliminary Evaluation". In: *Clinical Chemistry* 38.9, pp. 1618–1622. ISSN: 0009-9147. DOI: 10.1093/clinchem/38.9.1618. URL: https://doi.org/10.1093/clinchem/38.9.1618 (visited on 08/15/2023).

Rogal, Julia et al. (Feb. 1, 2019). "Stem-cell based organ-on-a-chip models for diabetes research". In: *Advanced Drug Delivery Reviews*. Human stem cell based organ-on-a-chip models for drug discovery and development 140, pp. 101–128. ISSN: 0169-409X. DOI: 10.1016/j.addr.2018.10.010. URL: https://www.sciencedirect.com/science/article/pii/S0169409X18302606 (visited on 08/29/2023).

Ronaldson-Bouchard, Kacey et al. (Apr. 2022). "A multi-organ chip with matured tissue niches linked by vascular flow". In: *Nature Biomedical Engineering* 6.4. Number: 4 Publisher: Nature Publishing Group, pp. 351–371. ISSN: 2157-846X. DOI: 10.1038/s41551-022-00882-6. URL: https://www.nature.com/articles/s41551-022-00882-6 (visited on 08/29/2023).

Rorsman, Patrik and Frances M. Ashcroft (Jan. 1, 2018). "Pancreatic β-Cell Electrical Activity and Insulin Secretion: Of Mice and Men". In: *Physiological Reviews* 98.1, pp. 117–214. ISSN: 0031-9333, 1522-1210. DOI: 10.1152/physrev.00008.2017. URL: https://www.physiology.org/doi/10.1152/physrev.00008.2017 (visited on 08/23/2023).

Rothbauer, Mario and Peter Ertl (Jan. 8, 2021). "Emerging Biosensor Trends in Organ-on-a-Chip". In: Advances in Biochemical Engineering/Biotechnology. Berlin, Heidelberg: Springer, pp. 1–12. DOI: 10.1007/10_2020_129. URL: https://doi.org/10.1007/10_2020_129 (visited on 01/08/2021).

Röder, Pia V. et al. (Mar. 2016). "Pancreatic regulation of glucose homeostasis". In: *Experimental & Molecular Medicine* 48.3. Number: 3 Publisher: Nature Publishing Group, e219–e219. ISSN: 2092-6413. DOI: 10.1038/emm.2016.6. URL: https://www.nature.com/articles/emm20166 (visited on 08/20/2023).

Sabu, Chinnu et al. (Sept. 2019). "Advanced biosensors for glucose and insulin". In: *Biosensors and Bioelectronics* 141, p. 111201. ISSN: 09565663. DOI: 10.1016/j.bios.2019.03.034. URL: https://linkinghub.elsevier.com/retrieve/pii/S0956566319302386 (visited on 01/23/2022).

Sassa, Fumihiro, Gokul Chandra Biswas, and Hiroaki Suzuki (2020). "Microfabricated electrochemical sensing devices". In: *Lab on a Chip* 20.8. Publisher: Royal Society of Chemistry, pp. 1358–1389. DOI: 10.1039/C9LC01112A. URL: https://pubs.rsc.org/en/content/articlelanding/2020/lc/c9lc01112a (visited on 09/19/2023).

Segeritz, Charis-P. and Ludovic Vallier (2017). "Cell Culture". In: *Basic Science Methods for Clinical Researchers*, pp. 151–172. DOI: 10.1016/B978-0-12-803077-6.00009-6. URL: https://www.ncbi.nlm.nih.gov/pmc/articles/PMC7149418/ (visited on 08/28/2023).

Shanbhag, Mahesh M. et al. (Nov. 15, 2023). "Fundamentals of bio-electrochemical sensing". In: *Chemical Engineering Journal Advances* 16, p. 100516. ISSN: 2666-8211. DOI: 10.1016/j.ceja.2023.100516. URL: https://www.sciencedirect.com/science/article/pii/S266682112300073X (visited on 09/19/2023).

Shoji, Jun-ya et al. (2023). "Global Meta-Analysis of Organoid and Organ-on-Chip Research". In: *Advanced Healthcare Materials* n/a (n/a), p. 2301067. ISSN: 2192-2659. DOI: 10.1002/adhm.202301067. URL: https://onlinelibrary.wiley.com/doi/abs/10.1002/adhm.202301067 (visited on 08/25/2023).

Shroff, Tanvi et al. (Mar. 2, 2022). "Studying metabolism with multi-organ chips: new tools for disease modelling, pharmacokinetics and pharmacodynamics". In: *Open Biology* 12.3, p. 210333. DOI: 10.1098/rsob.210333. URL: https://royalsocietypublishing.org/doi/full/10.1098/rsob.210333 (visited on 01/24/2023).

Singer, P et al. (Mar. 1985). "Postprandial hyperinsulinemia in patients with mild essential hypertension." In: *Hypertension* 7.2, pp. 182–186. ISSN: 0194-911X, 1524-4563. DOI: 10.1161/01.HYP.7.2.182. URL: https://www.ahajournals.org/doi/10.1161/01.HYP.7.2.182 (visited on 07/18/2023).

Skardal, Aleksander et al. (Aug. 18, 2017). "Multi-tissue interactions in an integrated three-tissue organ-on-a-chip platform". In: *Scientific Reports* 7.1. Number: 1 Publisher: Nature Publishing Group, p. 8837. ISSN: 2045-2322. DOI: 10.1038/s41598-017-08879-x. URL: https://www.nature.com/articles/s41598-017-08879-x (visited on 11/24/2020).

Soffe, Rebecca, Volker Nock, and James Geoffrey Chase (Jan. 25, 2019). "Towards Point-of-Care Insulin Detection". In: *ACS Sensors* 4.1. Number: 1 Publisher: American Chemical Society, pp. 3–19. DOI: 10.1021/acssensors.8b01253. URL: https://doi.org/10.1021/acssensors.8b01253 (visited on 11/19/2020).

Soucy, Jonathan R. et al. (Nov. 22, 2019). "Instrumented Microphysiological Systems for Real-Time Measurement and Manipulation of Cellular Electrochemical Processes". In: *iScience* 21, pp. 521–548. ISSN: 2589-0042. DOI: 10.1016/j.isci.2019.10.052. URL: http://www.sciencedirect.com/science/article/pii/S258900421930433X (visited on 01/08/2021).

Spanu, Andrea, Laura Martines, and Annalisa Bonfiglio (2021). "Interfacing cells with organic transistors: a review of in vitro and in vivo applications". In: *Lab on a Chip* 21.5. Publisher: Royal Society of Chemistry, pp. 795–820. DOI: 10.1039/D0LC01007C. URL: https://pubs.rsc.org/en/content/articlelanding/2021/lc/d0lc01007c (visited on 10/19/2023).

Sung, Jong Hwan, Ying Wang, and Michael L. Shuler (June 1, 2019). "Strategies for using mathematical modeling approaches to design and interpret multi-organ microphysiological systems (MPS)". In: *APL Bioengineering* 3.2. Number: 2 Publisher: American Institute of Physics, p. 021501. DOI: 10.1063/1.5097675. URL: https://aip.scitation.org/doi/full/10.1063/1.5097675 (visited on 11/02/2020).

Suzuki, Toshinobu et al. (Jan. 21, 2011). "Interleukin-6 Enhances Glucose-Stimulated Insulin Secretion From Pancreatic β-Cells: Potential Involvement of the PLC-IP3–Dependent Pathway". In: *Diabetes* 60.2, pp. 537–547. ISSN: 0012-1797. DOI: 10.2337/db10-0796. URL: https://doi.org/10.2337/db10-0796 (visited on 08/23/2023).

Sylow, Lykke et al. (Apr. 6, 2021). "The many actions of insulin in skeletal muscle, the paramount tissue determining glycemia". In: *Cell Metabolism* 33.4, pp. 758–780. ISSN: 1550-4131. DOI: 10.1016/j.cmet.2021.03.020. URL: https://www.sciencedirect.com/science/article/pii/S1550413121001273 (visited on 06/12/2023).

Tao, Tingting et al. (2022). "Microengineered Multi-Organoid System from hiPSCs to Recapitulate Human Liver-Islet Axis in Normal and Type 2 Diabetes". In: *Advanced Science* 9.5. _eprint: https://onlinelibrary.wiley.com/doi/pdf/10.1002/advs.202103495, p. 2103495. ISSN: 2198-3844. DOI: 10.1002/advs.202103495. URL: https://onlinelibrary.wiley.com/doi/abs/10.1002/advs.202103495 (visited on 08/29/2023).

The FDA Modernization Act 2.0 - What does it mean? (Jan. 9, 2023). *The FDA Modernization Act 2.0 - What does it mean? - CN Bio*. Section: Blog. URL: https://cn-bio.com/us-fda-modernization-act-2-what-does-it-mean/ (visited on 08/28/2023).

Thorens, Bernard (Feb. 1, 2015). "GLUT2, glucose sensing and glucose homeostasis". In: *Diabetologia* 58.2, pp. 221–232. ISSN: 1432-0428. DOI: 10.1007/s00125-014-3451-1. URL: https://doi.org/10.1007/s00125-014-3451-1 (visited on 08/30/2023).

Toral-Ojeda, Iván et al. (Oct. 10, 2018). "A Novel Functional In Vitro Model that Recapitulates Human Muscle Disorders". In: *Muscle Cell and Tissue - Current Status of Research Field*. Publisher: IntechOpen. DOI: 10.5772/intechopen.75903. URL: https://www.intechopen.com/books/muscle-cell-and-tissue-current-status-of-research-field/a-novel-functional-in-vitro-model-that-recapitulates-human-muscle-disorders (visited on 03/05/2021).

Tsuchiya, Ayako, Takeshi Kanno, and Tomoyuki Nishizaki (Nov. 28, 2013). "Stearic Acid Serves as a Potent Inhibitor of Protein Tyrosine Phosphatase 1B". In: *Cellular Physiology and Biochemistry* 32.5, pp. 1451–1459. ISSN: 1015-8987. DOI: 10.1159/000356582. URL: https://doi.org/10.1159/000356582 (visited on 07/18/2023).

Ugrinic, Martina et al. (Jan. 1, 2023). "Fabrication of high aspect ratio microfluidic devices for long term in vitro culture of 3D tumor models". In: *Microelectronic Engineering* 267-268, p. 111898. ISSN: 0167-9317. DOI: 10.1016/j.mee.2022.111898. URL: https://www.sciencedirect.com/science/article/pii/S0167931722001927 (visited on 09/14/2023).

Vashist, Sandeep Kumar et al. (Oct. 10, 2011). "Technology behind commercial devices for blood glucose monitoring in diabetes management: A review". In: *Analytica Chimica Acta* 703.2. Number: 2, pp. 124–136. ISSN: 0003-2670. DOI: 10.1016/j.aca.2011.07.024. URL: https://www.sciencedirect.com/science/article/pii/S0003267011009652 (visited on 03/08/2021).

Venzac, Bastien et al. (May 18, 2021). "PDMS Curing Inhibition on 3D-Printed Molds: Why? Also, How to Avoid It?" In: *Analytical Chemistry* 93.19. Number: 19 Publisher: American Chemical Society, pp. 7180–7187. ISSN: 0003-2700. DOI: 10.1021/acs.analchem.0c04944. URL: https://doi.org/10.1021/acs.analchem.0c04944 (visited on 06/04/2021).

Weltin, Andreas et al. (2014). "Cell culture monitoring for drug screening and cancer research: a transparent, microfluidic, multi-sensor microsystem". In: *Lab on a Chip* 14.1. Publisher: Royal Society of Chemistry, pp. 138–146. DOI: 10.1039/C3LC50759A. URL: https://pubs.rsc.org/en/content/articlelanding/2014/lc/c3lc50759a (visited on 09/19/2023).

Whitesides, George M. et al. (2001). "Soft Lithography in Biology and Biochemistry". In: *Annual Review of Biomedical Engineering* 3.1, pp. 335–373. DOI: 10.1146/annurev.bioeng.3.1.335. URL: https://doi.org/10.1146/annurev.bioeng.3.1.335 (visited on 08/28/2023).

Woerle, Hans J. et al. (Apr. 2003). "Pathways for glucose disposal after meal ingestion in humans". In: *American Journal of Physiology-Endocrinology and Metabolism* 284.4. Publisher: American Physiological Society, E716–E725. ISSN: 0193-1849. DOI: 10.1152/ajpendo.00365.2002. URL: https://journals.physiology.org/doi/full/10.1152/ajpendo.00365.2002 (visited on 07/10/2023).

Zambon, Alessandro et al. (2014). "Determination of glucose flux in live myoblasts by microfluidic nanosensing and mathematical modeling". In: *Integr. Biol.* 6.3, pp. 277–288. ISSN: 1757-9694, 1757-9708. DOI: 10.1039/C3IB40204E. URL: https://academic.oup.com/ib/article/6/3/277-288/5199139 (visited on 09/15/2022).

Zhang, Shuyu et al. (2023). "Microphysiological Constructs and Systems: Biofabrication Tactics, Biomimetic Evaluation Approaches, and Biomedical Applications". In: *Small Methods*.

Zhang, Yu Shrike et al. (Mar. 21, 2017). "Multisensor-integrated organs-on-chips platform for automated and continual in situ monitoring of organoid behaviors". In: *Proceedings of the National Academy of Sciences* 114.12. Number: 12 Publisher: National Academy of Sciences Section: PNAS Plus, E2293–E2302. ISSN: 0027-8424, 1091-6490. DOI: 10.1073/pnas.1612906114. URL: https://www.pnas.org/content/114/12/E2293 (visited on 12/07/2020).

Zheng, Yan, Sylvia H. Ley, and Frank B. Hu (Feb. 2018). "Global aetiology and epidemiology of type 2 diabetes mellitus and its complications". In: *Nature Reviews Endocrinology* 14.2, pp. 88–98. ISSN: 1759-5029, 1759-5037. DOI: 10.1038/nrendo.2017.151. URL: https://www.nature.com/articles/nrendo.2017.151 (visited on 08/25/2023).

Zhu, Chun-Hong et al. (2007). "Cellular senescence in human myoblasts is overcome by human telomerase reverse transcriptase and cyclin-dependent kinase 4: consequences in aging muscle and therapeutic strategies for muscular dystrophies". In: *Aging Cell* 6.4, pp. 515–523. ISSN: 1474-9726. DOI: https://doi.org/10.1111/j.1474-9726.2007.00306.x. URL: https://onlinelibrary.wiley.com/doi/abs/10.1111/j.1474-9726.2007.00306.x (visited on 05/27/2021).

Zhu, Lu et al. (May 16, 2019). "Intraislet glucagon signaling is critical for maintaining glucose homeostasis". In: *JCI Insight* 4.10. ISSN: 0021-9738. DOI: 10.1172/jci.insight.127994. URL: https://insight.jci.org/articles/view/127994 (visited on 09/26/2023).